THE POTENTIAL EFFECT AND MECHANISM OF TRADITIONAL MEDICINE ON VASCULAR HOMEOSTASIS AND REMODELING: AN UPDATE

EDITED BY: Yuliang Wang, Zhang Yuefan and Tie-Jun Li

PUBLISHED IN: Frontiers in Pharmacology and Frontiers in Neuroscience

frontiers Research Topics

ISSN 1664-8714
ISBN 978-2-88974-820-4
DOI 10.3389/978-2-88974-820-4

About Frontiers

Frontiers is more than just an open-access publisher of scholarly articles: it is a pioneering approach to the world of academia, radically improving the way scholarly research is managed. The grand vision of Frontiers is a world where all people have an equal opportunity to seek, share and generate knowledge. Frontiers provides immediate and permanent online open access to all its publications, but this alone is not enough to realize our grand goals.

Frontiers Journal Series

The Frontiers Journal Series is a multi-tier and interdisciplinary set of open-access, online journals, promising a paradigm shift from the current review, selection and dissemination processes in academic publishing. All Frontiers journals are driven by researchers for researchers; therefore, they constitute a service to the scholarly community. At the same time, the Frontiers Journal Series operates on a revolutionary invention, the tiered publishing system, initially addressing specific communities of scholars, and gradually climbing up to broader public understanding, thus serving the interests of the lay society, too.

Dedication to Quality

Each Frontiers article is a landmark of the highest quality, thanks to genuinely collaborative interactions between authors and review editors, who include some of the world's best academicians. Research must be certified by peers before entering a stream of knowledge that may eventually reach the public - and shape society; therefore, Frontiers only applies the most rigorous and unbiased reviews.
Frontiers revolutionizes research publishing by freely delivering the most outstanding research, evaluated with no bias from both the academic and social point of view. By applying the most advanced information technologies, Frontiers is catapulting scholarly publishing into a new generation.

What are Frontiers Research Topics?

Frontiers Research Topics are very popular trademarks of the Frontiers Journals Series: they are collections of at least ten articles, all centered on a particular subject. With their unique mix of varied contributions from Original Research to Review Articles, Frontiers Research Topics unify the most influential researchers, the latest key findings and historical advances in a hot research area! Find out more on how to host your own Frontiers Research Topic or contribute to one as an author by contacting the Frontiers Editorial Office: frontiersin.org/about/contact

THE POTENTIAL EFFECT AND MECHANISM OF TRADITIONAL MEDICINE ON VASCULAR HOMEOSTASIS AND REMODELING: AN UPDATE

Topic Editors:
Yuliang Wang, Shanghai Jiao Tong University, China
Zhang Yuefan, Shanghai University, China
Tie-Jun Li, Second Military Medical University, China

Citation: Wang, Y., Yuefan, Z., Li, T.-J., eds. (2022). The Potential Effect and Mechanism of Traditional Medicine on Vascular Homeostasis and Remodeling: An Update. Lausanne: Frontiers Media SA. doi: 10.3389/978-2-88974-820-4

Table of Contents

frontiers in Pharmacology

EDITORIAL
published: 10 March 2022
doi: 10.3389/fphar.2022.847333

Editorial: The Potential Effect and Mechanism of Traditional Medicine on Vascular Homeostasis and Remodeling: An Update

*Yuefan Zhang[1], Tie-Jun Li[1], Mengting Lv[1], Xinyu Li[1] and Yuliang Wang[2,3]**

[1]School of Medicine, Shanghai University, Shanghai, China, [2]Plant Biotechnology Research Center, Joint International Research Laboratory of Metabolic and Developmental Sciences, Fudan-SJTU-Nottingham Plant Biotechnology R&D Center, School of Agriculture and Biology, Shanghai Jiao Tong University, Shanghai, China, [3]Key Laboratory of Urban Agriculture (South) Ministry of Agriculture, Plant Biotechnology Research Center, Fudan-SJTU-Nottingham Plant Biotechnology R&D Center, School of Agriculture and Biology, Shanghai Jiao Tong University, Shanghai, China

Keywords: vascular homeostasis, vascular remodeling, nature product, cardiovascular, Chinese traditional and herbal drugs

Editorial on the Research Topic

The Potential Effect and Mechanism of Traditional Medicine on Vascular Homeostasis and Remodeling: An Update

OPEN ACCESS

Edited by:
Javier Echeverria,
University of Santiago, Chile

Reviewed by:
Ismail Laher,
University of British Columbia, Canada

****Correspondence:***
Yuliang Wang
wangyuliang@sjtu.edu.cn

Specialty section:
This article was submitted to Ethnopharmacology, a section of the journal Frontiers in Pharmacology

Received: *02 January 2022*
Accepted: *07 February 2022*
Published: *10 March 2022*

Citation:
Zhang Y, Li T-J, Lv M, Li X and Wang Y (2022) Editorial: The Potential Effect and Mechanism of Traditional Medicine on Vascular Homeostasis and Remodeling: An Update. Front. Pharmacol. 13:847333. doi: 10.3389/fphar.2022.847333

Cardiovascular diseases are the leading causes of death worldwide. And most cardiovascular diseases are accompanied by vascular homeostasis disorder and vascular remodeling. Vascular remodeling can disrupt the homeostasis of blood vessels, lead to vascular dysfunction and induce organ injury. Moreover, vascular remodeling is also the pathological basis of cardiovascular diseases and metabolic diseases such as hypertension, coronary heart disease, stroke, heart failure, diabetes, atherosclerosis (Koenen et al., 2021). In recent years, a growing body of experimental studies on the regulation of vascular remodeling and vascular homeostasis by natural products, which will lay the foundation for new drug discovery in cerebrovascular diseases.

Following the successful "The Potential Effect and Mechanism of Traditional Medicine on Vascular Homeostasis and Remodeling" Research Topic in *Frontiers in Pharmacology*, we organized a new Research Topic entitled "*The Potential Effect and Mechanism of Traditional Medicine on Vascular Homeostasis and Remodeling: An Update*" in *Frontiers in Pharmacology*. A total of nine articles has been published on this Research Topic, including eight research articles and one review. Here, we summarize the highlights of these articles.

Small vessel diseases are the disorders of cerebral microvessels that causes stroke and vascular dementia, which lead to white matter damage in cardiovascular diseases. The cerebral microvessel lesions manifest as blood-brain barrier dysfunction, impaired vasodilation, vessel stiffening, white matter rarefaction, and cerebral ischemia (Wardlaw et al., 2019). Many natural products have therapeutic effects on small vessel diseases. Quercetin is a flavonoid found in many plants. (Li M. et al, 2021).show that Quercetin mitigates HR-induced human brain microvascular endothelial cell injury by promoting the viability, migration and angiogenesis of HBMECs (Human Brain Microvascular Endothelial Cells), and inhibiting the apoptosis of HBMECs. Liquiritin is the main active component of *Glycyrrhiza uralensis Fisch*. The research article by (Li MT. et al, 2021)is focused on the protective effects of liquiritin on HR-induced human brain microvascular endothelial cells. The authors found that Liquiritin promotes proliferation, migration, angiogenesis, and inhibits the apoptosis of HBMECs. Quercetin and Liquiritin might serve as protective compounds in small vessel diseases by improving blood-brain barrier.

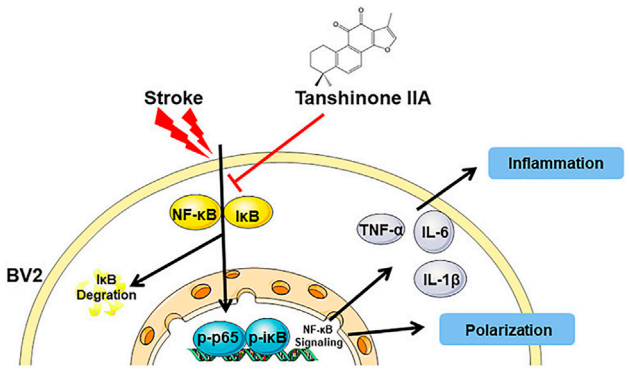

FIGURE 1 | The mechanism of the neuroprotective mechanisms of Tanshinone IIA in stroke-induced neuroinflammation.

The disruption of vascular homeostasis is closely related to the dysfunction of endothelial cells and smooth muscle cells in the blood vessels. Regulating the function of intravascular cells can effectively improve vascular remodeling and vascular homeostatic imbalance. Atherosclerosis is characterized by the dysfunction of lipid and vascular homeostasis. Chen et al. explore the therapeutic effects of Tongxinluo, a traditional Chinese medicine, on atherosclerosis, and find Tongxinluo can attenuate the accumulation of lipids, improve fat metabolism in macrophage. This effect relies on enhancing Beclin-1-induced autophagy. Resibufogenin is an active compound from *Bufo bufonis*. A study by Yang et al. shows Resibufogenin exerts the antiangiogenic effect on the HUVECs (Human Umbilical Endothelial Cells) in a VEGFR2 (Vascular Endothelial Growth Factor 2) dependent signal pathway.

Hu-zhang-qing-mai-yin is a Chinese traditional medicine formula, has been clinically used for many years. The research article by Yu et al. is focused on the anti-diabetic retinopathy effects of Hu-zhang-qing-mai-yin *in vitro*. They show Hu-zhang-qing-mai-yin can inhibit the cell proliferation and promote the mitochondria-related apoptosis of human retinal capillary endothelial cells through P38 and NF-κB signaling pathways. Avenanthramide C is a component of the phenolic compound of oats. Park et al. show Avenanthramide C can inhibit the expression of MMP (Matrix Metalloproteinase) and migration through MAPK (Mitogen-Activated Protein Kinase) signaling in human aortic smooth muscle cells. Avenanthramide C could be a promising candidate for atherosclerosis diseases.

Stroke is the sudden rupture of blood vessels in the brain, or the blockage of blood vessels in the brain, resulting in a series of brain damage. Now it is the main cause of death and disability worldwide. And the stroke burden is a huge public health issue (Owolabi et al., 2021). Drug research for stroke prevention and treatment has been a hot topic in medical research. A series of articles within this Research Topic identify novel natural products that can alleviate the cerebral ischemia injury. MQ (L-methionyl-L-glutamic acid) is one of the metabolites of monocyte locomotion inhibitory factor, a thermostable pentapeptide secreted by *Entamoeba histolytica*. The work by Zhang et al. describes the role of MQ in cerebral ischemia. They found that MQ exerts a neuroprotective effect in cerebral ischemia by blocking apoptosis via the p-JNK/Bax pathway. Tanshinone IIA is a fat-soluble diterpenoid isolated from *Salvia miltiorrhiza Bunge*. Song et al. show that Tanshinone IIA also has a neuroprotective effect by regulating microglia polarization from M1 to M2 in an NF-κB dependent signaling pathway (**Figure 1**). The review by Kang et al. brings the information regarding the protective effect and mechanism of astragaloside IV, an extract from *Radix Astragali*. Astragaloside IV exerts a protective effect on ischemia-reperfusion injury by relieving neuronal apoptosis, oxidative stress, BBB injury, leukocyte adhesion, and inhibiting inflammatory reaction.

Vascular remodeling is the pathological basis of vascular and circulatory dysfunction. The process of vascular remodeling is complex, which is closely related to abnormal hemodynamics, activation of vasoactive substances, cell proliferation and apoptosis, inflammation and oxidative stress. Natural products play an important role in regulating vascular remodeling and promoting vascular homeostasis because of their multi-target properties. Although articles presented in this Research Topic illustrate natural products that regulate vascular remodeling and vascular homeostasis, many natural products that regulate vascular function and the role of natural products in vascular remodeling and vascular homeostasis have not been clarified. We hope we can bring an update Research Topic soon.

AUTHOR CONTRIBUTIONS

YZ wrote the manuscript. T-JL, ML, and XL reviewed and edited this manuscript. YW conceptualized and reviewed the manuscript. All authors listed have made a substantial, direct, and intellectual contribution to the work and approved it for publication.

REFERENCES

Koenen, M., Hill, M. A., Cohen, P., and Sowers, J. R. (2021). Obesity, Adipose Tissue and Vascular Dysfunction. *Circ. Res.* 128 (7), 951–968. doi:10.1161/CIRCRESAHA.121.318093

Li, M., Ke, J., Deng, Y., Chen, C., Huang, Y., Bian, Y., et al. (2021a). The Protective Effect of Liquiritin in Hypoxia/Reoxygenation-Induced Disruption on Blood Brain Barrier. *Front. Pharmacol.* 12, 671783. doi:10.3389/fphar.2021.671783

Li, M. T., Ke, J., Guo, S. F., Wu, Y., Bian, Y. F., Shan, L. L., et al. (2021b). The Protective Effect of Quercetin on Endothelial Cells Injured by Hypoxia and Reoxygenation. *Front. Pharmacol.* 12, 732874. doi:10.3389/fphar.2021.732874

Owolabi, M. O., Thrift, A. G., Mahal, A., Ishida, M., Martins, S., Johnson, W. D., et al. (2021). Stroke Experts Collaboration GroupPrimary Stroke Prevention Worldwide: Translating Evidence into Action. *Lancet Public Health* S2468-2667 (21), 00230–00239.

Wardlaw, J. M., Smith, C., and Dichgans, M. (2019). Small Vessel Disease: Mechanisms and Clinical Implications. *Lancet Neurol.* 18 (7), 684–696. doi:10.1016/S1474-4422(19)30079-1

Conflict of Interest: The authors declare that the research was conducted in the absence of any commercial or financial relationships that could be construed as a potential conflict of interest.

Publisher's Note: All claims expressed in this article are solely those of the authors and do not necessarily represent those of their affiliated organizations, or those of the publisher, the editors and the reviewers. Any product that may be evaluated in this article, or claim that may be made by its manufacturer, is not guaranteed or endorsed by the publisher.

frontiers in Pharmacology

ORIGINAL RESEARCH
published: 25 March 2021
doi: 10.3389/fphar.2021.621854

Avenanthramide C Suppresses Matrix Metalloproteinase-9 Expression and Migration Through the MAPK/NF- κB Signaling Pathway in TNF-α-Activated HASMC Cells

*Junyoung Park[1], Hyunju Choi[1], Fukushi Abekura[1], Hak-Seong Lim[1], Jong-Hwan Im[2], Woong-Suk Yang[3], Cher-Won Hwang[4], Young-Chae Chang[5], Young-Choon Lee[6], Nam Gyu Park[2] and Cheorl-Ho Kim[1]**

[1]Department of Biological Sciences, College of Science, Sungkyunkwan University, Suwon, South Korea, [2]Department of Biotechnology, College of Fisheries Sciences, Pukyong National University, Busan, South Korea, [3]Nodaji Co., Ltd., Pohang, Republic of Korea, [4]Department of AGEE, Handong Global University, Pohang, South Korea, [5]Research Institute of Biomedical Engineering and Department of Medicine, College of Medicine, Catholic University of Daegu, Daegu, South Korea, [6]Faculty of Medicinal Biotechnology, Dong-A University, Busan, South Korea

OPEN ACCESS

Edited by:
Zhang Yuefan,
Shanghai University, China

Reviewed by:
Arunachalam Karuppusamy,
Federal University of Mato Grosso, Brazil
Sung-Kwon Moon,
Chung-Ang University, South Korea

***Correspondence:**
Cheorl-Ho Kim
chkimbio@skku.edu

Specialty section:
This article was submitted to Ethnopharmacology, a section of the journal Frontiers in Pharmacology

Received: 27 October 2020
Accepted: 05 February 2021
Published: 25 March 2021

Citation:
Park J, Choi H, Abekura F, Lim H-S, Im J-H, Yang W-S, Hwang C-W, Chang Y-C, Lee Y-C, Park NG and Kim C-H (2021) Avenanthramide C Suppresses Matrix Metalloproteinase-9 Expression and Migration Through the MAPK/NF- κB Signaling Pathway in TNF-α-Activated HASMC Cells. Front. Pharmacol. 12:621854. doi: 10.3389/fphar.2021.621854

In oat ingredients, flavonoids and phenolic acids are known to be the most important phenolic compounds. In phenolic compounds, wide-ranging biological responses, including antioxidative, anti-inflammatory, anti-allergic, and anti-cancer properties, were reported. Avenanthramide C (Avn C), a component of the phenolic compound of oats, has been reported to be highly antioxidant and anti-inflammatory, but its role in an anti-atherosclerosis response is unknown. The aim of this research was to assess the effect of Avn C on expression of MMP-9 on TNF-α-activated human arterial smooth-muscle cells (HASMC) and signaling involved in its anti-atherosclerosis activity. HASMC cells are known to produce inflammatory cytokines involving IL-6, IL-1β, and TNF-α during arteriosclerosis activity. Avn C specifically reduced IL-6 secretion in HASMC cells. Furthermore, we investigated whether Avn C could inhibit NF-κB nuclear protein translocation. Avn C suppressed nuclear protein translocation of NF-κB in TNF-α-stimulated HASMCs. The MMP-9 enzyme activity and expression are controlled through the MAPKs signaling path during the Avn C treatment. We confirmed that the levels of wound healing (p-value = 0.013, $^*p < 0.05$) and migration (p-value = 0.007, $^{**}p < 0.01$) are inhibited by 100 ng/ml TNF-α and 100 μM Avn C co-treated. Accordingly, Avn C inhibited the expression of MMP-9 and cell migration through the MAPK/NF-κB signaling pathway in TNF-α-activated HASMC. Therefore, Avn C can be identified and serve as disease prevention material and remedy for atherosclerosis.

Keywords: anti-atherosclerosis, MMP, TNF-α, HASMCs (human aortic smooth muscle cells), avenanthramide C

Abbreviations: Avn C, avenanthramide C; COX-2, cyclooxyenase-2; DMEM, Dulbecco's modified Eagle medium; DMSO, dimethyl sulfoxide; ECL, enhanced chemiluminescence; FBS, fetal bovine serum; FITC, fluorescein isothiocyanate; iNOS, inducible nitric oxide synthase; IL-1β, interleukin-1β; MAPKs, mitogen-activated protein kinases; MMP-9, matrix metallopeptidase 9; MTT, 3- (4,5-dimethylthiazol-2-yl)-2,5-diphenyl tetrazolium bromide; NF-κB, nuclear factor kappa-light-chain-enhancer of activated B cells; TBE, Tris-borate-EDTA; TNF-α, tumor necrosis factor-α

INTRODUCTION

Matrix metallopeptidases (MMP) play an important role in angiogenesis, cell behavior, differentiation, cell proliferation, migration, and host defense (Kuzuya and Iguchi, 2003; Flamant et al., 2007). MMP-9 can disassemble the extracellular matrix (ECM) and is prominent in the vulnerable areas of atherosclerosis (Watanabe and Ikeda, 2004; Johnson, 2017). MMP-9 and pro-inflammatory cytokines are significant factors that enable the disassembly of the ECM. Also, MMP is well known as the major cause of atherosclerosis (Beaudeux et al., 2004; Flamant et al., 2007). Atherosclerosis is a cause of vascular disease. Thus, the importance of research on metastasis and treatment, a disease of arteriosclerosis, is gradually increasing. MMP-9 and MMP-2 play a significant role in the migration of HASMC cells into the inner membrane of blood vessels, which further exacerbates many vascular diseases and atherosclerosis (Visse and Nagase, 2003; Wagsater et al., 2011; Park et al., 2019).

In oat ingredients, phenolic acid and flavonoid are the most important phenolic compounds. The phenolic compounds exhibit wide-ranging biological responses as antioxidants, anti-inflammatory, anti-allergic and anti-cancer agents (Cebeci and Sahin-Yesilcubuk, 2014; Meydani, 2009; Singh et al., 2013). Avenanthramides (Avns) are combinations of a 5-hydroxy anthranilic acid and phenylpropanoid. Avns extracted from oats are soluble phenolic compounds (Bei et al., 2020; Ishihara et al., 2014). Three main isoforms of Avn, A, B, and C (**Figure 1A**) have been verified, and the previous results have shown their anti-histamine, anti-tumor proliferative, anti-oxidant, and anti-inflammatory functions (Sur et al., 2008).

Recently, there have been several reports that Avn C restores impaired plasticity and cognition in an Alzheimer's disease model with mice and suppresses eccentric exercise-inflicted blood inflammatory markers (Koenig et al., 2016; Ramasamy et al., 2020). It has also been reported that Avn C decreases the cell survival of MDA-MB-231 cells via an apoptotic system and protects noise and drug-activated hearing loss by protecting auditory hair cells from oxidative stress (Hastings and Kenealey, 2017; Umugire et al., 2019). But the role of Avn C in anti-atherosclerosis responses is unknown.

In this study, we used TNF-α-induced HASMC cells as an arteriosclerosis model. The results showed that the Avn C decreased MMP-9 expression of HASMC cells activated with TNF-α dose-dependently. In addition, we studied the effect of Avn C on anti-arteriosclerosis activity with TNF-α treatment to find out its molecular mechanisms.

MATERIALS AND METHODS

Reagents

Avenanthramide C was purchased from Sigma–Aldrich (St. Louis, MO, United States; cat. no. 36465) and dissolved in dimethyl sulfoxide (DMSO) (St. Louis, MO, United States; cat.no. D2650) used in doses of 1 μM. It has a purity of 98% by SDS-PAGE gel and HPLC analyses and the grade is analytic standard. Human recombinant TNF-α protein (Purity: 98%) was purchased from PeproTech (Rocky Hill, NJ, United States). Griess reagent (cat. no. G4410), Hoechst staining solution (cat. no. 94403), 3- (4,5-dimethylthiazol-2-yl)-2,5-diphenyltetrazolium bromide (MTT) (cat. no. M5655), Corning trans-well Wright-Giemsa stain solution and 6-diamidino-2-phenylindole dihydrochloride (DAPI) (cat. no. D9542) were purchased from Sigma–Aldrich (St. Louis, MO, United States). p-ERK, ERK, p-p38, p-JNK, JNK and NF-kB were purchased from Cell signaling technology (Danvers, MA, United States). And, MMP-9, MMP-2, p38, β-actin, p-IkB and IkB antibodies were purchased from Santa Cruz Biotechnology (Paso Robles, CA, United States).

Cell Culture and MTT Assay

Human Aortic Smooth. Muscle Cells (HASMC) were purchased from American Type Culture Collection (ATCC; Rockville, MD, USA). These cells were cultured in DMEM (WelGENE Co., Daegu, Korea) after processing by 10% metal bovine serum

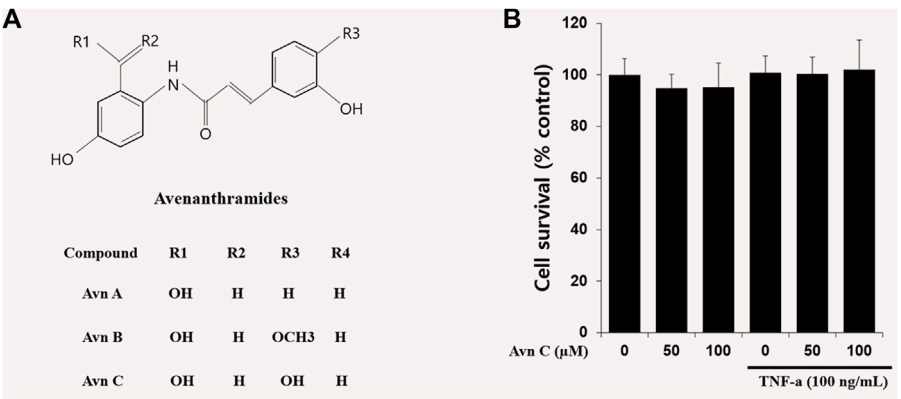

FIGURE 1 | Chemical structures of Avenanthramides and effects on cell viability in HASMC cells. **(A)** Avenanthramides: AvnA, AvnB and AvnC (Chemical structures) **(B)** Cell viability measured by MTT. 5×10^3 cell/well cells were treated with Avn C (0, 50, or 100 μM) and TNF-α (100 ng/ml) for 24 h.

(FBS), 100 U/ml penicillin, and 100 mg/ml streptomycin (P/S) on each medium in a humidified atmosphere containing 37°C and 5% CO_2 incubator. To assess cell viability, we seeded HASMC cells into a 96-well dish at a density of 1 X 10^4 cells/well and treated them with Avn C (0, 50, or 100 μM). We added MTT solution and incubated the cells for 4 h at 37°C in a CO2 incubator. We solubilized the reaction reagent with dimethyl sulfoxide (DMSO) and measured optical density at 550 nm after 15 min of incubation.

Gelatin Zymography Assay

Cultural medium with 100 ng/ml TNF-α with or without 100 μM Avn C treatment was collected from 12-well plates. The sample was mixed with a 5% Tris-glycine SDS sample buffer and loaded into 10% polyacrylamide gel with 1 mg/ml gelatin. After being run at 110 V for 1 h 20 min, the gel was washed with 2.5% Triton X-100 for 20 min and then incubated with incubation buffer (10 mM Tris base, 40 mM Tris–HCl, 200 mM NaCl, and 10 mM CaCl2) at 37°C for 12 h. The gel was then dyed for 2 h with comassie blue.

Western Blot

We extracted the protein from the HASMC cells using the 1% NP40 protein lysis buffer containing 100 mM Na-Northovanadate, 100 mM NaF, and 100 mM Na-pyrophosphate and centrifuged the extract at 4°C at 13,000 rpm. The extracted protein was quantified by Bio-Rad protein assay (Bio-Rad Laboratories Hercules, CA, United States) and separated the same amount (by size) of protein through SDS-PAGE (SDS-polyacrylamide). Then, we transferred the membrane to the NC (nitrocellulose) membrane, reacted it to the primary antibodies [MMP-9 (cat.no. sc-13520, 1:2000), MMP-2 (cat. no.13594, 1:2000), β-actin (cat. no. sc-47778; 1: 3000), NF-κB (cat. no. sc-372; 1:1000), Lamin B (cat no. sc-365962,1:1000), p-IκB (cat no. sc-8404,1:2000), IκB (cat. no. sc-1643, 1:2000), p-ERK (cat. no. 9101S; 1:2000), ERK (cat. no. 9101S; 1:2000), p-JNK (cat. no. #9255S; 1:2000), JNK (cat. no. 9252S; 1: 2000), p-p38 (cat. no. sc-7975; 1:2000) and p38 (cat. no. sc-535; 1: 2000) from Santa Cruz Biotechnology and Cell signaling technology, and horseradish peroxidase-linked anti-mouse (#31430, 1:2000), anti-rabbit (#31460, 1:2000), or anti-goat (#31402, 1:2000) immunoglobulin G secondary antibodies from Invitrogen and Thermo], and checked the results through the ECL (Enhanced chemiluminesence).

Reverse Transcription-Polymerase Chain Reaction (RT-PCR)

Total RNA of HASMC cells was extracted using TRizol agent (Invitrogen, USA), and the cDNA was synthesized using the oligo dT primer using RT-Premix kit (Takara Shuzo, Japan). The cDNA was amplified by a PCR machine using these primers: MMP-9, forward 5′-TCCCTGGAGACCTGAGAACC-3′, reverse 5′-CGGCAAGTCTTCCGAGTAGTT-3′; MMP-2, forward 5′-TGA AGG TCG GTG TGA ACG GA-3′ and reverse 5′-CAT GTA GCC ATG AGG TCC ACC AC-3′; and β-actin, forward 5′-TCCTTCTGCATCCTGTCGGC-3′, reverse 5′-CAAGAGATGGCCACGGCTGC-3′.

ELISA

We measured the levels of inflammatory cytokines such as TNF-α, IL-1β and IL-6 in culture medium using ELISA kits (Affymetrix, eBioscience) along with antibodies for each cytokine according to the protocol.

Immunofluorescence Assay

TNF-α was treated on HASMC cells, which were fixed 24 h later using 4% PFA (paraformaldehyde), increased permeability to 0.2% Triton-100, sequentially reacted with a primary antibody, a secondary antibody, and DAPAI, and checked by fluorescence microscope.

Trans-Well Migration Assay

We added the HASMC cells to the top of the transwell, added the TNF-α-treated badges to the bottom, and incubated them for 24 h. The cells moved through the 8-mm pore-size membrane, were fixed through methanol, were dyed with Giamsa, and then the dyed cells were identified by means of an optical microscope.

Wound Healing Assay

HASMCs were seeded into a 6-well dish at a density of 3×10^5 cells/well. The wound was artificially scratched with a yellow pipette tip (200 μl) and washed to a moderate extent three times. After 24 h of processing either Avn C or Avn C + TNF-α, each well was observed microscopically.

Statistical Analysis

All experiment results are representative of at least three independent experiments. The results of the data were assessed by one-way analysis of variance (ANOVA), followed by a post hoc Bonferoni test; a $p < 0.05$ was considered statistically significant. $^*p < 0.05$ and $^{**}p < 0.01$ indicate significant differences from the TNF-α-alone-treated cells.

RESULTS

Chemical Structures of Avenanthramides and Effects on Cell Viability in HASMC Cells

The chemical structures of Avn A, B and C (**Figure 1A**) of the major phenolic components of oats are specifically features of 5-hydroxy anthranilic acid and phenylpropanoid. The molecular weight of Avn C is 315.28 g/mol. To study the Avn C-influenced cell viability in HASMC cells, we did an MTT assay to assess the cellular proliferation. We could not observe any cell death following treatment with Avn C (0–100 μM) in the absence or presence of 100 ng/ml TNF-α. (**Figure 1B**). Thus, we have used 0–100 μM Avn C for all of the experiments.

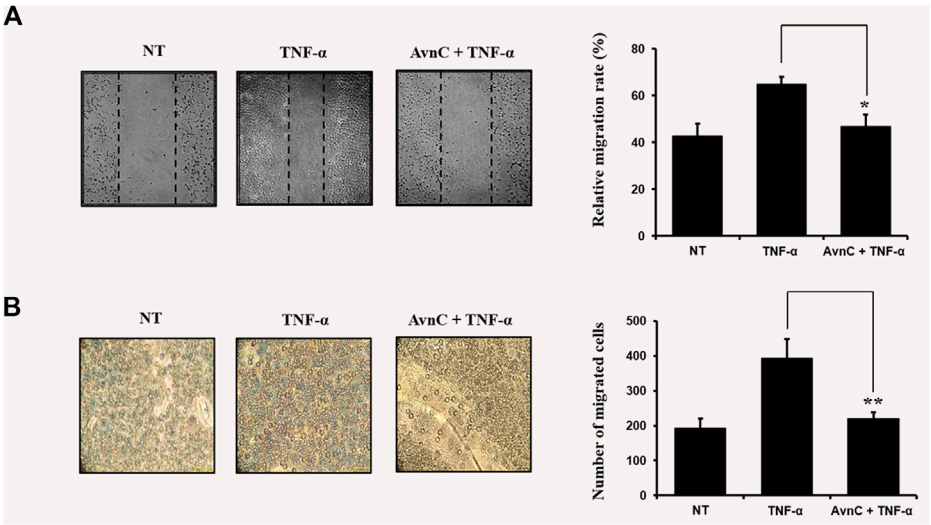

FIGURE 2 | Avn C inhibits TNF-α -stimulated migration and wound healing of HASMC cells **(A)** HASMC cells were scratched with a yellow pipette tip. The cells were treated with 100 ng/ml TNF-α with or without 100 μM Avn C for 24 h. Cells migrated into the wound area **(B)** The migration ability of HASMC cells was detected by a transwell assay. The cells were incubated with 100 ng/ml TNF-α with or without 100 μM Avn C for 24 h. Results shown are representative of three independent experiments. They are presented as mean ± SEM. *$p < 0.05$ and **$p < 0.01$, significant differences from TNF-α treated cells. NT, no treatment.

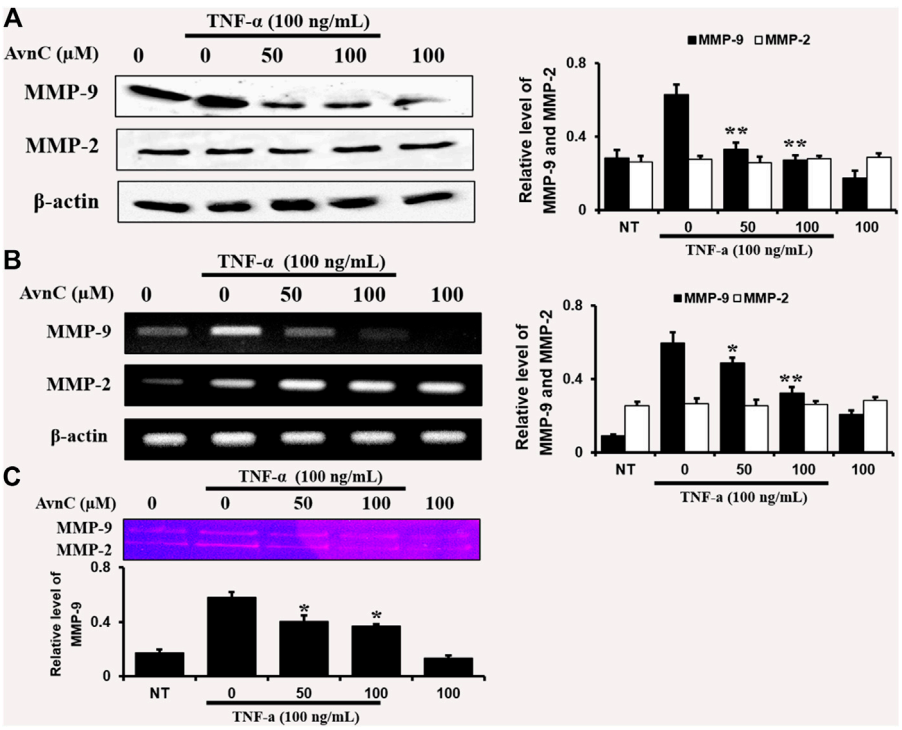

FIGURE 3 | Effects of Avn C on TNF-α-induced MMP-9 and MMP-2 expression levels in HASMC cells.HASMC cells were co-treated with 0–100 μM Avn C and 100 ng/ml TNF-α for 24 h. Protein **(A)** and mRNA **(B)** levels respectively were examined by Western blotting and RT-PCR **(C)** Gelatin zymography results of MMP-9 enzyme activity levels. Results shown are representative of three independent experiments. They are presented as mean ± SEM. *$p < 0.05$ and **$p < 0.01$, significant differences from the TNF-α treated cells. NT, no treatment.

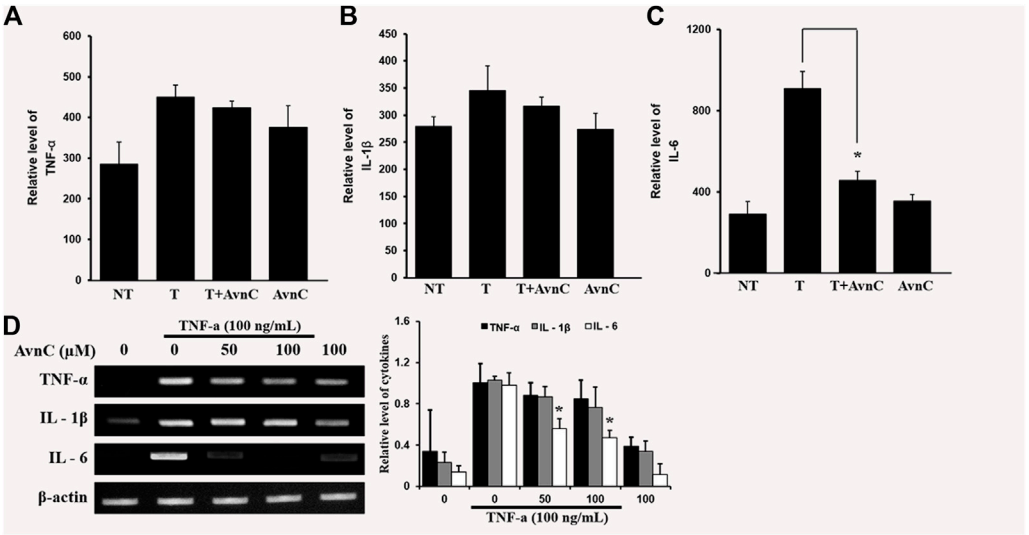

FIGURE 4 | Effects of Avn C on TNF-α-induced cytokines secretion levels of IL-1β, IL-6 and TNF-α in HASMC cells **(A)** and **(B)** were not different in the secretion of IL-1 β and TNF- α cytokines with treatment by AvnC according to ELISA, but **(C)** Avn C attenuated TNF-α-induced IL-6 inflammatory cytokines. Results shown are representative of three independent experiments. Also, Avn C showed no effect on the total expression level of IL-1β and TNF-α, but it specifically decreased the expression level of IL-6 in TNF-α -stimulated HASMC cells by RT-PCR analysis **(D)**. Results are presented was mean ± SEM. *$p < 0.05$ indicates a significant difference from TNF-α-treated cells. NT, no treatment; T, TNF-α; T + AvnC, TNF-α + Avn C.

Avn C Suppresses TNF-α-Stimulated Migration and Wound Healing of HASMC Cells

TNF-α has been reported to be involved in metastasis of tumor cells or invasive vascular cells (Balkwill, 2006). To confirm the effect of Avn C on the cell migration and wound healing in TNF-α-activated HASMC cells, the following experiments were conducted. As shown in **Figures 2A**,**B**, when TNF-α is treated with HASMC cells, wound healing and migration levels are increased. But when TNF-α and Avn C are co-treated, the levels of wound healing and migration are inhibited.

Effects of Avn C on Levels of mRNA and Protein Expression as Well as Enzyme Activities of mmp-9 and mmp-2 in HASMC Cells

To find out the anti-atherosclerotic effect of Avn C, we assessed the levels of protein expression of MMP-9 and MMP-2 in the cells stimulated by TNF-α (100 ng/ml) by Western blot, RT-PCR, and gelatin zymography analysis. The levels of protein and mRNA expression were evaluated after incubating HASMC cells with 100 ng/ml TNF-α and 0–100 μM Avn C for 24 h. In HASMC cells treated with Avn C, the level of protein expression in MMP-9 was decreased with no variation in MMP-2 expression (**Figure 3A**). The mRNA level of MMP-9 was also reduced in HASMC cells with high concentrations of 0 to 100 μM Avn C (**Figure 3B**). Moreover, MMP-9 enzyme activity in TNF-α activated HASMC cells with Avn C treatment was significantly increased when compared to the TNF-α -treated control cells (**Figure 3C**). The results showed that, by treatment with Avn C, the mRNA and protein levels of MMP-9 enzyme were specifically decreased.

Effects of Avn c on Secretion Levels of TNF-α-Activated Cytokines of IL-6, IL-1β and TNF-α in HASMC Cells

We assessed the effects of Avn C on secretions of well-known pro-inflammatory cytokines, such as IL-6, IL-1β, and TNF-α, by ELISA. In co-treatment of TNF-α and Avn C, there was no difference in the secretion levels of IL-1 β and TNF-α cytokines in the HASMC, but the secretion of IL-6 was inhibited (**Figures 4A–C–C**). Also, Avn C showed no effect on the total expression level of IL-1β and TNF-α, but it specifically decreased the expression level of IL-6 in TNF-α -stimulated HASMC cells by RT-PCR analysis (**Figure 4D**). The results showed that Avn C specifically inhibits IL-6 cytokine among the pro-inflammatory cytokines in HASMC cells.

Effects of Avn C on TNF-α-Stimulated Nuclear Translocation of NF-kb in HASMC Cells

To find the decrease in NF-κB translocation, we assessed the nuclear translocation level of the factor by direct immunofluorescence assay. The NF-κB translocation was decreased during processing of Avn C in the TNF-α activated HASMC, as detected by a fluorescence microscope, showing a specific reduction in NF- κB nuclear translocation (**Figure 5A**). Also, we investigated whether Avn C could control TNF-α-activated nuclear translocation of NF-κB in HASMC cells. Avn C inhibited the nuclear translocation from the cytosolic region to nucleus, because Avn C reduced cytosol nuclear translocation (**Figure 5B**). In this study, decreased IkB expressions and reduced the *p*-IkB level were observed, as

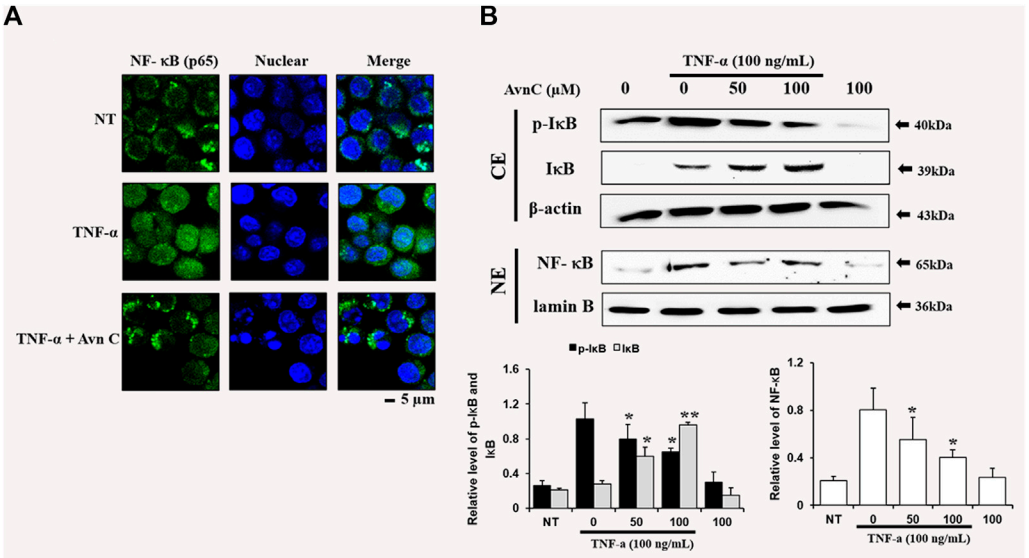

FIGURE 5 | Effects of Avn C on TNF-α-induced nuclear translocation of NF-kB in HASMC cells **(A)** Transfer of NF-κB to the nucleus was detected by immunofluorescence assay. HASMC cells were immune-stained by FITC and Hoechst. Scale bars, 5 μm. NE, Nuclear extracts; CE, Cytosolic extract; NT, no treatment **(B)** Nuclear extracts were subjected to translocation to the nuclear region of the NF-κB subunit by Western blot. They are presented as mean ± SEM. *$p < 0.05$ and **$p < 0.01$, significant differences from the TNF-α treated cells. NT, no treatment.

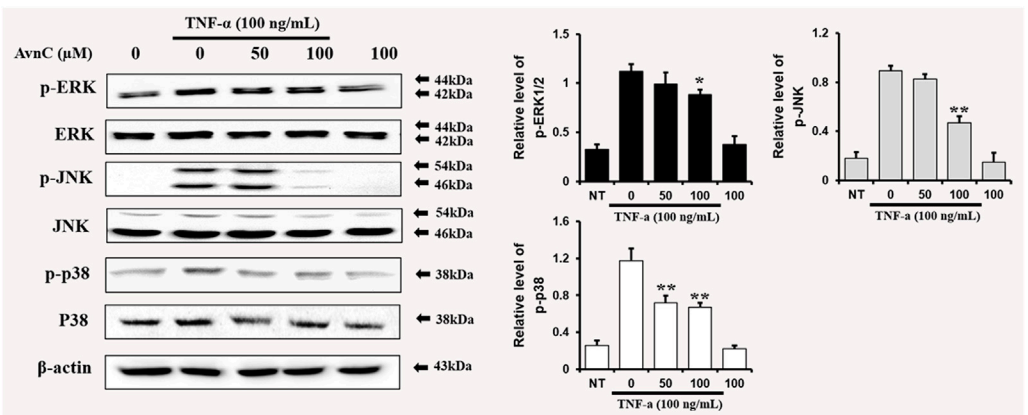

FIGURE 6 | Avn C inhibits MAPK phosphorylation in TNF-α-activated HASMC cells.Levels of phosphorylated ERK, p38, and JNK were assessed by Western blotting. Levels of ERK, JNK, and p38 were indicated by loaded protein as individual control. Results shown are representative of three independent experiments. Results are presented as mean ± SEM. *$p < 0.05$ and **$p < 0.01$ indicate significant differences from TNF-α treated cells. NT, no treatment.

expected (**Figure 5B**). These results show that Avn C could inhibit TNF-α-stimulated nuclear translocation of HASMC cells.

Avn C Inhibits MAPK Phosphorylation in TNF-α-Activated HASMC Cells

To find out whether Avn C affects MAPKs phosphorylation in TNF-α-induced HASMC cells, cells were treated with Avn C prior to TNF-α treatment, and then consequent levels of p38, JNK, and ERK phosphorylation were examined. Avn C decreased the phosphorylation levels of JNK, ERK, and p38 in TNF-α-activated HASMC cells (**Figure 6**). These results show that Avn C suppresses arteriosclerosis activity by downregulating the MAPK signaling pathway in HASMC cells induced by TNF-α.

DISCUSSION

Pathogenic atherosclerosis is associated with the secretion of MMP-9 and inflammatory cytokines to plasma and also in HASMC cells (Tayebjee et al., 2005; Nabata et al., 2008). Inflammatory cytokines, including IL-6, IL-1β, and TNF-α, are

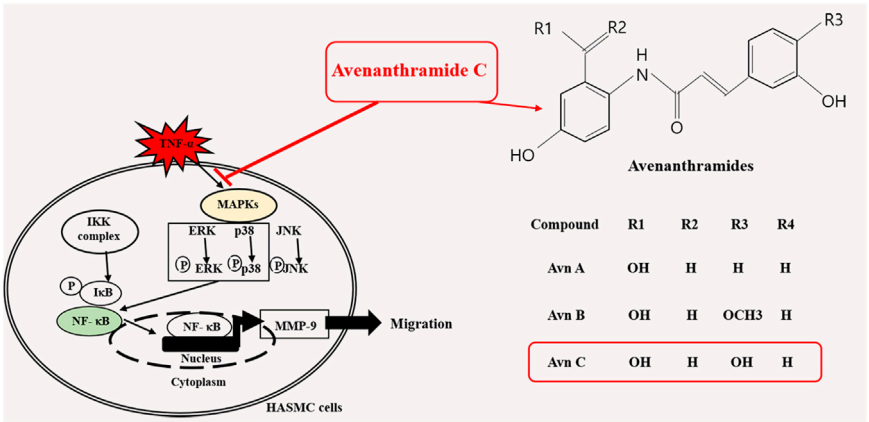

FIGURE 7 | A schematic illustration of anti-atherosclerosis action of Avn C.

also directly associated with the MMP-9 expression in the *in vivo* and *in vitro* experimental subjects (Kang et al., 2005; Stanley and Lacy, 2010; Li et al., 2017).

In this study, TNF-α-induced HASMC cells were used as an *in vitro* experiment model of arteriosclerosis (Kallenbach et al., 2003). We assessed the effect of Avn C (**Figure 1**) on TNF-α-activated atherosclerosis responses to understand the molecular mechanism underlying the anti-atherosclerotic potential of Avn-C. We confirmed the inhibition effect of Avn C on cell migration and wound healing in TNF-α-activated HASMC cells. These results indicate that the wound healing and migration activity of the vascular cells were suppressed by Avn C treatment (**Figure 2**). Avn C dose-dependently suppressed the increased MMP-9 protein and mRNA levels in HASMC cells upon TNF-α treatment. Avn C also inhibited MMP-9 enzyme activity (**Figure 3**). HASMC cells are known to produce inflammatory cytokines involving IL-6, IL-1β, and TNF-α during arteriosclerosis activity (Demyanets et al., 2011; Munoz-Garcia et al., 2006). Avn C specifically reduced IL-6 secretion in HASMC cells (**Figure 4**). Furthermore, we investigated whether Avn C could inhibit NF-κB nuclear protein translocation. Avn C suppressed nuclear protein translocation of NF-κB in TNF-α-stimulated HASMC cells dose-dependently (**Figure 5**). NF-κB is an important factor of the atherosclerotic manifest (Dabek et al., 2010). And the NF-κB regulator, IκB, has previously been identified as ensuring the level of nuclear translocation diminution (Ho et al., 2005; Ye et al., 2000). Next, we investigated whether Avn C influences the MAPKs phosphorylation. Avn C reduced the level of expression of ERK, JNK, and p38 phosphorylation in HASMC cells activated by TNF-α (**Figure 6**). The MAPK signaling pathway includes phosphorylation of p38, JNK, and ERK regulated by TNF-α (Chin et al., 1998; Zhao et al., 2019). Consequently, Avn C was shown to reduce the secretion of the cell migration and pro-cytokine through MAPK signaling, and to suppress arteriosclerosis progression (**Figure 7**). Therefore, we propose that Avn C could be a promising candidate for atherosclerosis diseases.

DATA AVAILABILITY STATEMENT

The raw data supporting the conclusions of this article will be made available by the authors, without undue reservation, to any qualified researcher.

AUTHOR CONTRIBUTIONS

CK (Supervision, Conceptualized, Project administration), JP (Data curation, Funding acquisition, Software, Visualization, Writing – original draft), JP, CK (Formal analysis), JP, FA, HL (Investigation), JP, JI, WY(Validation), JP, FA, LHS, HC (Methodology), CH, YC (Resources), CK, YL, NP (Writing – review & editing).

FUNDING

The study has in part supported by the Korea Institute of Planning and Evaluation for Technology in Food, Agriculture and Forestry (IPET 119010032HD050 derived from the IPET No.119010032CG000) during 2019–2021. The funders had no role in study design, data collection and analysis, decision to publish, or preparation of the manuscript.

REFERENCES

Balkwill, F. (2006). TNF-alpha in promotion and progression of cancer. *Cancer Metastasis Rev.* 25 (3), 409–416. doi:10.1007/s10555-006-9005-3

Beaudeux, J. L., Giral, P., Bruckert, E., Foglietti, M. J., and Chapman, M. J. (2004). Matrix metalloproteinases, inflammation and atherosclerosis: therapeutic perspectives. *Clin. Chem. Lab. Med.* 42 (2), 121–31. doi:10.1515/CCLM.2004.024

Bei, Q., Wu, Z., and Chen, G. (2020). Dynamic changes in the phenolic composition and antioxidant activity of oats during simultaneous hydrolysis

and fermentation. *Food Chem.* 305, 125269. doi:10.1016/j.foodchem.2019.125269

Cebeci, F., and Şahin-Yeşilçubuk, N. (2014). The matrix effect of blueberry, oat meal and milk on polyphenols, antioxidant activity and potential bioavailability. *Int. J. Food Sci. Nutr.* 65 (1), 69–78. doi:10.3109/09637486.2013.825699

Chin, B. Y., Choi, M. E., Burdick, M. D., Strieter, R. M., Risby, T. H., and Choi, A. M. (1998). Induction of apoptosis by particulate matter: role of TNF-alpha and MAPK. *Am. J. Physiol.* 275 (5), L942–9. doi:10.1152/ajplung.1998.275.5.L942

Dabek, J., Kulach, A., and Gasior, Z. (2010). Nuclear factor kappa-light-chain-enhancer of activated B cells (NF-kappaB): a new potential therapeutic target in atherosclerosis? *Pharmacol Rep.* 62 (5), 778–783. doi:10.1016/s1734-1140(10)70338-8

Demyanets, S., Kaun, C., Rychli, K., Pfaffenberger, S., Kastl, S. P., Hohensinner, P. J., et al. (2011). Oncostatin M-enhanced vascular endothelial growth factor expression in human vascular smooth muscle cells involves PI3K-, p38 MAPK-, Erk1/2- and STAT1/STAT3-dependent pathways and is attenuated by interferon-γ. *Basic Res. Cardiol.* 106 (2), 217–231. doi:10.1007/s00395-010-0141-0

Flamant, M., Placier, S., Dubroca, C., Esposito, B., Lopes, I., Chatziantoniou, C., et al. (2007). Role of matrix metalloproteinases in early hypertensive vascular remodeling. *Hypertension* 50 (1), 212–218. doi:10.1161/HYPERTENSIONAHA.107.089631

Hastings, J., and Kenealey, J. (2017). Avenanthramide-C reduces the viability of MDA-MB-231 breast cancer cells through an apoptotic mechanism. *Cancer Cel Int.* 17, 93. doi:10.1186/s12935-017-0464-0

Ho, R. C., Hirshman, M. F., Li, Y., Cai, D., Farmer, J. R., Aschenbach, W. G., et al. (2005). Regulation of IkappaB kinase and NF-kappaB in contracting adult rat skeletal muscle. *Am. J. Physiol. Cel Physiol.* 289 (4), C794–C801. doi:10.1152/ajpcell.00632.2004

Ishihara, A., Kojima, K., Fujita, T., Yamamoto, Y., and Nakajima, H. (2014). New series of avenanthramides in oat seed. *Biosci. Biotechnol. Biochem.* 78 (12), 1975–1983. doi:10.1080/09168451.2014.946390

Johnson, J. L. (2017). Metalloproteinases in atherosclerosis. *Eur. J. Pharmacol.* 816, 93–106. doi:10.1016/j.ejphar.2017.09.007

Kallenbach, K., Fernandez, H. A., Seghezzi, G., Baumann, F. G., Patel, S., Grossi, E. A., et al. (2003). A quantitative *in vitro* model of smooth muscle cell migration through the arterial wall using the human amniotic membrane. *Arterioscler Thromb. Vasc. Biol.* 23 (6), 1008–1013. doi:10.1161/01.ATV.0000069880.81136.38

Kang, Y. J., Kim, W. J., Bae, H. U., Kim, D. I., Park, Y. B., Park, J. E., et al. (2005). Involvement of TL1A and DR3 in induction of pro-inflammatory cytokines and matrix metalloproteinase-9 in atherogenesis. *Cytokine* 29 (5), 229–235. doi:10.1016/j.cyto.2004.12.001

Koenig, R. T., Dickman, J. R., Kang, C. H., Zhang, T., Chu, Y. F., and Ji, L. L. (2016). Avenanthramide supplementation attenuates eccentric exercise-inflicted blood inflammatory markers in women. *Eur. J. Appl. Physiol.* 116 (1), 67–76. doi:10.1007/s00421-015-3244-3

Kuzuya, M., and Iguchi, A. (2003). Role of matrix metalloproteinases in vascular remodeling. *J. Atheroscler. Thromb.* 10 (5), 275–282. doi:10.5551/jat.10.275

Li, Q. Y., Xu, H. Y., and Yang, H. J. (2017). (Effect of proinflammatory factors TNF-alpha,IL-1beta, IL-6 on neuropathic pain). *Zhongguo Zhong Yao Za Zhi* 42 (19), 3709–3712. doi:10.19540/j.cnki.cjcmm.20170907.004

Meydani, M. (2009). Potential health benefits of avenanthramides of oats. *Nutr. Rev.* 67 (12), 731–735. doi:10.1111/j.1753-4887.2009.00256.x

Muñoz-García, B., Martín-Ventura, J. L., Martínez, E., Sánchez, S., Hernández, G., Ortega, L., et al. (2006). Fn14 is upregulated in cytokine-stimulated vascular smooth muscle cells and is expressed in human carotid atherosclerotic plaques: modulation by atorvastatin. *Stroke* 37 (8), 2044–2053. doi:10.1161/01.STR.0000230648.00027.00

Nabata, A., Kuroki, M., Ueba, H., Hashimoto, S., Umemoto, T., Wada, H., et al. (2008). C-reactive protein induces endothelial cell apoptosis and matrix metalloproteinase-9 production in human mononuclear cells: implications for the destabilization of atherosclerotic plaque. *Atherosclerosis* 196 (1), 129–35. doi:10.1016/j.atherosclerosis.2007.03.003

Park, J., Ha, S. H., Abekura, F., Lim, H., Magae, J., Ha, K. T., et al. (2019). 4-O-Carboxymethylascochlorin inhibits expression levels of on inflammation-related cytokines and matrix metalloproteinase-9 through NF-κB/MAPK/TLR4 signaling pathway in LPS-activated RAW264.7 cells. *Front. Pharmacol.* 10, 304. doi:10.3389/fphar.2019.00304

Ramasamy, V. S., Samidurai, M., Park, H. J., Wang, M., Park, R. Y., Yu, S. Y., et al. (2020). Avenanthramide-C restores impaired plasticity and cognition in Alzheimer's disease model mice. *Mol. Neurobiol.* 57 (1), 315–330. doi:10.1007/s12035-019-01707-5

Singh, R., De, S., and Belkheir, A. (2013). Avena sativa (Oat), a potential neutraceutical and therapeutic agent: an overview. *Crit. Rev. Food Sci. Nutr.* 53 (2), 126–44. doi:10.1080/10408398.2010.526725

Stanley, A. C., and Lacy, P. (2010). Pathways for cytokine secretion. *Physiology (Bethesda)* 25 (4), 218–229. doi:10.1152/physiol.00017.2010

Sur, R., Nigam, A., Grote, D., Liebel, F., and Southall, M. D. (2008). Avenanthramides, polyphenols from oats, exhibit anti-inflammatory and anti-itch activity. *Arch. Dermatol. Res.* 300 (10), 569–574. doi:10.1007/s00403-008-0858-x

Tayebjee, M. H., Karalis, I., Nadar, S. K., Beevers, D. G., MacFadyen, R. J., and Lip, G. Y. (2005). Circulating matrix metalloproteinase-9 and tissue inhibitors of metalloproteinases-1 and -2 levels in gestational hypertension. *Am. J. Hypertens.* 18 (3), 325–329. doi:10.1016/j.amjhyper.2004.09.014

Umugire, A., Lee, S., Kim, D., Choi, M., Kim, H. S., and Cho, H. H., 2019. Avenanthramide-C prevents noise- and drug-induced hearing loss while protecting auditory hair cells from oxidative stress. *Cel. Death Discov.* 5, 115. doi:10.1038/s41420-019-0195-1

Visse, R., and Nagase, H. (2003). Matrix metalloproteinases and tissue inhibitors of metalloproteinases: structure, function, and biochemistry. *Circ. Res.* 92 (8), 827–839. doi:10.1161/01.RES.0000070112.80711.3D

Wågsäter, D., Zhu, C., Björkegren, J., Skogsberg, J., and Eriksson, P. (2011). MMP-2 and MMP-9 are prominent matrix metalloproteinases during atherosclerosis development in the Ldlr(-/-)Apob(100/100) mouse. *Int. J. Mol. Med.* 28 (2), 247–253. doi:10.3892/ijmm.2011.693

Watanabe, N., and Ikeda, U. (2004). Matrix metalloproteinases and atherosclerosis. *Curr. Atheroscler. Rep.* 6 (2), 112–20. doi:10.1007/s11883-004-0099-1

Ye, J., Xie, X., Tarassishin, L., and Horwitz, M. S. (2000). Regulation of the NF-kappaB activation pathway by isolated domains of FIP3/IKKgamma, a component of the IkappaB-alpha kinase complex. *J. Biol. Chem.* 275 (13), 9882–9889. doi:10.1074/jbc.275.13.9882

Zhao, X. W., Zhou, J. P., Bi, Y. L., Wang, J. Y., Yu, R., Deng, C., et al. (2019). The role of MAPK signaling pathway in formation of EMT in oral squamous carcinoma cells induced by TNF-α. *Mol. Biol. Rep.* 46 (3), 3149–3156. doi:10.1007/s11033-019-04772-0

Conflict of Interest: WY was employed by the company Nodaji Co., Ltd.

The remaining authors declare that the research was conducted in the absence of any commercial or financial relationships that could be construed as a potential conflict of interest

frontiers in Pharmacology

ORIGINAL RESEARCH
published: 19 April 2021
doi: 10.3389/fphar.2021.641848

Tanshinone IIA Protects Against Cerebral Ischemia Reperfusion Injury by Regulating Microglial Activation and Polarization *via* NF-κB Pathway

Zhibing Song[1,2†], *Jingjing Feng*[2†], *Qian Zhang*[1], *Shanshan Deng*[3], *Dahai Yu*[4], *Yuefan Zhang*[3*] *and Tiejun Li*[1*]

[1]Department of Pharmacy, Punan Hospital, Pudong New District, Shanghai, China, [2]College of Pharmacology, Anhui University of Chinese Medicine, Hefei, China, [3]School of Medicine, Shanghai University, Shanghai, China, [4]970 Hospital, Weihai, China

Tanshinone IIA, a fat-soluble diterpenoid isolated from Salvia miltiorrhiza Bunge, has been shown to attenuate the cerebral ischemic injury. The aim of this study was to examine the effects on neuroprotection and microglia activation of Tanshinone IIA. Male Sprague-Dawley rats were subjected to middle cerebral artery occlusion (MCAO). We found that Tanshinone IIA significantly reduced infarction volume, alleviated neuronal injuries, reduced the release of TNF-α, IL-1β, and IL-6, increased SOD activity, and decrease the content of MDA in MCAO rats. Hematoxylin and eosin staining, Nissl staining, TUNEL staining and immunofluorescence staining showed that Tanshinone IIA improved the distribution and morphology of neurons in brain tissues and reduced apoptosis. In addition, Co-immunofluorescence staining of rat brain tissues and the mRNA expression levels of CD11b, CD32, iNOS, and Arg-1, CD206, IL-10 in BV2 cells indicated that Tanshinone IIA can downregulate M1 microglia and upregulate M2 microglia in MCAO rats. Further, BV2 microglial cells were subjected to oxygen-glucose deprivation, the protein expression levels were detected by western blot. Tanshinone IIA inhibited the expression levels of NF-κB signaling pathway related proteins. Taken together, this study suggested that Tanshinone IIA modulated microglial M1/M2 polarization *via* the NF-κB signaling pathway to confer anti-neuroinflammatory effects.

Keywords: tanshinone IIA, cerebral ischemia, microglia, polarization, inflammation

OPEN ACCESS

Edited by:
Cheorl-Ho Kim, Sungkyunkwan University, South Korea

Reviewed by:
Bhakta Prasad Gaire, University of Maryland, Baltimore, United States
Zhijun Zhang, Shanghai Jiao Tong University, China

***Correspondence:**
Yuefan Zhang
yuefanzhang@shu.edu.cn
Tiejun Li
ltj204@163.com

[†]*These authors have contributed equally to this work*

Specialty section:
This article was submitted to Ethnopharmacology, a section of the journal Frontiers in Pharmacology

Received: *15 December 2020*
Accepted: *05 March 2021*
Published: *19 April 2021*

Citation:
Song Z, Feng J, Zhang Q, Deng S, Yu D, Zhang Y and Li T (2021) Tanshinone IIA Protects Against Cerebral Ischemia Reperfusion Injury by Regulating Microglial Activation and Polarization via NF-κB Pathway. Front. Pharmacol. 12:641848. doi: 10.3389/fphar.2021.641848

INTRODUCTION

Senile neurological diseases stroke has become the third leading cause of death in developed countries and the main cause of global disability (Collaborators, 2018). Among stroke patients, stroke caused by cerebral artery thrombosis or cerebral ischemia accounts for 80–85% (Alves et al., 2019). The molecular mechanism of stroke pathology is very complex as this process includes oxidative stress, blood-brain barrier destruction, apoptosis, and inflammatory response. It causes brain swelling and leads to brain cell death (Wahul et al., 2018).

The main pathophysiological mechanism of ischemic stroke neurological injury is inflammatory response. Microglia are one of the resident immune cells in the central nervous system. Affected by its environment, microglia have multiple phenotypes and retain metastatic function to maintain tissue homeostasis (Orihuela et al., 2016). Similar to macrophages, microglia's polarization can be

divided into different phenotypes; M1 and M2 type (Hansen et al., 2018). Traditionally, in the case of ischemic stroke, microglia rapidly transform from a resting state to an active "amebic-like" state, releasing a variety of inflammatory and cytotoxic mediators, causing cell damage and death, thus aggravating brain damage (Zhao et al., 2017; Lamkanfi and Dixit, 2014). M2 type can promote nerve repair during central nervous system injury (Chen et al., 2015; Kalkman and Feuerbach, 2016; Liu et al., 2019) and has a vital role in resolving inflammatory responses and debris removal, tissue remodeling, and angiogenesis (Mantovani et al., 2013).

The traditional Chinese medicine Radix Salviae Miltiorrhizae belongs to the blood-activating and stasis-relieving medicine. Tanshinone IIA, a fat-soluble diterpenoid isolated from Salvia miltiorrhiza Bunge, is one of the main active components of this red sage. It has several pharmacological effects, such as anti-atherosclerosis and myocardial protection, anti-platelet aggregation, and anti-tumor effect (Fei et al., 2017; Pan et al., 2017; Ye et al., 2020). Several studies have shown that Tanshinone IIA has neuroprotective effects against cerebral ischemia injury (Wang et al., 2014.; Chen et al., 2019). Over the past decade, Tanshinone IIA was demonstrated to have potential protective effects against cerebral ischemia-reperfusion injury through a variety of mechanisms (Zhu et al., 2017; Ma et al., 2019; He et al., 2020; Huang et al., 2020). Tanshinone IIA decreased the expression of cleaved caspase-3 protein and increased the expression of B-cell lymphoma 2 (bcl-2) protein in the ischemic cortex (Chen et al., 2012b). This would indicate that the neuroprotective effects of Tanshinone IIA against focal cerebral ischemic/reperfusion injury are likely to be related to the attenuation of apoptosis. Another study showed that Tanshinone IIA exerts neuroprotective effects through activation of nuclear factor erythroid 2-related factor-dependent antioxidant responses (Cai et al., 2017). A recent study reported that Tanshinone IIA can reduces the number of inflammatory cells in the brain after cerebral ischemia-reperfusion and decreases ischemia-induced upregulation of autophagy-related proteins, such as such as LC3-II, Beclin-1 and Sirt 6 (Wang et al., 2020). These findings suggest that Tanshinone IIA can provide protection against ischemic stroke by inhibiting inflammation and autophagy. However, there is no report on its effect on microglia after cerebral ischemia-reperfusion injury, and the mechanism of its neuroprotection is unclear.

The main objective of this study was to investigate the neuroprotective effect of Tanshinone IIA on rat brain after ischemia-reperfusion injury and its effect on microglia, and to further demonstrate the potential mechanism.

MATERIALS AND METHODS

Reagent

Tanshinone IIA (T4952) and 2,3,5-triphenyltetrazolium chloride (TTC) were purchased from Sigma-Aldrich (United States).; BPL (3-n-Butylphthalide, a marketed drug for acute ischemic stroke) (H20100041) was purchased from CSPC (China); BAY-11-7082 (a NF-κB inhibitor) (S2913) was purchased from Selleck (United States); ELISA Kit was purchased from R&D Systems (United States); superoxide dismutase (SOD) and malondialdehyde (MDA) assay kit were purchased from Nanjing Jiancheng Bioengineering Institute (China); total RNA Kit was purchased from Takara (Japan). Primary antibodies: NeuN (24307), Iba-1 (17198), iκB (76041), NF-κB (p65) (8242), GAPDH (5174) were purchased from Cell Signaling Technology (United States); p-iκB (ab133462) and p-NF-κB (p-p65) (ab239882) were purchased from Abcam (United States); CD16/32 (AF1460) and CD206 (AF2535) were purchased from R&D Systems (United States). Secondary antibodies: Alexa Fluor® 488 AffiniPure Goat Anti-Rabbit IgG, Alexa Fluor® 488 AffiniPure Donkey Anti-Goat IgG and Cy™3 AffiniPure Donkey Anti-Rabbit IgG were purchased from Jackson (United States).

Animal Care and Experimental Protocol

Male Sprague-Dawley (SD) adult rats (~250 g) were purchased from Slack Laboratory Animals Co., Ltd. (Shanghai, China). Food and water were available under constant temperature (23 ± 2°C) and controlled light conditions (12 h light/dark cycle). All experiments were in accordance with the guidelines of the Animal Care Committee of Shanghai University. During the experiment, all experimental animals were treated humanized.

All rats were divided randomly into six groups: Sham group (sham-operation treated with 0.9%NaCl, N = 12); MCAO group (MCAO treated with 0.9%NaCl, N = 12); BPL group (MCAO treated with 10 mg/kg butyphthalide, N = 12); TanIIA 1 mg/kg group (MCAO treated with 1 mg/kg Tanshinone IIA, N = 12); TanIIA 3 mg/kg group (MCAO treated with 3 mg/kg Tanshinone IIA, N = 12); and TanIIA 9 mg/kg group (MCAO treated with 9 mg/kg Tanshinone IIA, N = 12). After cerebral ischemia 10min, drugs were injected (tail vein injection). And after reperfusion, drugs were injected (tail vein injection) again.

Middle Cerebral Artery Occlusion Model and Neurological Deficit Scores

Middle cerebral artery occlusion (MCAO) was performed according to the Longa's method (Longa et al., 1989). SD rats were anesthetized with intraperitoneal 2% sodium pentobarbital (3 ml/kg). Then an incision was cut in the cervical midline. The exposed external carotid arteries were closed by sterile suture, and the vascular clamp was used to clamp internal carotid artery. Subsequently, an incision in the common carotid artery was made, the proximal common carotid artery is tightly tied, and the suture line (0.26°mm; Cinontech, China) is inserted into the skull along the internal carotid artery along the small hole, inserted into the black mark (~18 mm), then the internal carotid artery is ligated. During surgery, the cerebral blood flow (CBF) in the left cortex of rats was monitored by Laser Doppler Flowmeter (Oxylab LDF; B&E TEKSYSTEMS LTD., China), and the reduction of CBF in rats to less than 20% of the initial value was a sign of successful surgery. After 2 h, the rats underwent reperfusion. Sham-operated rats receive identical surgery without arterial ligation and monofilament insertion. Animals were warmed under warm light before waking up.

After 24 h of reperfusion, the neurological deficit score was assessed. The neurological dysfunction in rats was assessed as previous (Longa et al., 1989) in a double-blinded manner with the following definitions: Score 0: no detectable neurological deficits; Score 1: failure to extend the right forepaw fully; Score 2: circling to the left; Score 3: falling to the left; Score 4: did not walk spontaneously and had a depressed level of consciousness.

Assessment of Cerebral Infarct Volume

After analysis of neurological function, the rats were sacrificed by sodium pentobarbital injection and the brains were harvested. Brains were rinsed with saline to remove excess water, and immediately placed in the freezer for 15 min. Then forebrains were dissected into six sections in coronal plane (2-mm slice) (Chiang et al., 2011). The slices were placed in 2% TTC (Sigma- Aldrich, United States) for 20 min at room temperature. followed by fixation in 4% formaldehyde at 4°C for 24 h. Brain slices were photographed and analyzed by ImageJ analysis software (v6.0). The infarct volume was calculated as follows: the left infarct volume/whole brain volume × 100%.

Hematoxylin and Eosin Staining

Rats were anesthetized, and perfused with physiological saline and 4% paraformaldehyde (Sinopharm, China) *via* cardiac puncture. Brains were harvested, fixed with 4% formaldehyde, embedded in paraffin, sliced into 5-μm-thick coronal sections. Slices were stained with hematoxylin for 3–8 min, washed with tap water, alcoholic fractionation with 1% hydrochloric acid for a few seconds, rinsed with tap water, returned to blue with 0.6% ammonia, and rinsed with running water, then slices were stained in eosin staining solution for 1–3 min. Areas of interest were observed with a light microscope.

Nissl Staining

Paraffin sections went through xylene (Sinopharm, China) dewaxing and an alcohol gradient rehydration as above and stained with Nissl solution (Beyotime, China) for 5–10 min. Then slices were treated with 95% alcohol until Nissl bodies were dark blue and the background was light blue or colorless. They were placed under microscope for observing Nissl bodies in cortical neurons.

TUNEL Staining

TUNEL staining was performed using an apoptosis kit (Roche, China) according to the manufacturer's instructions. In brief, after the sections were dewaxed, proteinase K was added and incubated at 37°C for 30 min, the film-breaking solution was added dropwise and incubated at room temperature for 30 min, after washing, TUNEL reagent was added and incubated at 37°C for 1 h. Then the sections were incubated in 3% hydrogen peroxide solution at room temperature for 15 min, converter-POD was added and incubated at 37°C for 30 min, and finally DAB was added dropwise for color development. TUNEL-positive neurons surrounding the injury areas were observed and counted under high magnification on a fluorescence microscope (Olympus, Japan).

Immunofluorescence Assessment

The sections were placed in a 0.1 M sodium citrate buffer solution (pH = 6.0) at 100°C for 30 min for antigen retrieval. After cooled to room temperature, the membrane was lysed for 5 min using 0.1% Triton X-100, sections were blocked with 1% bovine serum albumin (BSA, Sigma, MO, United States) + 0.1% TritonTM X-100 for 1 h and incubated at 4°C overnight with primary antibodies: NeuN (1:250) or Iba-1 (1:250), followed by incubation with appropriate fluorescence-conjugated secondary antibodies: Cy™ 3 AffiniPure Donkey Anti-Rabbit IgG (1:200) for 2 h in the dark. In addition, 4, 6-diamidino-2-phenylindole (DAPI) (Beyotime, China) was used to counterstain nuclei for 10 min in the dark, and then mounted with a sealing liquid. The ischemic lateral hemicortical region was observed by laser confocal microscopy and photographed. Fluorescence intensity was analyzed and calculated by ImageJ software (National Institutes of Health, Bethesda, MD, United States).

Co-Immunofluorescence Staining

The brain sections were incubated overnight at 4°C in a humidified box with primary antibody Iba-1 (1:250). Then, the samples were incubated with secondary antibody: Alexa Fluor® 488 AffiniPure Goat Anti-Rabbit IgG (Jackson; 1:200) for 2 h in the dark at room temperature. The following antibodies CD16/32 (1:250) and CD206 (1:250) were used overnight at 4°C. Next, the fluorescent secondary antibody Alexa Fluor® 488 AffiniPure Donkey Anti-Goat IgG (1:200) was incubated for 2 h at room temperature in the dark at room temperature. In addition, DAPI was used to counterstain nuclei for 10 min in the dark. Finally, the sections were photographed using a laser confocal microscope (Leica TCS SP5, Germany). The merged yellow fluorescence intensity was detected by ImageJ software. And the relative quantification of each groups were based on fluorescence intensity.

Cell Culture and Oxygen-Glucose Deprivation

The BV2 microglia (Concord Cell Resource Center, China) growth in 90% high glucose Dulbecco's Modified Eagle Medium (DMEM) medium supplemented with 10% fetal calf serum (Gibco, United States), 1% penicillin-streptomycin (Gibco, United States), and cells were cultured at 37°C in humidified 5% CO2/95% air for 7–10 days prior to experimentation. The liquid was changed every other day.

BV2 microglia were exposed to OGD for establishing an *in vitro* model of cerebral ischemia. Before exposure, cultured cells were pretreated with Tanshinone IIA (10 μM) and then the cells seeded in glucose free DMEM medium (Gibco, United States) transferred into an anoxic device (Billups Rothenberg, United States), and flushed of a 95% N_2 and 5% CO_2 gas mixture for 4 h. Control group cells grow normally in the incubator.

Cell Counting Kit-8 Assay

A Cell Counting Kit-8 (Beyotime, China) was used to assess cell survival. The experimental steps were strictly performed

according to the manufacturer's manual. Briefly, BV2 cells were plated at a density of 1.0×10^5 cells/ml in 96-well cell culture plates. 10 μl of CCK-8 solution was added to each culture well of a 96-well plate and incubated for 1–4 h at 37°C. The absorbance at 450 nm was measured with a microplate reader (Multiskan MK3; Thermo Fisher Scientific, Inc.).

Enzyme-Linked Immunosorbent Assay

The ischemic hemibrain tissue were placed in PBS and were homogenized, then supernatants were obtained by centrifugation at 12,000 r/min, 4°C for 15 min. The levels of interleukin-6 (IL-6), tumor necrosis factor-α (TNF-α), and interleukin-1 β (IL-1β) were detected by the corresponding ELISA kits (R&D, United States) according to the manufacturer's instructions. Measurements were made using a microplate reader (Multiskan MK3; Thermo Fisher Scientific, United States).

Superoxide dismutase and Malondialdehyde Measurement

The ischemic hemibrain tissue were placed in PBS and then supernatants were obtained by centrifugation at 12.000 r/min, 4°C for 15 min. The levels of SOD were detected by the SOD kit (Jiancheng Bioengineerinng, China). The levels of MDA were detected by the MDA kit (Jiancheng Bioengineerinng, China).

Real-Time Polymerase Chain Reaction Assay

BV2 microglia cells were collected from each group. Total RNA was isolated as following: Add 500 μl of RNAiso Trizol (Takara, Japan) to 100 μl of chloroform (Sinopharm, China) for 5 min. Centrifuge for 15 min. Add equal volume of isopropanol to the supernatant and mix for 10 min. Centrifuge for 10 min, add 1 ml of 75% ethanol (Sinopharm, China), and centrifuge for 5 min. Add RNase-free H_2O (Takara, Japan) to dissolve. All centrifugation was carried out at 12,000g at 4°C. After the RNA concentration was determined by ultraviolet absorption. Then, 1000 ng of total RNA was reverse transcribed in a 20-μl reaction at 37°C for 15 min followed by 85°C for 5 s using PrimeScript RT Master Mix (Takara, Japan). Real-time PCR was performed in a 20-μl reaction according to the manufacturer's manual for SYBR Premix Ex Taq (Takara, Japan). The primer sequences were as follows:

GAPDH Forward: 5′-CTTCACCACCATGGAGAAGGC-3′
Reverse: 5′-GGCATGGACTGTGGTCATGAG-3′
CD11b Forward: 5′-CCAAGACGATCTCAGCATCA-3′
Reverse: 5′-TTCTGGCTTGCTGAATCCTT-3′
CD32 Forward: 5′-AATCCTGCCGTTCCTACTGATC-3′
Reverse: 5′-GTGTCACCGTGTCTTCCTTGAG-3′
iNOS Forward: 5′-GGCAGCCTGTGAGACCTTTG-3′
Reverse: 5′-GCATTGGAAGTGAAGCGTTTC-3′
Arg-1 Forward: 5′-GAACACGGCAGTGGCTTTAAC-3′
Reverse: 5′-TGCTTAGCTCTGTCTGCTTTGC-3′
CD206 Forward: 5′-TTCGGTGGACTGTGGACGAGCA-3′
Reverse: 5′-ATAAGCCACCTGCCACTCCGGT-3′
IL-10 Forward: 5′-TAACTGCACCCACTTCCCAG-3′
Reverse: 5′-AGGCTTGGCAACCCAAGTAA-3′

The reaction was performed at 95°C for 30 s followed by 45 cycles of 95°C for 15 s and 55°C for 5 s, 72°C, 5 s on the Real-Time PCR Detection System (AB7500, United States). The relative mRNA expression were analyzed by the $2^{-\Delta\Delta Ct}$ method.

Western Blot Analysis

The BV2 cells were collected, and the total cellular protein was extracted by standard extraction reagent (Thermo, United States) supplemented with protease inhibitors (Merck, Germany) and phosphatase inhibitor (Merck, Germany). Protein concentration was determined by bicinchoninic acid protein assay kit (Pierce, Thermo, United States). The extracted proteins were separated by SDS-PAGE and electrically transferred to nitrocellulose membranes (Millipore, United States). Then, the membranes were blocked with Tris-buffered saline with 5% non-fat milk for 1–2 h at room temperature. The following primary antibodies were used: iκB (1:1,000), p-iκB (1:1,000), NF-κB (p65) (1:1,000), p-NF-κB (p-p65) (1:1,000), GAPDH (1:1,000) from Abcam and Cell signaling technology. The membranes were shaken at 4°C overnight and incubated with fluorescent secondary antibody: Alexa Fluor® 488 AffiniPure Goat Anti-Rabbit IgG (1:10,000) for 1 h at room temperature in dark. Protein bands were visualized using the Odyssey Imager with Odyssey 1.1 software (Li-Cor). Digital images were quantified using densitometry measurements by ImageJ software.

Statistical Analysis

The statistical analysis was performed using SPSS software. Data were expressed as the mean ± standard deviation. Comparison among groups was analyzed by one-way analysis (One-way ANOVA) of variance. $p < 0.05$ was considered statistically significant.

RESULTS

Tanshinone IIA Ameliorated Neurological Deficits and Reduced Infarct Volumes in Rats

The molecular structure of Tanshinone IIA, 1,6,6-trimethyl-6,7,8,9-tetrahydrophenanthro[1,2-b] furan-10,11-dione, was shown in **Figure 1A**. BPL and Tanshinone IIA (3 mg/kg, 9 mg/kg) decreased the neurological deficit scores in rats ($p < 0.05$; **Figure 1B**). Additionally, the infarct volumes of rat brains were measured with TTC staining (**Figure 1C**).

Tanshinone IIA treatment at 1 mg/kg dose did not decrease the cerebral infarct volume compared to the MCAO group. However, when used at higher doses (3 and 9 mg/kg), it induced a significant neuroprotection after MCAO ($p < 0.05$; **Figure 1D**) (Two rats died in the MCAO group and one in the Tanshinone IIA (1 mg/kg) group after 24 h of reperfusion).

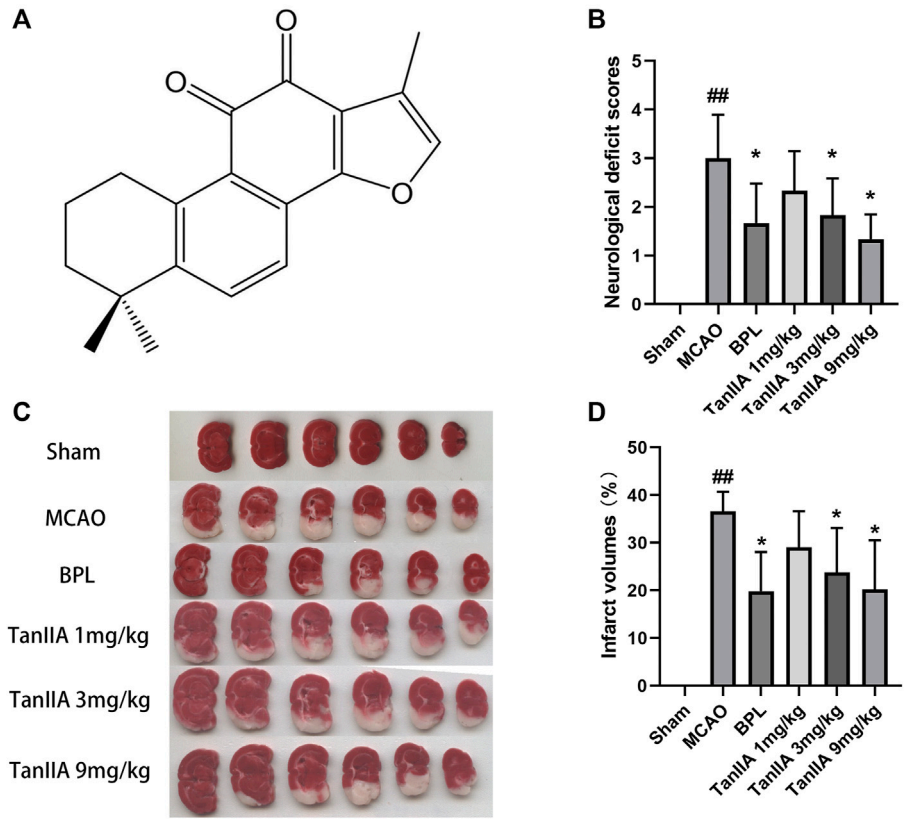

FIGURE 1 | Tanshinone IIA treatment ameliorated neurological deficits and reduced infarct volumes in rats. Tanshinone IIA, BPL or control saline was injected into the tail vein at the indicated time after occlusion. After 24 h, the neurological deficit scores were measured, and the rats were euthanatized and the brain sections were stained with TTC for infarct volume measurement. **(A)** The molecular structure of Tanshinone IIA. **(B)** The neurological deficit scores of rats in each group. **(C)** TTC staining in each group. **(D)** Statistical results of cerebral infarct volumes in each group. ##$p < 0.01$, compared with the Sham group. *$p < 0.05$, compared with the MCAO group. Sham, sham operation group; MCAO, middle cerebral artery occlusion; BPL, butyphthalide (positive control); TanIIA, Tanshinone IIA, $n = 6$.

Tanshinone IIA Alleviated the Inflammatory Response and Oxidative Damage

After 24 h reperfusion, the expression levels of pro-inflammatory cytokines were detected by Enzyme-linked Immunosorbent Assay (ELISA). Compared with the sham group, MCAO treatment significantly upregulated levels of IL-1β ($p < 0.01$; **Figure 2A**), IL-6 ($p < 0.01$; **Figure 2B**), and TNF-α ($p < 0.01$; Tanshinone IIA 3 mg/kg treatment group vs. MCAO group; **Figure 2C**) in rat cerebral cortex. Tanshinone IIA (3 mg/kg) inhibited the MCAO-induced inflammatory cytokines and reversed the decrease of SOD ($p < 0.05$; Tanshinone IIA 3 mg/kg treatment group vs. MCAO group; **Figure 2D**) and the increase of MDA ($p < 0.05$; Tanshinone IIA 3 mg/kg treatment group vs. MCAO group; **Figure 2E**) in rats ischemic brain tissues. These results suggest that Tanshinone IIA can reduce the expression of oxidative damage and inflammatory factors.

Pathological Changes and Apoptosis Levels in Rat Cortex

Next, we examined the protective effects of Tanshinone IIA on cell injury in the rat brain tissues after MCAO. H&E staining was used to check the morphological changes. As showed in **Figure 3A**, cells of Sham group were neatly arranged, showing full cell morphology and distinct nuclei. In the MCAO group, most neurons in the cerebral cortex's ischemic penumbra presented cell edema and nucleus solidification. Contrary to the MCAO group, cortical neuronal cell vacuolization was reduced, and cell morphology returned to normal in the Tanshinone IIA treatment group. The important components of neurons are the neuron nucleosomes, which are mainly composed of nucleic acids, ribose, and proteins, and are closely related to neuronal function. Nissl staining indicated that a large number of cells were shrunk down with an enlarged intercellular space and more dark color staining in the MCAO group relative to the Sham group. Meanwhile, these characteristic changes were all improved in the Tanshinone IIA treatment group. Furthermore, TUNEL staining was used to detect apoptosis in rat brains (**Figure 3A**). Apoptotic bodies stained brown were not observed in brain tissue cells of the Sham group, and a large number of apoptotic bodies were observed in the MCAO group. By counting the apoptotic cells in each group, we found that the number of apoptotic cells in the

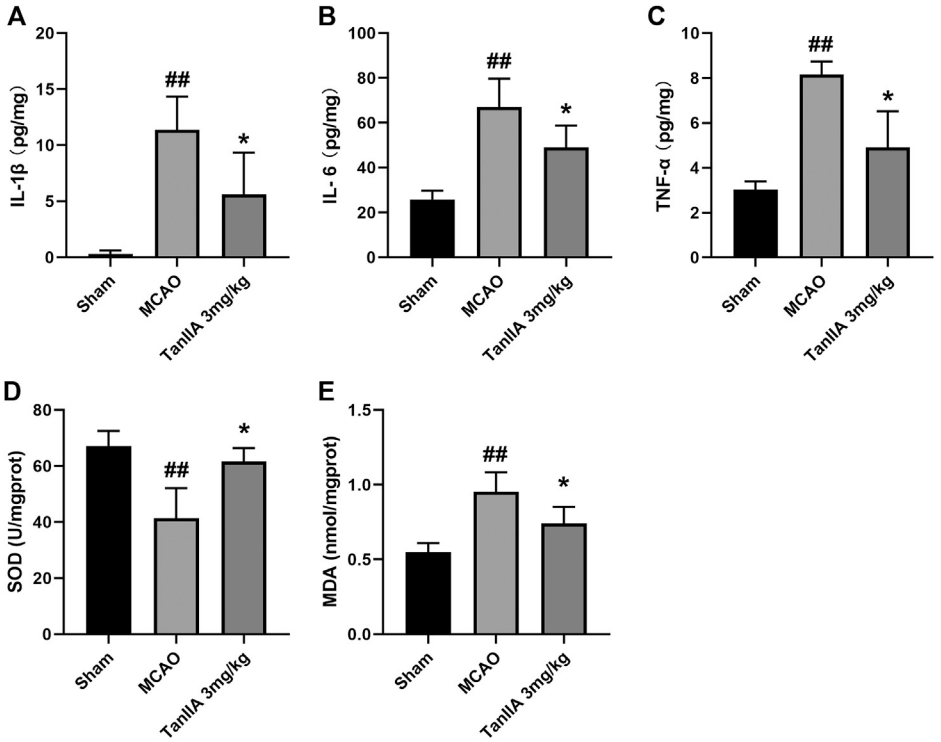

FIGURE 2 | Tanshinone IIA inhibited inflammatory cytokines and Oxidative Damage in MCAO rats. Tanshinone IIA or control saline was injected into the tail vein at the indicated time after MCAO. After reperfusion, the rat brains were harvested. ELISA was used to detect levels of IL-1β **(A)**, IL-6 **(B)** and TNF-α **(C)**. SOD kit and MDA kit were used to detect the levels of SOD **(D)** and MDA **(E)**. ##$p < 0.01$, compared with the Sham group, *$p < 0.05$, compared with the MCAO group. Sham, sham operation group; MCAO, middle cerebral artery occlusion; TanIIA, Tanshinone IIA, $n = 3$.

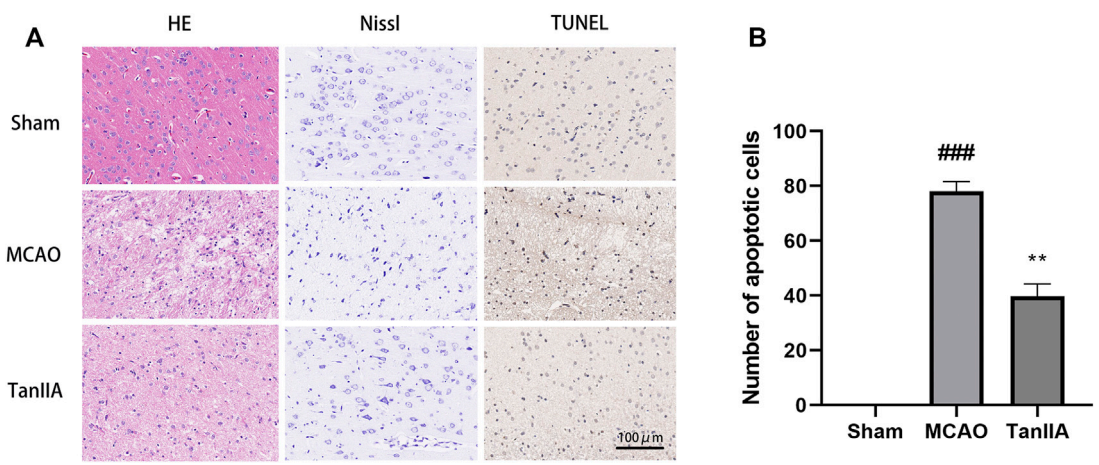

FIGURE 3 | Effects of Tanshinone IIA on pathology and apoptosis after MCAO in rat brains. Tanshinone IIA or control saline was injected into the tail vein at the indicated time after MCAO. After reperfusion, the rat brains were harvested. **(A)** Pathological changes of rat cortex tissues were detected by HE staining and Nissl staining, apoptotic cells in rat cortex were detected by TUNEL staining (Scale bar: 100 μm). **(B)** The apoptotic cells of different groups were calculated and shown. ###$p < 0.001$, compared with the Sham group, **$p < 0.01$, compared with the MCAO group. Sham, sham operation group; MCAO, middle cerebral artery occlusion; TanIIA, Tanshinone IIA, $n = 3$.

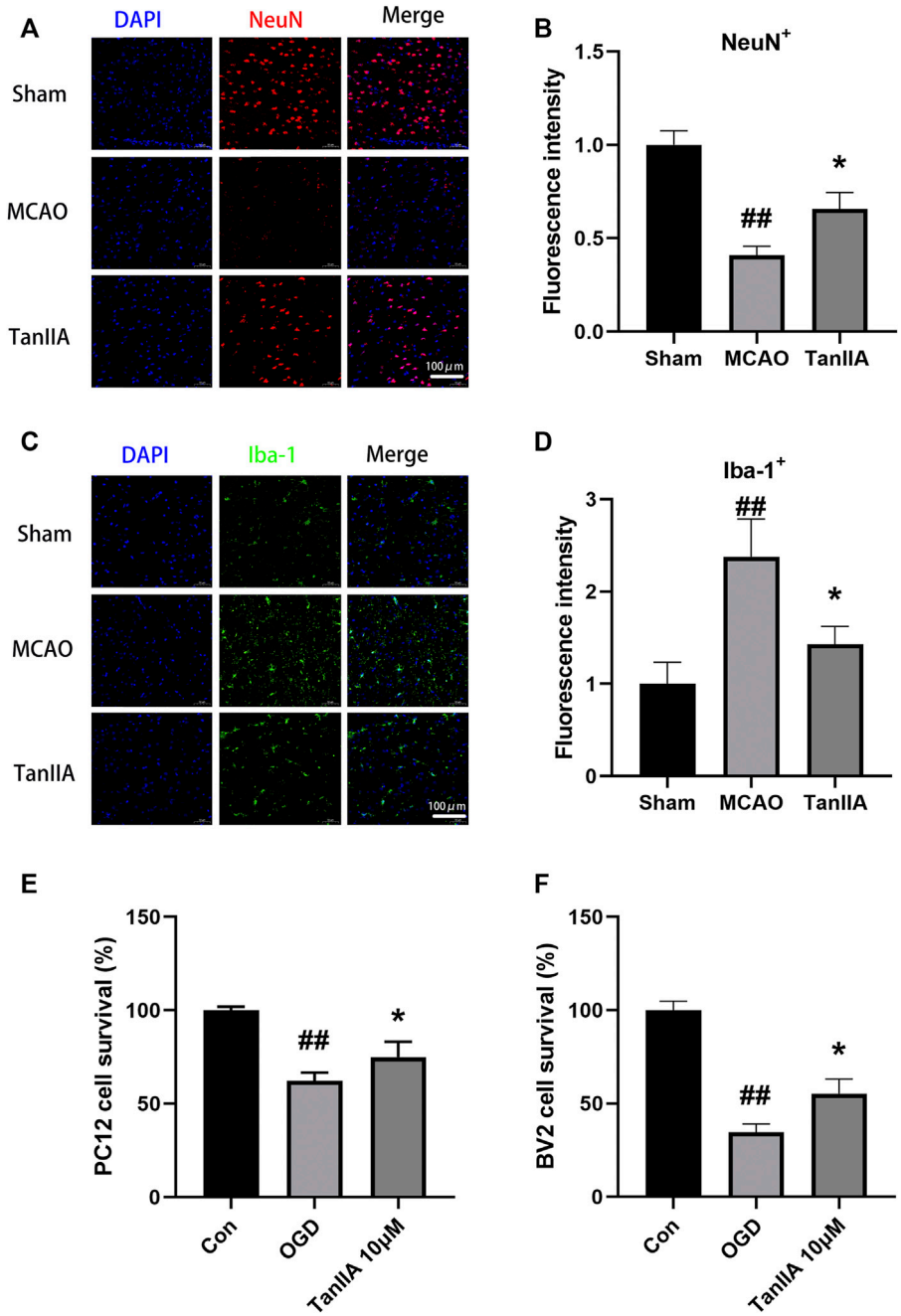

FIGURE 4 | Effects of Tanshinone IIA on neuroprotection *in vivo* and *in vitro*. Immunofluorescence staining was used to detect the levels of NeuN-positive neuron **(A)** and Iba-1-positive microglia **(C)** in rat ischemic penumbra area. NeuN was shown as red, Iba-1 was shown as green and DAPI was shown as blue (Scale bar: 100 μm). **(B)** Fluorescence intensity of NeuN-positive neuron in rat ischemic penumbra area. **(D)** Fluorescence intensity of Iba-1-positive microglia in rat ischemic penumbra area. ##$p < 0.01$, compared with the Sham group, *$p < 0.05$, compared with the MCAO group. Sham, sham operation group; MCAO, middle cerebral artery occlusion; TanIIA, Tanshinone IIA, $n = 3$. OGD-induced BV2 cells were treated with Tanshinone IIA. CCK-8 assay was used to measure the cell survival of PC12 cells **(E)** and BV2 cells **(F)** after oxygen-glucose deprivation (OGD). ##$p < 0.01$, compared with the control group, *$p < 0.05$, compared with the OGD group. Con, control group; OGD, oxygen-glucose deprivation; TanIIA, Tanshinone IIA, $n = 6$.

Tanshinone IIA treatment group was significantly reduced compared with the MCAO group ($p < 0.01$, **Figure 3B**). These results suggested that Tanshinone IIA relieves the damage caused by cerebral ischemia.

Tanshinone IIA Reduced Hypoxia-Induced Neuronal Cell Death

The results of immunofluorescence showed that the fluorescence intensity of NeuN-positive neuron was decreased in the MCAO

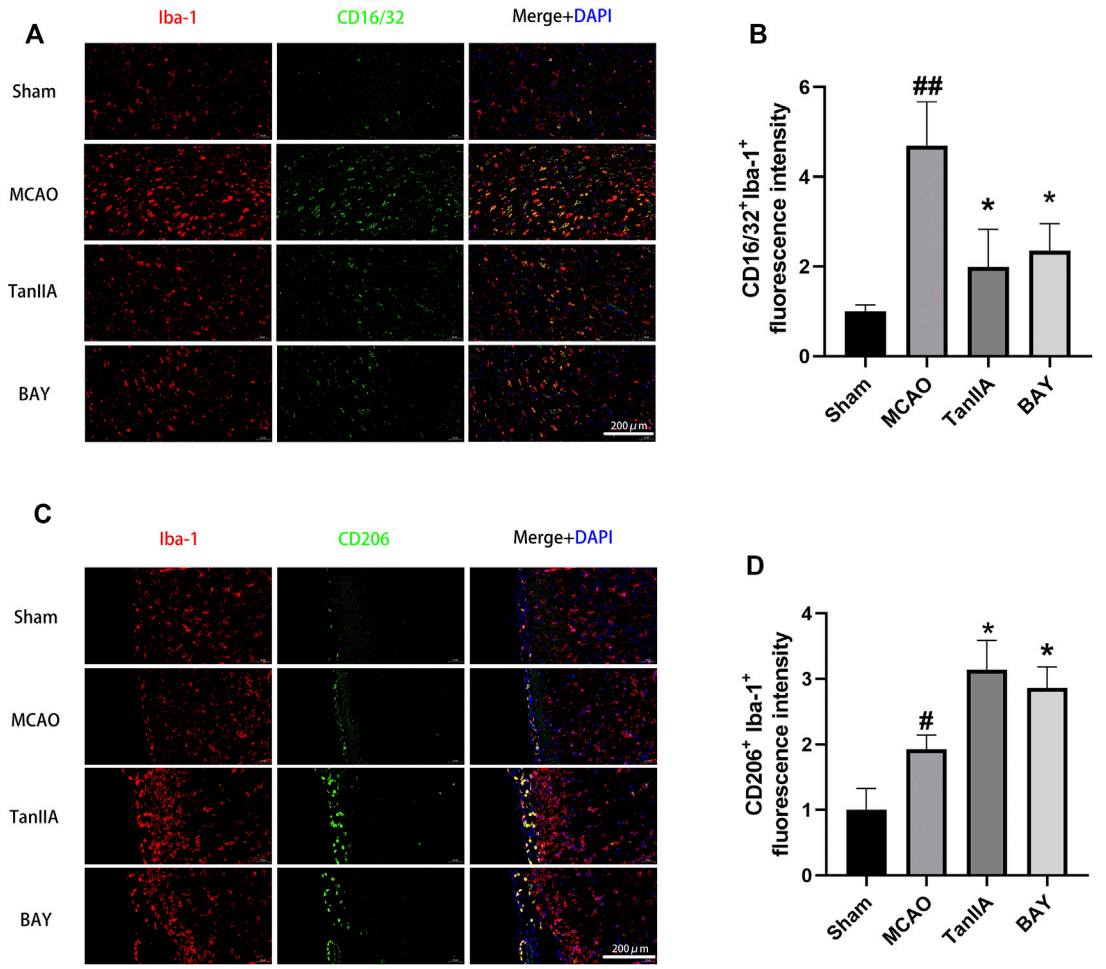

FIGURE 5 | Tanshinone IIA regulated the polarization of microglia in rat cortex. Tanshinone IIA or control saline was injected into the tail vein at the indicated time after MCAO. After reperfusion, the rat brains were harvested. **(A)** Co-immunofluorescence staining of rat brain tissues for microglia marker Iba-1 (red) and M1 marker CD16/32 (green), **(B)** and the level of $CD16/32^{+}$ $Iba\text{-}1^{+}$ cells were analyzed and shown. **(C)** Co-immunofluorescence staining of rat brain tissues for microglia marker Iba-1 (red) and M2 marker CD206 (green), **(D)** the level of $CD206^{+}$ $Iba\text{-}1^{+}$ cells were analyzed and shown. ##$p < 0.01$, compared with the Sham group, *$p < 0.05$, compared with the MCAO group. Sham, sham operation group; MCAO, middle cerebral artery occlusion; TanIIA, Tanshinone IIA, BAY, BAY-11-7082, a NF-κB inhibitor, $n = 3$. (Scale bar: 200 μm).

group. By calculating the fluorescence intensity of each group, we found that Tanshinone IIA significantly increased the fluorescence intensity of NeuN-positive neuron in rat cortex ($p < 0.05$; Tanshinone IIA 3 mg/kg treatment group vs. MCAO group; **Figures 4A,B**). Meanwhile, compared with the sham group, the fluorescence intensity of Iba-1-positive microglia was significantly increased in the MCAO group ($p < 0.01$). After Tanshinone IIA treatment, the fluorescence intensity of Iba-1-positive microglia reduced compared to the MCAO group ($p < 0.05$, **Figures 4C,D**).

Next, we investigated the protective effect of Tanshinone IIA on PC12 cells and BV2 cells exposed to hypoxia. We established an OGD model with a hypoxia time of 4 h. CCK-8 assay was used to detect the cell viability. Compared with the OGD group, Tanshinone IIA treatment group significantly increased the cell survival of PC12 cells and BV2 cells ($p < 0.05$; Tanshinone IIA 3 mg/kg treatment group vs. OGD group; **Figures 4E,F**). These results were indicated that Tanshinone IIA reduced hypoxia-induced neuronal cell death.

Tanshinone IIA Regulated the Polarization of Microglia *in Rats*

After cerebral ischemia, microglia were activated and polarized into pro-inflammatory M1 and anti-inflammatory M2. Co-immunofluorescence staining was performed to observe the polarization of M1 and M2 microglia in rat brains (**Figures 5A,C**). The result of fluorescence intensity assay showed that Tanshinone IIA and BAY-11-7082 (a NF-κB inhibitor) treatments down-regulated $CD16/32^{+}Iba\text{-}1^{+}$ microglia cells activated by MCAO ($p < 0.05$; Tanshinone IIA 3 mg/kg treatment group vs. MCAO group; **Figure 5B**). Meanwhile, Tanshinone IIA and BAY-11-7082 (a NF-κB inhibitor) treatments upregulated $CD206^{+}Iba\text{-}1^{+}$ microglia cells

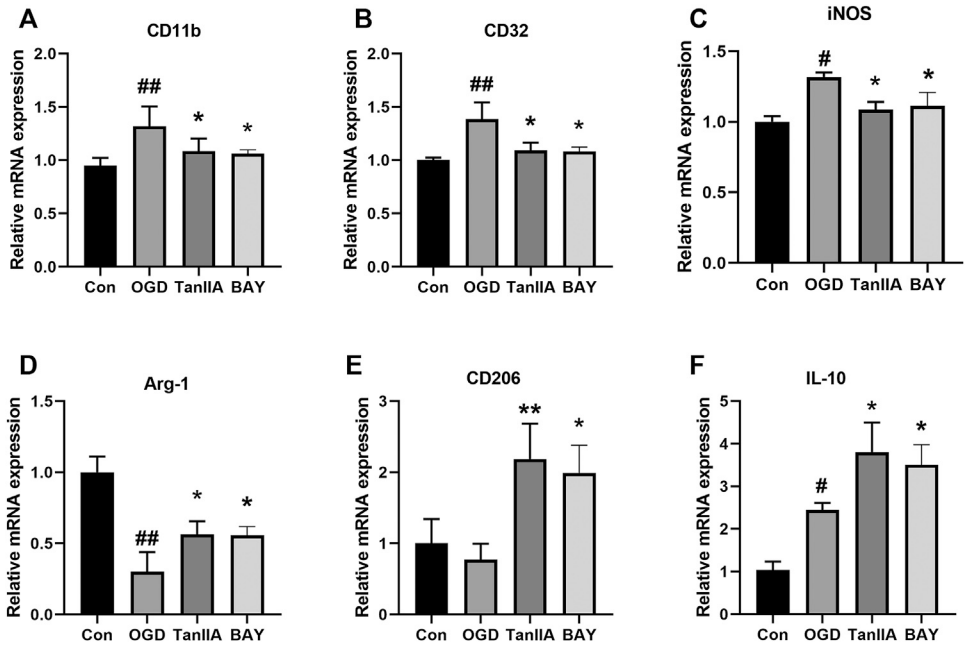

FIGURE 6 | Effect of Tanshinone IIA on polarization-related mRNA expressions after OGD in BV2 cells. OGD-induced BV2 cells were treated with Tanshinone IIA. Quantitative RT-PCR was used to assess the mRNA expression levels of M1 microglia markers: CD11b **(A)**, CD32 **(B)**, iNOS **(C)**, and M2 microglia markers: Arg-1 **(D)**, CD206 **(E)**, IL-10 **(F)**. ##$p < 0.01$, compared with the Con group, *$p < 0.05$, compared with the OGD group. Con, control group; OGD, oxygen-glucose deprivation; TanIIA, Tanshinone IIA. BAY, BAY-11-7082, a NF-κB inhibitor, $n = 3$.

compared with the MCAO group ($p < 0.05$; Tanshinone IIA 3 mg/kg or BAY-11-7082 3 mg/kg treatment group vs. MCAO group; **Figure 5D**).

The mRNA Expression Levels of BV2 Cells After Oxygen-Glucose Deprivation

To further investigate the effect of Tanshinone IIA on microglia, we used quantitative RT-PCR to detect the mRNA expression levels of M1 and M2 markers in BV2 cells. Tanshinone IIA and BAY-11-7082 (a NF-κB inhibitor) downregulated the mRNA expressions of M1 markers in OGD-induced BV2 cells: CD11b, CD32, iNOS ($p < 0.05$; Tanshinone IIA 10 μM or BAY-11-7082 5 μM treatment group vs. OGD group; **Figures 6A–C**), and upregulated the mRNA expression levels of M2 markers: Arg-1, CD206 and IL-10 ($p < 0.05$; Tanshinone IIA 10 μM or BAY-11-7082 5 μM treatment group vs. OGD group; **Figures 6D–F**). The above data were shown that Tanshinone IIA and BAY-11-7082 could inhibit M1 type and promote M2 type of microglia's polarization.

Tanshinone IIA Regulated the Polarization of Microglia by NF-κB Signaling Pathway

Previous studies have shown that the NF-κB signaling pathway has an important role in inflammatory signaling (Bruno et al., 2018). Western blot was used to detect the protein expression of NF-κB signaling pathway in BV2 cells after oxygen-glucose deprivation (OGD). Tanshinone IIA down-regulated the expression levels of p-iκB and p-p65 proteins in BV2 cells ($p < 0.01$; Tanshinone IIA 10 μM treatment group vs. OGD group; **Figures 7A,B**). In addition, BAY-11-7082 (a NF-κB inhibitor) also downregulated the expression of *p*-iκB and p-p65 in BV2 cells, and strengthened the inhibiton of p-p65 by Tanshinone IIA ($p < 0.05$; BAY-11-7082 5 μM treatment group vs. OGD group; **Figures 7C,D**). These results indicated that Tanshinone IIA may inhibit the polarization of microglia *via* NF-κB signaling pathway (**Figure 8**).

DISCUSSION

Stroke is a major cause of death and disability worldwide, and traditional Chinese medicine has high application value and therapeutic potential in stroke (Liu et al., 2018). In the previous research, Chen et al. (2012a) reported that intraperitoneal injection of Tanshinone IIA (25 mg/kg) can significantly reduce the brain infarct volume of cerebral ischemia in rats. And a recent study showed that Tanshinone IIA (20 and 40 mg/kg) reduced brain water content and normalized neurological deficit score after cerebral ischemia-reperfusion injury in rats (Wang et al., 2020). In this study, we found that tail vein injection of Tanshinone IIA (3 and 9 mg/kg) significantly reduced the brain infarct volume and normalized neurological deficit score after cerebral ischemia-reperfusion injury in rats. Furthermore, H&E staining and Nissl staining were used to detect the pathological changes in rat brain tissues. The results showed that Tanshinone IIA

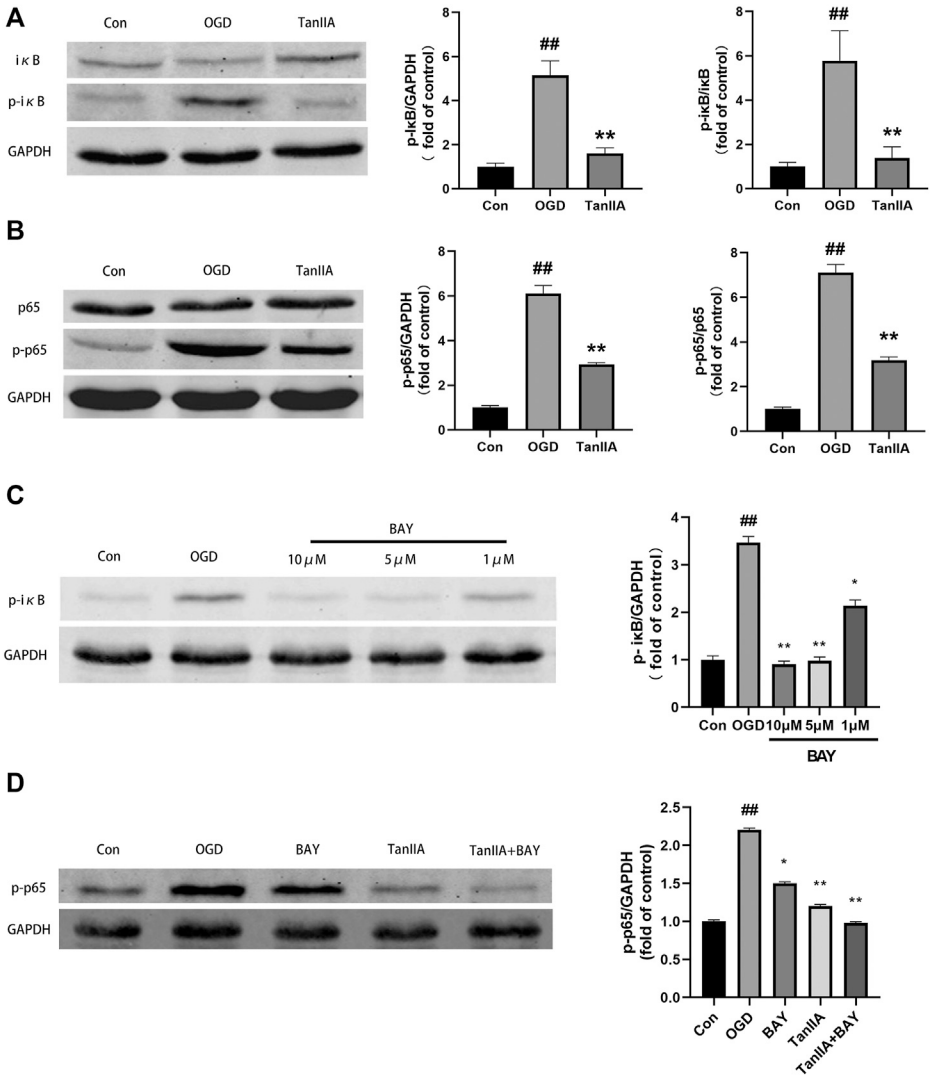

FIGURE 7 | Tanshinone IIA regulated NF-κB signaling pathway in BV2 cells after oxygen-glucose deprivation (OGD). **(A)** The protein level of p-IκB in BV2 cells treated with Tanshinone IIA. **(B)** The protein level of p-p65 in BV2 cells treated with Tanshinone IIA. **(C)** The protein level of p-IκB in BV2 cells treated with BAY-11-7082. **(D)** The protein level of p-p65 in BV2 cells treated with Tanshinone IIA and BAY-11–7082. ##$p < 0.01$, compared with the control group. *$p < 0.05$, **$p < 0.01$, compared with the OGD group. Con, control group; OGD, oxygen-glucose deprivation; TanIIA, Tanshinone IIA; BAY, BAY-11-7082, a NF-κB inhibitor, $n = 3$.

treatment significantly improved the distribution and morphological structure of neurons. TUNEL staining showed that Tanshinone IIA treatment can reduce apoptotic cells in rat brain after MCAO. These results indicated that Tanshinone IIA can moderate the cerebral ischemia damage in rats.

The inflammatory response has an important role in cerebral ischemia-reperfusion injury, and most of the damage is caused by a secondary inflammatory cascade. Overexpression of inflammatory factors, such as TNF-α, IL-6, IL-1β, promotes the inflammatory response's progression (Tobin et al., 2014; Ai et al., 2017; Wei et al., 2017). In acute cerebral ischemic injury, the excessive formation of oxygen free radicals leads to excessive oxidative stress, which, in turn, leads to cells and tissue damage (Naderi et al., 2017). SOD, as a major antioxidant enzyme, represents the strength of the antioxidant system. MDA is a product of lipid peroxidation in the cell membrane, which indicates the degree of damage caused by oxidative stress (Sun et al., 2016). Our results showed that Tanshinone IIA could inhibit the expression of pro-inflammatory factors TNF-α, IL-6, and IL-1β and regulate the levels of SOD and MDA in the brain tissue of rats with cerebral ischemia.

Microglia, representing the brain's major innate immune cells, play an important role in neuroinflammation (Pape et al., 2019). Affected by the environment, microglia have various phenotypes, which participate in innate immunity and the central nervous system (Orihuela et al., 2016). Under normal conditions, they clear cellular debris and toxic cells by phagocytosis. Once these cells are activated, they transmit and translate peripheral-initiated inflammatory signaling factors (Yenari et al., 2010). Previous studies have found that resveratrol promotes neuronal protection by

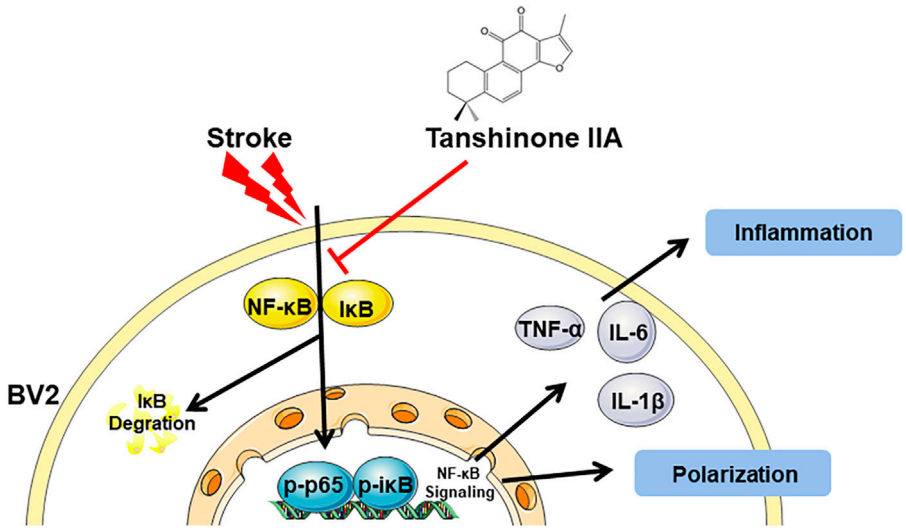

FIGURE 8 | A graphical representation of the neuroprotective mechanisms of Tanshinone IIA against the stroke-induced neuroinflammation by NF-κB signaling pathway.

limiting inflammatory cytokines production, thereby reducing induced microglial activation (Zhao et al., 2018). In the activation of BV2 and primary glial cells, some scholars have found that ingredients in Cudrania tricuspidata can inhibit the production of pro-inflammatory factors in cells against acute neuroinflammation (Kim et al., 2017). After activation, microglia can be divided into classically activated microglia (M1) and selectively activated microglia (M2) (Orihuela et al., 2016). M1 type can produce pro-inflammatory factors and mediators (IL-1β, IL-6, TNF-α, CCL2, ROS, NO, glutamate, etc.), resulting in peripheral inflammatory cell infiltration. They also initiate an inflammatory response, causing apoptosis and secondary damage (Devanney et al., 2020). In contrast, activated M2 cells produce an anti-inflammatory cytokine IL-10 that inhibits neuronal inflammation, expressing tissue remodeling receptors (Arg-1, CD36, CD163, CD206, etc.), transforming growth factor β (TGF-β), brain-derived neurotrophic factor (BDNF) (Boche et al., 2013; Hu et al., 2015), and help restore the homeostasis of the central nervous system (Gogoleva et al., 2019). Therefore, promoting microglia conversion to M2 type is considered a therapeutic strategy for cerebral ischemic injury (Lu et al., 2020). In this study, we found that Tanshinone IIA reduced ischemia-induced neuronal cell death by increasing neuron and microglia cell numbers *in vivo*. Then we established an OGD model of PC12 and BV2 cells to mimic the cerebral ischemic environment in rats. Tanshinone IIA increased the survival of PC12 and BV2 cells after OGD. In a recent study, Tanshinone IIA can shift microglia phenotype from M1 to M2 in A. cantonensis-infected BALB/c mice (Feng et al., 2019). Tanshinone IIA treatment downregulated M1 macrophage markers and upregulated M2 macrophage markers in BV-2 cells under LPS stimulation (Chen et al., 2020). Next in our experiments, co-immunofluorescence staining was used to detect the polarization of microglia in rat brain. Interestingly, we found that Tanshinone IIA could inhibit the M1 type of microglia's polarization and promote the polarization of the M2 type in rat cortex. In addition, we also found that Tanshinone IIA could significantly downregulated the mRNA expressions of M1 markers in OGD-induced BV2 cells: CD11b, CD32, iNOS and upregulated the mRNA expression levels of M2 markers: Arg-1, CD206 and IL-10. These results suggest that Tanshinone IIA may play a neuroprotective role by regulating microglia polarization. However, its mechanism was unknown.

NF-κB factors have been shown to regulate cell survival and proliferation, inflammation, and immune response processes (Pires et al., 2018). Its protein products p65/p50 and Rel/p52 are relatively stable dimers (Huang et al., 1997; Cai et al., 2020). The function of NF-κB members may depend on specific cellular stimuli (Freire and Conneely, 2018). Pattern recognition receptors, cytokine or antigen receptor-mediated signaling cascades eventually culminate in the activation of the IκB kinase (IKK) complex, followed by inhibition of intracellular NF-κB chaperone IκBα and related protein phosphorylation. This phosphorylation results in ubiquitination and degradation of K48-linked IκBα, thus allowing NF-κB dimers to translocate into the nucleus and initiate specific gene transcription, increase nuclear NF-κB, initiate inflammatory responses and downstream pathways (Liu et al., 2017; Zhang et al., 2018). The relationship between NF-κB and stroke was studied by detecting the expression of RelA and p50 in brain tissue in six patients after death (Harari and Liao, 2010). During cerebral ischemia, NF-κB is activated (Taetzsch et al., 2015), and M1 type microglia is polarized (Wang et al., 2017). Dong et al. (2009) reported that Tanshinone IIA inhibited the translocation of NF-κB in the nucleus on H_2O_2 induced astrocytes. And Wang et al. (2014) reported that Tanshinone IIA reduced the expression of NF-κB in rat brain after I/R. In this study, we examined proteins associated with the NF-κB pathway, finding that Tanshinone IIA inhibited expression levels of NF-κB signaling pathway-related

proteins in BV2 cells. And further studies showed that BAY-11-7082 (a NF-κB inhibitor) could also inhibit M1 type and promote M2 type of microglia's polarization *in vivo* and *in vitro*. These results suggested that Tanshinone IIA may inhibit the inflammatory response by inhibiting M1 microglia polarization and promoting the polarization of the M2 type through the NF-κB pathway.

In conclusion, in this study, we again demonstrated that Tanshinone IIA is effective for the treatment of cerebral I/R injury in rats. We also found that Tanshinone IIA could modulate microglia polarization. Above all, the research suggested that Tanshinone IIA might regulate microglia polarization from M1 to M2 through NF-κB signaling pathway and thus have anti-neuroinflammatory effects.

DATA AVAILABILITY STATEMENT

The original contributions presented in the study are included in the article/Supplementary Material, further inquiries can be directed to the corresponding authors.

ETHICS STATEMENT

The animal study was reviewed and approved by the Animal Committee of Shanghai University.

AUTHOR CONTRIBUTIONS

TL and YZ conceived and designed the study. ZS, JF, QZ, constructed the animal model. ZS, DY performed the cell experiments, Western Blot experiments, analyzed the data and wrote the manuscript. TL, ZS and YZ revised the manuscript. All authors read and approved the final manuscript.

FUNDING

This work was supported by The Outstanding Clinical Project of Shanghai Pudong (PWYgy 2018-04) and The Important Weak Subject Construction Project of Shanghai Pudong (PWZbr 2017-16).

REFERENCES

Ai, J., Wan, H., Shu, M., Zhou, H., Zhao, T., Fu, W., et al. (2017). Guhong injection protects against focal cerebral ischemia-reperfusion injury via anti-inflammatory effects in rats. *Arch. Pharm. Res.* 40 (5), 610–622. doi:10.1007/s12272-016-0835-4

Alves, H. C., Treurniet, K. M., Jansen, I. G. H., Yoo, A. J., Dutra, B. G., Zhang, G., et al. (2019). Thrombus migration paradox in patients with acute ischemic stroke. *Stroke* 50 (11), 3156–3163. doi:10.1161/strokeaha.119.026107

Boche, D., Perry, V. H., and Nicoll, J. A. R. (2013). Review: activation patterns of microglia and their identification in the human brain. *Neuropathol. Appl. Neurobiol.* 39 (1), 3–18. doi:10.1111/nan.12011

Bruno, V., Svensson-Arvelund, J., Rubér, M., Berg, G., Piccione, E., Jenmalm, M. C., et al. (2018). Effects of low molecular weight heparin on the polarization and cytokine profile of macrophages and T helper cells in vitro. *Scientific reports*, 8 (1), 4166. doi:10.1038/s41598-018-22418-2

Cai, M., Guo, Y., Wang, S., Wei, H., Sun, S., Zhao, G., et al. (2017). Tanshinone IIA elicits neuroprotective effect through activating the nuclear factor erythroid 2-related factor-dependent antioxidant response. *Rejuvenation Res.* 20 (4), 286–297. doi:10.1089/rej.2016.1912

Cai, M., Liao, Z., Zou, X., Xu, Z., Wang, Y., Li, T., et al. (2020). Herpes simplex virus 1 UL2 inhibits the TNF-alpha-mediated NF-kappaB activity by interacting with p65/p50. *Front. Immunol.* 11, 549. doi:10.3389/fimmu.2020.00549

Chen, Y., Wu, X., Yu, S., Lin, X., Wu, J., Li, L., et al. (2012a). Neuroprotection of Tanshinone IIA against cerebral ischemia/reperfusion injury through inhibition of macrophage migration inhibitory factor in rats. *PLoS One* 7 (6), e40165. doi:10.1371/journal.pone.0040165

Chen, Y., Wu, X., Yu, S., Fauzee, N. J. S., Wu, J., Li, L., et al. (2012b). Neuroprotective capabilities of Tanshinone IIA against cerebral ischemia/reperfusion injury via anti-apoptotic pathway in rats. *Biol. Pharm. Bull.* 35 (2), 164–170. doi:10.1248/bpb.35.164

Chen, P., Piao, X., and Bonaldo, P. (2015). Role of macrophages in Wallerian degeneration and axonal regeneration after peripheral nerve injury. *Acta Neuropathol.* 130 (5), 605–618. doi:10.1007/s00401-015-1482-4

Chen, W., Li, X., Guo, S., Song, N., Wang, J., Jia, L., et al. (2019). Tanshinone IIA harmonizes the crosstalk of autophagy and polarization in macrophages via miR-375/KLF4 pathway to attenuate atherosclerosis. *Int. Immunopharmacol.* 70, 486–497. doi:10.1016/j.intimp.2019.02.054

Chen, M., Chen, Q., and Tao, T. (2020). Tanshinone IIA promotes M2 microglia by erβ/IL-10 pathway and attenuates neuronal loss in mouse TBI model. *Neuropsychiatr. Dis. Treat* Vol. 16, 3239–3250. doi:10.2147/ndt.s265478

Chiang, T., Messing, R. O., and Chou, W. H. (2011). Mouse model of middle cerebral artery occlusion. *J. Vis. Exp.* 48, 2716. doi:10.3791/2761

Collaborators, G. B. D. C. o. D. (2018). Global, regional, and national age-sex-specific mortality for 282 causes of death in 195 countries and territories, 1980-2017: a systematic analysis for the Global Burden of Disease Study 2017. *Lancet* 392 (10159), 1736–1788. doi:10.1016/S0140-6736(18)32203-7

Devanney, N. A., Stewart, A. N., and Gensel, J. C. (2020). Microglia and macrophage metabolism in CNS injury and disease: the role of immunometabolism in neurodegeneration and neurotrauma. *Exp. Neurol.* 329, 113310. doi:10.1016/j.expneurol.2020.113310

Dong, K., Xu, W., Yang, J., Qiao, H., and Wu, L. (2009). Neuroprotective effects of Tanshinone IIA on permanent focal cerebral ischemia in mice. *Phytother. Res.* 23 (5), 608–613. doi:10.1002/ptr.2615

Fei, Y. X., Wang, S. Q., Yang, L. J., Qiu, Y. Y., Li, Y. Z., Liu, W. Y., et al. (2017). Salvia miltiorrhiza Bunge (Danshen) extract attenuates permanent cerebral ischemia through inhibiting platelet activation in rats. *J. Ethnopharmacol.* 207, 57–66. doi:10.1016/j.jep.2017.06.023

Feng, Y., Feng, F., Zheng, C., Zhou, Z., Jiang, M., Liu, Z., et al. (2019). Tanshinone IIA attenuates demyelination and promotes remyelination in A. cantonensis-infected BALB/c mice. *Int. J. Biol. Sci.* 15 (10), 2211–2223. doi:10.7150/ijbs.35266

Freire, P. R., and Conneely, O. M. (2018). NR4A1 and NR4A3 restrict HSC proliferation via reciprocal regulation of C/EBPα and inflammatory signaling. *Blood* 131 (10), 1081–1093. doi:10.1182/blood-2017-07-795757

Gogoleva, V. S., Drutskaya, M. S., and Atretkhany, K. S. (2019). [The role of microglia in the homeostasis of the central nervous system and neuroinflammation]'. *Mol. Biol. (Mosk)* 53 (5), 790–798. doi:10.1134/s0026893319050054

Hansen, D. V., Hanson, J. E., and Sheng, M. (2018). Microglia in Alzheimer's disease. *J. Cell Biol.* 217 (2), 459–472. doi:10.1083/jcb.201709069

Harari, O. A., and Liao, J. K. (2010). NF-κBand innate immunity in ischemic stroke. *Ann. N. Y Acad. Sci.* 1207, 32–40. doi:10.1111/j.1749-6632.2010.05735.x

He, Y., Ruganzu, J. B., Lin, C., Ding, B., Zheng, Q., Wu, X., et al. (2020). Tanshinone IIA ameliorates cognitive deficits by inhibiting endoplasmic reticulum stress-induced apoptosis in APP/PS1 transgenic mice. *Neurochem. Int.* 133, 104610. doi:10.1016/j.neuint.2019.104610

Hu, X., Leak, R. K., Shi, Y., Suenaga, J., Gao, Y., Zheng, P., et al. (2015). Microglial and macrophage polarization-new prospects for brain repair. *Nat. Rev. Neurol.* 11 (1), 56–64. doi:10.1038/nrneurol.2014.207

Huang, D. B., Huxford, T., Chen, Y.-Q., and Ghosh, G. (1997). The role of DNA in the mechanism of NFκB dimer formation: crystal structures of the dimerization domains of the p50 and p65 subunits. *Structure* 5 (11), 1427–1436. doi:10.1016/s0969-2126(97)00293-1

Huang, Y., Long, X., Tang, J., Li, X., Zhang, X., Luo, C., et al. (2020). The attenuation of traumatic brain injury via inhibition of oxidative stress and apoptosis by Tanshinone IIA. *Oxid Med. Cell Longev* 2020, 4170156. doi:10.1155/2020/4170156

Kalkman, H. O., and Feuerbach, D. (2016). Antidepressant therapies inhibit inflammation and microglial M1-polarization. *Pharmacol. Ther.* 163, 82–93. doi:10.1016/j.pharmthera.2016.04.001

Kim, D. C., Quang, T. H., Oh, H., and Kim, Y. C. (2017). Steppogenin isolated from Cudrania tricuspidata shows antineuroinflammatory effects via NF-kappaB and MAPK pathways in LPS-stimulated BV2 and primary rat microglial cells'. *Molecules* 22 (12). doi:10.3390/molecules22122130

Lamkanfi, M., and Dixit, V. M. (2014). Mechanisms and functions of inflammasomes. *Cell* 157 (5), 1013–1022. doi:10.1016/j.cell.2014.04.007

Liu, X., Pichulik, T., Wolz, O.-O., Dang, T. M., Stutz, A., Dillen, C., et al. (2017). Human NACHT, LRR, and PYD domain-containing protein 3 (NLRP3) inflammasome activity is regulated by and potentially targetable through Bruton tyrosine kinase. *J. Allergy Clin. Immunol.* 140 (4), 1054–1067. doi:10.1016/j.jaci.2017.01.017

Liu, T., Ding, Y., and Wen, A. (2018). Traditional Chinese medicine for ischaemic stroke. *Lancet Neurol.* 17 (9), 745. doi:10.1016/s1474-4422(18)30290-4

Liu, P., Peng, J., Han, G. H., Ding, X., Wei, S., Gao, G., et al. (2019). Role of macrophages in peripheral nerve injury and repair. *Neural Regen. Res.* 14 (8), 1335–1342. doi:10.4103/1673-5374.253510

Longa, E. S., Weinstein, P. R., Carlson, S., and Cummins, R. (1989). Reversible middle cerebral artery occlusion without craniectomy in rats. *Stroke.* 20, 84–91. doi:10.1161/01.str.20.1.84

Lu, E., Wang, Q., Li, S., Chen, C., Wu, W., Xu, Y. X. Z., et al. (2020). 'Profilin 1 knockdown prevents ischemic brain damage by promoting M2 microglial polarization associated with the RhoA/ROCK pathway', *J Neurosci Res*, 98 (6), 1198–1212.

Ma, J., Hou, D., Wei, Z., Zhu, J., Lu, H., Li, Z., et al. (2019). Tanshinone IIA attenuates cerebral aneurysm formation by inhibiting the NFκBmediated inflammatory response. *Mol. Med. Rep.* 20 (2), 1621–1628. doi:10.3892/mmr.2019.10407

Mantovani, A., Biswas, S. K., Galdiero, M. R., Sica, A., and Locati, M. (2013). Macrophage plasticity and polarization in tissue repair and remodelling. *J. Pathol.* 229 (2), 176–185. doi:10.1002/path.4133

Naderi, Y., Sabetkasaei, M., Parvardeh, S., and Zanjani, T. M. (2017). Neuroprotective effect of minocycline on cognitive impairments induced by transient cerebral ischemia/reperfusion through its anti-inflammatory and anti-oxidant properties in male rat. *Brain Res. Bull.* 131, 207–213. doi:10.1016/j.brainresbull.2017.04.010

Orihuela, R., McPherson, C. A., and Harry, G. J. (2016). Microglial M1/M2 polarization and metabolic states. *Br. J. Pharmacol.* 173 (4), 649–665. doi:10.1111/bph.13139

Pan, Y., Qian, J. X., Lu, S. Q., Chen, J. W., Zhao, X. D., Jiang, Y., et al. (2017). Protective effects of Tanshinone IIA sodium sulfonate on ischemia-reperfusion-induced myocardial injury in rats. *Iran J. Basic Med. Sci.* 20 (3), 308–315. doi:10.22038/ijbms.2017.8361

Pape, K., Tamouza, R., Leboyer, M., and Zipp, F. (2019). Immunoneuropsychiatry - novel perspectives on brain disorders. *Nat. Rev. Neurol.* 15 (6), 317–328. doi:10.1038/s41582-019-0174-4

Pires, B. R. B., Silva, R., Ferreira, G. M., and Abdelhay, E. (2018). NF-kappaB: two sides of the same coin. *Genes (Basel)* 9 (1). doi:10.3390/genes9010024

Sun, J., Ling, Z., Wang, F., Chen, W., Li, H., Jin, J., et al. (2016). *Clostridium* butyricum pretreatment attenuates cerebral ischemia/reperfusion injury in mice via anti-oxidation and anti-apoptosis. *Neurosci. Lett.* 613, 30–35. doi:10.1016/j.neulet.2015.12.047

Taetzsch, T., Levesque, S., McGraw, C., Brookins, S., Luqa, R., Bonini, M. G., et al. (2015). Redox regulation of NF-κB p50 and M1 polarization in microglia. *Glia* 63 (3), 423–440. doi:10.1002/glia.22762

Tobin, M. K., Bonds, J. A., Minshall, R. D., Pelligrino, D. A., Testai, F. D., and Lazarov, O. (2014). Neurogenesis and inflammation after ischemic stroke: what is known and where we go from here. *J. Cereb. Blood Flow Metab.* 34 (10), 1573–1584. doi:10.1038/jcbfm.2014.130

Wahul, A. B., Joshi, P. C., Kumar, A., and Chakravarty, S. (2018). Transient global cerebral ischemia differentially affects cortex, striatum and hippocampus in Bilateral Common Carotid Arterial occlusion (BCCAo) mouse model. *J. Chem. Neuroanat.* 92, 1–15. doi:10.1016/j.jchemneu.2018.04.006

Wang, C., Yeo, S., Haas, M. A., and Guan, J. L. (2017). Autophagy gene FIP200 in neural progenitors non-cell autonomously controls differentiation by regulating microglia. *J. Cell Biol.* 216 (8), 2581–2596. doi:10.1083/jcb.201609093

Wang, J.-G., Bondy, S. C., Zhou, L., Yang, F.-Z., Ding, Z.-G., Hu, Y., et al. (2014). Protective effect of Tanshinone IIA against infarct size and increased HMGB1, NFκB, GFAP and apoptosis consequent to transient middle cerebral artery occlusion. *Neurochem. Res.* 39 (2), 295–304. doi:10.1007/s11064-013-1221-y

Wang, L., Xiong, X., Zhang, X., Ye, Y., Jian, Z., Gao, W., et al. (2020). Sodium Tanshinone IIA sulfonate protects against cerebral ischemia-reperfusion injury by inhibiting autophagy and inflammation. *Neuroscience* 441, 46–57. doi:10.1016/j.neuroscience.2020.05.054

Wei, Y., Hong, H., Zhang, X., Lai, W., Wang, Y., Chu, K., et al. (2017). Salidroside inhibits inflammation through PI3K/akt/HIF signaling after focal cerebral ischemia in rats. *Inflammation* 40 (4), 1297–1309. doi:10.1007/s10753-017-0573-x

Ye, T., Li, Y., Xiong, D., Gong, S., Zhang, L., Li, B., et al. (2021). Combination of Danshen and ligustrazine has dual anti-inflammatory effect on macrophages and endothelial cells. *J. Ethnopharmacol.* 266, 113425. doi:10.1016/j.jep.2020.113425

Yenari, M. A., Kauppinen, T. M., and Swanson, R. A. (2010). Microglial activation in stroke: therapeutic targets. *Neurotherapeutics* 7 (4), 378–391. doi:10.1016/j.nurt.2010.07.005

Zhang, F., Yan, C., Wei, C., Yao, Y., Ma, X., Gong, Z., et al. (2018). Vinpocetine inhibits NF-κB-Dependent inflammation in acute ischemic stroke patients. *Transl. Stroke Res.* 9 (2), 174–184. doi:10.1007/s12975-017-0549-z

Zhang, S. C., Ma, L. S., Chu, Z. H., Xu, H., Wu, W. Q., Liu, F., et al. (2017). Regulation of microglial activation in stroke. *Acta Pharmacol. Sin.* 38, 445–458. doi:10.1038/aps.2016.162

Zhao, H., Wang, Q., Cheng, X., Li, X., Li, N., Liu, T., et al. (2018). Inhibitive effect of resveratrol on the inflammation in cultured astrocytes and microglia induced by aβ1-42. *Neuroscience* 379, 390–404. doi:10.1016/j.neuroscience.2018.03.047

Zhu, J., Xu, Y., Ren, G., Hu, X., Wang, C., Yang, Z., et al. (2017). Tanshinone IIA Sodium sulfonate regulates antioxidant system, inflammation, and endothelial dysfunction in atherosclerosis by downregulation of CLIC1. *Eur. J. Pharmacol.* 815, 427–436. doi:10.1016/j.ejphar.2017.09.047

Conflict of Interest: The authors declare that the research was conducted in the absence of any commercial or financial relationships that could be construed as a potential conflict of interest.

frontiers in Pharmacology

ORIGINAL RESEARCH
published: 30 April 2021
doi: 10.3389/fphar.2021.682735

Resibufogenin Suppresses Triple-Negative Breast Cancer Angiogenesis by Blocking VEGFR2-Mediated Signaling Pathway

Ting Yang[1†], Yi-Xin Jiang[1†], Ye Wu[1†], Dong Lu[1], Rui Huang[1], Long-Ling Wang[1], Shi-Qi Wang[1], Ying-Yun Guan[2], Hong Zhang[1]* and Xin Luan[1]**

[1]Institute of Interdisciplinary Integrative Medicine Research, Shanghai University of Traditional Chinese Medicine, Shanghai, China, [2]Department of Pharmacy, Ruijin Hospital, School of Medicine, Shanghai Jiaotong University, Shanghai, China

OPEN ACCESS

Edited by:
Tie-Jun Li,
Second Military Medical University, China

Reviewed by:
Jiang-Jiang Qin,
Chinese Academy of Sciences (CAS), China
Fu Peng,
Sichuan University, China

***Correspondence:**
Xin Luan
luanxin@shutcm.edu.cn
Hong Zhang
zhanghong@shutcm.edu.cn
Ying-Yun Guan
gyy40696@rjh.com.cn

[†]These authors have contributed equally to this work

Specialty section:
This article was submitted to Ethnopharmacology, a section of the journal Frontiers in Pharmacology

Received: 19 March 2021
Accepted: 12 April 2021
Published: 30 April 2021

Citation:
Yang T, Jiang Y-X, Wu Y, Lu D, Huang R, Wang L-L, Wang S-Q, Guan Y-Y, Zhang H and Luan X (2021) Resibufogenin Suppresses Triple-Negative Breast Cancer Angiogenesis by Blocking VEGFR2-Mediated Signaling Pathway. Front. Pharmacol. 12:682735. doi: 10.3389/fphar.2021.682735

Resibufogenin (RBF), an active compound from *Bufo bufonis*, has been used for the treatment of multiple malignant cancers, including pancreatic cancer, colorectal cancer, and breast cancer. However, whether RBF could exert its antitumor effect by inhibiting angiogenesis remains unknown. Here, we aimed to explore the antiangiogenic activity of RBF and its underlying mechanism on human umbilical vein endothelial cell (HUVEC), and the therapeutic efficacy with regard to antiangiogenesis *in vivo* using two triple-negative breast cancer (TNBC) models. Our results demonstrated that RBF can inhibit the proliferation, migration, and tube formation of HUVECs in a dose-dependent manner. Spheroid sprouts were thinner and shorter after RBF treatment *in vitro* 3D spheroid sprouting assay. RBF also significantly suppressed VEGF-mediated vascular network formation *in vivo* Matrigel plug assay. In addition, Western blot analysis was used to reveal that RBF inhibited the phosphorylation of VEGFR2 and its downstream protein kinases FAK and Src in endothelial cells (ECs). Molecular docking simulations showed that RBF affected the phosphorylation of VEGFR2 by competitively binding to the ATP-bound VEGFR2 kinase domain, thus preventing ATP from providing phosphate groups. Finally, we found that RBF exhibited promising antitumor effect through antiangiogenesis *in vivo* without obvious toxicity. The present study first revealed the high antiangiogenic activity and the underlying molecular basis of RBF, suggesting that RBF could be a potential antiangiogenic agent for angiogenesis-related diseases.

Keywords: resibufogenin, antiangiogenic cancer therapy, VEGFR2, tumor angiogenesis, triple-negative breast cancer

INTRODUCTION

Updated Global Cancer Statistics indicated that female breast cancer has surpassed lung cancer as the leading cause of global cancer incidence in 2020 with an estimated 2.3 million new cases, representing 11.7% of all cancer cases (Sung et al., 2021). Triple-negative breast cancer (TNBC) is the most challenging heterogenous subtype of breast cancer often associated with an aggressive phenotype, high recurrence, metastasis, and poor prognosis (Bianchini et al., 2016). Approximately 12% of breast cancer patients are TNBC in the United States from 2012 to 2016, with a 5-year survival rate is 8–16% lower than other subtypes (DeSantis et al., 2019; Howard and Olopade, 2021). Owing to the absence

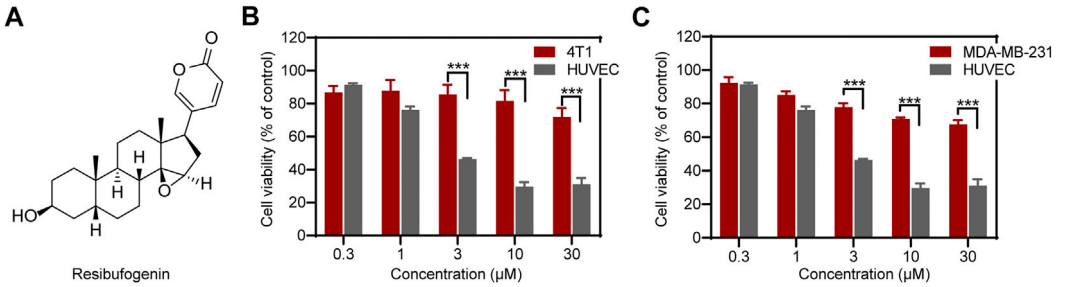

FIGURE 1 | RBF effectively inhibited the viability of HUVECs relative to 4T1 and MDA-MB-231 cells. **(A)** The chemical structure of RBF drawn through ChemDraw 19.0. **(B, C)** RBF dose-dependently inhibited the viability of HUVECs at concentrations without affecting 4T1 and MDA-MB-231 cells. Values are expressed as mean ± SD, $n = 4$. ***$p < 0.001$ *vs.* 4T1 or MDA-MB-231 cells.

of expression of the estrogen receptor (ER), progesterone receptor (PgR), and human epidermal growth factor receptor 2 (HER2), conventional cytotoxic chemotherapy remains the mainstay of treatment (Waks and Winer, 2019). However, chemotherapeutics may cause the acute nonspecific side effects for normal tissues and multidrug resistance (MDR), leading to therapeutic failure (Nedeljkovic and Damjanovic, 2019). Therefore, discovery of neoadjuvant drugs with highly selective antitumor mechanism has become a promising approach for the treatment of TNBC.

Angiogenesis plays a critical role in tumor formation, progression, and metastasis. Through excessive secretion of pro-angiogenic factors, tumor cells continue to activate ECs to "sprout" in the original blood vessels and form new vascular structures (Duran et al., 2017). Correspondingly, angiogenesis provides cancer cells with the essential nutrients and oxygen, and also a route for metastasis (Viallard and Larrivée, 2017). Therefore, inhibiting tumor angiogenesis keeps an attractive strategy for oncotherapy since decades ago. To date, bevacizumab is the only antiangiogenic drug approved by FDA (Food and Drug Administration) for TNBC (Xie et al., 2021), whereas bevacizumab has little effect on overall survival due to acquired drug resistance (Liu et al., 2020) and its limitation of blocking VEGFA expression (Zou et al., 2020). It is essential to find antiangiogenic medicines with novel skeleton for antiangiogenesis therapy and to overcome drug resistance.

Natural products provide unparalleled source with unique molecular scaffolds for antiangiogenic drug discovery. Among them, resibufogenin (RBF) (**Figure 1A**), the main component of the antitumor traditional Chinese medicine (TCM) *Bufo bufonis* from the dry secretions of *Bufo gargarizans Cantor* and *Bufo melanostictus Schneider* (Chu et al., 2016), is a compound with the steroid mother nucleus structure of cardiotonic aglycone (Qi et al., 2011). Studies have shown that RBF has antitumor activity and can inhibit the tumor growth through different mechanisms. For instance, RBF can suppress transforming growth factor-β activated kinase 1 (Tak1)–mediated nuclear transcription factor-kappa B (NF-κB) activity through protein kinase C–dependent inhibition of glycogen synthase kinase-3 (GSK-3) on pancreatic cancer cells, PANC-1 and ASPC (Liu et al., 2018). RBF also can inhibit the growth and metastasis of colorectal cancer by triggering RIP3-dependent necrotizing ptosis and inducing glutathione peroxidase 4 (Gpx4) inactivation to induce oxidative stress (Han et al., 2018; Shen et al., 2021). Moreover, RBF treatment exhibited antitumorigenic and anti-Warburg effect in breast cancer through upregulating the inhibitory effect of miR-143–3p/HK2 axis (Guo et al., 2020). However, there is no study on RBF-mediated regulation of angiogenesis, the essential step for TNBC growth.

In present study, we first investigated the antiangiogenic effect of RBF and its mechanism on human umbilical vein endothelial cell (HUVEC). The antiangiogenic activity of RBF *in vivo* was evaluated by Matrigel plug assay. Furthermore, the *in vivo* antiangiogenic efficacy of RBF was evaluated in 4T1 and MDA-MB-231 orthotopic mice models. This study provided a new theoretical basis and reference for the potential clinical application of RBF.

MATERIALS AND METHODS

Materials, Cell Lines, and Animals

RBF was purchased from Wuhan Zhongbiao Technology Company (Wuhan, China). Recombinant human vascular endothelial growth factor (VEGF165), Rabbit polyclonal antibodies against phospho-VEGFR-2, VEGFR-2, FAK, phosphor-FAK, Src, and phosphor-Src were obtained from Cell Signaling Technology (Danvers, MA).

Breast cancer cell lines 4T1 and MDA-MB-231 were obtained from Shanghai Cell Bank, Chinese Academy of Sciences (Shanghai, China). 4T1 cells were cultured in RPMI 1640 medium (meilunbio, Dalian, China), and MDA-MB-231 cells were cultured in Leibovitz's L-15 medium (Gibco, United States). All culture media were supplemented with 10% fetal bovine serum (FBS, Gibco, United States), 1% penicillin, and 1% streptomycin. Human umbilical vein endothelial cells (HUVECs) were obtained using Lifeline Cell Technology® and cultured in completed endothelial cell medium (Lifeline® Cell Technology, Frederick, MD). 4T1 cells and HUVECs were cultured at 37°C in a humidified atmosphere containing 5% carbon dioxide (CO_2), and MDA-MB-231 cells were cultured at 37°C without CO_2.

BALB/c miceBALB/c nude mice, and C57 BL/6 mice were supplied by Shanghai Laboratory Animal Center (Shanghai, China). The animals were kept in an environment-controlled

room (temperature: 20–25°C, relative humidity: 55–65%, and 12 h light/12 h dark cycle) with free access to water and fodder. All animal experimental protocols were approved by the Animal Ethics Committee of Shanghai University of Traditional Chinese Medicine.

Cell Viability Assay

The effect of RBF on cell viability of the HUVECs, 4T1 and MDA-MB-231 cells was measured using Cell Counting Kit-8 (CCK-8, meilunbio, Dalian, China). Briefly, these cells were seeded in 96 well plates (5×10^3 cells/well), respectively. After 24–h incubation, the cells were treated with different concentrations of RBF (0.3, 1, 3, 10, and 30 μM) for 24 h. Then, 100 μl medium containing 10% CCK-8 was added to each well and incubated at 37°C for additional 2 h. The absorbance at 450 nm was determined by microplate reader (Spark 10M, Tecan, Switzerland). The percentage of cell viability was calculated against control. Each condition included replicate wells with at least four independent repeats.

Endothelial Cell Wound Healing Assay

HUVECs (2×10^5 cells/well) were seeded in a 6-well plate and incubated at 37°C for 24 h. Subsequently, confluent HUVECs were scratched with the pipette tips, washed with PBS and photographed, and then the cells were treated with various concentrations of RBF (0.3, 1, 3, 10, and 30 μM). After drug stimulation for 12 h, the plate was photographed with microscope (Spark 10M, Tecan, Switzerland) and EC migration was quantified by Image-Pro Plus 6.0 software (Media Cybernetics, Bethesda, MD).

Endothelial Cell Tube Formation Assay

Tube formation assay was carried out as described previously with some modifications (Dai et al., 2016; Lu et al., 2017). In brief, a precooled 96-well plate was coated with 50 μl/well Matrigel (BD Biosciences, San Jose, CA), which was thawed at 4°C overnight in advance and then incubated at 37°C for at least 30 min. HUVECs (1×10^4 cells/well) were dispersed in the completed medium containing different concentrations of RBF (0.3, 1, 3, and 10 μM) and then seeded on the Matrigel layer. After 10 h of incubation (37°C with 5% CO_2), the tubular structure formed by HUVECs stained with calcein AM with a final concentration of 2 μM for 15 min, then fluorescence photography was performed with Cytation 5 (BioTek, United States). The tube length was quantified by Image Pro Plus 6.0 software.

Endothelial Cell Transwell Migration Assay

The chemotactic motility of HUVEC was investigated using a transwell migration assay with 24-well transwell plates of polycarbonate filter with 8 μm pore diameter and 6.5 mm diameter inserts. Briefly, complete medium containing 20 ng/ml VEGF165 was added to the lower chamber, and HUVECs (2×10^4 cells/well) was suspended in the medium which containing different concentrations of RBF (0.3, 1, 3, and 10 μM) and seeded in the top chamber. After incubation for 8 h in an incubator (37°C with 5% CO_2), the migrated cells were fixed with 4% paraformaldehyde for 20 min, then stained with 0.1% crystal violet, while the nonmigrated cells on the upper surface of polycarbonate membrane were gently wiped off with a cotton swab. The cells on the other side of the membrane were photographed under an inverted microscope (Laica, Germany) after washing the membrane three times with PBS. The number of migrated cells was determined by Image-Pro Plus 6.0 software.

Spheroid-Based Angiogenesis Assay

ECs spheroids of defined cell number were generated as described previously (Heiss et al., 2015; Wu et al., 2019) with minor modifications. In brief, HUVECs (1.6×10^4 cells/ml) were suspended in a culture medium containing 0.24% (wt/vol) methylcellulose (Adamas, China) and the mixture seeded alternately in a 100-mm × 20-mm dish (Corning, United States). Under these conditions, all suspended cells contributed to the formation of a single spheroid of defined size and cell number (400 cells/spheroid). Spheroids were cultured for 24 h in an incubator (37°C with 5% CO_2). Afterward, the spheroids were suspended with a solution of rat tail collagen type I (BD, United States), then rapidly transferred into prewarmed 24-well plates and allowed to polymerize (30 min). After the collagen gels were set, 100 μl of complete medium containing 500 ng/ml $VEGF_{165}$ and different concentrations of RBF (1 or 3 μM) or complete medium only containing 500 ng/ml VEGF165 was added to each well, and the spheroids formed sprouts after 24 h. The sprouts were photographed with microscope (Spark 10 M, Tecan, Switzerland).

Matrigel Plug Assay

Six-week-old female C57BL/6 mice were subcutaneously injected with Matrigel mixture (400 μl/plug) containing 400 ng/ml VEGF and different concentrations of RBF (10 or 30 μM), and the Matrigel was mixed with PBS for mock control or 400 ng/ml VEGF for vehicle control. After 7 days of implantation, Matrigel plugs were removed and fixed with 4% paraformaldehyde, then photographed with a digital camera. After Matrigel plugs were embedded and fixed in paraffin, neovascularization was determined by CD31 staining.

Western Blot

The effect of RBF on VEGF-dependent angiogenesis signaling pathways was determined by Western blot assay. HUVECs (1×10^5 cells/well) were seeded in a 6-well plate and incubated overnight in an incubator (37°C with 5% CO_2). When the cell density reached about 80%, the cells were starved in a serum-free medium for 6 h. The serum-free medium containing different concentrations of RBF was then changed and continued to culture for 30 min and stimulated for 4 min with 100 ng/ml VEGF, subsequently. RIPA Lysis Buffer (Beyotime, Shanghai, China) supplemented with complete protease inhibitor cocktail and PhosSTOP phosphatase inhibitor cocktail (Roche, Rotkreuz, Switzerland) were used for cell lysis extraction. The concentration of protein was determined by BCA Protein Assay Kit (Beyotime, Shanghai, China) and equalized before loading. Then, 20 μg of membrane

protein from each sample was applied to 7.5% SDS–PAGE. Polyvinylidene fluoride (PVDF) was incubated with primary antibody (Cell Signaling Technology, Danvers, MA) at 4°C and then co-incubated with horseradish peroxidase–coupled second antibody. The luminescent images were detected using ECL kits.

Anticancer Therapy of Resibufogenin *In Vivo*

Mouse triple-negative breast cancer cells 4T1 (1×10^7 cells/ml) and human triple-negative breast cancer cells MDA-MB-231 (5×10^7 cells/mL) were suspended in PBS, and then inoculated in 6-week-old female BALB/c mice and female BALB/c nude mice on the fourth pair of fat pads (100 μl/mouse) to establish orthotopic model of breast cancer. Once the tumor volume reached ~50 mm^3, the all of mice were randomly divided into two groups (n = 6 per group): control group and RBF treatment group (10 mg/kg/day). The mice of the control group received intraperitoneal injection with oil and the mice in the RBF treatment group were injected with oil-containing RBF (10 mg/kg/day). The body weight, tumor length, and width of mice were monitored every 2 days. The formula for calculating tumor volume is as follows: tumor volume (mm^3) = (length) × $(width)^2/2$. After administration for 12 days, the mice were sacrificed and the tumor was dissected. And all of the tumors were photographed and weighed, and then fixed with 4% paraformaldehyde to prepare for paraffin section and immunohistochemical assay. The hematoxylin and eosin (H&E) staining evaluated tumor necrosis, and the immunohistochemical assay of CD31 staining was used to observe the tumor vessels according to the previous studies. All of the slices were photographed by photomicroscope. The tumor necrosis area, microvessel density, Ki67-positive cells, and TUNEL-positive cells of the slices were analyzed by Image-Pro Plus 6.0 software.

Molecular Docking

Through the computer virtual docking of molecular operating environment (MOE), the molecular interaction between VEGFR2 and RBF was explored. First, the three-dimensional structure of RBF is generated by energy minimization in MOE. Then the x-ray crystals of VEGFR2 kinase domain and its ligands were obtained from the Protein Data Bank (http://www.rcsb.org). Two crystal structures of 3B8R and 3B8Q, which belong to DFG-in and DFG-out conformations, were selected to dock with RBF. The interaction between the molecules was analyzed and visualized by ligand interaction module and PyMOL.

Statistical Analysis

All data were presented as mean ± SD. Statistical analysis and graphical representation of the data were performed using GraphPad Prism 6.0 (GraphPad Software, San Diego, CA). The differences between groups were examined with Student's t-test or ANOVA with Bonferroni's multiple comparisons tests. Differences were considered significant if the p value was less than 0.05.

RESULTS

Resibufogenin Inhibits Viability of Human Umbilical Vein Endothelial Cells at Concentrations Not Affecting Triple-Negative Breast Cancers

As shown in **Figures 1B,C**, RBF inhibited the cell viability of HUVECs in a dose-dependent manner with a low half-maximal inhibitory concentration (IC_{50}) value, 3 μM. The cell viability of HUVECs was distinctly inhibited at RBF concentration of 10 μM. In contrast, RBF had almost no obvious effect on the viability of the TNBCs 4T1 and MDA-MB-231 at the same concentrations of HUVECs. These results proved that ECs are more sensitive to RBF than 4T1 and MDA-MB-231 cells. Moreover, RBF did not exert significant anti-proliferative effect toward HUVECs at the dose from 0.3 to 30 μM within 12 h.

Resibufogenin Inhibits Endothelial Cell Migration, Invasion, and Tube Formation

The migration of ECs is the important step in the process of angiogenesis (Varinska et al., 2018). Thus, we performed a wound healing assay and transwell migration assay to investigate the effect of RBF on the horizontal and vertical migration ability of HUVECs. As shown in **Figures 2A,D**, RBF dose-dependently inhibited the lateral migration of ECs, and it was obvious that the migration ability of HUVECs was completely inhibited at the concentration of 10 μM. The transwell assay (**Figures 2B,E**) showed that RBF could inhibit the vertical migration of HUVECs to the bottom chamber at 0.3 μM. To evaluate the antiangiogenesis ability of RBF, we performed a tube formation assay to verify the effects of RBF on tube formation of HUVECs on a Matrigel substratum. HUVECs could form a complete tubular network after VEGF stimulation (**Figures 2C,F**), while RBF markedly restrained HUVECs tube formation at the concentration of 3 μM. These results suggested that RBF has a strong inhibitory effect on HUVEC motility, migration, and tube formation at the nontoxic concentrations.

Resibufogenin Inhibits Human Umbilical Vein Endothelial Cells Spheroid Sprouting

In the sprout formation assay, HUVECs were formed a single spheroid and then embedded in a 3D collagen matrix. In the control group, the HUVEC spheroid was sprouting significantly under the stimulation of $VEGF_{165}$. However, when treated with different concentrations of RBF, the sprouts became thinner. Sprouting was almost completely inhibited by the treatment with RBF at 3 μM (**Figure 3A**).

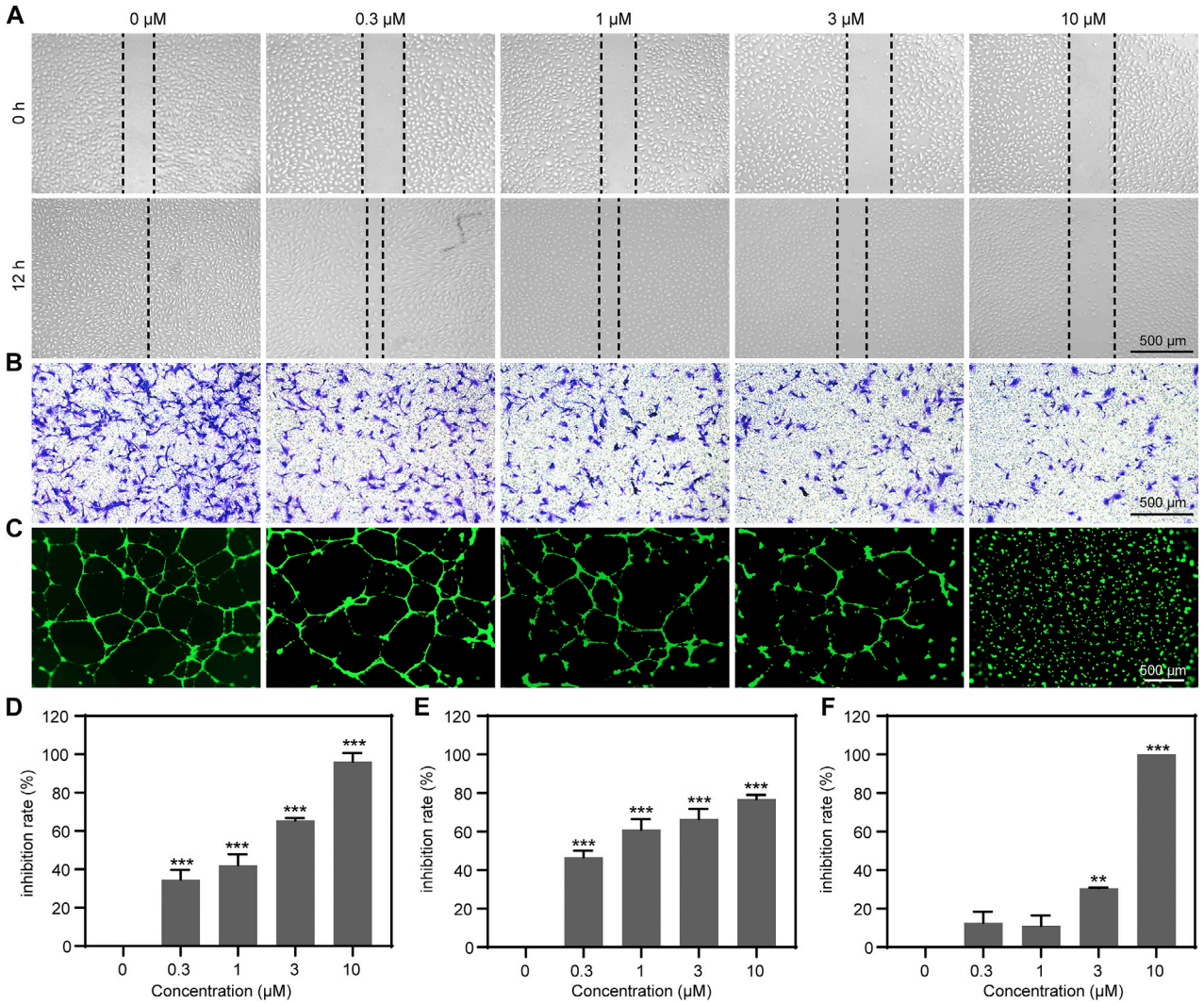

FIGURE 2 | RBF significantly suppressed HUVEC motility, migration, and tube formation. **(A)** RBF inhibited HUVEC migration in wound healing assay. Dotted lines indicated the boundary of initial scraping. **(B)** RBF suppresses HUVEC vertical migration in transwell assay. HUVEC migration after 8 h treatment of RBF was assayed using transwell Boyden chamber. **(C)** RBF inhibited tube formation of HUVECs. HUVECs were placed in the Matrigel coated 96-well plate. After 10 h, the tubular structures were photographed. **(D)** The inhibition rate of wound healing after treatment with different concentrations of RBF. **(E)** The inhibition rate of the migrated cells after treatment with different concentrations of RBF. **(F)** The inhibition rate of tube formation after treatment with different concentrations of RBF. Values are expressed as mean ± SD, $n = 4$. $^{**}p < 0.01$ and $^{***}p < 0.001$ as compared with control.

These results suggested that RBF has an inhibitory effect on HUVEC spheroid sprouting.

Resibufogenin Inhibits Angiogenesis in Matrigel Plugs *In Vivo*

Next, we performed the Matrigel plug assay to further explore whether RBF could inhibit angiogenesis *in vivo*. As illustrated in **Figure 3B**, compared with the PBS group, Matrigel plugs mixed with VEGF exhibited obvious red area after 1 week of implantation, indicating a large number of new blood vessels in Matrigel plugs. In contrast, Matrigel plugs mixed with RBF were almost colorless and transparent, suggesting almost no angiogenesis existed. These results indicated that RBF could significantly inhibit neovascularization in the Matrigel plugs *in vivo*. The existence of blood vessels was verified by staining of CD31, a specific marker on the surface of ECs (Privratsky and Newman, 2014; Lertkiatmongkol et al., 2016). The results in **Figure 3C** displayed that RBF (10 μM) had a significant inhibitory effect on angiogenesis stimulated by VEGF. The number of blood vessels in the high-dose group (30 μM) was similar to that in the PBS alone group.

Resibufogenin Suppressed the Activation of VEGFR2-Mediated Signaling Pathway

The VEGF signaling pathway and its main receptor, VEGFR2, could stimulate tumor angiogenesis in most solid tumors (Simons

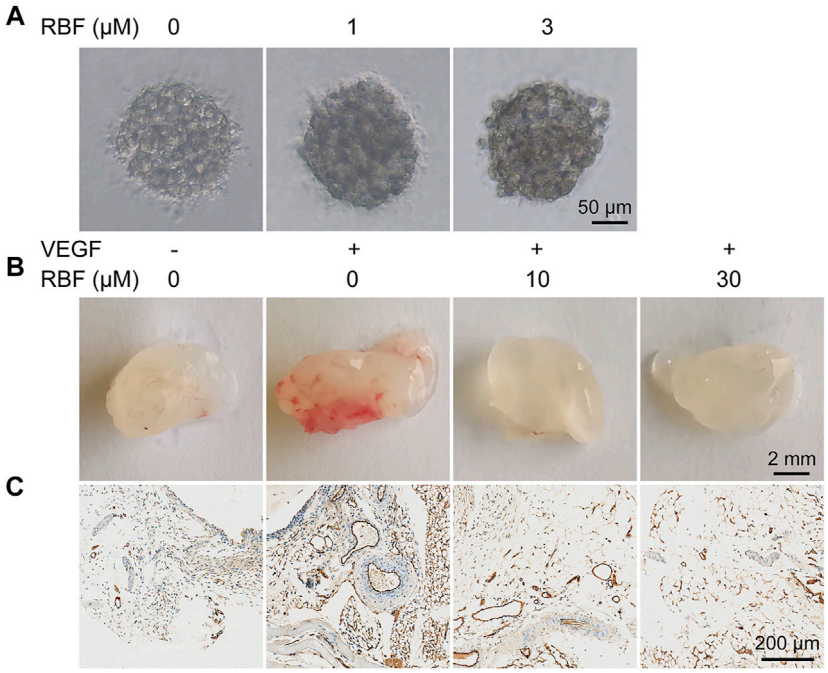

FIGURE 3 | RBF blocked angiogenesis in 3D HUVEC spheroid and Matrigel plug. **(A)** Sprouting from HUVEC spheroids stimulated with VEGF were inhibited by RBF. **(B)** Representative photographs of Matrigel plug treated with different concentrations of RBF. **(C)** Representative CD31 staining sections showing the vessel in each Matrigel plug.

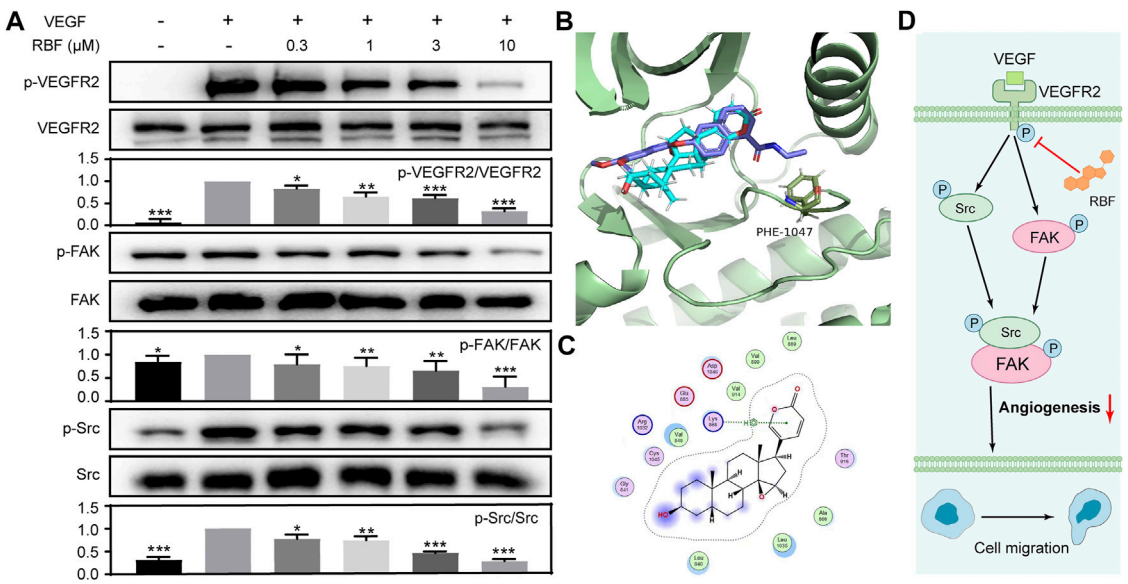

FIGURE 4 | RBF inhibited the phosphorylation of VEGFR2 and its downstream signaling molecules in endothelial cells. **(A)** RBF inhibited the activation of VEGFR2 and its downstream signaling kinases in HUVECs. HUVECs were pretreated with various concentrations of RBF for 0.5 h followed by the stimulation with 100 ng/ml of VEGF for 4 min. The activation of VEGFR2 and its downstream cascade (FAK and Src) were analyzed by Western blot. The quantified results were shown as the grayscale ratio of phosphorylated protein to the total protein. $^{*}p < 0.05$, $^{**}p < 0.01$, and $^{***}p < 0.001$ as compared with control (HUVECs stimulated by VEGF), $n = 3$. **(B)** The predicted binding interactions between RBF and VEGFR2. Side chains of crucial residues in the binding site are shown as blue sticks. **(C)** Two-dimensional interaction map of RBF and ATP binding pocket of VEGFR2 kinase domain was visualized by ligand interaction module. **(D)** Signaling pathway diagram of RBF-mediated antiangiogenesis.

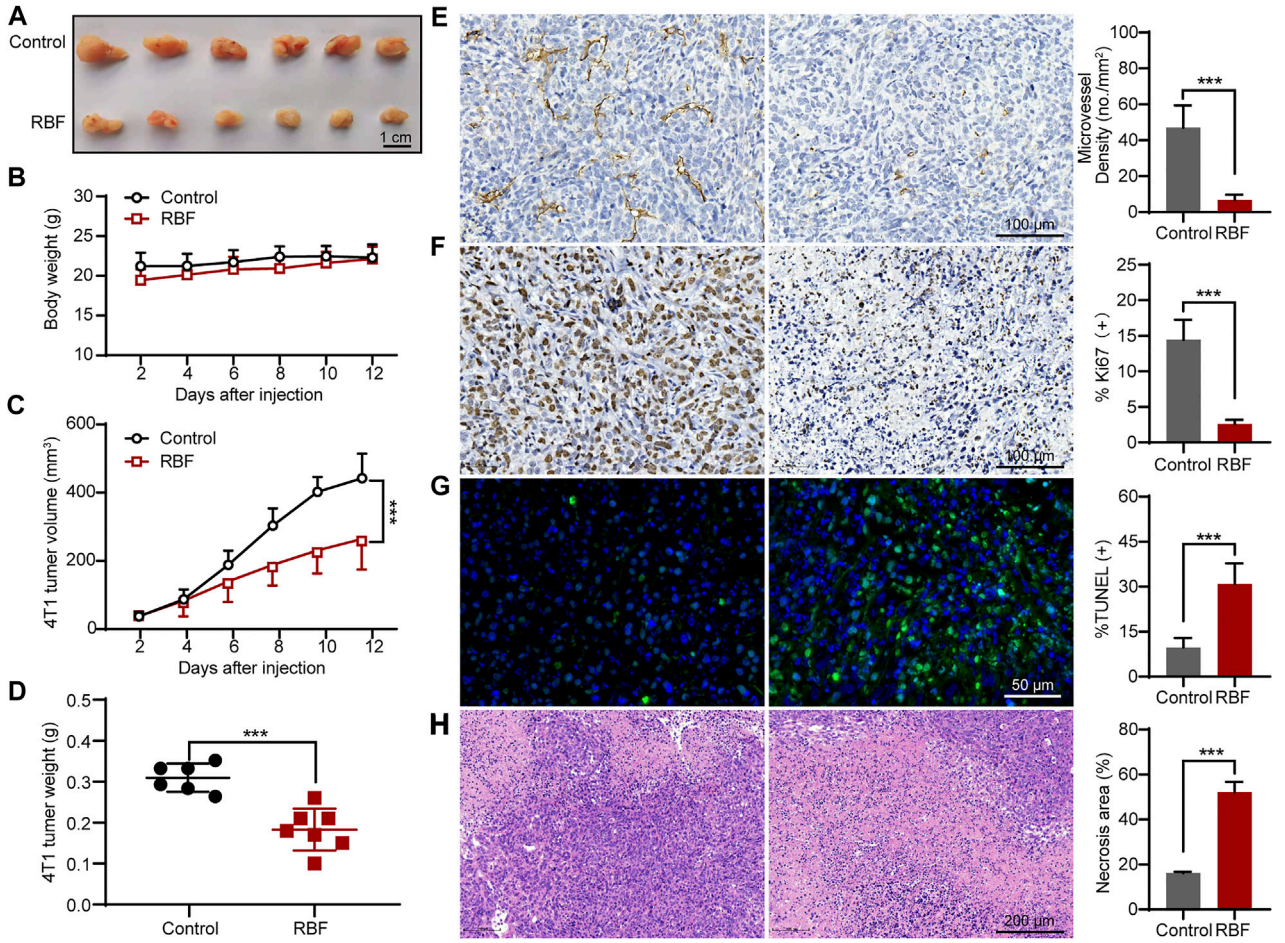

FIGURE 5 | RBF inhibited tumor angiogenesis and growth in 4T1 xenograft mice model. **(A)** Photograph of the resected tumors from the control and RBF groups. **(B)** Mice body weight. **(C)** RBF treatment decreased the tumor weight compared with the control. **(D)** RBF treatment delayed the tumor growth compared with the control. **(E)** Intratumoral CD31-positive vessel (microvessel density, MVD). **(F)** Ki67-positive proliferation tumor cells. **(G)** TUNEL-positive apoptotic tumor cells **(H)** H&E staining sections and statistical analysis of necrosis area. All values were shown as mean ± SD, $n = 5$. $^{**}p < 0.01$ and $^{***}p < 0.001$ as compared with control.

et al., 2016). To verify the mechanisms involved in the antiangiogenic function of RBF, we first examined whether RBF could affect VEGF-mediated phosphorylation of VEGFR2 by Western-blotting assay. It was shown that the expression of tyrosine phosphorylation of VEGFR2 was significantly increased after VEGF stimulation, and RBF could inhibit the phosphorylation level of VEGFR2 in a dose-dependent manner (**Figure 4A**). As known, the downstream signaling pathway could be activated by the VEGFR2, which regulate multiple activities of ECs, including migration, proliferation, and survival (Simons et al., 2016; Wang et al., 2020). We further investigated the effect of RBF on the expression level of downstream proteins of VEGFR2. The results suggested that RBF could downregulate the level of phospho-FAK and phospho-Src. Taken together, the above results proved that RBF could inhibit the phosphorylation of VEGFR2, FAK, and Src to block the angiogenesis ability of ECs.

Resibufogenin Competitively Bound ATP-Binding VEGFR2 Kinase Domain

As RBF downregulate the phosphorylation of VEGFR2 and its downstream signal molecules, it was speculated that RBF may be an inhibitor of VEGFR2 kinase. So, molecular docking simulation was carried out to predict the possible binding mode between RBF and VEGFR2 kinase domain. Studies have shown that VEGFR2 inhibitors can be divided into two types according to different binding modes, namely, type I (conformational complex with DFG-in) and type II (conformational complex with DFG-out) protein kinase inhibitors (Huang et al., 2012). Type I inhibitors affect phosphorylation of VEGFR2 by competitively binding ATP- binding VEGFR2 kinase domain, thereby preventing ATP from providing phosphate groups. While type II inhibitors inhitbit phosphorylation by occupying the space position of Phe1047 in active conformation (DFG-in) and

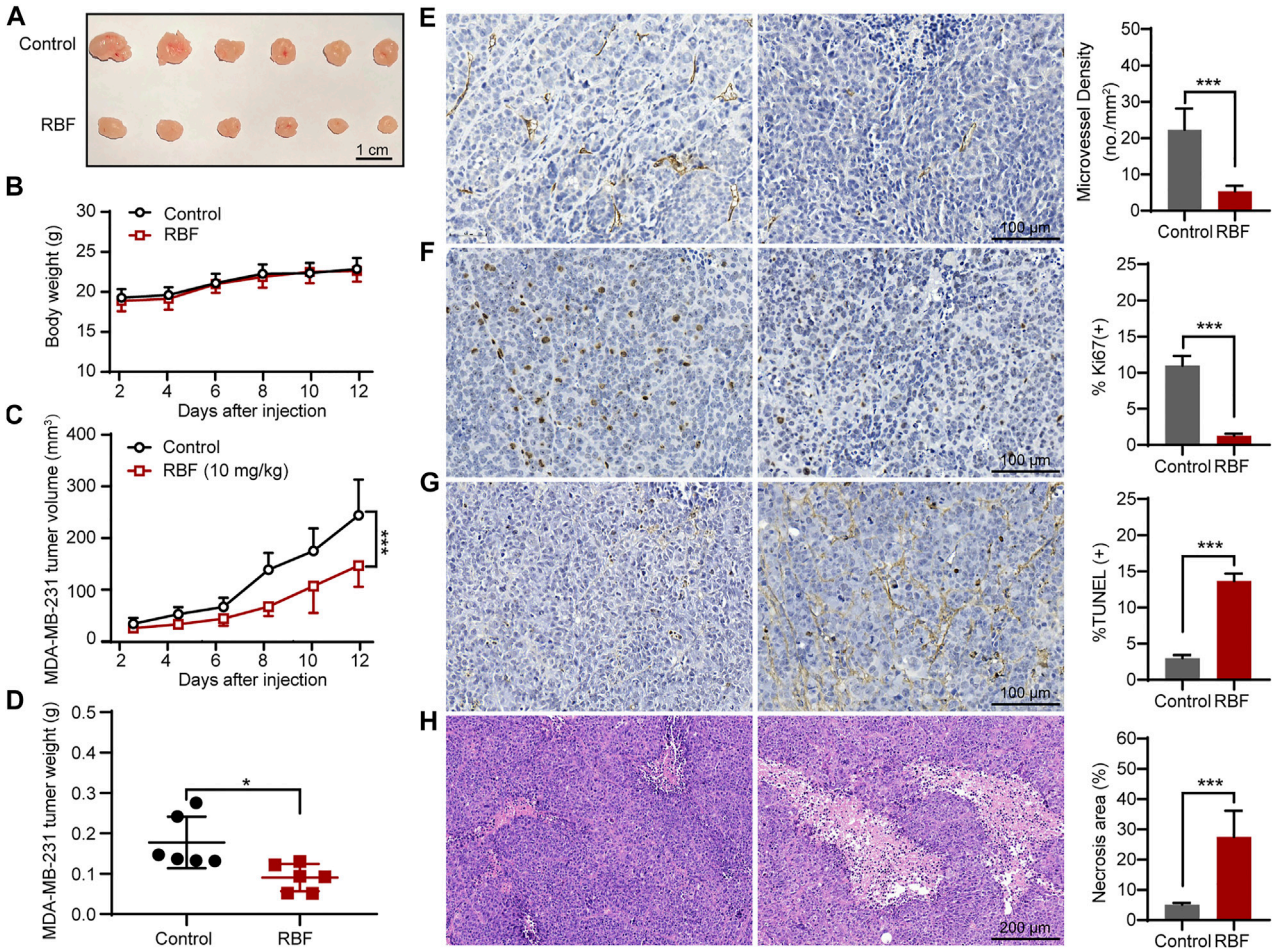

FIGURE 6 | RBF inhibited tumor angiogenesis and growth in MDA-MB-231 xenograft mice model. **(A)** The photograph of the resected tumors from the control and RBF groups. **(B)** Mice body weight. **(C)** RBF treatment decreased the tumor weight compared with the control. **(D)** RBF treatment delayed the tumor growth compared with the control. **(E)** Intratumoral CD31-positive vessel (microvessel density, MVD). **(F)** Ki67-positive proliferation of tumor cells. **(G)** TUNEL-positive apoptotic tumor cells **(H)** H&E staining sections and statistical analysis of the necrosis area. All values were shown as mean ± SD, $n = 5$. $^{**}p < 0.01$ and $^{***}p < 0.001$ as compared with control.

preventing VEGFR2 from transforming from inactive to active (Weiss et al., 2008; Huang et al., 2012). Then, DFG-in and DFG-out protein states were selected for docking. As shown in **Figures 4B,C**, RBF could bind to the DFG-in protein state and cannot penetrate into the Phe1047 pocket to further prevent VEGFR2 activation. RBF mainly interacted with amino acid residues, including Leu840, Val848, Ala866, Leu889, Val899, Val914, and Leu1035 via the hydrophobic interaction. There was also H–pi interaction between the arene moiety of RBF and the key residues of Lys868. These results indicated that RBF was a Type I inhibitor which inhibited the phosphorylation of VEGFR2.

Resibufogenin Inhibited Tumor Angiogenesis and Growth in 4T1 and MDA-MB-231 Orthotopic Mouse Models

In order to investigate the inhibiting effects of RBF on tumor angiogenesis and growth *in vivo*, the tumor models were first established by *in situ* inoculation of 4T1 cells in BALB/c mice (Duan et al., 2019; Tsui et al., 2019). RBF was injected intraperitoneally at a dose of 10 mg/kg/day for 12 days. The results showed (**Figures 5A,C,D**) that RBF significantly inhibited the growth of tumor, the tumor volume was 246.15 ± 69.9 mm^3, and the average tumor weight was only 0.17 ± 0.04 g, whereas the tumor volume was 471.89 ± 45.1 mm^3 and the average tumor weight was 0.31 ± 0.03 g in the control group. In addition, there was no significant change in the body weight of mice at this dose (**Figure 5B**), indicating that RBF had no obvious toxicity to the mice at the curative dose. Immunohistochemistry and pathological examination showed that RBF not only effectively inhibited tumor cell proliferation and increase tumor necrotic area but also reduced tumor microvessel density and elevate TUNEL-positive cells.

Meanwhile, we also established another TNBC model by *in situ* inoculation of human TNBC cell line (MDA-MB-231) into BALB/c nude mice (Shi et al., 2019; Kachamakova-Trojanowska et al., 2020; Xu et al., 2020). As shown in **Figure 6C**, RBF also

showed significant antitumor activity in this tumor model, and the tumor volume was 146.77 ± 37.5 mm^3 much smaller than that in the control group (244.31 ± 62.9 mm^3). In contrast to untreated controls, RBF-treated group showed a profound decrease in the number of CD31-positive microvessel and Ki67-positive cells, while the rate of TUNEL-positive cells and the area of tumor necrosis increased. These results suggested that the antiangiogenic activity of RBF effectively contributed to its antitumor effect *in vivo*.

DISCUSSION

Neovascularization is the critical characteristic of solid tumors to contribute tumor rapid progression and metastasis. Therefore, targeting tumor blood vessels has been considered as a reasonable approach to the treatment of various malignancies (Rajabi and Mousa, 2017). Bevacizumab, a recombinant humanized monoclonal IgG1 antibody that binds to VEGF, provides a new hope of improved survival for patients with intractable TNBC in combination with paclitaxel and capecitabine (Liu et al., 2020). However, this neoadjuvant therapy cannot fully meet the expectations of patients for higher overall survival owing to acquired resistance. Given that, it is imperative to explore alternative novel antiangiogenic agents to improve the therapeutic effectiveness.

Active small components derived from TCM have been demonstrated to possess excellent bioactivity with low toxicity in the treatment of many diseases. Taking these advantages, we successfully identified a TCM *Bufo bufonis*–derived small molecule, RBF, which have high selectivity between TNBCs and HUVECs. Multiple mechanisms for RBF antitumor activity have been elucidated, but none of them touched its antiangiogenic activity in breast cancers, especially TNBC. We first demonstrated the potent antiangiogenic ability and mechanisms of RBF *in vitro* as well as the anti-TNBC effect *in vivo*.

We successfully proved that RBF could perform the antiangiogenic function toward migration, invasion, and tube formation of HUVECs in a dose-dependent inhibition. Meanwhile, we found that the sprouting 3D spheroid sprouts were thinner and shorter after treatment of RBF. The Matrigel plug assay was used to verify the antiangiogenesis effect of RBF *in vivo*. Then, we constructed 4T1 and MDA-MB-231 orthotopic mouse models to evaluate the therapeutic effect of RBF through antiangiogenic potency. As expected, the results exhibited that RBF can not only suppress the growth of mouse TNBC *in vivo*, but also inhibit human TNBC progression in mice through the successful blocking effect on tumor-related angiogenesis, thereby highlighting the potential clinical transformation of RBF. Immunohistochemical assay further revealed that RBF could significantly increase the necrotic area of tumor, inhibited tumor cell proliferation, and promoted apoptosis. More importantly, the intratumoral CD31-positive vessel in the RBF treatment group decreased pronouncedly, suggesting that its antitumor effect was closely related to antiangiogenesis. Collectively, these *in vitro* and *in vivo* results both suggested that the antiangiogenic activity of RBF played a critical role in suppressing tumor growth *in vivo* (Guo et al., 2020).

Among angiogenic factors, VEGF has the strongest effect to the process of angiogenesis. VEGFR2 plays a principal role in mediating VEGF-induced series of downstream signals of angiogenesis (such as Akt pathway, NF- κB pathway, and MAPK pathway) that subsequently promote the activation of endothelial cells (Simons et al., 2016). Thus, targeting VEGFR2 signaling pathway to inhibit tumor angiogenesis is regarded as vital strategy. We also observed that RBF dose-dependently decreased the VEGF-induced VEGFR2 phosphorylation and its downstream signals, including FAK and Src. Molecular docking test indicated that RBF could locate at the ATP-bound VEGFR2 kinase domain through hydrophobic interaction and H–pi interaction, thereby blocking the phosphorylation of VEGFR2. Such bioinformatics of the binding pattern of RBF and VEGFR2 can help us better understand the antiangiogenic effect of RBF, and we could reinforce this binding by chemical structure modification of RBF.

In conclusion, we successfully elucidated the antiangiogenic effect and corresponding mechanism of RBF on the HUVECs by attenuating VEGFR2 signal pathway. More importantly, this new antitumor mechanism further contributed to slow tumor growth and lower microvessel density in two TNBC mice, which provide a promising candidate for angiogenesis in TNBC treatment.

DATA AVAILABILITY STATEMENT

The original contributions presented in the study are included in the article/Supplementary Material, further inquiries can be directed to the corresponding authors.

ETHICS STATEMENT

The animal study was reviewed and approved. All animal experimental protocols were approved by the Animal Ethics Committee of Shanghai University of Traditional Chinese Medicine.

AUTHOR CONTRIBUTIONS

XL, HZ, Y-YG, and TY conceived and designed the experiments. TY, Y-XJ, DL and L-LW performed the experiments. TY, RH, YW, and S-QW analyzed the data and made the figures. TY, Y-XJ, and YW wrote the paper. XL and HZ helped to proofread the article. All the authors contributed to the article and approved the submitted version.

FUNDING

This work was supported by the National Natural Science Foundation of China (No. 81903654), Program for Professor of Special Appointment (Young Eastern Scholar) at Shanghai Institutions of Higher Learning (No. QD2018035), Shanghai "Chenguang Program" of Education Commission of Shanghai

Municipality (No. 18CG46), Shanghai Sailing Program (No. 19YF1449400), Ruijin Youth NSFC Cultivation Fund (No. KY20194297), National key subject of drug innovation (No. 2019ZX09201005–007), and National key R & D program for key research project of modernization of traditional Chinese medicine (No. 2019YFC1711602).

REFERENCES

Bianchini, G., Balko, J. M., Mayer, I. A., Sanders, M. E., and Gianni, L. (2016). Triple-negative Breast Cancer: Challenges and Opportunities of a Heterogeneous Disease. *Nat. Rev. Clin. Oncol.* 13, 674–690. doi:10.1038/nrclinonc.2016.66

Chu, Q. C., Xu, H., Gao, M., Guan, X., Liu, H. Y., Deng, S., et al. (2016). Liver-targeting Resibufogenin-Loaded Poly(lactic-Co-Glycolic Acid)-D-α-Tocopheryl Polyethylene Glycol 1000 Succinate Nanoparticles for Liver Cancer Therapy. *Int. J. Nanomedicine.* 11, 449–463. doi:10.2147/IJN.S93541

Dai, F., Gao, L., Zhao, Y., Wang, C., and Xie, S. (2016). Farrerol Inhibited Angiogenesis through Akt/mTOR, Erk and Jak2/Stat3 Signal Pathway. *Phytomedicine* 23, 686–693. doi:10.1016/j.phymed.2016.03.008

DeSantis, C. E., Ma, J., Gaudet, M. M., Newman, L. A., Miller, K. D., Goding Sauer, A., et al. (2019). Breast Cancer Statistics, 2019. *CA A. Cancer J. Clincancer J. Clin.* 69, 438–451. doi:10.3322/caac.21583

Duan, X.-C., Yao, X., Zhang, S., Xu, M.-Q., Hao, Y.-L., Li, Z.-T., et al. (2019). Antitumor Activity of the Bioreductive Prodrug 3-(2-nitrophenyl) Propionic Acid-Paclitaxel Nanoparticles (NPPA-PTX NPs) on MDA-MB-231 Cells: In Vitro and In Vivo. *Ijn* 14, 195–204. doi:10.2147/IJN.S186556

Duran, C. L., Howell, D. W., Dave, J. M., Smith, R. L., Torrie, M. E., Essner, J. J., et al. (2017). Molecular Regulation of Sprouting Angiogenesis. *Compr. Physiol.* 8, 153–235. doi:10.1002/cphy.c160048

Guo, Y., Liang, F., Zhao, F., and Zhao, J. (2020). Resibufogenin Suppresses Tumor Growth and Warburg Effect through Regulating miR-143-3p/HK2 axis in Breast Cancer. *Mol. Cel Biochem.* 466, 103–115. doi:10.1007/s11010-020-03692-z

Han, Q., Ma, Y., Wang, H., Dai, Y., Chen, C., Liu, Y., et al. (2018). Resibufogenin Suppresses Colorectal Cancer Growth and Metastasis through RIP3-Mediated Necroptosis. *J. Transl. Med.* 16, 201. doi:10.1186/s12967-018-1580-x

Heiss, M., Hellström, M., Kalén, M., May, T., Weber, H., Hecker, M., et al. (2015). Endothelial Cell Spheroids as a Versatile Tool to Study Angiogenesis In Vitro. *FASEB j.* 29, 3076–3084. doi:10.1096/fj.14-267633

Howard, F. M., and Olopade, O. I. (2021). Epidemiology of Triple-Negative Breast *Cancer:* A Review. *Cancer J.* 27, 8–16. doi:10.1097/PPO.0000000000000500

Huang, L., Huang, Z., Bai, Z., Xie, R., Sun, L., and Lin, K. (2012). Development and Strategies of VEGFR-2/KDR Inhibitors. *Future Med. Chem.* 4, 1839–1852. doi:10.4155/fmc.12.121

Kachamakova-Trojanowska, N., Podkalicka, P., Bogacz, T., Barwacz, S., Józkowicz, A., Dulak, J., et al. (2020). HIF-1 Stabilization Exerts Anticancer Effects in Breast Cancer Cells In Vitro and In Vivo. *Biochem. Pharmacol.* 175, 113922. doi:10.1016/j.bcp.2020.113922

Lertkiatmongkol, P., Liao, D., Mei, H., Hu, Y., and Newman, P. J. (2016). Endothelial Functions of Platelet/endothelial Cell Adhesion Molecule-1 (CD31). *Curr. Opin. Hematol.* 23, 253–259. doi:10.1097/MOH.0000000000000239

Liu, L., Liu, Y., Liu, X., Zhang, N., Mao, G., Zeng, Q., et al. (2018). Resibufogenin Suppresses Transforming Growth Factor-β-activated Kinase 1-mediated Nuclear factor-κB Activity through Protein Kinase C-dependent Inhibition of Glycogen Synthase Kinase 3. *Cancer Sci.* 109, 3611–3622. doi:10.1111/cas.13788

Liu, Y., Ji, X., Kang, N., Zhou, J., Liang, X., Li, J., et al. (2020). Tumor Necrosis Factor α Inhibition Overcomes Immunosuppressive M2b Macrophage-Induced Bevacizumab Resistance in Triple-Negative Breast Cancer. *Cell Death Dis.* 11, 993. doi:10.1038/s41419-020-03161-x

Lu, H., Zhou, X., Kwok, H.-H., Dong, M., Liu, Z., Poon, P.-Y., et al. (2017). Ginsenoside-Rb1-Mediated Anti-angiogenesis via Regulating PEDF and miR-33a through the Activation of PPAR-γ Pathway. *Front. Pharmacol.* 8, 783. doi:10.3389/fphar.2017.00783

Nedeljkovic, M., and Damjanovic, A. (2019). Mechanisms of Chemotherapy Resistance in Triple-Negative Breast Cancer-How We Can Rise to the Challenge. *Cells* 8, 957. doi:10.3390/cells8090957

Privratsky, J. R., and Newman, P. J. (2014). PECAM-1: Regulator of Endothelial Junctional Integrity. *Cell Tissue Res.* 355, 607–619. doi:10.1007/s00441-013-1779-3

Qi, F., Li, A., Inagaki, Y., Kokudo, N., Tamura, S., Nakata, M., et al. (2011). Antitumor Activity of Extracts and Compounds from the Skin of the Toad *Bufo bufo* Gargarizans Cantor. *Int. Immunopharmacol.* 11, 342–349. doi:10.1016/j.intimp.2010.12.007

Rajabi, M., and Mousa, S. (2017). The Role of Angiogenesis in Cancer Treatment. *Biomedicines* 5, 34. doi:10.3390/biomedicines5020034

Shen, L. D., Qi, W. H., Bai, J. J., Zuo, C. Y., Bai, D. L., Gao, W. D., et al. (2021). Resibufogenin Inhibited Colorectal Cancer Cell Growth and Tumorigenesis through Triggering Ferroptosis and ROS Production Mediated by GPX4 Inactivation. *Anat. Rec.* 304, 313–322. doi:10.1002/ar.24378

Shi, D., Zhao, S., Jiang, W., Zhang, C., Liang, T., and Hou, G. (2019). TLR5: A Prognostic and Monitoring Indicator for Triple-Negative Breast Cancer. *Cel Death Dis.* 10, 954. doi:10.1038/s41419-019-2187-8

Simons, M., Gordon, E., and Claesson-Welsh, L. (2016). Mechanisms and Regulation of Endothelial VEGF Receptor Signalling. *Nat. Rev. Mol. Cel Biol.* 17, 611–625. doi:10.1038/nrm.2016.87

Sung, H., Ferlay, J., Siegel, R. L., Laversanne, M., Soerjomataram, I., Jemal, A., et al. (2021). Global Cancer Statistics 2020: GLOBOCAN Estimates of Incidence and Mortality Worldwide for 36 Cancers in 185 Countries. *CA A. Cancer J. Clin.* doi:10.3322/caac.21660

Tsui, K.-H., Wu, M.-Y., Lin, L.-T., Wen, Z.-H., Li, Y.-H., Chu, P.-Y., et al. (2019). Disruption of Mitochondrial Homeostasis with Artemisinin Unravels Anti-angiogenesis Effects via Auto-Paracrine Mechanisms. *Theranostics* 9, 6631–6645. doi:10.7150/thno.33353

Varinská, L., Fáber, L., Kello, M., Petrovová, E., Balážová, Ľ., Solár, P., et al. (2018). β-Escin Effectively Modulates HUVECs Proliferation and Tube Formation. *Molecules* 23, 197. doi:10.3390/molecules23010197

Viallard, C., and Larrivée, B. (2017). Tumor Angiogenesis and Vascular Normalization: Alternative Therapeutic Targets. *Angiogenesis* 20, 409–426. doi:10.1007/s10456-017-9562-9

Waks, A. G., and Winer, E. P. (2019). Breast *Cancer* Treatment. *JAMA* 321, 288–300. doi:10.1001/jama.2018.19323

Wang, X., Bove, A. M., Simone, G., and Ma, B. (2020). Molecular Bases of VEGFR-2-Mediated Physiological Function and Pathological Role. *Front. Cel Dev. Biol.* 8, 599281. doi:10.3389/fcell.2020.599281

Weiss, M. M., Harmange, J.-C., Polverino, A. J., Bauer, D., Berry, L., Berry, V., et al. (2008). Evaluation of a Series of Naphthamides as Potent, Orally Active Vascular Endothelial Growth Factor Receptor-2 Tyrosine Kinase Inhibitors¶. *J. Med. Chem.* 51, 1668–1680. doi:10.1021/jm701098w

Wu, X.-G., Zhou, C.-F., Zhang, Y.-M., Yan, R.-M., Wei, W.-F., Chen, X.-J., et al. (2019). Cancer-derived Exosomal miR-221-3p Promotes Angiogenesis by Targeting THBS2 in Cervical Squamous Cell Carcinoma. *Angiogenesis* 22, 397–410. doi:10.1007/s10456-019-09665-1

Xie, W., Zhao, H., Wang, F., Wang, Y., He, Y., Wang, T., et al. (2021). A Novel Humanized Frizzled-7-Targeting Antibody Enhances Antitumor Effects of Bevacizumab against Triple-Negative Breast Cancer via Blocking Wnt/β-Catenin Signaling Pathway. *J. Exp. Clin. Cancer Res.* 40 (1), 30. doi:10.1186/s13046-020-01800-x

Xu, P., Yan, F., Zhao, Y., Chen, X., Sun, S., Wang, Y., et al. (2020). Green Tea Polyphenol EGCG Attenuates Mdscs-Mediated Immunosuppression through Canonical and Non-canonical Pathways in a 4T1 Murine Breast Cancer Model. *Nutrients* 12 (4), 1042. doi:10.3390/nu12041042

Zou, G., Zhang, X., Wang, L., Li, X., Xie, T., Zhao, J., et al. (2020). Herb-sourced Emodin Inhibits Angiogenesis of Breast Cancer by Targeting VEGFA Transcription. *Theranostics* 10 (15), 6839–6853. doi:10.7150/thno.43622

Conflict of Interest: The authors declare that the research was conducted in the absence of any commercial or financial relationships that could be construed as a potential conflict of interest.

frontiers in Pharmacology

ORIGINAL RESEARCH
published: 18 June 2021
doi: 10.3389/fphar.2021.689007

Anti-Inflammatory Dipeptide, a Metabolite from Ambioba Secretion, Protects Cerebral Ischemia Injury by Blocking Apoptosis Via p-JNK/Bax Pathway

Qian Zhang[1,2†], Jinwei Dai[3†], Zhibing Song[2], Yuchen Guo[2], Shanshan Deng[1], Yongsheng Yu[1], Tiejun Li[1] and Yuefan Zhang[1]**

[1]School of Medicine, Shanghai University, Shanghai, China, [2]College of Pharmacology, Anhui University of Chinese Medicine, Hefei, China, [3]Department of Pharmacology, School of Life Science and Biopharmaceutics, Shenyang Pharmaceutical University, Shenyang, China

OPEN ACCESS

Edited by:
David M. Pereira, University of Porto, Portugal

Reviewed by:
Nahid Aboutaleb, Iran University of Medical Sciences, Iran
Hung-Hsiang Yu, Academia Sinica, Taiwan

***Correspondence:**
Tiejun Li
ltj204@163.com
Yuefan Zhang
yuefanzhang@shu.edu.cn

[†]These authors have contributed equally to this work

Specialty section:
This article was submitted to Neuropharmacology, a section of the journal Frontiers in Pharmacology

Received: *31 March 2021*
Accepted: *03 June 2021*
Published: *18 June 2021*

Citation:
Zhang Q, Dai J, Song Z, Guo Y, Deng S, Yu Y, Li T and Zhang Y (2021) Anti-Inflammatory Dipeptide, a Metabolite from Ambioba Secretion, Protects Cerebral Ischemia Injury by Blocking Apoptosis Via p-JNK/Bax Pathway. Front. Pharmacol. 12:689007. doi: 10.3389/fphar.2021.689007

MQ (L-methionyl-L-glutamic acid), anti-inflammatory dipeptide, is one of the metabolites of monocyte locomotion inhibitory factor, a thermostable pentapeptide secreted by *Entamoeba histolytica*. Monocyte locomotion inhibitory factor injection has been approved as an investigational drug for the potential neural protection in acute ischemic stroke. This study further investigated the neuroprotective effect of MQ in ischemic brain damage. Ischemia-reperfusion injury of the brain was induced in the rat model by middle cerebral artery occlusion. 2,3,5-triphenyltetrazolium chloride staining assay was used to measure cerebral infarction areas in rats. Laser Doppler measurement instrument was used to detect blood flow changes in the rat model. Nissl staining and NeuN staining were utilized to observe the numbers and structures of neuron cells, and the pathological changes in the brain tissues were examined by hematoxylin–eosin staining. Terminal deoxynucleotidyl transferase deoxyuridine triphosphate nick end labeling (TUNEL) staining was used to assess cell apoptosis. The changes in oxidative stress indexes, superoxide dismutase and malondialdehyde (MDA), were measured in serum. Methyl thiazolyl tetrazolium was used to measure the survival rates of PC12 cells. Flow cytometry assessed the apoptosis rates and the levels of reactive oxygen species. Real-time PCR was used to evaluate the mRNA expression levels, and Western blotting was used to analyze the changes in protein levels of p-JNK, Bax, cleaved Caspase3. We revealed that MQ improved neurobehavior, decreased cerebral infarction areas, altered blood flow volume, and the morphology of the cortex and hippocampus. On the other hand, it decreased the apoptosis of cortical neurons and the levels of MDA, and increased the levels of superoxide dismutase. *In vitro* studies demonstrated that MQ enhanced the cell survival rates and decreased the levels of reactive oxygen species. Compared to the oxygen-glucose deprivation/reperfusion group, the protein and mRNA expressions of p-JNK, Bax, cleaved Caspase3 was decreased significantly. These findings suggested that MQ exerts a neuroprotective effect in cerebral ischemia by blocking apoptosis via the p-JNK/Bax pathway.

Keywords: cerebral ischemia, apoptosis, anti-inflammation dipeptide, neuroprotection, oxygen-glucose deprivation/reperfusion

INTRODUCTION

Ischemic stroke, with high morbidity, high disability, and high mortality, accounts for about 80% of all stroke cases and causing severe nerve injuries (Poustchi et al., 2021). Prolonged cerebral ischemia leads to irreversible neuronal death, and reperfusion after ischemia results in brain injury, as assessed in animal studies or clinical trials (Lapchak and Zhang, 2017; Wu et al., 2020). Apoptosis is a regulated and programmed cell death that plays a crucial role in cerebral ischemia-induced brain injury in human and animal models (Sairanen et al., 2009; Liang et al., 2014). Hitherto, there are only a few effective drugs to treat ischemia/reperfusion (I/R) injury, especially for neural damage (Liang et al., 2011). Therefore, finding the anti-neuroapoptosis drugs for the treatment of ischemic stroke is clinically significant.

Animal medicine is a vital part of traditional Chinese medicine, such as *earthworm* and *Leech*. Peptides from animal medicine have various pharmacological activities. *Entamoeba histolytica*, an anaerobic pathogenic enteric protozoan and tissue-invasive parasite (Lee et al., 2019), is responsible for amoebic dysentery and amoebic liver abscess, resulting in human suffering and death (Soares et al., 2019). The pathogen is commonly found in low-resource regions, including Africa, India, Mexico, and parts of central/south America, and Southeast Asia (Wingfield et al., 2018). MLIF, a natural product derived from *Entamoeba histolytica* axenic cultures (Kretschmer et al., 1989; Rico et al., 1998), has been approved as an investigational drug for the potential neural protection in acute ischemic stroke (Liu et al., 2018). It was first identified as an anti-inflammatory peptide that inhibited the migration of monocytes (Kretschmer et al., 2001; Barrientos-Salcedo et al., 2009; Silva-Garcia and Rico-Rosillo, 2011) and the expression of interleukin (IL)-1β, IL-5, IL-6, and interferon (IFN)-γ and increased the expression of IL-10 in macrophages (Utrera-Barillas et al., 2003; Rojas-Dotor et al., 2006; Silva-Garcia et al., 2008). Subsequent studies showed that MLIF participated in other biological effects, such as expression of immunomodulatory genes (Silva-Garcia et al., 2008; Rojas-Dotor et al., 2018), cell proliferation, extracellular matrix formation, angiogenesis, and axon guidance. In a previous study, we discovered that MLIF exerts a protective effect on the vascular system by acting on eukaryotic elongation factor1A1 (eEF1A1) to upregulate the expression of vascular endothelial nitric oxide synthase (eNOS) and reduce the level of ICAM-1 and VCAM-1 (Zhang et al., 2012). In addition, MLIF decreased cerebral infarction areas and the level of malondialdehyde (MDA), myeloperoxidase (MPO), tumor necrosis factor-alpha (TNF-α), and IL-1β and increased the level of superoxide dismutase (SOD) (Yao et al., 2011). It also acted on eEF1A2 and the p-JNK/p53 pathways to protect the nerves (Zhu et al., 2016). Both native and synthetic MLIF presented selective anti-inflammatory properties, thereby inhibiting the human monocyte locomotion and respiratory burst and altering the expression of both anti-inflammatory and pro-inflammatory cytokines (Liu et al., 2018). However, due to the disadvantages of high synthesis cost, the related structure of MLIF is under continuous improvement. Finally, another peptide, an anti-inflammatory dipeptide, was found.

MQ is one of the metabolites of MLIF, which consists of methionine and glutamine. Endogenous peptides play a critical role in human function. A previous study (Baek et al., 2014) stated that carnosine, an endogenous dipeptide, converted LC3-I to LC3-II and reduced the expression of phosphorylated mTOR/p70S6K in the ischemic brain by improving brain mitochondrial function and mitophagy signaling. The dimeric dipeptide mimetic GK-2 prevented $H_2O_2^-$ or glutamic acid-induced destruction of hippocampal neurons and improved cognitive and memory functions to exert neuroprotective effects (Povarnina et al., 2013). Additionally, it prevented delayed neuronal damage and axonal degeneration and reduced TBI-related disruptions of brain functions (Genrikhs et al., 2018).

Therefore, the present study investigated the neuroprotective effect of MQ by blocking apoptosis via p-JNK/Bax pathway *in vitro* and *in vivo*.

MATERIALS AND METHODS

The experimental procedures were conducted according to the ARRIVE guidelines. Adult male Sprague–Dawley (SD) rats (220–270 g), purchased from the Changzhou Cavens Experimental Animals Co., Ltd (Changzhou, China), were housed in controlled conditions and given rat chow and tap water ad libitum. The surgery was executed after one week. The animal experiments were conducted under the supervision of the Animal Ethics Committee of Shanghai University (Shanghai, China), according to the National Institutes of Health Guide for the Care and Use of Laboratory Animals. We also made efforts to meet the principle of "3Rs" (Reduction, Refinement, and Replacement), according to the law.

MQ was synthesized by the Chinese Peptide Company (Hangzhou, China), with purity >98% determined by HPLC. MLIF were synthesized by the Chinese Peptide Company (Hangzhou, China), with purity >98%. 2,3,5-triphenyltetrazolium chloride (TTC) was purchased from Sigma (St. Louis, MO, United States). SOD and MDA kits were bought from Nanjing Jiancheng Bioengineering Institute (Nanjing, China). Reactive Oxygen Species (ROS) kit, Annexin V-fluorescein isothiocyante kit, TUNEL kit, and 2-(4-Amidinophenyl)-6-indolecarbamidine dihydrochloride (DAPI) were obtained from Beyotime (Shanghai, China). p-JNK, Caspase3, Bax, GAPDH, NeuN antibodies were purchased from Cell Signaling Technology (CST, Danvers, MA, United States). JNK inhibitor (SP600125) was purchased from Selleck (Shanghai, China). BCA protein kit was bought from Thermo Scientific (Waltham, MA, United States).

Middle Cerebral Artery Occlusion (MCAO)

Cerebral I/R was induced by MCAO, as described previously (Fan et al., 2011; Zhang et al., 2012). The rats were anesthetized with an intraperitoneal injection of 10% chloral hydrate (3 mL/kg). Then, the neck skin incision was scissored, and the tissues were bluntly dissected with tweezers to expose the left common carotid artery (CCA). The internal carotid artery and the external carotid artery were separated, and the external carotid artery was ligatured.

After a small incision was made in the proximal CCA, the occlusion line (0.26 mm) was inserted (18 mm) into the internal carotid artery through the CCA, thereby occluding the origin of the MCA. The body temperature was maintained at 37°C with warm light for 2 h, following which the occlusion line was pulled out with the curved tweezer for reperfusion. After 24 h, the rats were sacrificed for subsequent experiments.

Experimental Groups and Drug Treatment

The experimental rats were randomly divided into the following groups: sham operation (sham + saline solution), cerebral I/R (model + saline solution), I/R + MQ (3 mg/kg) hydrochloric, and I/R + MQ (1 mg/kg) hydrochloric. At 30 min post-MCAO surgery, MQ and normal saline were administered through the caudal vein.

In the comparison experiment of MQ and MLIF, the experimental rats were randomly divided into sham group + saline solution, model group + saline solution, I/R + MQ (3 mg/kg) hydrochloric group, and I/R + MLIF (3 mg/kg) hydrochloric group. At 30 min post-MCAO surgery, MQ, MLIF, and normal saline were administered through the caudal vein.

Cerebral Blood Flow (CBF) Monitoring

The rat was fixed on the stereotaxic instrument after anesthesia, and a scalp wound was made along the centerline. Then, a 30% hydrogen peroxide solution was applied to the scalp to remove the periosteum. The dental drill was used to drill the skull until the meninges were visible behind the anterior fontanelle at 3 mm or near the midline at 3.5 mm. The laser sensor was mounted on the drill hole with glue. Subsequently, Doppler blood flow meter monitoring was used to evaluate CBF at the following time points: (a) 30 min before cerebral ischemia, (b) 30 min after cerebral ischemia, and (c) 30 min after cerebral I/R. CBF decrease (%) = $(CBF_c - CBF_b)/CBF_a \times 100\%$.

Neurological Deficit

The neurological function was assessed, as described previously (Longa et al., 1989; Fan et al., 2011) on a five-point scale system: 0, no neurological deficit; 1, failure to extend left forepaw fully; 2, circling to the contralateral side; 3, leaning to the contralateral side; 4, no initiative in walking with consciousness (Gu et al., 2016). The high scores indicated severe neurological functional damage. The investigators were blinded to both the type of surgery and the treatment.

Quantitative Analyses

Image J software (National Institute of Health) was used for quantitative analyses of the data. The quantitative analyses were conducted by two independent examiners blinded to the treatment, and the average of the data was calculated.

Measurement of Infarct Volume

The rats were anesthetized with intraperitoneal administration of 10% chloral hydrate (3 mL/kg). The brain tissues were excised and immediately placed at −20°C for 15 min. Then, the brain tissue was cut evenly into six coronary sections and placed in the 1% TTC for 15 min at 37°C and fixed in 4% paraformaldehyde. The researcher measuring the infarct area was blinded to the treatment group. The infarct volume was quantified and analyzed using Image J software (Li et al., 2020).

H&E Staining

Rats were deeply anesthetized, and the heart was perfused with saline. The brain was removed after perfusion, followed by 4% paraformaldehyde fixation for 24 h. Subsequently, the brain tissues were sectioned at 5-μm thickness using a paraffin slicing machine. Then, the sections were dewaxed with xylene and dehydrated with graded alcohol. Finally, the sections were stained with H&E, as described previously (Feng et al., 2020), and observed under an optical microscope (×400). The sections used in the following staining were observed by two experienced pathologists blinded to the groups.

Nissl Staining

Brain tissue was embedded in paraffin and sliced into 10-μm-thick coronal sections. Next, the slices were dewaxed, rehydrated (Shen et al., 2021), stained for 10 min in methyl violet solution, 2% acetic acid for 6 s, followed by anhydrous ethanol for 30 s and observed under a fluorescent microscope; the neuronal cells were counted and analyzed using Image J.

Terminal Deoxynucleotidyl Transferase (TdT) Deoxyuridine Triphosphate Nick-End Labeling (TUNEL) Staining

The apoptotic brain cells were counted using the TdT-mediated dUTP-streptavidin-HRP method. Then, the sections were dewaxed as described above, and the nucleases were inactivated with the proteinase K. The endogenous peroxidase activity was quenched by adding 3% Triton X-100. The sections were blocked with 1% bovine serum albumin (BSA) and permeabilized with 3% Triton X-100 for 1 h, followed by incubation with the TUNEL detection liquid. Subsequently, the sections were incubated with streptavidin-horseradish peroxidase (HRP) and observed under a microscope at ×400. The number of apoptotic cells in three different fields of non-overlapping brain tissue was counted for further analysis.

NeuN Staining

The sections were dewaxed with xylene and dehydrated with graded alcohol. The antigen was retrieved using proteinase K for 30 min. Then, the sections were incubated with primary antibody (NeuN, 1:20) at 4°C overnight, mounted in glycerin and phosphate-buffered saline (PBS) (1:1), and observed under laser confocal microscopy (×400).

SOD and MDA Assay

The blood serum was collected by centrifugation at 12,000×*g* for 10 min at 4°C. The BCA Protein Assay Kit (Tiangen Biotech, Beijing, China) was used to determine the protein concentration of serum. The MDA and SOD levels were detected using the MDA kit (TBA colorimetry) and the SOD kit (WST-1 method). The OD values of the serum were measured on a microplate reader (Bio-Rad, CA, United States) at 532 and 450 nm.

Cell Culture

Rat adrenal pheochromocytoma PC12 cells were obtained from the Cell Bank of Chinese Academy of Sciences (Shanghai, China) and cultured in Dulbecco's modified Eagle medium (DMEM) (Hyclone, Logan, UT, United States) with 100 μg/mL penicillin-streptomycin solution (Thermo Scientific, Waltham, MA, United States) and 10% fetal bovine serum (FBS; Gibco, Carlsbad, CA, United States) at 37°C under 5% CO_2 and 95% humidified atmosphere.

Oxygen-Glucose Deprivation/Reperfusion (OGD/R) Model and MQ Treatment

Before OGD, the PC12 cells were washed three times with PBS and pretreated for 1 h with MQ (10 μg/mL) and diluted in PBS (0.001 μg/mL) with neurobasal and glucose-free DMEM. Then, the cells were placed in an oxygen-deficiency incubation device with 95% N_2 and 5% CO_2 for 2, 4, and 6 h at 37°C. For reperfusion, PC12 cells were cultured in a normal medium at 37°C for 12 h for subsequent experiments. A normal normoxia medium served as the control.

Methyl Thiazolyl Tetrazolium (MTT) Assay

Cells were inoculated in 96-well culture plates at a density of 1×10^5 cells/mL, and OGD/R was carried out as described above. Then, 20 μL MTT (5 mg/kg) was added to each well for 4 h at 37°C, and the reaction was quenched with 150 μL dimethyl sulfoxide (DMSO). The absorbance was measured at 490 nm on a microplate reader. The percentage of cell viability was calculated as follows: Cell viability (%) = absorbance value of sample/absorbance value of control × 100%.

Annexin V-Fluorescein Isothiocyanate (FITC) Assay

To detect cell apoptosis, Annexin V-FITC assay was conducted according to the manufacturer's protocol. Briefly, PC12 cells were collected by centrifugation at 1,000 *g* for 5 min at 4°C and stained with 200 μL Annexin V-FITC for 15 min and 10 μL propidium iodide (PI) at room temperature in the dark for 15 min. Then, the apoptosis rate of each group was detected by flow cytometry.

ROS Assay

Flow cytometry was used to analyze the generation of intracellular ROS using a fluorescence probe 2′7′-dichlorodihydrofluorescein diacetate (DCFH-DA, Beyotime, China), which was diluted with serum-free medium (1:1,000). Then, the cells were added and the reaction incubated for 30 min at 37°C, followed by PBS washes before analysis (Xiang et al., 2019).

Real-Time Quantitative Polymerase Chain Reaction (RT-qPCR)

The cells were lysed with RNAiso Reagent (TaKaRa, Shiga, Japan) to obtain total RNA. Reverse transcription reaction was carried out using an All-in-One cDNA Synthesis SuperMix assay kit (TaKaRa). The cDNA was synthesized in a 10 μL reaction containing 500 ng of total RNA, 2 μL of 5× qRT Super Mix, and RNase-free water at 42°C for 15 min or 85°C for 2 min. The PCR reaction (20 μL) consisted of 10 μL of 2× SYBR Green qPCR Master Mix kit (Bimake, Shanghai, China), 1 μL of cDNA, 1 μL of each primer, and 7 μL RNase-free water. The reaction conditions were as follows: initial denaturation at 95°C for 5 min, followed by 40 cycles of denaturation at 95°C for 5 s, primer annealing at 55°C for 30 s, and extension at 72°C for 30 s on a 7500 Real-Time PCR System (Applied Biosystems, Shanghai, China). The mRNA expression levels were evaluated using the $2^{-\Delta\Delta Cq}$ method. The primer sequences were as follows: *JNK* (Forward: 5′-GGGCCT TTTTGCTACAGGGT-3′, Reverse: 5′-TTCTTGGTGGATGCG TCCTG-3′), *Bax* (Forward: 5′-TGACGCCTTATGTGGTGACT-3′, Reverse: 5′-TGATGTATGGGTGGTGGAGA-3′), *GAPDH* (Forward: 5′-ACCACAGTCCATGCCATCAC-3′, Reverse: 5′-TCCACCACCCTGTTGCTGTA-3′), *Caspase3* (Forward: 5′-GAGCTTGGAACGCGAAGAAA-3′, Reverse: 5′-TAACCG GGTGCGGTAGAGTA-3′).

Western Blot

Western blot was performed as described previously (Li et al., 2020; Si et al., 2020). The whole-cell lysate was prepared using M-PER Protein Extraction Reagent (Pierce, Rockford, IL, United States) supplemented with protease inhibitor cocktail. The protein concentration was measured using the BCA protein kit (Thermo). The protein lysate was resolved on 10% sodium dodecyl sulfate-polyacrylamide gel electrophoresis (10% SDS-PAGE), according to the molecular weight, and transferred to a nitrocellulose membrane. The membranes were blocked with 5% BSA in Tris-buffered saline with Tween-20 (TBST) at room temperature for 2 h before probing with the primary antibodies against p-JNK, Bax, cleaved Caspase-3, and GAPDH (1:1,000, CST) overnight at 4°C. The immunoreactive proteins were detected using enhanced chemiluminescence (ECL) (Thermo Scientific). All bands were quantified using Image J software.

Statistical Analysis

All statistical analyses of experimental data were carried out using SPSS 17.0 (SPSS, Chicago, IL, United States). Data were reported as mean ± standard error of the mean (SEM). The differences among more than two groups were assessed using one-way analysis of variance (ANOVA) after the assessment of the normal distribution and homogeneity of variance of data, followed by Dunnett's multiple comparison tests. $p < 0.05$ indicated statistically significant difference. Data were analyzed using Image J and Prism 8.0 (GraphPad Software, San Diego, CA, United States).

RESULTS

MQ Increased Reperfusion CBF, Decreased Infarct Volume, and Neurological Deficits in MCAO Rats

To investigate the *in vivo* effect of MQ, we explored the ischemic brain model in SD rats. The cerebral infarction was estimated by TTC staining on the day following artery occlusion. As shown in

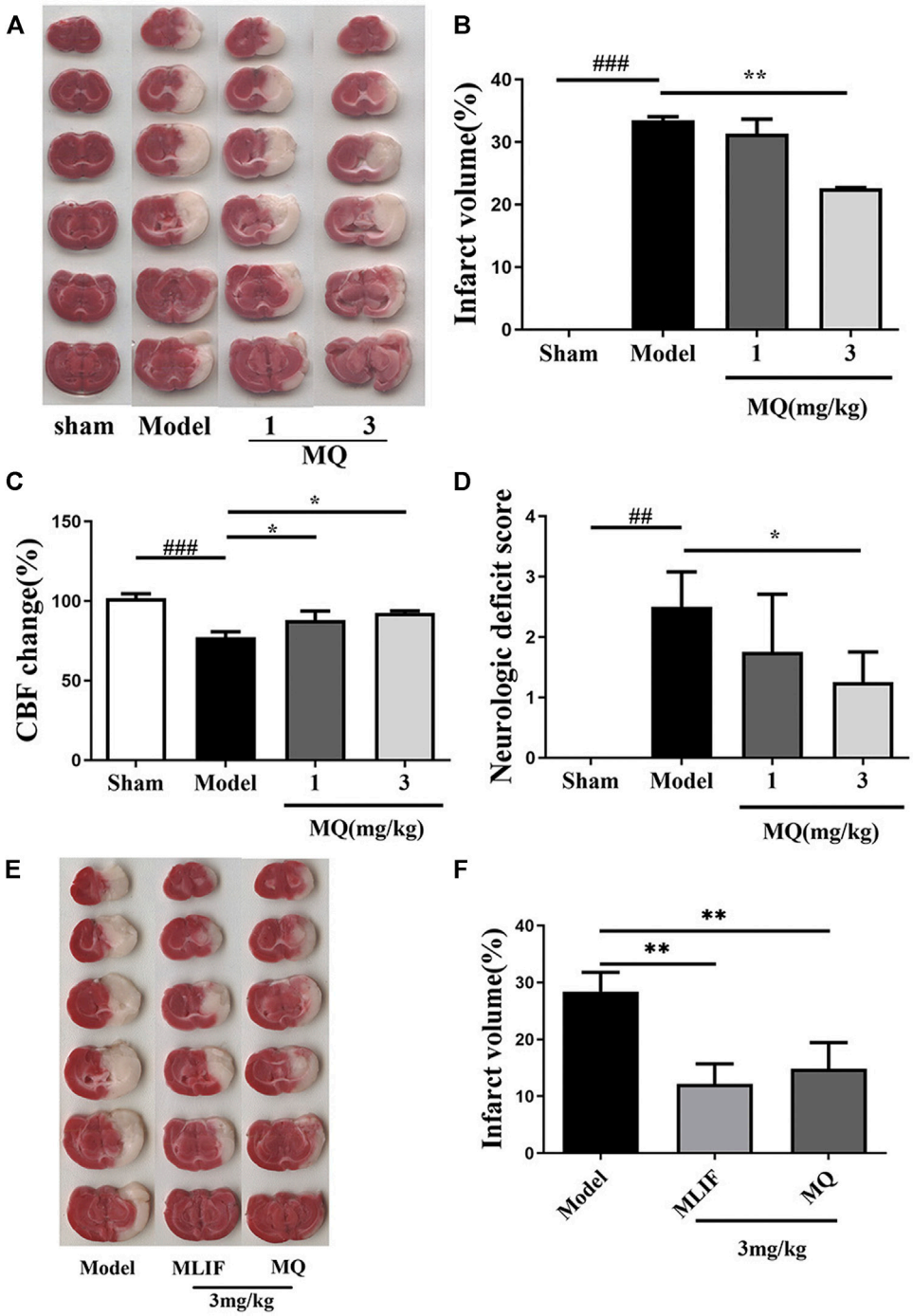

FIGURE 1 | MQ increased reperfusion CBF, decreased infarct volume, and neurological deficits in MCAO rats; MLIF decreased infarct volume similar to MQ. **(A)** TTC staining was used to assess the infarct areas of the brain, **(B)** brain infarct areas were analyzed by Image J to estimate the infarct areas in the whole hemisphere after MCAO, **(C)** effect of MQ on the values of cerebral blood flow after cerebral I/R in rats, **(D)** effects of MQ on the neurological function after cerebral I/R in rats, **(E)** the infarct areas of the model group (28.42 ± 3.08%) increased dramatically compared to those of the sham group, and **(F)** the infarct areas of the MLIF and MQ (11.55 ± 3.81%, 14.85 ± 4.20%) decreased significantly compared to the model group. $^{###}p < 0.001$, Model group vs. Sham group; $^{*}p < 0.05$, $^{**}p < 0.01$, MQ group vs. Model group, $n \geq 3$.

Figure 1A, the infarct areas of the model group (33.46 ± 0.83%) increased significantly compared to those of the sham group ($p < 0.001$). The infarct area of the high-dose group (3 mg/kg) (22.60 ± 0.163%) decreased significantly ($p < 0.01$) compared to the model group (**Figure 1B**). The rate of cerebral blood flow in the rats was measured by a laser Doppler flow analyzer, and a significant

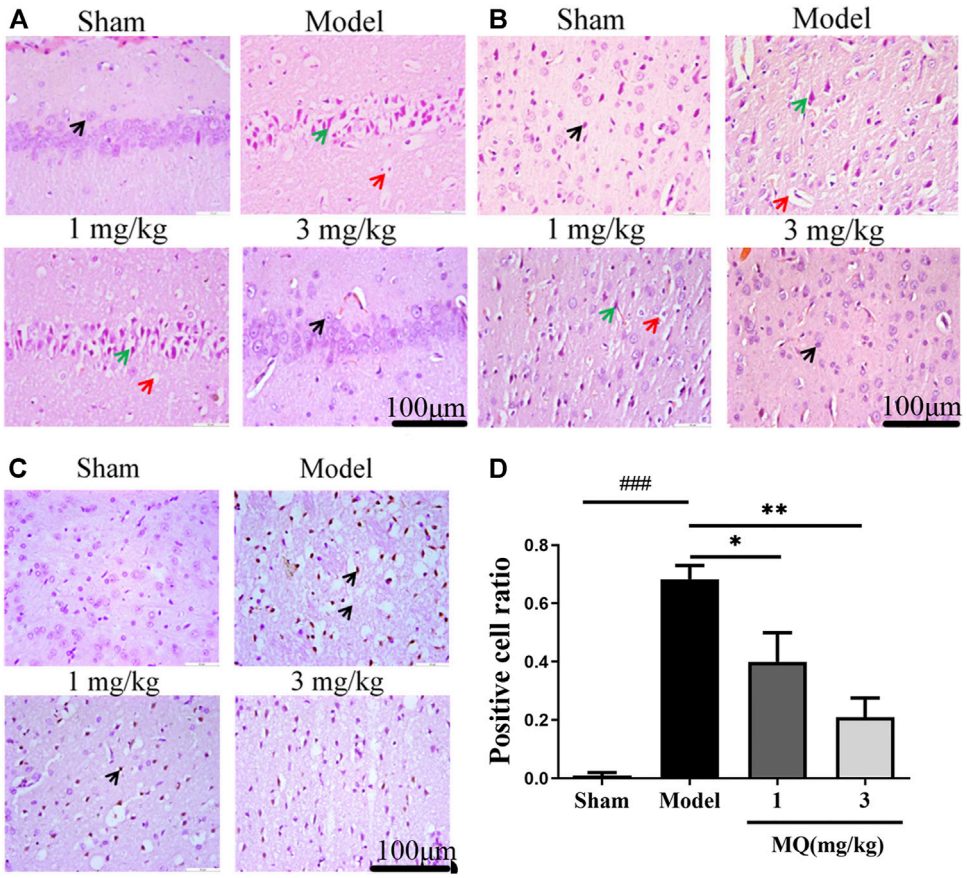

FIGURE 2 | MQ reduced cell apoptosis of the brain in MCAO rats. **(A)** The hippocampi were stained with H&E (magnification ×400), **(B)** the cortices were stained with H&E (magnification ×400). Normal neurons (black arrow), atrophic neurons (green arrow), and cavitation edema neurons (red arrow), **(C)** the cortices were stained with TUNEL (magnification ×400) (D) The percentage of positive cells after I/R in different groups. $^{###}p < 0.001$, Sham group vs. Model group; $^{**}p < 0.01$, Model group vs. 3 mg/kg group; $^{*}p < 0.05$, Model group vs. 1 mg/kg group, $n = 3$.

increase was detected in the low-dose and high-dose groups compared to the model group ($p < 0.05$) (**Figure 1C**). The neurological functions in the rats were observed 24 h after cerebral I/R. The sham group did not show any neurological deficits, while the high-dose group showed a decreasing trend of neurological deficits compared to the model and low-dose groups ($p < 0.05$) (**Figure 1D**).

To compare the neuroprotective effect of MLIF to that of MQ, we assessed the ischemic brain model in SD rats. Cerebral infraction was estimated by TTC staining after the day of artery occlusion. As shown in **Figure 1E**, the infarct areas of the model group (28.42 ± 3.08%) increased dramatically compared to those of the sham group ($p < 0.01$). The infarct area of the MLIF and MQ (3 mg/kg) (11.55 ± 3.81% and 14.85 ± 4.20%, respectively) decreased significantly ($p < 0.01$) compared to that of the model group (**Figure 1F**).

MQ Reduced Cell Apoptosis of the Brain in MCAO Rats

The morphological differences of SD rats were assessed by H&E staining one day after the operation (**Figures 2A,B**). We observed that the cell nucleus was full and clear, the structure was unbroken, and cells were arranged closely in the sham group, while the cell nucleus was shrunk and vacuoles appeared in the model and low-dose groups. Moreover, a large number of cells were detected in the cortex and the hippocampus in the high-dose group of MQ.

TUNEL staining was used to detect the apoptosis of the brain tissues, and the number of TUNEL-positive cells was calculated using Image J software. As shown in **Figure 2D**, no positive neurons were detected in the sham group. However, after treatment with MQ, the low-dose ($p < 0.05$) and the high-dose ($p < 0.01$) groups had fewer dark-brown positive neurons in the cortex compared to the model group. Additionally, we observed that MQ protects the nerve cells after cerebral ischemia injury by reducing apoptosis.

MQ Alleviated Nerve Injury Induced by MCAO

To further assess the neuroprotection of MQ, we performed Nissl staining to count neurons on the day after MCAO. The numbers and morphological changes in Nissl bodies were speculated as

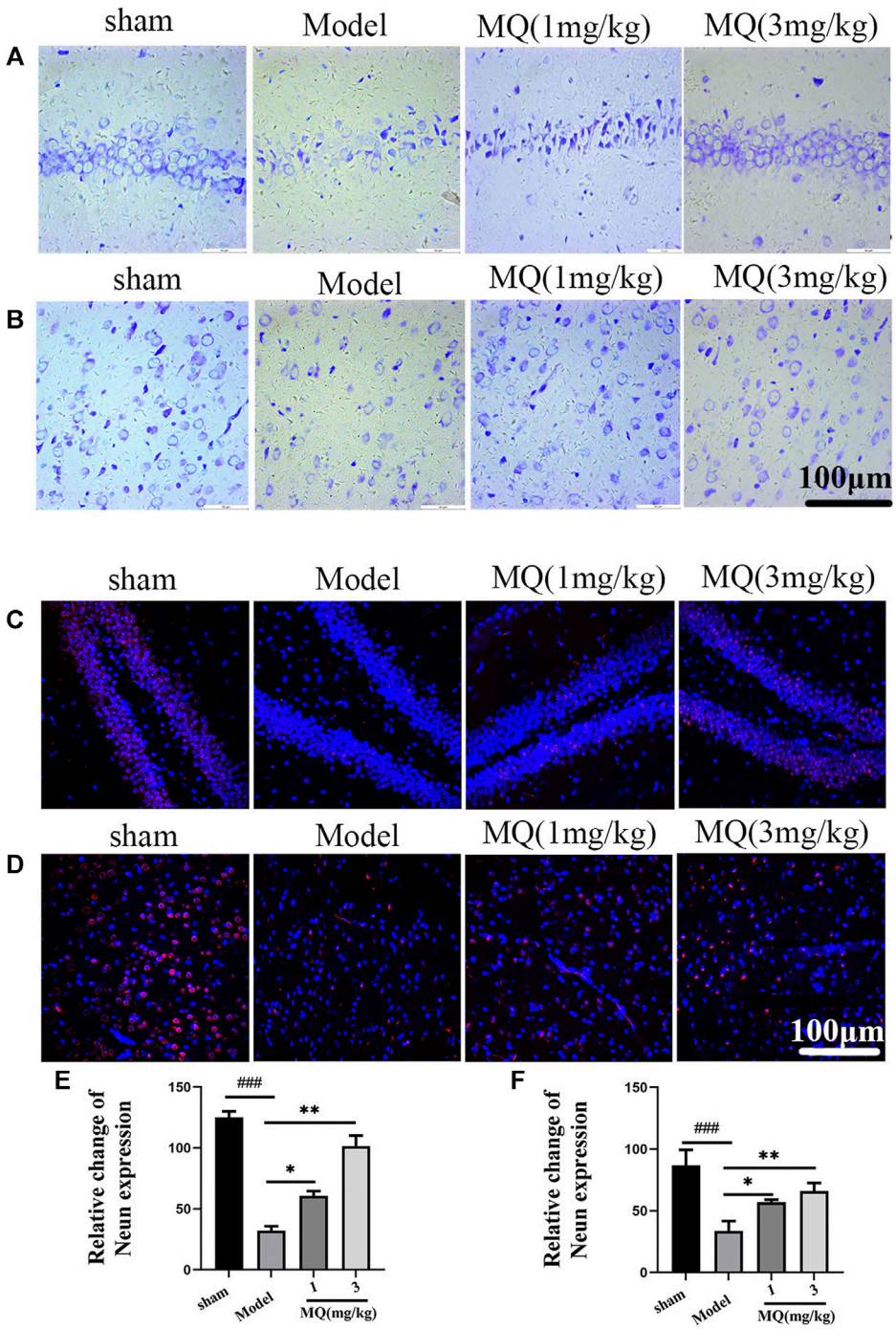

FIGURE 3 | MQ alleviated the nerve injury induced by MCAO **(A)** The hippocampi were stained with Nissl (magnification ×400), **(B)** the cortices were stained with Nissl (magnification ×400), **(C)** the hippocampi were stained with NeuN (magnification ×400), **(D)** the cortices were stained with NeuN (magnification ×400), **(E)** number of nerve cells in hippocampi, **(F)** number of nerve cells in cortices. Dark brown-positive apoptotic cells (black arrow). $^{###}p < 0.001$, $^{##}p < 0.01$, Sham group vs. Model group; $^{***}p < 0.001$, $^{**}p < 0.01$, $^{*}p < 0.05$, MQ group vs. Model group, $n = 3$.

vital components reflecting the growth and development of the neurons and the material energy exchange and functions among nerve cells. As shown in **Figure 3**, the nerve cells were arranged orderly and did not show any damage in the sham group, while in the mode group, the cells were shrunken and disordered. Furthermore, interstitial spaces were detected in the cells, but the number decreased in the model group compared to the sham group ($p < 0.001$). After the treatment with high-dose dipeptide, the number and morphology of the nerve cells were improved significantly ($p < 0.01$).

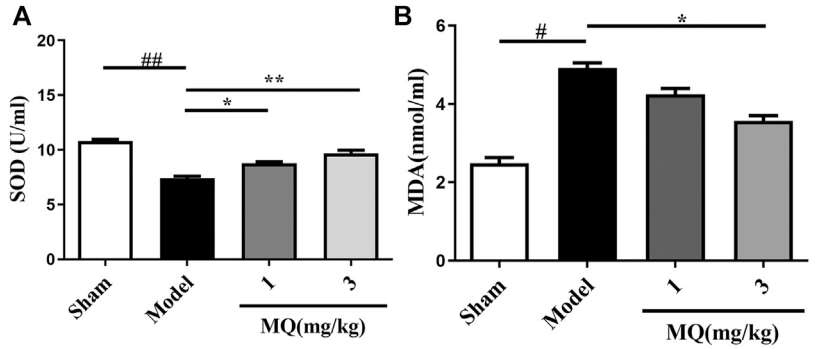

FIGURE 4 | Effects of MQ on the levels of SOD and MDA in MCAO rats. **(A)** The activity of SOD after I/R in different groups, **(B)** the levels of MDA after I/R in different groups. $^{**}p < 0.01$, Model group vs. 3 mg/kg group; $^{**}p < 0.01$, Model group vs. 3 mg/kg group; $^{*}p < 0.05$, Model group vs. 1 mg/kg group, $n = 3$.

NeuN staining revealed the modifications in nerve cells after cerebral ischemia. NeuN-positive cells were marked red, and DAPI-positive cells were marked blue. As shown in **Figure 3**, the number of NeuN-DAPI-positive cells (white arrow) in the high-dose group was more than the number in the model group ($p < 0.01$). These findings indicated that MQ alleviated nerve injury after ischemia.

Effects of MQ on the Levels of SOD and MDA in MCAO Rats

Since oxidative stress plays a major role in MCAO injury, we investigated the effect of MQ on SOD activities and MDA levels in the serum. As shown in **Figure 4A**, an obvious decline was observed in the SOD levels in the serum of the model group compared to that of the sham group ($p < 0.01$). After treatment with MQ, the SOD levels increased subsequently; significant differences were observed in the low-dose ($p < 0.05$) and high-dose ($p < 0.01$) groups vs. the model group. On the other hand, a declining trend was noted in the MDA levels in the high-dose group compared to the model group ($p < 0.05$) (**Figure 4B**).

MQ Decreased Cell Apoptosis in OGD/R-Induced PC12 Cells

To further evaluate the protective roles of MQ, we determined the effect of MQ on OGD/R-induced apoptosis in PC12 Cells. After OGD/R, MTT assay was used to detect the best time of OGD and the optimum concentration of MQ. We found that the cell survival rate was the lowest (32.81 ± 0.828%) after OGD treatment for 2 h. **Figure 5A** shows that the pretreatment with MQ (0.01 and 0.001 μg/mL) showed that the survival rate differed significantly compared to that of the OGD/R group ($p < 0.01$, $p < 0.05$). The results of the flow cytometry showed that the cells treated with 0.01 μg/mL MQ had a lower percentage of total apoptotic cells than the OGD group ($p < 0.01$; **Figure 5B**). Furthermore, the ROS level was decreased in PC12 cells treated with 0.01 μg/L MQ compared to that of the OGD/R group, as revealed by flow cytometry data ($p < 0.01$; **Figure 5C**).

MQ Decreased Cell Apoptosis Via p-JNK/Bax Pathway

As shown in **Figure 6A**, the expression of p-JNK, Bax, and cleaved Caspase 3 proteins was significantly upregulated in the OGD/R group compared to the control group ($p < 0.05$, $p < 0.01$). However, the expression of p-JNK, Bax, and cleaved Caspase 3 declined after treatment with MQ compared to the OGD/R group ($p < 0.05$, $p < 0.01$, and $p < 0.05$, respectively). Compared to the normal control group, the level of p-JNK and Bax proteins was markedly higher ($p < 0.05$); whereas, the treatment with MQ and JNK inhibitors (SP600125) significantly decreased the level of these two proteins compared to the OGD/R group ($p < 0.01$).

We also observed that the mRNA levels of *JNK*, *Bax*, and *Caspase3* decreased after MQ treatment of PC12 cells. The results showed that MQ inhibited cell apoptosis through the p-JNK/Bax pathway.

DISCUSSION

Acute stroke therapy has significantly evolved over the last two decades. Intravenous chemical thrombolysis and intra-arterial mechanical thrombectomy have been utilized worldwide. However, the recovery of blood flow by thrombolytic therapy damaged brain tissues. On the other hand, inhibiting I/R injury is the most effective treatment strategy for alleviating the clinical symptoms (Jin et al., 2017; Koh and Park, 2017). Oxidative stress is involved in reperfusion (Lu et al., 2018), following which the abnormal mitochondria activities caused by I/R injury produce a large amount of ROS (Hsu et al., 2017; Wu et al., 2018) that causes cell apoptosis (Kim et al., 2018) or necrosis (Andrabi et al., 2017; Ji et al., 2017). Interestingly, folk remedies are derived from animal medicine, such as earthworm, hirudo, and *Zaocys dhumnades* conus. The secretions of these animals have also shown to have pharmacological activity; for instance, related peptides secreted by earthworm (Cornwell and Krajniak, 2014), hirudin secreted by hirudo (Ren et al., 2021), and conotoxin secreted by conus (AlSharari et al., 2020). Similarly, MQ is a metabolite of MILF,

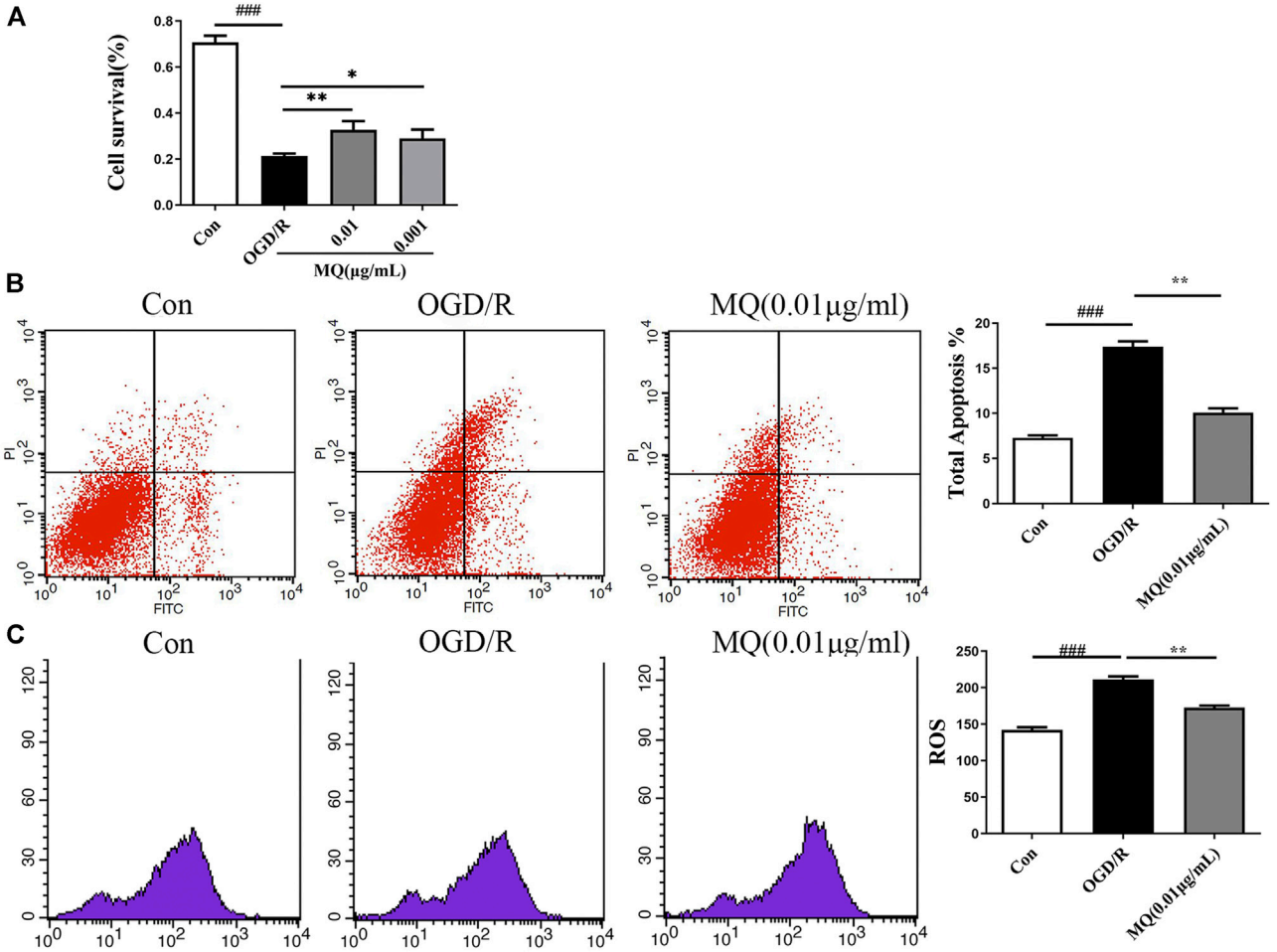

FIGURE 5 | MQ decreased cell apoptosis in OGD/R-induced PC12 cells. **(A)** MTT was used to test PC12 cell viability, **(B)** flow cytometry data showed the percentage of total apoptotic cells compared to the OGD groups, **(C)** flow cytometry data showed the level of ROS in PC12 cells. MQ: 0.01 μg/mL; $^{###}p < 0.001$, control group vs. OGD group, $^{*}p < 0.05$, $^{**}p < 0.01$, MQ group vs. OGD group, $n \geq 3$.

which is also animal secretion from *Entamoeba histolytica*. Several studies have reported the neuroprotective effects of MQ (Jiang et al., 2016; Zhu et al., 2016), which are small molecules and cheaper to produce compared to MLIF. The TTC staining results and infarct volume measurements did not detect any significant difference in the neuroprotection efficacy between MQ and MLIF. MQ exerts an antioxidant effect by decreasing the MDA and increasing the SOD serum content. Simultaneously, MQ significantly downregulated the apoptosis rate and ROS level compared to the OGD/R group.

Apoptosis is programmed cell death, and the process is an energy-dependent manner (D'Arcy, 2019; Farhood et al., 2019). In the early stage of acute ischemia, apoptosis may be a protective reaction of OGD, which maintains the survival of vital cells. However, calcium overload and the release of oxygen free radicals and lysosomal enzymes cause cell death during ischemia (Shi et al., 2015; Secondo et al., 2018; Yang, 2018). Furthermore, Caspase3 is an apoptosis-associated enzyme (Zheng et al., 2019) that plays a key role in cell apoptosis. Cerebral ischemia triggers the release of cytochrome c (cytC) from the mitochondria and promotes the activation of endogenous Caspase3 and apoptosis (Li et al., 2017; Jin et al., 2019; Wang et al., 2019). The two different forms of Caspase3, inactive and active (cleaved Caspase3), were used as the indexes of apoptosis because the expression of cleaved Caspase3 was elevated in the process of cell death (Adams and Cory, 1998). Conversely, the expression of cleaved Caspase3 was decreased in the An-Dong-Niu-Huang-Wan group compared to the MCAO group in ischemia (Wang et al., 2014). The current data showed that MQ treatment downregulated the expression of cleaved Caspase3.

The mitogen-activated protein kinase (MAPK) family proteins are serine-threonine kinases (Wang et al., 2017). The MAPK family mainly consists of c-Jun N-terminal kinases (JNKs), extracellular signal-regulated kinases (ERKs), and P38 (Wang et al., 2017; Chen et al., 2018). ERK1/2 upregulates B cell lymphoma 2 (Bcl-2), JNK regulates the transcription-dependent apoptotic signals to promote cell survival, and p38 is implicated in cell death, cell cycle, senescence, and

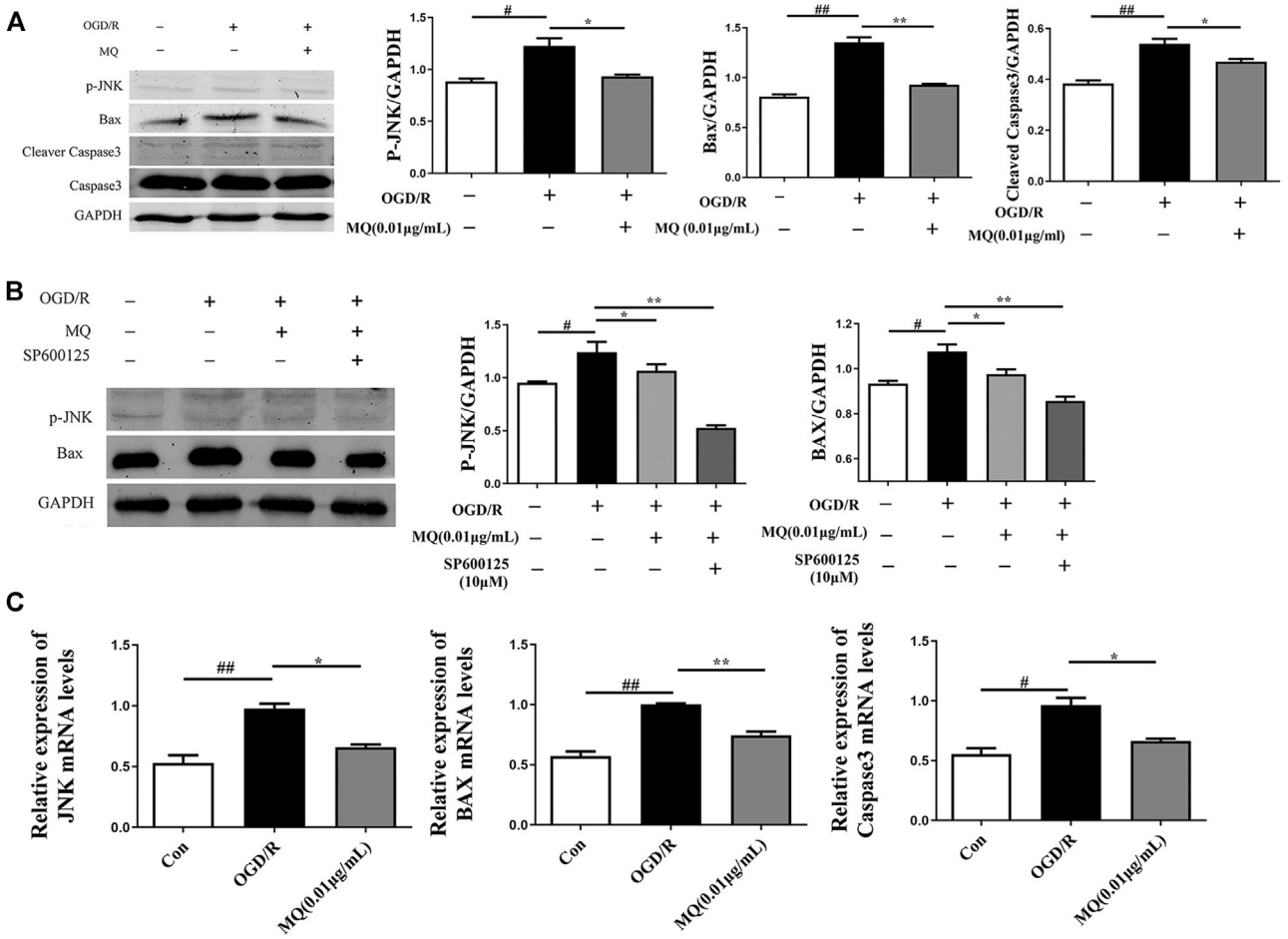

FIGURE 6 | MQ decreased cell apoptosis via p-JNK/Bax pathway. **(A)** Protein expression of p-JNK, Bax, and cleaved Caspase3 levels in PC12 cells, as examined by Western blot, **(B)** representative protein expression of p-JNK and Bax treated with JNK inhibitor (SP600125), as examined by Western blot, **(C)** Effects of MQ on the mRNA levels of *JNK*, *Bax*, and *Caspase3* after OGD/R. $^{\#}p < 0.05$, $^{\#\#}p < 0.01$, OGD/R group vs. Con group; $^{*}p < 0.05$, $^{**}p < 0.01$, OGD/R group vs. MQ 0.01 μg/mL group; $n = 3$.

carcinogenesis (Naoi et al., 2019). The MAPK pathway is triggered by various stimuli and physiological responses, including cell proliferation, differentiation, growth, inflammation, and apoptosis in mammalian cells (Zhang and Liu, 2002). The JNK signaling pathway plays a major role in the CNS, including the regulation of apoptosis and regeneration of both neuronal and glial cells (Salman et al., 2017). A recent study showed that the activation of JNK signaling pathways contributes to oxidative stress in ischemic kidney cell death (Yang et al., 2016). Additionally, the expression of JNKs, ERKs, and P38 and p-JNK, p-ERK, and p-P38 of the MAPK pathway is elevated in the cerebral ischemia mammalian brain model (Ferrer et al., 2003). Our preliminary experiment confirmed that MLIF inhibits the p-JNK/p53 pathway that exerts neural protection (Yao et al., 2011). Based on previous studies, we investigated the effect of MQ on p-JNK expression. The findings demonstrated that the level of p-JNK was markedly downregulated and further reduced by inhibiting the JNK activity with SP600125. The Bcl-2 protein family consists of anti-apoptotic (Bcl-2 and Mcl-1) and proapoptotic (Bax and Bad) molecules (Adams and Cory, 1998; Ruiz et al., 2018). Additional studies confirmed that Bcl-2 protein family adjusts the mitochondrial pathway by controlling the permeability of the outer membrane of the organelle (Sharma et al., 2019). The Bcl-2 proteins are localized in the mitochondria, endoplasmic reticulum, and nuclear membrane and are effective cell apoptosis inhibitors. Although Bax protein exists in the cytoplasm and endothelial surface (Singh et al., 2019), a configurational modification transfers it to the mitochondrial membrane as a response to apoptotic stimuli, such as the activation of Caspase (Bruel et al., 1997; Wolter et al., 1997; Gross et al., 1998). However, the apoptosis adjustment mechanism of Bcl-2 and Bax is not yet clarified. Jin et al. reported that simvastatin alleviated spleen atrophy and spleen cell apoptosis caused by stroke via increased protein expression of Bcl-2 and reduced level of Bax (Jin et al., 2013). In this study, we found that Bax, a JNK downstream protein, plays a role in the mechanism of cerebral ischemia after MQ treatment.

Overall, the current study showed that MQ reduced neurological dysfunction, neuronal injury, cerebral infarction, and the MDA level and increased the SOD level in a rat model, which might be associated with the downregulated oxidation processes. This finding indicates that the treatment of MQ exerts antioxidant and anti-apoptotic effects, rendering it beneficial for stroke because it prevents reperfusion-induced injury. Nevertheless, the current study has some limitations. We studied the protective effect of I/R injury; thrombolysis was not involved as the main treatment. Importantly, MQ can be proposed as an auxiliary treatment as a part of rehabilitation after thrombolysis. Future studies are expected to design therapeutic medicine based on MQ for controlling cerebral I/R injury.

DATA AVAILABILITY STATEMENT

The raw data supporting the conclusions of this article will be made available by the authors, without undue reservation, to any qualified researcher.

ETHICS STATEMENT

The animal study was reviewed and approved by Ethics Committee of Shanghai University.

AUTHOR CONTRIBUTIONS

YZ and TL conceived and designed the study. QZ, ZS, YG, SD, YY constructed the animal model. QZ, JD performed the cell experiments, Western Blot experiments, analyzed the data and wrote the manuscript. YZ, TL and QZ revised the manuscript. All authors read and approved the final manuscript.

FUNDING

This work was supported by the Grants from the National Natural Science Foundation of China (No. 81971017).

REFERENCES

Adams, J. M., and Cory, S. (1998). The Bcl-2 Protein Family: Arbiters of Cell Survival. *Science* 281 (5381), 1322–1326. doi:10.1126/science.281.5381.1322

AlSharari, S. D., Toma, W., Mahmood, H. M., Michael McIntosh, J., and Imad Damaj, M. (2020). The α9α10 Nicotinic Acetylcholine Receptors Antagonist α-conotoxin RgIA Reverses Colitis Signs in Murine Dextran Sodium Sulfate Model. *Eur. J. Pharmacol.* 883, 173320. doi:10.1016/j.ejphar.2020.173320

Andrabi, S. S., Parvez, S., and Tabassum, H. (2017). Progesterone Induced Neuroprotection in Reperfusion Promoted Mitochondrial Dysfunction Following Focal Cerebral Ischemia in Rats. *Dis. Models Mech.* 10 (6), 787–796. doi:10.1242/dmm.025692

Baek, S.-H., Noh, A. R., Kim, K.-A., Akram, M., Shin, Y.-J., Kim, E.-S., et al. (2014). Modulation of Mitochondrial Function and Autophagy Mediates Carnosine Neuroprotection against Ischemic Brain Damage. *Stroke* 45 (8), 2438–2443. doi:10.1161/strokeaha.114.005183

Barrientos-Salcedo, C., Rico-Rosillo, G., Giménez-Scherer, J. A., and Soriano-Correa, C. (2009). Computational Study of the Electronic Structure Characterization of a Novelanti-Inflammatory Tripeptide Derived from Monocyte Locomotion Inhibitoryfactor (MLIF)-pentapeptide. *Eur. J. Med. Chem.* 44 (8), 3114–3119. doi:10.1016/j.ejmech.2009.03.003

Bruel, A., Karsenty, E., Schmid, M., McDonnell, T. J., and Lanotte, M. (1997). Altered Sensitivity to Retinoid-Induced Apoptosis Associated with Changes in the Subcellular Distribution of Bcl-2. *Exp. Cel Res.* 233 (2), 281–287. doi:10.1006/excr.1997.3594

Chen, K., Lu, Y., Liu, C., Zhang, L., Fang, Z., and Yu, G. (2018). Morroniside Prevents H2O2 or Aβ1-42-Induced Apoptosis via Attenuating JNK and P38 MAPK Phosphorylation. *Eur. J. Pharmacol.* 834, 295–304. doi:10.1016/j.ejphar.2018.07.047

Cornwell, F. J., and Krajniak, K. G. (2014). The Effects of FMRFamide and its Related Peptides on the Isolated Crop-Gizzard of the Earthworm Lumbricus Terrestris. *Integr. Comp. Biol.* 54, E257. doi:10.1016/s1095-6433(99)00083-5

D'Arcy, M. S. (2019). Cell Death: a Review of the Major Forms of Apoptosis, Necrosis and Autophagy. *Cell Biol Int* 43 (6), 582–592. doi:10.1002/cbin.11137

Fan, Y.-Y., Hu, W.-W., Dai, H.-B., Zhang, J.-X., Zhang, L.-Y., He, P., et al. (2011). Activation of the central Histaminergic System Is Involved in Hypoxia-Induced Stroke Tolerance in Adult Mice. *J. Cereb. Blood Flow Metab.* 31 (1), 305–314. doi:10.1038/jcbfm.2010.94

Farhood, B., Najafi, M., and Mortezaee, K. (2019). CD8+cytotoxic T Lymphocytes in Cancer Immunotherapy: A Review. *J. Cel Physiol* 234 (6), 8509–8521. doi:10.1002/jcp.27782

Feng, C., Wan, H., Zhang, Y., Yu, L., Shao, C., He, Y., et al. (2020). Neuroprotective Effect of Danhong Injection on Cerebral Ischemia-Reperfusion Injury in Rats by Activation of the PI3K-Akt Pathway. *Front. Pharmacol.* 11, 13. doi:10.3389/fphar.2020.00298

Ferrer, I., Friguls, B., Dalfó, E., and Planas, A. M. (2003). Early Modifications in the Expression of Mitogen-Activated Protein Kinase (MAPK/ERK), Stress-Activated Kinases SAPK/JNK and P38, and Their Phosphorylated Substrates Following Focal Cerebral Ischemia. *Acta Neuropathol.* 105 (5), 425–437. doi:10.1007/s00401-002-0661-2

Genrikhs, E. E., Voronkov, D. N., Kapkaeva, M. R., Gudasheva, T. A., Glibka, Y. A., Isaev, N. K., et al. (2018). The Delayed Protective Effect of GK-2, A Dipeptide Mimetic of Nerve Growth Factor, in a Model of Rat Traumatic Brain Injury. *Brain Res. Bull.* 140, 148–153. doi:10.1016/j.brainresbull.2018.05.002

Gross, A., Jockel, J., Wei, M. C., and Korsmeyer, S. J. (1998). Enforced Dimerization of BAX Results in its Translocation, Mitochondrial Dysfunction and Apoptosis. *Embo j* 17 (14), 3878–3885. doi:10.1093/emboj/17.14.3878

Gu, J., Chen, J., Yang, N., Hou, X., Wang, J., Tan, X., et al. (2016). Combination of Ligusticum Chuanxiong and Radix Paeoniae Ameliorate Focal Cerebral Ischemic in MCAO Rats via Endoplasmic Reticulum Stress-dependent Apoptotic Signaling Pathway. *J. Ethnopharmacology* 187, 313–324. doi:10.1016/j.jep.2016.04.024

Hsu, L.-W., Shiao, W.-C., Chang, N.-C., Yu, M.-C., Yen, T.-L., Thomas, P. A., et al. (2017). The Neuroprotective Effects of Tao-Ren-Cheng-Qi Tang against Embolic Stroke in Rats. *Chin. Med.* 12, 112. doi:10.1186/s13020-017-0128-y

Ji, Y., Yan, X., Hu, Y., Xue, H., Sun, J., Chen, H., et al. (2017). DhHP-6 Attenuates Cerebral Ischemia-Reperfusion Injury in Rats through the Inhibition of Apoptosis. *Mol. Med. Rep.* 16 (5), 7229–7236. doi:10.3892/mmr.2017.7569

Jiang, S., Liu, Y., Wang, J., Zhang, Y., Rui, Y., Zhang, Y., et al. (2016). Cardioprotective Effects of Monocyte Locomotion Inhibitory Factor on Myocardial Ischemic Injury by Targeting Vimentin. *Life Sci.* 167, 85–91. doi:10.1016/j.lfs.2016.10.021

Jin, J., Sun, H., Liu, D., Wang, H., Liu, Q., Chen, H., et al. (2019). LRG1 Promotes Apoptosis and Autophagy through the TGFβ-Smad1/5 Signaling Pathway to Exacerbate Ischemia/Reperfusion Injury. *Neuroscience* 413, 123–134. doi:10.1016/j.neuroscience.2019.06.008

Jin, R., Zhu, X., Liu, L., Nanda, A., Granger, D. N., and Li, G. (2013). Simvastatin Attenuates Stroke-Induced Splenic Atrophy and Lung Susceptibility to Spontaneous Bacterial Infection in Mice. *Stroke* 44 (4), 1135–1143. doi:10.1161/strokeaha.111.000633

Jin, Y., Barnett, A., Zhang, Y., Yu, X., and Luo, Y. (2017). Poststroke Sonic Hedgehog Agonist Treatment Improves Functional Recovery by Enhancing Neurogenesis and Angiogenesis. *Stroke* 48 (6), 1636–1645. doi:10.1161/strokeaha.117.016650

Kim, S. W., Kim, I. K., Ha, J. H., Yeo, C. D., Kang, H. H., Kim, J. W., et al. (2018). Normobaric Hyperoxia Inhibits the Progression of Lung Cancer by Inducing Apoptosis. *Exp. Biol. Med. (Maywood)* 243 (9), 739–748. doi:10.1177/1535370218774737

Koh, S.-H., and Park, H.-H. (2017). Neurogenesis in Stroke Recovery. *Transl. Stroke Res.* 8 (1), 3–13. doi:10.1007/s12975-016-0460-z

Kretschmer, R. R., Castro, E. M., Rico, G., Pacheco, G., Noriega, R., and Arellano, J. (1989). Further Characterization of a Human Monocyte Locomotion Inhibitory Factor Produced by Axenically grownEntamoeba Histolytica. *Parasitol. Res.* 75 (3), 245–246. doi:10.1007/bf00931283

Kretschmer, R. R., Rico, G., and Giménez, J. A. (2001). A Novel Anti-inflammatory Oligopeptide Produced by Entamoeba Histolytica. *Mol. Biochem. Parasitol.* 112 (2), 201–209. doi:10.1016/s0166-6851(00)00367-4

Lapchak, P. A., and Zhang, J. H. (2017). The High Cost of Stroke and Stroke Cytoprotection Research. *Transl. Stroke Res.* 8 (4), 307–317. doi:10.1007/s12975-016-0518-y

Lee, Y. A., Kim, K. A., Min, A., and Shin, M. H. (2019). NOX4 Activation Is Involved in ROS-dependent Jurkat T-cell Death Induced by Entamoeba Histolytica. *Parasite Immunol.* 41 (11), 7. doi:10.1111/pim.12670

Li, H., Han, W., Wang, H., Ding, F., Xiao, L., Shi, R., et al. (2017). Tanshinone IIA Inhibits Glutamate-Induced Oxidative Toxicity through Prevention of Mitochondrial Dysfunction and Suppression of MAPK Activation in SH-Sy5y Human Neuroblastoma Cells. *Oxidative Med. Cell Longevity* 2017, 1–13. doi:10.1155/2017/4517486

Li, L., Sun, L., Qiu, Y., Zhu, W., Hu, K., and Mao, J. (2020). Protective Effect of Stachydrine against Cerebral Ischemia-Reperfusion Injury by Reducing Inflammation and Apoptosis through P65 and JAK2/STAT3 Signaling Pathway. *Front. Pharmacol.* 11, 64. doi:10.3389/fphar.2020.00064

Liang, H., Liu, P., Wang, Y., Song, S., and Ji, A. (2011). Protective Effects of Alkaloid Extract from Leonurus Heterophyllus on Cerebral Ischemia Reperfusion Injury by Middle Cerebral Ischemic Injury (MCAO) in Rats. *Phytomedicine* 18 (10), 811–818. doi:10.1016/j.phymed.2011.01.020

Liang, X., Hu, Q., Li, B., McBride, D., Bian, H., Spagnoli, P., et al. (2014). Follistatin-Like 1 Attenuates Apoptosis via Disco-Interacting Protein 2 Homolog A/Akt Pathway after Middle Cerebral Artery Occlusion in Rats. *Stroke* 45 (10), 3048–3054. doi:10.1161/strokeaha.114.006092

Liu, X., Hu, P., Wang, Y., Wang, X., Huang, J., Li, J., et al. (2018). A Validated UPLC-MS/MS Method for the Quantitation of an Unstable Peptide, Monocyte Locomotion Inhibitory Factor (MLIF) in Human Plasma and its Application to a Pharmacokinetic Study. *J. Pharm. Biomed. Anal.* 157, 75–83. doi:10.1016/j.jpba.2018.04.009

Longa, E. Z., Weinstein, P. R., Carlson, S., and Cummins, R. (1989). Reversible Middle Cerebral Artery Occlusion without Craniectomy in Rats. *Stroke* 20 (1), 84–91. doi:10.1161/01.str.20.1.84

Lu, H., Wang, B., Cui, N., and Zhang, Y. (2018). Artesunate Suppresses Oxidative and Inflammatory Processes by Activating Nrf2 and ROS-dependent P38 MAPK and Protects against Cerebral Ischemia-reperfusion Injury. *Mol. Med. Rep.* 17 (5), 6639–6646. doi:10.3892/mmr.2018.8666

Naoi, M., Wu, Y., Shamoto-Nagai, M., and Maruyama, W. (2019). Mitochondria in Neuroprotection by Phytochemicals: Bioactive Polyphenols Modulate Mitochondrial Apoptosis System, Function and Structure. *Int. J. Mol. Sci.* 20 (10), 2451. doi:10.3390/ijms20102451

Poustchi, F., Amani, H., Ahmadian, Z., Niknezhad, S. V., Mehrabi, S., Santos, H. A., et al. (2021). Combination Therapy of Killing Diseases by Injectable Hydrogels: From Concept to Medical Applications. *Adv. Healthc. Mater.* 10 (3), 2001571. doi:10.1002/adhm.202001571

Povarnina, P. Y., Vorontsova, O. N., Gudasheva, T. A., Ostrovskaya, R. U., and Seredenin, S. B. (2013). Original Nerve Growth Factor Mimetic Dipeptide GK-2 Restores Impaired Cognitive Functions in Rat Models of Alzheimer's Disease. *Acta Naturae* 5 (3), 84–91. doi:10.32607/20758251-2013-5-3-84-91

Ren, K., Gong, H., Hu, L., He, K., Yu, A., Hu, S., et al. (2021). Study on the Activity of Recombinant Mutant Tissue-type Plasminogen Activator Fused with the C-Terminal Fragment of Hirudin. *J. Thromb. Thrombolysis* 11, 121. doi:10.1007/s11239-021-02440-4

Rico, G., Arellano, J., and Kretschmer, R. R. (1998). The Human Monocyte Locomotion-Inhibitory Factor Produced by Entamoeba Histolytica Does Not Inhibit the Locomotion of Human Eosinophils. *Parasitol. Res.* 84 (6), 522–523. doi:10.1007/s004360050441

Rojas-Dotor, S., Araujo-Monsalvo, V. M., Sánchez-Rojas, M. J., and Domínguez-Hernández, V. M. (2018). The Monocyte Locomotion Inhibitory Factor Inhibits the Expression of Inflammation-Induced Cytokines Following Experimental Contusion in Rat Tibia. *Scand. J. Immunol.* 88 (3), e12702. doi:10.1111/sji.12702

Rojas-Dotor, S., Rico, G., Pérez, J., Velázquez, J., Silva, R., Morales, E., et al. (2006). Cytokine Expression in CD4+ Cells Exposed to the Monocyte Locomotion Inhibitory Factor Produced by Entamoeba Histolytica. *Parasitol. Res.* 98 (5), 493–495. doi:10.1007/s00436-005-0090-y

Ruiz, A., Alberdi, E., and Matute, C. (2018). Mitochondrial Division Inhibitor 1 (Mdivi-1) Protects Neurons against Excitotoxicity through the Modulation of Mitochondrial Function and Intracellular Ca2+ Signaling. *Front. Mol. Neurosci.* 11, 16. doi:10.3389/fnmol.2018.00003

Sairanen, T., Szepesi, R., Karjalainen-Lindsberg, M.-L., Saksi, J., Paetau, A., and Lindsberg, P. J. (2009). Neuronal Caspase-3 and PARP-1 Correlate Differentially with Apoptosis and Necrosis in Ischemic Human Stroke. *Acta Neuropathol.* 118 (4), 541–552. doi:10.1007/s00401-009-0559-3

Salman, M. M., Kitchen, P., Woodroofe, M. N., Bill, R. M., Conner, A. C., Heath, P. R., et al. (2017). Transcriptome Analysis of Gene Expression Provides New Insights into the Effect of Mild Therapeutic Hypothermia on Primary Human Cortical Astrocytes Cultured under Hypoxia. *Front. Cel. Neurosci.* 11, 15. doi:10.3389/fncel.2017.00386

Secondo, A., Bagetta, G., and Amantea, D. (2018). On the Role of Store-Operated Calcium Entry in Acute and Chronic Neurodegenerative Diseases. *Front. Mol. Neurosci.* 11, 14. doi:10.3389/fnmol.2018.00087

Sharma, A., Boise, L., and Shanmugam, M. (2019). Cancer Metabolism and the Evasion of Apoptotic Cell Death. *Cancers* 11 (8), 1144. doi:10.3390/cancers11081144

Shen, L., Zhang, T., Yang, Y., Lu, D., Xu, A., and Li, K. (2021). FPS-ZM1 Alleviates Neuroinflammation in Focal Cerebral Ischemia Rats via Blocking Ligand/RAGE/DIAPH1 Pathway. *ACS Chem. Neurosci.* 12 (1), 63–78. doi:10.1021/acschemneuro.0c00530

Shi, J., Gu, J.-h., Dai, C.-l., Gu, J., Jin, X., Sun, J., et al. (2015). O-GlcNAcylation Regulates Ischemia-Induced Neuronal Apoptosis through AKT Signaling. *Sci. Rep.* 5, 14500. doi:10.1038/srep14500

Si, W., Li, B., Lenahan, C., Li, S., Gu, R., Qu, H., et al. (2020). AT1R/GSK-3β/mTOR Signaling Pathway Involved in Angiotensin II-Induced Neuronal Apoptosis after HIE Both *In Vitro* and *In Vivo*. *Oxid Med. Cel Longev.* 2020, 1–14. doi:10.1155/2020/8864323

Silva-García, R., Estrada-García, I., Ramos-Payán, R., Torres-Salazar, A., Morales-Martínez, M. E., Arenas-Aranda, D., et al. (2008). The Effect of an Anti-inflammatory Pentapeptide Produced by Entamoeba Histolytica on Gene Expression in the U-937 Monocytic Cell Line. *Inflamm. Res.* 57 (4), 145–150. doi:10.1007/s00011-007-6199-y

Silva-García, R., and Rico-Rosillo, G. (2011). Anti-inflammatory Defense Mechanisms of Entamoeba Histolytica. *Inflamm. Res.* 60 (2), 111–117. doi:10.1007/s00011-010-0261-x

Singh, R., Letai, A., and Sarosiek, K. (2019). Regulation of Apoptosis in Health and Disease: the Balancing Act of BCL-2 Family Proteins. *Nat. Rev. Mol. Cel Biol.* 20 (3), 175–193. doi:10.1038/s41580-018-0089-8

Soares, N. M., Azevedo, H. C., Pacheco, F. T. F., de Souza, J. N., Del-Rei, R. P., Teixeira, M. C. A., et al. (2019). A Cross-Sectional Study ofEntamoeba histolytica/dispar/moshkovskiiComplex in Salvador, Bahia, Brazil. *Biomed. Res. Int.* 2019, 1–7. doi:10.1155/2019/7523670

Utrera-Barillas, D., Velazquez, J. R., Enciso, A., Muñoz Cruz, S., Rico, G., Curiel-Quesada, E., et al. (2003). An Anti-inflammatory Oligopeptide Produced byEntamoeba Histolyticadown-Regulates the Expression of Pro-inflammatory Chemokines. *Parasite Immunol.* 25 (10), 475–482. doi:10.1111/j.1365-3024.2003.00657.x

Wang, G.-H., Lan, R., Zhen, X.-D., Zhang, W., Xiang, J., and Cai, D.-F. (2014). An-Gong-Niu-Huang Wan Protects against Cerebral Ischemia Induced Apoptosis in Rats: Up-Regulation of Bcl-2 and Down-Regulation of Bax and Caspase-3. *J. Ethnopharmacology* 154 (1), 156–162. doi:10.1016/j.jep.2014.03.057

Wang, T., Liao, Y., Sun, Q., Tang, H., Wang, G., Zhao, F., et al. (2017). Upregulation of Matrix Metalloproteinase-9 in Primary Cultured Rat Astrocytes Induced by 2-Chloroethanol via MAPK Signal Pathways. *Front. Cel. Neurosci.* 11, 10. doi:10.3389/fncel.2017.00218

Wang, Y. Q., Tang, Y. F., Yang, M. K., and Huang, X. Z. (2019). Dexmedetomidine Alleviates Cerebral Ischemia-reperfusion Injury in Rats via Inhibition of Hypoxia-inducible Factor-1α. *J. Cel Biochem.* 120 (5), 7834–7844. doi:10.1002/jcb.28058

Wingfield, T., Ball, R., Woolley, S. D., Campbell, F., Heath, R. M., Beeching, N. J., et al. (2018). The Brief Case: A Rare Case of Invasive Amebiasis Requiring Emergency Subtotal Colectomy in an HIV-Positive Man. *J. Clin. Microbiol.* 56 (8), 8. doi:10.1128/jcm.01703-17

Wolter, K. G., Hsu, Y.-T., Smith, C. L., Nechushtan, A., Xi, X.-G., and Youle, R. J. (1997). Movement of Bax from the Cytosol to Mitochondria during Apoptosis. *J. Cel Biol.* 139 (5), 1281–1292. doi:10.1083/jcb.139.5.1281

Wu, M.-Y., Yiang, G.-T., Liao, W.-T., Tsai, A. P.-Y., Cheng, Y.-L., Cheng, P.-W., et al. (2018). Current Mechanistic Concepts in Ischemia and Reperfusion Injury. *Cell Physiol Biochem.* 46 (4), 1650–1667. doi:10.1159/000489241

Wu, Q., Mao, Z., Liu, J., Huang, J., and Wang, N. (2020). Ligustilide Attenuates Ischemia Reperfusion-Induced Hippocampal Neuronal Apoptosis via Activating the PI3K/Akt Pathway. *Front. Pharmacol.* 11, 10. doi:10.3389/fphar.2020.00979

Xiang, J., Zhang, J., Cai, X., Yang, F., Zhu, W., Zhang, W., et al. (2019). Bilobalide Protects Astrocytes from Oxygen and Glucose Deprivation-induced Oxidative Injury by Upregulating Manganese Superoxide Dismutase. *Phytotherapy Res.* 33 (9), 2329–2336. doi:10.1002/ptr.6414

Yang, C.-F. (2018). Clinical Manifestations and Basic Mechanisms of Myocardial Ischemia/reperfusion Injury. *Tzu Chi Med. J.* 30 (4), 209–215. doi:10.4103/tcmj.tcmj_33_18

Yang, Y., Zhang, S., Fan, C., Yi, W., Jiang, S., Di, S., et al. (2016). Protective Role of Silent Information Regulator 1 against Hepatic Ischemia: Effects on Oxidative Stress Injury, Inflammatory Response, and MAPKs. *Expert Opin. Ther. Targets* 20 (5), 519–531. doi:10.1517/14728222.2016.1153067

Yao, J., Xu, Y., Ji, F., Wang, C., Zhang, Y., Ni, J., et al. (2011). Protective Effects of MLIF Analogs on Cerebral Ischemia-Reperfusion Injury in Rats. *Peptides* 32 (5), 1047–1054. doi:10.1016/j.peptides.2011.03.005

Zhang, W., and Liu, H. T. (2002). MAPK Signal Pathways in the Regulation of Cell Proliferation in Mammalian Cells. *Cell Res.* 12 (1), 9–18. doi:10.1038/sj.cr.7290105

Zhang, Y., Chen, J., Li, F., Li, D., Xiong, Q., Lin, Y., et al. (2012). A Pentapeptide Monocyte Locomotion Inhibitory Factor Protects Brain Ischemia Injury by Targeting the eEF1A1/Endothelial Nitric Oxide Synthase Pathway. *Stroke* 43 (10), 2764–2773. doi:10.1161/strokeaha.112.657908

Zheng, J.-H., Xie, L., Li, N., Fu, Z.-Y., Tan, X.-F., Tao, R., et al. (2019). PD98059 Protects the Brain against Mitochondrial-Mediated Apoptosis and Autophagy in a Cardiac Arrest Rat Model. *Life Sci.* 232, 116618. doi:10.1016/j.lfs.2019.116618

Zhu, Q., Zhang, Y., Liu, Y., Cheng, H., Wang, J., Zhang, Y., et al. (2016). MLIF Alleviates SH-Sy5y Neuroblastoma Injury Induced by Oxygen-Glucose Deprivation by Targeting Eukaryotic Translation Elongation Factor 1A2. *Plos One* 11 (2), e0149965. doi:10.1371/journal.pone.0149965

Conflict of Interest: The authors declare that the research was conducted in the absence of any commercial or financial relationships that could be construed as a potential conflict of interest.

frontiers in Pharmacology

ORIGINAL RESEARCH
published: 25 June 2021
doi: 10.3389/fphar.2021.673366

Traditional Chinese Medication Tongxinluo Attenuates Lipidosis in Ox-LDL-Stimulated Macrophages by Enhancing Beclin-1-Induced Autophagy

*Yifei Chen[1,2], Fangpu Yu[1], Yu Zhang[1], Mengmeng Li[1], Mingxue Di[1], Weijia Chen[1], Xiaolin Liu[1], Yun Zhang[1] and Mei Zhang[1]**

[1]The Key Laboratory of Cardiovascular Remodeling and Function Research, Chinese Ministry of Education, Chinese National Health Commission and Chinese Academy of Medical Sciences, The State and Shandong Province Joint Key Laboratory of Translational Cardiovascular Medicine, Qilu Hospital of Shandong University, Jinan, China, [2]Department of Echocardiography, Beijing Anzhen Hospital, Capital Medical University, Beijing, China

Tongxinluo (TXL), a traditional Chinese medication, plays a key role in the formation and progression of plaques in atherosclerosis. The formation of foam cells by macrophages accelerates the destabilisation of plaques. In previous research, we had found that TXL significantly inhibits ox-LDL-induced apoptosis in macrophages *in vitro* by improving the dissociation of the Beclin-1-Bcl-2 complex. Therefore, here, we explored the effect of TXL on lipid metabolism in macrophages and the mechanism involved. To evaluate the role of TXL in atherosclerotic plaques, we construct the atherosclerotic animal model with lentiviral injection and performed immunofluorescence staining analysis *in vivo*. Western blot, immunofluorescence staining and microscopy were performed to elucidate the mechanism underlying TXL-mediated regulation of autophagy in THP-1 macrophages *in vitro*. Immunofluorescence assay revealed that TXL treatment inhibited lipid deposition in advanced atherosclerotic plaques. *In vitro* TXL treatment inhibited lipid deposition in THP-1 macrophages by enhancing autophagy via Beclin-1. TXL reversed the high expression of class I histone deacetylases (HDACs) induced by ox-LDL ($p < 0.05$). Compared with the TXL + ox-LDL group, TXL failed to promote intracellular lipid droplet decomposition after the addition of the histone deacetylase agonist. We found that TXL attenuates the accumulation of lipids in macrophage by enhancing Beclin-1-induced autophagy, and additionally, it inhibits the inhibitory effect of class I HDAC on the expression of Beclin-1.

Keywords: atherosclerosis, tongxinluo, macrophages, lipid metabolism, autophagy

OPEN ACCESS

Edited by:
Zhang Yuefan,
Shanghai University, China

Reviewed by:
Min Wu,
China Academy of Chinese Medical Sciences, China
Xianwei Wang,
Xinxiang Medical University, China

****Correspondence:***
Mei Zhang
daixh@vip.sina.com

Specialty section:
This article was submitted to Ethnopharmacology, a section of the journal Frontiers in Pharmacology

Received: *27 February 2021*
Accepted: *15 June 2021*
Published: *25 June 2021*

Citation:
Chen Y, Yu F, Zhang Y, Li M, Di M, Chen W, Liu X, Zhang Y and Zhang M (2021) Traditional Chinese Medication Tongxinluo Attenuates Lipidosis in Ox-LDL-Stimulated Macrophages by Enhancing Beclin-1-Induced Autophagy. Front. Pharmacol. 12:673366. doi: 10.3389/fphar.2021.673366

INTRODUCTION

Atherosclerosis is a chronic inflammatory disease caused because of lipid dysfunction that occurs in the walls of the large and middle arterial blood vessels (Lusis, 2000). In the initial stages of atherosclerosis, endothelial function is disturbed and apolipoprotein B lipoproteins, such as low-density lipoprotein (LDL), are retained in the subendothelium, while the endothelium is activated to secrete chemokines and monocyte adhesion molecules. After monocytes enter the vascular

endothelium, they differentiate into macrophages, which take up the subcutaneous lipoproteins. With the accumulation of lipids in macrophages, large amounts of lipid droplets (LDs) accumulate in the cytoplasm of macrophages, which eventually transform into foam cells. As a major component of atherosclerotic lesions, foam cells play a particularly important role in the development of atherosclerosis. The formation of foam cells can promote the development of atherosclerosis (Mannarino and Pirro, 2008; Libby et al., 2011; Moore et al., 2013). Therefore, the reduction in the conversion of macrophages to foam cells will be an effective therapeutic strategy for reversing plaque lipid accumulation.

Cholesteryl esters (CEs), which are taken up into macrophage lipoproteins, are hydrolysed to free cholesterol (FC) and fatty acids. It has been found that the ATP-binding cassette transporters ABCA1 and ABCG1 play an important role in the transfer of FCs to the extracellular surface of the cells. Knockout of ABCA1 and ABCG1 in macrophages promotes atherosclerosis in mice (Westerterp et al., 2014).

Autophagy is a conserved cellular catabolism process in which the cytoplasmic components are encapsulated by autophagosomes that fuse with lysosomes to form autolysosomes, where they undergo substance degradation (Levine and Kroemer, 2019). The autophagy of cytoplasmic lipid droplets, also known as lipophagy, involves catalysis of the triglycerides stored in cells and promotes fatty acid oxidation to maintain cellular energy homeostasis (Singh et al., 2009). By increasing autophagy, cells can enhance the absorption and re-decomposition of oxidised LDL and acetylated lipoprotein, thereby enhancing plaque stability. In addition to the cholesterol transport pathway, autophagy-lysosome system is another important way to regulate intracellular cholesterol metabolism (Ouimet et al., 2011; Robinet et al., 2013).

Tongxinluo (TXL) is a traditional Chinese medicine made of 12 kinds of animal and plant products. Since its approval by the State Drug Administration of China in 1996, it has been widely used in the treatment of various cardiovascular diseases such as atherosclerosis (Chen et al., 2009; Hao et al., 2015). A large number of clinical and basic studies have found that TXL has anti-atherosclerotic effects, including improvement of the stability of atherosclerotic plaques, inhibition of systemic inflammation, and regulation of lipid metabolism. Using mouse genechip (Ma et al., 2019), it was found that 114 genes in the aortic tissue of atherosclerosis animal model were modified, including 48 genes that were up-regulated and 56 genes that were down-regulated in atherosclerosis. In the TXL treatment group, these changes were reversed. One of these genes is lectin-like oxidised low density lipoprotein receptor 1 (LOX-1), which is one of the scavenger receptors for oxidised LDL cholesterol (ox-LDL) and plays a vital role in the uptake of ox-LDL in cells (Pothineni et al., 2017).

TXL can effectively delay the progression of atherosclerotic lesions (Zhang et al., 2019). A multicentre randomised double-blind parallel group placebo-controlled study found that TXL decreased the mean carotid intima-media thickness (IMT), plaque area, and the progress of vascular remodeling. And it also reduced the incidence of unstable angina. Anti-inflammation and regulation of lipid metabolism are important anti-atherosclerotic mechanisms of TXL (Zhang et al., 2018; Ma et al., 2019). However, the mechanism of TXL on autophagy-mediated lipid homeostasis is not clear.

The purpose of this study was to examine and describe the therapeutic effects of TXL on lipid metabolism in macrophages both *in vitro* and *in vivo*, and to explore the underlying mechanisms.

MATERIALS AND METHODS

Ethics Statement

All experiments *in vitro* were approved by the Key Laboratory of Cardiovascular Remodelling and Function Research, Qilu Hosipital, China. All *in vivo* protocols involving animal care and experiments complied with the Guide for Care and Use of Laboratory Animals published by the National Institutes of Health, United States (8th Edition, 2011) and the Animal Management Rules of the Chinese Ministry of Health (Project No. 55, 2001).

Preparation of Tongxinluo

TXL ultrafine powder was obtained from Yiling Pharmaceutical Co. Ltd. (Shijiazhuang, Hebei, China). For *in vitro* experiments, TXL ultrafine powder was dissolved in serum-free RPMI 1640 medium (Gibco, United States) with the ultrasound technology to melt it well. The solution was centrifuged at 3,500 rpm for 10 min, and the supernatant was filtered with Sterile Syringe Filters (Millex-GP Syringe Filter Unit, 0.22 μm, Merck KGaA, Darmstadt, Germany). For *in vivo* experiments, TXL ultrafine powder was dissolved in saline and was administrated to mice daily.

Cell Culture

Human acute monocytic leukaemia cell line (THP-1) was obtained from American Type Culture Collection (ATCC) and was cultivated in RPMI 1640 medium supplemented with 10% foetal bovine serum (FBS) and 1% penicillin/streptomycin at 37°C in 5% CO2. For adherence and differentiation of THP-1 cells into macrophages, 160 nM phorbol myristate acetate (PMA) was used overnight. THP-1 macrophages were incubated with or without TXL for 24 h before being stimulated with 50 mg/L recombinant human ox-LDL for indicated time.

siRNA and RNA Interference

Upon reaching 40–60% confluence, HUVECs were transfected with specific siRNA or negative control siRNA (GenePharma, Shanghai, China) using Lipofectamine 3,000 (Thermo Fisher Scientific, Waltham, MA, United States) in Opti-MEM (Gibco, Thermo Fisher Scientific, Waltham, MA, United States). After 6 h of transfection, the medium was replaced with complete 1,640, and the cells were cultured for an additional 24 h. The transfected cells were treated with ox-LDL at the designated concentrations and for the indicated times. The DNA target sequence for Beclin-1 siRNA is 5'-CAGTTTGGCACAATCAATA-3'.

Protocol for Development of Atherosclerosis Animal Models

Male apoE$^{-/-}$ mice (8 weeks old, 18–23 g) were purchased from the Peking University Animal Research Center (Beijing). All mice were fed atherogenic chow (1.25% cholesterol and 40% cocoa butter). The atherosclerotic models were created as previously described (Zhang et al., 2014). The mice were randomly divided into four groups (n = 24 per group): normal saline group (NS), low-dose TXL group, which received an oral dose of 0.38 g/kg/day TXL, medium-dose TXL group, which received an oral dose of 0.75 g/kg/day TXL, and high-dose TXL group, which received an oral dose of 1.5 g/kg/day TXL. Four weeks after the carotid-artery surgery, a 200 μl of suspension (4*10^8 TU Beclin-1i per ml) was injected into each mouse through the tail vein. All mice underwent euthanasia 4 weeks post-transfection.

Lentiviral Silencing

The lentivirus vector pGLV3/H1/GFP + Puro (pGLV3) was purchased from GeneChem (Shanghai, China) and a short-hairpin RNA sequence targeting Beclin-1 and scrambled control RNA were cloned into the vector. The following duplexes targeted murine Beclin-1: sense 5'-UAAUAUUAA ACCACAUGUUUACA-3', antisense 5'-UGUAACGGAUCC UUAACAAAUGU-3'.

Measurements of Serum Biological Parameters

Blood samples were collected by retro-orbital blood. After incubation at room temperature for 30 min and serum was separated by centrifugation (4°C, 2,500 r.p.m., 20 min). Lipid groups including TC, total TG, LDL cholesterol and HDL cholesterol were detected by automatic chemical modification technology (Roche Modular DPP System, Roche, Basel, Switzerland).

Immunofluorescence Staining and Microscopy

The aortic roots were dissected, fixed in 4% formaldehyde overnight at 4°C, embedded in OCT compound, and prepared into 5-μm-thick sections. The cryosections or cell slides were blocked with 5% BSA and were incubated with primary antibodies at 4°C overnight. The sections were washed with PBS and were incubated with Alexa Fluor 488 or Alexa Fluor 594 conjugated secondary antibodies. LDs were stained with BODIPY 493/503 (Thermo, D-3922). Autophagolysosomes were stained with LysoTracker Red (Beyotime, C1046). Nuclei were stained with 4', 6-diamidino-2-phenylindole (DAPI, 1:2000, Roche, Mannheim, Germany) for 15 min. The samples were rinsed three times in PBS and were examined under an epifluorescence microscope (Nikon, Japan).

Western Blot Analysis

THP-1 macrophages and tissue samples were lysed using Minute™ Protein Extraction Kits containing 1 mM phosphatase inhibitors and protease inhibitor (Invitrogen, Carlsbad, CA, United States) and were collected after centrifugation at 16,000 × rpm for 10 min. The protein concentrations were determined using a BCA assay kit. Equal amounts of proteins and pre-stained protein ladder (Thermo Fisher Scientific) were separated on 12% SDS-PAGE gels, transferred to the Immovilon PVDF membranes (Millipore, Billerica, MA, United States), and incubated with primary antibodies overnight at 4°C. The membranes were incubated with secondary antibodies (ProteinTech, Rosemont, Penn., United States) the next day for overnight at 4°C. Bands were visualised using Immobilon ECL substrate (Millipore, Billerica, MA, United States), and blots were imaged with an Amersham Imager 600 (GE, United States). Protein expression was quantified using Adobe Photoshop CS6 (Adobe Systems, San Jose, CA, United States), normalised to the GAPDH expression in each sample, and expressed as percentage of the control.

Reagents

Antibodies used for immunoblotting were as follows: LC3B antibody (abcam 51,520), ABCA1 antibody (abcam 7,360), ABCG1 antibody (abcam 52,617), LOX-1 antibody (abcam 60,178), HDAC one antibody (abcam 109,411), HDAC two antibody (abcam 32,117), HDAC three antibody (abcam 32,369), HDAC eight antibody (abcam 187,139), GAPDH antibody (ptg 60,004–1), Beclin-1 antibody (CST #3495). 3-MA (Sigma-Aldrich, 5 mM). Trichostatin A (TSA) (MCE HY-15144, 300 nM) and ITSA-1 (MCE HY-100508, 50 μm).

Statistical Analysis

Data were analysed using SPSS software v16.0 (SPSS Inc., Chicago, IL, United States). Data were presented as the mean ± S.E.M. of at least three independent experiments. The normality of variable distribution was tested by the Kolmogorov–Smirnov test. Comparisons were analysed using Student's t-test or one-way ANOVA followed by Bonferroni post hoc test. $p < 0.05$ was considered statistically significant.

RESULTS

Tongxinluo Treatment Inhibited Lipid Deposition in Advanced Atherosclerotic Plaques by Enhancing Macrophage Autophagy

We used low-, medium-, and high-dose TXL treatment (0.38, 0.75, and 1.5 g/kg/day, respectively) for apoE−/− mice. There was no difference in mouse body weight between experimental groups. The TC and TG values of NS + TXL-H group were lower than those of NS + Saline group ($p < 0.05$), and the TC and TG values of shBeclin-1 + TXL-H group were higher than those of NS + TXL-H group ($p < 0.05$), while there was no significant difference in the values of HDL-C and LDL-C between the groups (**Figure 1A**).

To test whether TXL reduces lipid accumulation in atherosclerotic plaques by promoting autophagy in

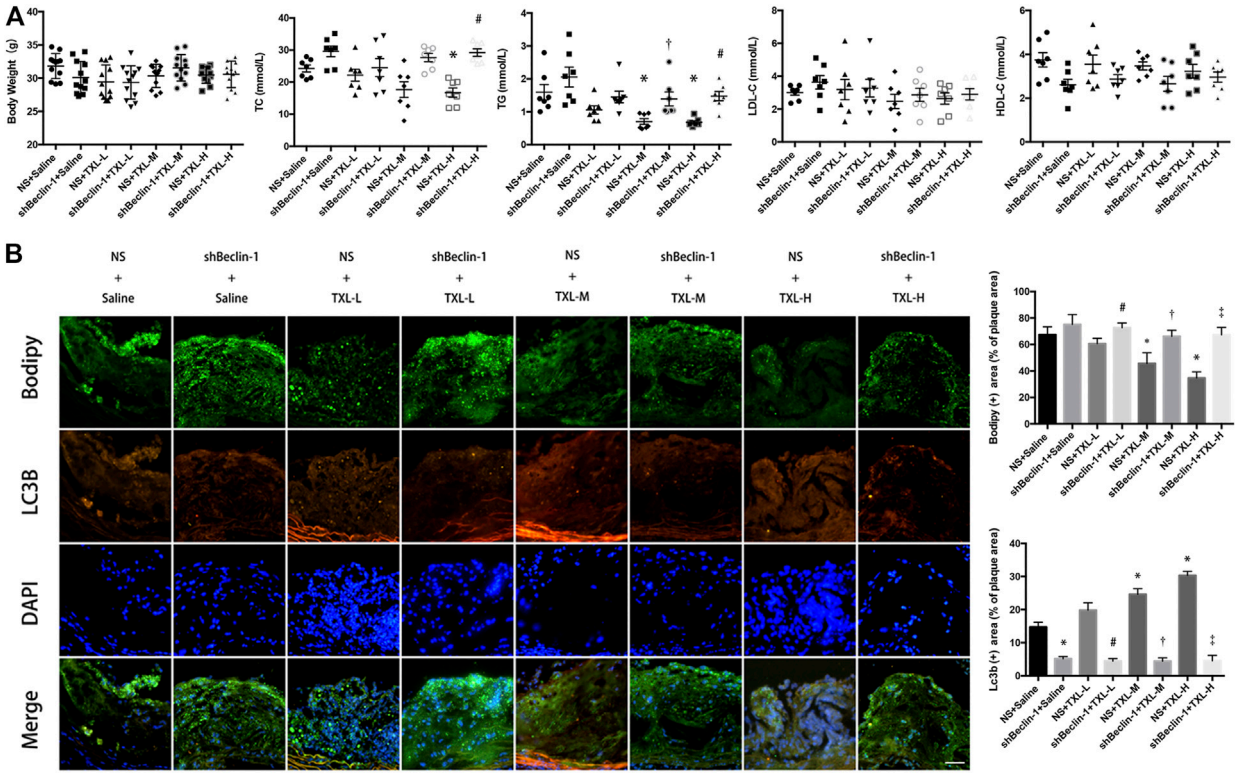

FIGURE 1 | TXL treatment inhibited lipid deposition in advanced atherosclerotic plaques. **(A)** Mouse body weight and blood lipids, $n = 7$, $^{*}p < 0.05$ vs. NS + Saline, $^{\#}p < 0.05$ vs. NS + TXL-H, $^{\dagger}p < 0.05$ vs. NS + TXL-M. **(B)** Effects of TXL on autophagy and lipid deposition in advanced atherosclerotic plaques, $n = 3$, bar = 50 μm $^{*}p <$ 0.05 vs. NS + Saline, $\#p < 0.05$ vs. NS + TXL-L, $^{\dagger}p < 0.05$ vs. NS + TXL-M, $^{\ddagger}p < 0.05$ vs. NS + TXL-H.

macrophages, we used lentivirus to silence Beclin-1, which was injected in the tail of mice. Then autophagosomes were labelled with LC3B and lipids were labelled with BODIPY. Co-localised staining of lipid droplets and autophagosomes in mouse aortic root plaques was observed. In the NS + TXL-M and NS + TXL-H groups, the lipid content in the plaque decreased ($p < 0.05$, **Figure 1B**), and the level of autophagy was increased compared with the NS group ($p < 0.05$). However, this difference was not observed in the shBeclin-1 groups. In connection with the earlier research findings (Chen et al., 2018), these data indicate that TXL improves lipid deposition in advanced atherosclerotic plaques, and this effect is induced by autophagy.

Tongxinluo Treatment Inhibited Lipid Deposition in THP-1 Macrophages and the Formation of Foam Cells

To study the effect of TXL on the formation of ox-LDL-induced macrophage foam cells, the successfully induced macrophages were pre-treated with TXL, stimulated with ox-LDL, and detected by oil red O staining and BODIPY staining. As shown in **Figures 2A,B**, ox-LDL caused an increase in lipid content in macrophages compared to the control group ($p < 0.05$). Compared with the ox-LDL group, the lipid content in the macrophages of 200 mg/L TXL + ox-LDL and 500 mg/L TX + ox-LDL was reduced ($p <$ 0.05), and the inhibitory effect of 500 mg/L TXL was more pronounced. Green fluorescence is expressed as a positive concentration of LDs in the macrophage, and green fluorescence in the ox-LDL group is stronger than that in the control group ($p < 0.05$), indicating that ox-LDL induces lipid deposition in macrophages to foam cells. After treatment with TXL, the green fluorescence in macrophages decreased in a dose-dependent manner ($p < 0.05$), indicating that TXL can inhibit ox-LDL-induced macrophage lipid deposition.

LDs is where the foam cells store cholesterol. Reducing the foaming and lipid deposition of macrophages is a potential therapeutic target for reversing atherosclerosis. In order to explore the effect of TXL on the breakdown of lipids LDs, autophagosomes were labeled with LC3B antibody and LDs were labelled with BODIPY. Compared with the ox-LDL group, in 200 mg/L TXL + ox-LDL and 500 mg/L TXL + ox-LDL groups, the number of lipid LDs co-localised with autophagosomes was decreased ($p < 0.05$, **Figure 2C**).

Tongxinluo Promotes Lipid Degradation in Lipid Droplets by Enhancing Autophagy

To explore the effect of TXL on the autophagic outflow of lipid droplets in macrophages, autophagy lysosomes were labeled with LysoTracker Red and LDs were labelled with BODIPY. Co-localisation of BODIPY and LysoTracker Red showed that in

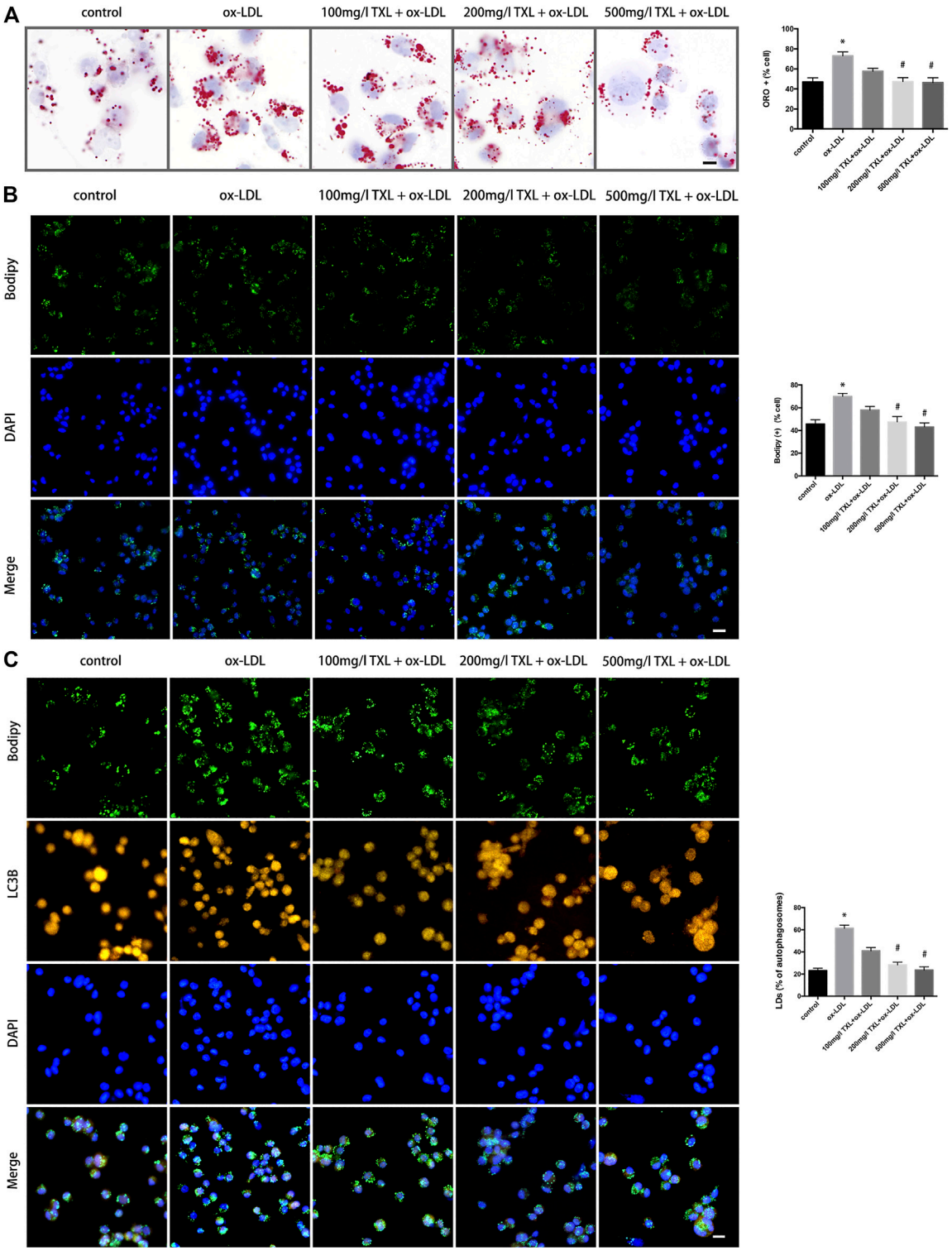

FIGURE 2 | TXL treatment inhibited lipid deposition in THP-1 Macrophages. **(A)** Cell oil red O detected the effect of TXL on ox-LDL-induced macrophage lipid deposition, $n = 3$, bar = 10 μm, $^{*}p < 0.05$ vs. control, $^{\#}p < 0.05$ vs. ox-LDL. **(B)** Cell Bodipy staining detected the effect of TXL on ox-LDL-induced macrophage lipid deposition, $n = 3$, bar = 25 μm, $^{*}p < 0.05$ vs. control, $^{\#}p < 0.05$ vs. ox-LDL. **(C)** Effects of TXL on autophagy and intracellular lipid in macrophages. $n = 3$, bar = 10 μm $^{*}p < 0.05$ vs. control, $^{\#}p < 0.05$ vs. ox-LDL.

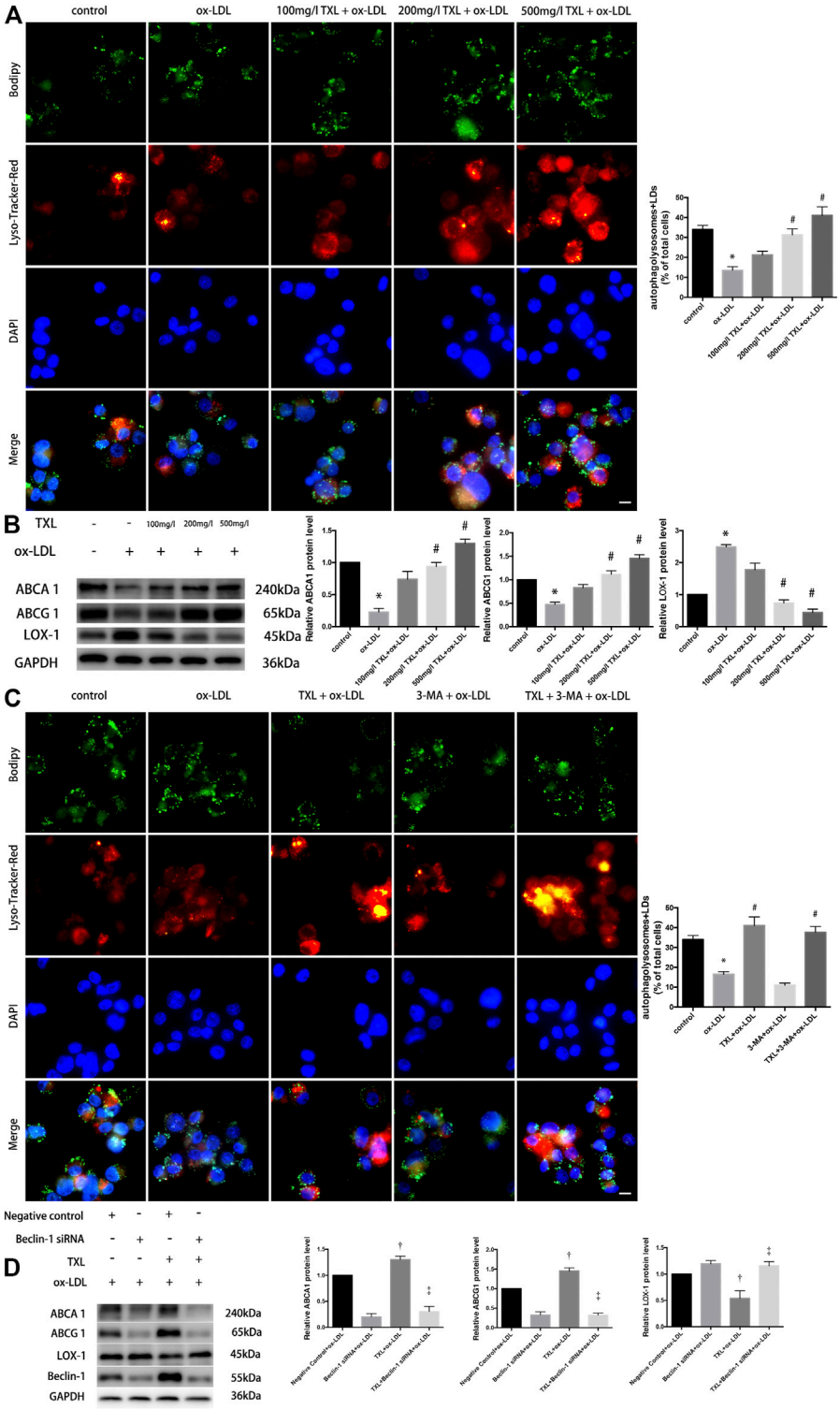

FIGURE 3 | TXL treatment reduced lipid deposition by increasing autophagy in THP-1 Macrophages. **(A)** Effects of TXL on intracellular lipid metabolism of macrophages mediated by autophagy, $n = 3$, bar = 10 μm, $^{*}p < 0.05$ vs. control, $^{\#}p < 0.05$ vs. ox-LDL. **(B)** Western Blot detection of TXL on ox-LDL-induced macrophage lipid efflux, $n = 3$, $^{*}p < 0.05$ vs. control, $^{\#}p < 0.05$ vs. ox-LDL. **(C)** Detection of autophagy in TXL inhibited ox-LDL-induced macrophage lipid deposition *via* cellular immunofluorescence, $n = 3$, bar = 10 μm, $^{*}p < 0.05$ vs. control, $^{\#}p < 0.05$ vs. ox-LDL. **(D)** Western blot revealed the effect of Beclin-1 in inhibition of ox-LDL-induced lipid deposition in TXL-treated macrophages. $n = 5$, $^{\dagger}p < 0.05$ vs. Negative control + ox-LDL, $^{\ddagger}p < 0.05$ vs. TXL + ox-LDL.

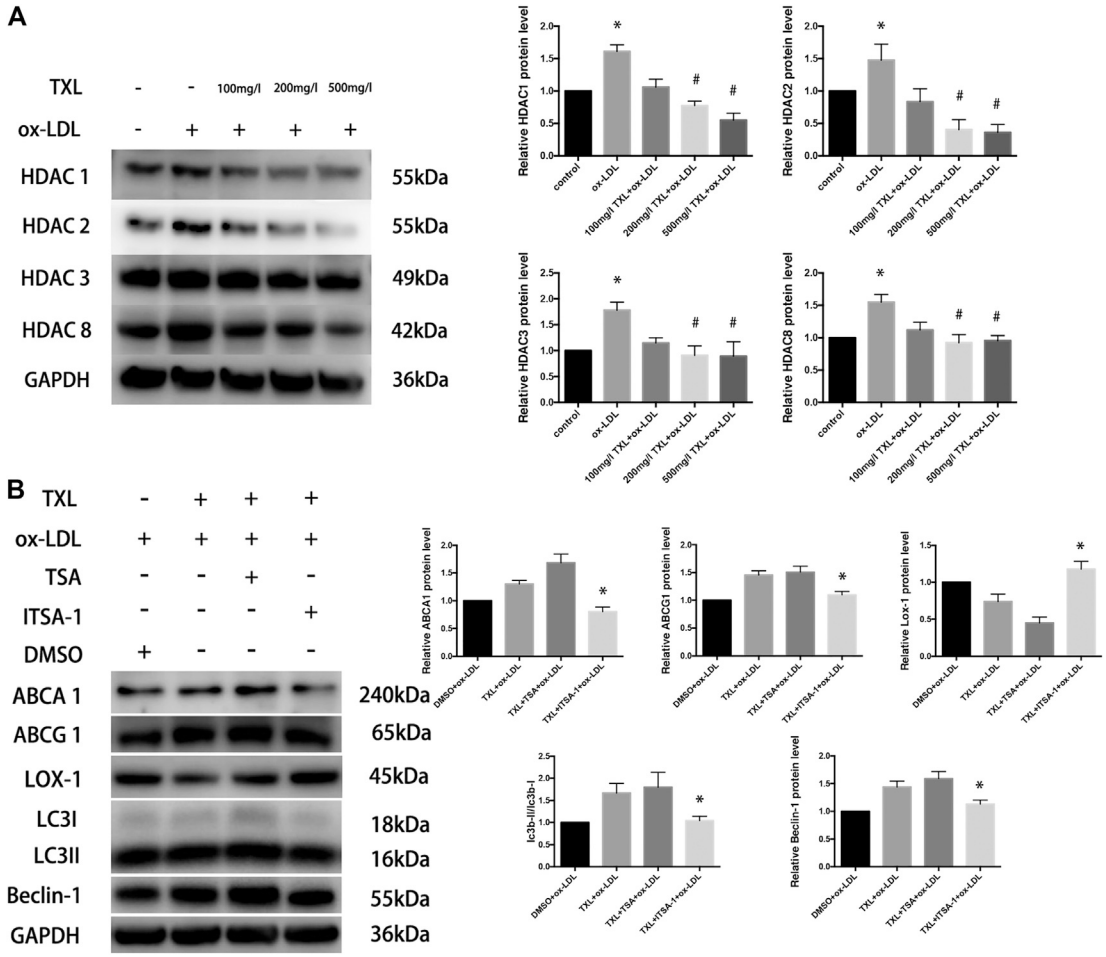

FIGURE 4 | TXL increase macrophage autophagy through histone deacetylase inhibition. **(A)** Western blot revealed the effect of TXL on ox-LDL-induced macrophage type I histone deacetylase expression, $n = 5$, $^{*}p < 0.05$ vs. control, $^{\#}p < 0.05$ vs. ox-LDL. **(B)** Western blot revealed histone deacetylase inhibited the effect of TXL on macrophage lipid deposition, $n = 5$, $^{*}p < 0.05$ vs. TXL + ox-LDL.

200 mg/L TXL + ox-LDL and 500 mg/L TXL + ox-LDL groups, the number of lipid LDs co-localised with autophagosomes was increased, more lipids were co-localised with autophagy lysosomes ($p < 0.05$, **Figure 3A**). And in **Figure 3B**, ox-LDL stimulation by western blot decreased the expression of ABCA1, ABCG1 protein expression and increased the expression of LOX-1 protein expression, but pretreatment of TXL significantly inhibit it with the effects at 200 mg/L and 500 mg/L concentrations ($p < 0.05$, **Figure 3B**).

After macrophages were pre-treated with TXL and ox-LDL stimulation, macrophage autophagy was quantified by co-localisation with BODIPY and LysoTracker Red, with or without autophagy inhibitor 3-MA. As shown in **Figure 3C**, the number of autophagolysosomes in the macrophages of the 3-MA + ox-LDL group was lower than that of the control group. After treatment with TXL, more lipids in the macrophages of the ox-LDL group were bound to autophagosomes ($p < 0.05$), and the number of autophagosomes became higher. Lipid deposition in 3-MA + ox-LDL group was significantly higher than that in TXL + ox-LDL group, but it was lower in 3-MA + TXL + ox-LDL group and in the TXL group. The autophagic level of the lipid droplets in the cells was increased ($p < 0.05$). These results suggested that TXL reduced lipid deposition by increasing autophagy levels.

To show the role of autophagy-related gene Beclin-1 in inhibition of ox-LDL-induced lipid deposition in TXL-treated macrophages, Beclin-1 gene was silenced using siRNA. Compared with the TXL + ox-LDL group, ABCA1, ABCG1 protein expression decreased and LOX-1 protein expression increased ($p < 0.05$) in TXL + Beclin-1 siRNA + ox-LDL group ($p < 0.05$, **Figure 3D**).

Tongxinluo Inhibits the Expression of Histone Deacetylase to Increase Macrophage Autophagy

In the past few decades, drugs targeting histone deacetylase (HDACs) have been identified and developed for the treatment of cancer, and more non-oncological applications of these drugs have been discovered. It has been confirmed that

histone deacetylase can directly participate in the regulation of autophagy key proteins and autophagy-related proteins, to regulate autophagy. To explore the mechanism by which TXL regulates autophagy in macrophages, we suppose that TXL can alter HDAC regulate autophagy and observe the effect of TXL on HDAC. Compared with the control group, ox-LDL caused an increase in macrophage class I histone deacetylases (HDAC1, HDAC2, HDAC3, and HDAC8) protein expression ($p < 0.05$) while TXL reversed the HDACs high expression ($p < 0.05$) induced by ox-LDL (**Figure 4A**). In addition, compared with TXL + ox-LDL group, after addition of HDAC agonist (ITSA-1), the ratio of LC3II/LC3I, Beclin-1 protein expression, ABCA1 and ABCG1 protein expression decreased, and LOX-1 protein expression increased ($p < 0.05$, **Figure 4B**).

DISCUSSION

In this study, we investigated how TXL affects lipid deposition in advanced atherosclerotic plaques and lipid metabolism in macrophages. The following conclusions were generated: 1) TXL treatment inhibited lipid deposition in advanced atherosclerotic plaques by enhancing macrophage autophagy. 2) TXL treatment inhibited lipid deposition in THP-1 macrophages and the formation of foam cells. 3) TXL promotes lipid degradation in lipid droplets by enhancing autophagy. 4) TXL inhibits the expression of histone deacetylase to increase macrophage autophagy.

To evaluate the role of TXL in atherosclerotic plaques, we construct the atherosclerotic animal model with lentiviral injection and performed histopathology and immunofluorescence staining analysis *in vivo*. Immunofluorescence staining revealed that TXL treatment inhibited lipid deposition in advanced atherosclerotic plaques by enhancing macrophage autophagy. *In vitro* TXL treatment inhibited lipid deposition in THP-1 macrophages by enhancing autophagy *via* Beclin-1. TXL reversed the high expression of class I histone deacetylases (HDACs) induced by ox-LDL. Trichostatin A (TSA) is a specific inhibitor of class I histone deacetylase. ITSA-1 is an agonist of histone deacetylase. In order to study the effect of class I histone deacetylase on TXL treatment, we added TSA or ITSA-1 to THP-1 macrophages. Compared with the TXL + ox-LDL group, TXL failed to promote intracellular lipid droplet decomposition after the addition of the histone deacetylase agonist.

Atherosclerosis is a progressive disease characterised by the accumulation of lipid and fibre elements in the aortic walls, leading to myocardial infarction or stroke. Tongxinluo (TXL), a traditional Chinese medication, plays a key role in the formation and progression of plaques in atherosclerosis. In previous research (Chen et al., 2018), we had found that TXL significantly inhibits ox-LDL-induced apoptosis in macrophages *in vitro* by improving the dissociation of the Beclin-1-Bcl-2 complex. *In vivo*, TXL treatment significantly reduced macrophage apoptosis dose-dependently and the result was blocked by Beclin-1 silencing. In addition, the increased Lc3b dots by TXL almost localized to macrophages in advanced atherosclerotic plaque. Compared with the same dose of TXL shBeclin-1 group, plaque area (showed by positive oil red O-stained area of en face staining or staining of aortic root sections with H&E) and the vulnerability index of TXL groups decreased. The anti-apoptosis effects of TXL on atherosclerosis was related to the improvement of autophagy *via* Beclin-1. Our current study reveals that TXL inhibits the lipid deposition through increasing autophagy related Beclin-1 both *in vitro* and *in vivo*. TXL also reduces the expression of histone deacetylase, which are involved in autophagy inhibition and counteracts atherogenic effect of ox-LDL in THP-1 macrophages.

After apolipoprotein E (apoE) knockout animals were exposed to a high-fat diet, lipoprotein particles and their aggregates accumulated in the damaged intima, and mononuclear cells adhered to the surface of the endothelium migrate through the endothelial monolayer to the intima. Then, the cells proliferate and differentiate into macrophages and ingest lipoproteins, forming foam cells. Over time, the foam cells undergo apoptosis, lysis, and their lipid-filled contents turn into the necrotic core of the plaque (Ross, 1993; Tamminen et al., 1999). The accumulation of ox-LDL in the intima significantly promotes monocyte recruitment and foam cell formation (Cyrus et al., 1999; Libby, 2000; Maxfield and Van Meer, 2010). In the present research, *in vivo* experiments showed that the accumulation of lipids in macrophage promotes the development of atherosclerotic plaques, so TXL maybe inhibit the progress of atherosclerotic plaques by attenuating the accumulation of lipid in macrophage by enhancing Beclin-1-induced autophagy. *In vitro* experiments showed that TXL could inhibit macrophage lipid deposition induced by ox-LDL. However, after the Beclin-1 gene was silenced, these effects disappeared, indicating that TXL achieves its effects through autophagic key molecule Beclin-1.

The cell itself has a complete and complex mechanism to ensure the distribution and content of free cholesterol in order to prevent the cell membrane from being destroyed due to excess of cholesterol (Maxfield and Van Meer, 2010). In the state of increased cholesterol levels, cellular feedback mechanisms can reduce cholesterol uptake and synthesis and increase reverse cholesterol transport (Maxfield and Tabas, 2005). If these compensatory mechanisms do not adequately reduce free cholesterol levels, excess free cholesterol will be esterified and stored as lipid-free non-cytotoxic cholesterol esters to maintain normal cell function. The export of cholesterol mediated by autophagy is an ABCA1-dependent process (Orsó et al., 2000; Neufeld et al., 2001). ABCA1 promotes intracellular cholesterol efflux and increases high-density lipoprotein levels to achieve reverse cholesterol transport (RCT). Through RCT, i.e., cholesterol is transferred from macrophages, cleared by the liver, and eventually excreted (Chen et al., 2001; Cuchel and Rader, 2006). This study confirmed that TXL can up-regulate the expression of ABCA1 and ABCG1 protein and inhibit the expression of LOX-1 protein. This indicates that TXL can promote the RCT by initiating Beclin-1 mediated autophagic pathway, in order to achieve the inhibition of atherosclerotic plaque lipid deposition and to improve plaque stability.

LDs are metabolically active but atypical intracellular organelles composed of a hydrophobic core of neutral lipids (Ouimet and Marcel, 2012). In eukaryotic cells, various forms of autophagy can maintain the homeostasis of the intracellular environment and thus regulate cell survival. Experimental studies have found that autophagy dysfunction is associated with cancer, neurodegenerative diseases, inflammatory diseases, and immunodeficiency diseases (Ouimet et al., 2011). Autophagy, by releasing excess cholesterol, prevents the harmful effects of excessive cellular cholesterol accumulation in macrophages. The main mechanism is that cholesterol esters are stored in LDs, soluble in lysosomes, and hydrolysed by lysosomal acid lipase (LAL) into free cholesterol, then flows out of the cell (Sergin et al., 2017). Animal experiments indicated that in plaques of advanced atherosclerosis, autophagy occurs in macrophages. TXL promoted autophagy in plaque macrophages and suppressed lipid deposition in plaques. In the results of cell experiments, after TXL treatment, the more autophagic macrophages, the less lipid deposition, and most of the lipid was bound to autolysosomes, leading to significant increase in the volume of lysosomes. TXL also reversed the effect of inhibition of autophagy caused by 3-MA, but after silencing of Beclin-1, the drug of TXL was inhibited. These results suggest that TXL can exert its effect of inhibiting macrophage lipid deposition through Beclin-1 mediated autophagy pathway.

Class I HDAC shares homology with yeast Tpd3, including HDAC1, HDAC2, HDAC3 and HDAC8. Moreover, they are expressed in various tissues and organs. HDAC1, HDAC2 and HDAC3 play a regulation role in gene expression in the nucleus, and HDAC8 can deacetylate a variety of non-histone proteins in the nucleus and cytoplasm (Gammoh et al., 2012). Class I and class IIa HDACs inhibit the initiation of autophagy by altering the transcription or expression of an important autophagy-related protein (e.g., Beclin-1) or an extension (e.g., ATG7 or LC3B) during nucleation. In contrast, class IIb HDACs can promote autophagy maturation. These family members are involved in the process of promoting the transfer of autophagosomes to lysosomes and fusion with lysosomes. Class I HDAC specific inhibitors can reduce the inhibition of autophagy and thus promote the initiation of autophagy flow (Schipper et al., 2014). Results of this study indicate that TXL can inhibit the expression of type I HDAC, and after addition of HDAC agonists, the effect of TXL on promoting the expression of autophagy and lipid efflux protein is inhibited. The HDAC agonist used in this study is not a type I HDAC-specific agonist, therefore, the regulation of other types of HDAC by TXL needs further study.

In summary, TXL can inhibit the expression of type I HDAC, thereby inhibiting the inhibitory effect of histone deacetylase on the expression of autophagic key molecule Beclin-1 and promoting the autophagic outflow of intracellular lipids. This study provides experimental basis for the clinical application of TXL in regulating lipid metabolism and stabilising atherosclerotic plaques.

DATA AVAILABILITY STATEMENT

The raw data supporting the conclusion of this article will be made available by the authors, without undue reservation.

ETHICS STATEMENT

This animal study was reviewed and approved by the Animal Care Committee of Shandong University.

AUTHOR CONTRIBUTIONS

YC and FY designed and performed the research, YuZ and ML analysed data, WC, XL and MZ conceived the project, reviewed the data, and wrote the manuscript. All authors read and approved the final manuscript.

FUNDING

This work was supported by the National Natural Science Foundation of China (Grant Nos.81970377, 81470559, 81770439, 81700387), International Collaboration and Exchange Program of China (Grant No. 81320108004).

REFERENCES

Chen, W. Q., Zhong, L., Zhang, L., Ji, X. P., Zhao, Y. X., Zhang, C., et al. (2009). Chinese Medicine Tongxinluo Significantly Lowers Serum Lipid Levels and Stabilizes Vulnerable Plaques in a Rabbit Model. *J. Ethnopharmacology* 124, 103–110. doi:10.1016/j.jep.2009.04.009

Chen, W., Sun, Y., Welch, C., Gorelik, A., Leventhal, A. R., Tabas, I., et al. (2001). Preferential ATP-Binding Cassette Transporter A1-Mediated Cholesterol Efflux from Late Endosomes/lysosomes. *J. Biol. Chem.* 276, 43564–43569. doi:10.1074/jbc.m107938200

Chen, Y., Li, M., Zhang, Y., Di, M., Chen, W., Liu, X., et al. (2018). Traditional Chinese Medication Tongxinluo Attenuates Apoptosis in Ox-LDL-Stimulated Macrophages by Enhancing Beclin-1-Induced Autophagy. *Biochem. biophysical Res. Commun.* 501, 336–342. doi:10.1016/j.bbrc.2018.03.094

Cuchel, M., and Rader, D. J. (2006). Macrophage Reverse Cholesterol Transport. *Circulation* 113, 2548–2555. doi:10.1161/circulationaha.104.475715

Cyrus, T., Witztum, J. L., Rader, D. J., Tangirala, R., Fazio, S., Linton, M. F., et al. (1999). Disruption of the 12/15-lipoxygenase Gene Diminishes Atherosclerosis in Apo E-Deficient Mice. *J. Clin. Invest.* 103, 1597–1604. doi:10.1172/jci5897

Gammoh, N., Lam, D., Puente, C., Ganley, I., Marks, P. A., and Jiang, X. (2012). Role of Autophagy in Histone Deacetylase Inhibitor-Induced Apoptotic and Nonapoptotic Cell Death. *Proc. Natl. Acad. Sci.* 109, 6561–6565. doi:10.1073/pnas.1204429109

Hao, P.-P., Jiang, F., Chen, Y.-G., Yang, J., Zhang, K., Zhang, M.-X., et al. (2015). Traditional Chinese Medication for Cardiovascular Disease. *Nat. Rev. Cardiol.* 12, 115–122. doi:10.1038/nrcardio.2014.177

Levine, B., and Kroemer, G. (2019). Biological Functions of Autophagy Genes: a Disease Perspective. *Cell* 176, 11–42. doi:10.1016/j.cell.2018.09.048

Libby, P. (2000). Changing Concepts of Atherogenesis. *J. Intern. Med.* 247, 349–358. doi:10.1046/j.1365-2796.2000.00654.x

Libby, P., Ridker, P. M., and Hansson, G. K. (2011). Progress and Challenges in Translating the Biology of Atherosclerosis. *Nature* 473, 317–325. doi:10.1038/nature10146

Lusis, A. J. (2000). Atherosclerosis. *Nature* 407, 233–241. doi:10.1038/35025203

Ma, J., Qiao, L., Meng, L., Ma, L., Zhao, Y., Liu, X., et al. (2019). Tongxinluo May Stabilize Atherosclerotic Plaque via Multiple Mechanisms Scanning by Genechip. *Biomed. Pharmacother.* 113, 108767. doi:10.1016/j.biopha.2019.108767

Mannarino, E., and Pirro, M. (2008). Molecular Biology of Atherosclerosis. *Clin. Cases Miner Bone Metab.* 5, 57–62.

Maxfield, F. R., and Tabas, I. (2005). Role of Cholesterol and Lipid Organization in Disease. *Nature* 438, 612–621. doi:10.1038/nature04399

Maxfield, F. R., and Van Meer, G. (2010). Cholesterol, the central Lipid of Mammalian Cells. *Curr. Opin. Cel. Biol.* 22, 422–429. doi:10.1016/j.ceb.2010.05.004

Moore, K. J., Sheedy, F. J., and Fisher, E. A. (2013). Macrophages in Atherosclerosis: a Dynamic Balance. *Nat. Rev. Immunol.* 13, 709–721. doi:10.1038/nri3520

Neufeld, E. B., Remaley, A. T., Demosky, S. J., Stonik, J. A., Cooney, A. M., Comly, M., et al. (2001). Cellular Localization and Trafficking of the Human ABCA1 Transporter. *J. Biol. Chem.* 276, 27584–27590. doi:10.1074/jbc.m103264200

Orsó, E., Broccardo, C., Kaminski, W. E., Böttcher, A., Liebisch, G., Drobnik, W., et al. (2000). Transport of Lipids from Golgi to Plasma Membrane Is Defective in Tangier Disease Patients and Abc1-Deficient Mice. *Nat. Genet.* 24, 192–196. doi:10.1038/72869

Ouimet, M., Franklin, V., Mak, E., Liao, X., Tabas, I., and Marcel, Y. L. (2011). Autophagy Regulates Cholesterol Efflux from Macrophage Foam Cells via Lysosomal Acid Lipase. *Cel Metab.* 13, 655–667. doi:10.1016/j.cmet.2011.03.023

Ouimet, M., and Marcel, Y. L. (2012). Regulation of Lipid Droplet Cholesterol Efflux from Macrophage Foam Cells. *Arterioscler Thromb. Vasc. Biol.* 32, 575–581. doi:10.1161/atvbaha.111.240705

Pothineni, N. V. K., Karathanasis, S. K., Ding, Z., Arulandu, A., Varughese, K. I., and Mehta, J. L. (2017). LOX-1 in Atherosclerosis and Myocardial Ischemia. *J. Am. Coll. Cardiol.* 69, 2759–2768. doi:10.1016/j.jacc.2017.04.010

Robinet, P., Ritchey, B., and Smith, J. D. (2013). Physiological Difference in Autophagic Flux in Macrophages from 2 Mouse Strains Regulates Cholesterol Ester Metabolism. *Arterioscler Thromb. Vasc. Biol.* 33, 903–910. doi:10.1161/atvbaha.112.301041

Ross, R. (1993). The Pathogenesis of Atherosclerosis: a Perspective for the 1990s. *Nature* 362, 801–809. doi:10.1038/362801a0

Schipper, H., Alla, V., Meier, C., Nettelbeck, D. M., Herchenröder, O., and Pützer, B. M. (2014). Eradication of Metastatic Melanoma through Cooperative Expression of RNA-Based HDAC1 Inhibitor and P73 by Oncolytic Adenovirus. *Oncotarget* 5, 5893–5907. doi:10.18632/oncotarget.1839

Sergin, I., Evans, T. D., Zhang, X., Bhattacharya, S., Stokes, C. J., Song, E., et al. (2017). Exploiting Macrophage Autophagy-Lysosomal Biogenesis as a Therapy for Atherosclerosis. *Nat. Commun.* 8, 1–20. doi:10.1038/ncomms15750

Singh, R., Kaushik, S., Wang, Y., Xiang, Y., Novak, I., Komatsu, M., et al. (2009). Autophagy Regulates Lipid Metabolism. *Nature* 458, 1131–1135. doi:10.1038/nature07976

Tamminen, M., Mottino, G., Qiao, J. H., Breslow, J. L., and Frank, J. S. (1999). Ultrastructure of Early Lipid Accumulation in ApoE-Deficient Mice. *Arterioscler Thromb. Vasc. Biol.* 19, 847–853. doi:10.1161/01.atv.19.4.847

Westerterp, M., Bochem, A. E., Yvan-Charvet, L., Murphy, A. J., Wang, N., and Tall, A. R. (2014). ATP-binding Cassette Transporters, Atherosclerosis, and Inflammation. *Circ. Res.* 114, 157–170. doi:10.1161/circresaha.114.300738

Zhang, K., Liu, X., Yu, Y., Luo, T., Wang, L., Ge, C., et al. (2014). Phospholipid Transfer Protein Destabilizes Mouse Atherosclerotic Plaque. *Arterioscler Thromb. Vasc. Biol.* 34, 2537–2544. doi:10.1161/atvbaha.114.303966

Zhang, L., Li, Y., Yang, B.-S., Li, L., Wang, X.-Z., Ge, M.-L., et al. (2018). A Multicenter, Randomized, Double-Blind, and Placebo-Controlled Study of the Effects of Tongxinluo Capsules in Acute Coronary Syndrome Patients with High On-Treatment Platelet Reactivity. *Chin. Med. J.* 131, 508–515. doi:10.4103/0366-6999.226064

Zhang, M., Liu, Y., Xu, M., Zhang, L., Liu, X., Zhao, Y., et al. (2019). Carotid Artery Plaque Intervention with Tongxinluo Capsule (CAPITAL): A Multicenter Randomized Double-Blind Parallel-Group Placebo-Controlled Study. *Scientific Rep.* 9, 1–11. doi:10.1038/s41598-019-41118-z

Conflict of Interest: The authors declare that the research was conducted in the absence of any commercial or financial relationships that could be construed as a potential conflict of interest.

frontiers in Pharmacology

ORIGINAL RESEARCH
published: 06 July 2021
doi: 10.3389/fphar.2021.671783

The Protective Effect of Liquiritin in Hypoxia/Reoxygenation-Induced Disruption on Blood Brain Barrier

Mengting Li[1†], Jia Ke[1†], Yiqing Deng[2], Chunxiang Chen[1], Yichen Huang[1], Yuefeng Bian[1], Shufen Guo[1], Yang Wu[1], Hong Zhang[2], Mingyuan Liu[1]* and Yan Han[1]**

[1]Department of Neurology, Yueyang Hospital of Integrated Traditional Chinese and Western Medicine, Shanghai University of Traditional Chinese Medicine, Shanghai, China, [2]Institute of Interdisciplinary Integrative Biomedicine Research, Shanghai University of Traditional Chinese Medicine, Shanghai, China

OPEN ACCESS

Edited by:
Tie-Jun Li,
Second Military Medical University, China

Reviewed by:
Danhong Wu,
Fudan University, China
Abraham Jacob Al-Ahmad,
Texas Tech University Health Sciences Center, United States

***Correspondence:**
Hong Zhang
hqzhang51@126.com
Mingyuan Liu
liu.mingyuan@foxmail.com
Yan Han
hanyan.2006@aliyun.com

[†]These authors have contributed equally to this work

Specialty section:
This article was submitted to Ethnopharmacology, a section of the journal Frontiers in Pharmacology

Received: 24 February 2021
Accepted: 19 April 2021
Published: 06 July 2021

Citation:
Li M, Ke J, Deng Y, Chen C, Huang Y, Bian Y, Guo S, Wu Y, Zhang H, Liu M and Han Y (2021) The Protective Effect of Liquiritin in Hypoxia/Reoxygenation-Induced Disruption on Blood Brain Barrier. Front. Pharmacol. 12:671783. doi: 10.3389/fphar.2021.671783

Background: Stroke is the second leading cause of death in human life health, but current treatment strategies are limited to thrombolytic therapy, and because of the tight time window, many contraindications, and only a very small number of people can benefit from it, new therapeutic strategies are needed to solve this problem. As a physical barrier between the central nervous system and blood, the blood-brain barrier (BBB) maintains the homeostasis of the central nervous system. Maintaining the integrity of the BBB may emerge as a new therapeutic strategy. Liquiritin (LQ) is a flavonoid isolated from the medicinal plant *Glycyrrhiza uralensis* Fisch. ex DC. (Fabaceae), and this study aims to investigate the protective effects of LQ on brain microvascular endothelial cells (BMECs), to provide a new therapeutic strategy for stroke treatment, and also to provide research ideas for the development of traditional Chinese medicine (TCM).

Methods: The protective effects of LQ on HBMECs under the treatment of hypoxia reoxygenation (H/R) were investigated from different aspects by establishing a model of H/R injury to mimic ischemia-reperfusion *in vivo* while administrating different concentrations of LQ, which includes: cell proliferation, migration, angiogenesis, mitochondrial membrane potential as well as apoptosis. Meanwhile, the mechanism of LQ to protect the integrity of BBB by antioxidation and inhibiting endoplasmic reticulum (ER) stress was also investigated. Finally, to search for possible targets of LQ, a proteomic analysis approach was employed.

Results: LQ can promote cell proliferation, migration as well as angiogenesis and reduce mitochondrial membrane potential damage and apoptosis. Meanwhile, LQ can also reduce the expression of related adhesion molecules, and decrease the production of reactive oxygen species. In terms of mechanism study, we demonstrated that LQ could activate Keap1/Nrf2 antioxidant pathway, inhibit ER stress, and maintain the integrity of BBB. Through differential protein analysis, 5 disease associated proteins were found.

Conclusions: Studies have shown that LQ can promote cell proliferation, migration as well as angiogenesis, and reduce cell apoptosis, which may be related to its inhibition of oxidative and ER stress, and then maintain the integrity of BBB. Given that five differential

proteins were found by protein analysis, future studies will revolve around the five differential proteins.

Keywords: liquiritin, vascular protection, human brain microvascular endothelial cells, blood-brain barrier, oxidative stress, endoplasmic reticulum stress

INTRODUCTION

With the increase of human life span and the aging of population, the incidence rate of age-related cerebrovascular diseases such as stroke has increased dramatically (GBD 2016 Lifetime Risk of Stroke Collaborators, 2018). According to the Global Burden of Diseases (GBD), the age-standardized mortality rate of cerebral infarction is 56.9/100000, which is the second leading cause of death in the world and the first cause of death in China (GBD 2017 Causes of Death Collaborators, 2018). At present, the most effective method for ischemic brain injury is limited to vascular recanalization, and the recovery of blood flow will increase the reperfusion injury (Powers et al., 2019). In addition, high time window and many contraindications lead to less than 20% of patients can benefit from thrombolysis (Molina, 2011; Widimsky et al., 2014). Therefore, there is an urgent need for new treatment strategies and drugs to expand the beneficiaries.

After the occurrence of ischemic stroke, blood-brain barrier (BBB), the physical barrier between the central nervous system (CNS) and blood, is destroyed, which accelerates the damage process of brain parenchyma. Under physiological conditions, BBB protects brain tissue from inflammatory and toxic substances, and maintains the stability of CNS (Abbott et al., 2010; Keep et al., 2014). Brain microvascular endothelial cells (BMECs), pericytes and astrocytes jointly maintain the integrity of BBB. Ischemia reperfusion can mediate BBB rupture, resulting in edema and brain parenchymal damage (Granger and Kvietys, 2015; Keaney and Campbell, 2015). It has been reported that BMECs injury plays an important role in ischemia-reperfusion injury after cerebral infarction (Wu et al., 2019). Therefore, protecting BMECs may be a potential therapeutic strategy for stroke treatment.

With a history of more than 2000 years, Chinese herbs is an important part of traditional Chinese medicine (TCM) (Hao et al., 2015). Although TCM is used as a supplementary and alternative medicine in many developed countries, in China, it's applied to prevent and treat diverse diseases by more than 70% Chinese (Chen and Lu, 2006). In recent years, with the development of TCM, it is accepted by more and more countries, such as the United States and Australia (Guo et al., 2013). According to the Pharmacopoeia of the People's Republic of China, *Glycyrrhiza uralensis* has the effects of tonifying spleen and Qi, clearing away heat and detoxification. Liquiritin (LQ), the main active component of *Glycyrrhiza uralensis* Fisch. ex DC. (Fabaceae), has anti-inflammatory and anti-oxidation effects, and can enter the brain tissue through BBB after ischemia-reperfusion injury (Li et al., 2015). However, whether it can exert a cerebroprotective effect remains unknown.

In our study, we discussed the protective effect of LQ on HBMECs injured by hypoxia reoxygenation (H/R), and studied the possible mechanism of LQ, so as to provide more theoretical basis for the clinical promotion of LQ and provide new ideas for the treatment of stroke.

MATERIALS AND METHODS

Media, Reagents and Antibodies

Liquiritin (purity > 98%) was acquired from DingRich Chemical Co., Ltd (Shanghai, China). HBMECs were bought from Qingqi Biotechnology Development Co., Ltd (Shanghai, China). Fetal bovine serum (FBS) was purchased from Biological Industries (Israel). Penicillin/streptomycin, phosphate buffer saline (PBS) and dulbecco's modified eagle medium (DMEM) were obtained from Hyclone (United States). Cell Counting Kit-8 (CCK-8) was purchased from Dongren Chemical Technology (Shanghai, China). Matrigel was bought from Corning (New York, United States). Mitochondrial membrane potential (JC-1) test kit, BCA protein test kit and NP40 lysate were purchased from Beyotime Biotechnology (Shanghai, China). Apoptosis Kit was purchased from Becton, Dickinson and Company (New York, United States). Human Superoxide dismutase (SOD) ELISA kit was obtained from Novus (United States). Malondialdehyde (MDA) ELISA kit was purchased from Biovision (San Francisco, United States). Human intercellular cell adhesion molecule-1 (ICAM-1) ELISA kit, human vascular cell adhesion molecule-1 (VCAM-1) ELISA kit and anti-Claudin-5 antibody were purchased from Abcam company (Cambridge, UK). GAPDH antibody was purchased from Affinity (United States). Nuclear factor E2-related factor 2 (Nrf2), Kelch Like ECH Associated Protein 1 (Keap1), ATF6, glucose-regulated protein 78 (GRP78), zonula occludens 1 (ZO-1) antibodies were purchased from Cell Signaling Technology (Danvers, United States). Horseradish peroxidase (HRP)-conjugated anti-rabbit IgG was brought from Jackson company (Pennsylvania, United States). SDS-PAGE rapid dispensing kit and ECL chromogenic solution were obtained from EpiZyme Biotechnology (Shanghai, China). TBST, electrophoretic buffer and electrotransfer solution were purchased from Beijing Solarbio Technology (Beijing, China).

Cell Culture and H/R Treatment

HBMECs were cultured in high glucose medium containing 10% FBS, 1% streptomycin and penicillin, and were cultured in 5% CO_2 at 37°C incubator. To simulate ischemia-reperfusion injury *in vivo*, the cell injury model of HBMECs was described previously with slight modifications (Liberale et al., 2020). The specific operation is as follows: HBMECs were firstly cultured in the basic medium without FBS under hypoxic conditions (1% O_2, 5% CO_2 and 94% N_2) for 12 h. The medium then replaced by the

complete medium containing FBS, and cultured under normal conditions (5% CO_2 and 95% air) for 8 h.

The Treatment of LQ

LQ was dissolved by DMSO at a stock concentration of 1 mmol/L. Then diluted to different concentrations with medium before use. The model group and the normal group were given medium containing 0.1% DMSO.

Cell Viability Assay

HBMECs were seeded in 96-well plates with 5×10^3 cells/well and incubated in complete medium under normal oxygen incubator overnight. To explore the safety dose of LQ, cells were incubated in the presence of 0.1, 0.5, 1, 2, 5, 10 μmol/L for 24 h in serum free medium under normal incubators. Then the safe dose was chosen for the next experiment. Cells were incubated in the presence of LQ (0.1, 0.5, 1 μmol/L) for 12 h in serum free medium under hypoxic incubators. Cells were then incubated with the same concentration of LQ as above for 8 h in complete medium under normal condition. Cell viability was determined by CCK-8 method according to the manufacturer's instructions. Six holes were designed and repeated three times.

Scratch Healing Assay

HBMECs were seeded in a 12-well plate with 2×10^5 cells/mL and incubated in normal condition. Since the cells were covered in the holes, a straight line was drawn along the bottom of the plate with a 10 μL gunhead and photographed immediately (0 h). After the scratched cells were washed with PBS, different concentrations of LQ were added, and after H/R treatment, photographs were taken again. ImageJ was used to calculate the size of the damaged area enclosed by cells photographed twice. The final expression was the area relative to the control group. Two duplicate holes were set for each concentration and repeated three times.

Tube Formation Assay

Matrigel (9–12 mg/ml) was plated in a 96-well plate with 50 μL/well and allowed to curdle at 37°C in normal incubator for 30 min. HBMECs were seeded in a 24-well plate with 2×10^5 cells/mL and incubated in normal condition overnight. Different concentrations of LQ were added and the cells were digested and collected after the treatment of H/R. HBMECs were placed 5×10^5 cells/mL per well on the pre-solidified matrigel, then cultured in a 37°C normal incubator for 8 h. The tube formation was observed under the microscope, and take pictures, five pieces per well. The length and number of the branch of the tube was calculated by software, which was finally expressed as the length relative to the control group. Two multiple holes were set for each concentration, and the experiment was repeated three times.

Mitochondrial Membrane Potentials Assay

HBMECs were seeded in 12-well plates with 5×10^4 cells/mL and incubated in 37°C, containing 5%CO_2 incubator overnight. After treatment of different concentrations of LQ under H/R condition, JC-1 probe was employed to measure the change of mitochondrial membrane potentials. Briefly, 500 μL 1 × JC-1 staining working fluid was added into each well, incubated in the incubator for 20 min, washed twice with 1 × JC-1 buffer, and finally 300 μL PBS was added to take pictures with high content cell analyzer, and the fluorescence intensity was calculated with ImageJ software. Two multiple wells were set for each concentration and the experiment was repeated three times.

Apoptosis Assay

Annexin V and PI staining were employed to measure apoptosis detection. HBMECs were treated with different concentrations of LQ and incubated in H/R condition. Then cells were digested and collected, after centrifuged and washed with pre-cooled PBS, 1 × binding buffer was used to resuspended. The fluorescein-conjugated Annexin V and PI reagent were added to cell suspensions. Then the suspensions were incubated in dark for 10 min and were assessed by Beckman flow cytometer. The experiment was repeated three times.

Enzyme-Linked Immunosorbent Assay (ELISA)

After treatment of HBMECs with LQ and H/R, the supernatants were collected. The expression of ICAM-1, VCAM-1, SOD and MDA were detected by ELISA according to the manufacturer's protocol.

Reactive Oxygen Species (ROS) Assay

HBMECs were treated with different concentrations of LQ and H/R, DCFH-DA probe was loaded into cells, which can be oxidized by ROS to generate fluorescence and can be detected. After incubating at 37°C for 30 min, the probes that did not enter the cells were fully removed by washing them three times with serum-free medium. Finally, the high content cell analyzer was used to take pictures, and the fluorescence intensity was calculated by software with the control group as the reference. The experiment was repeated at least three times.

Western Blot Assay

HBMECs were treated with LQ (0.1, 0.5, 1 μmol/L) and H/R, then the cells were collected for subsequent experiments. BCA kit was employed to measure the protein concentration, and 30 μg proteins were used in isolation of SDS-PAGE. After the proteins were transferred to polyvinylidene difluoride (PVDF) membrane, 5% of skimmed milk powder is used to block making the binding of the first and second antibodies. Membranes were then incubated with antibodies against Nrf2 (Rabbit, 1:1,000), Keap1 (Rabbit, 1:1,000), ATF6 (Rabbit, 1:1,000), GRP78 (Rabbit, 1:1,000), ZO-1 (Rabbit, 1:1,000), Claudin-5 (Rabbit, 1:1000) 16–18 h at 4°C. Subsequently, the first antibodies were adsorbed and membranes were washed with Tris Buffered saline Tween (TBST) for three times, horseradish peroxidase conjugated goat-anti-rabbit secondary antibodies (IgG-HRP, 1: 10,000) were incubated within 1 h. Finally, the enhanced chemiluminescent (ECL) reagents were used for development. The expression of GAPDH (Rabbit, 1:10,000) was used as an internal reference. The experiment was repeated at least three times.

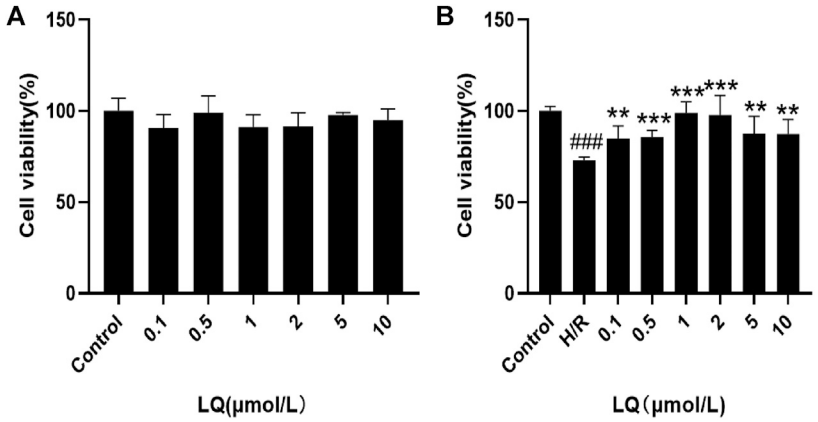

FIGURE 1 | LQ increase cell vitality. **(A)** LQ under the concentrations of 0.1–10 μmol/L had no effect on HBMECs. **(B)** The ability of H/R-HBMECs could be increased under various concentrations of LQ (0.1, 0.5, 1 μmol/L). Every experiment was performed less than three times. $^{###}p < 0.001$, compared to control. $^{**}p < 0.01$, $^{***}p < 0.001$, compared to H/R.

Proteomic Analysis

HBMECs were treated with LQ of 1 μmol/L and H/R, then the cells were collected. The cells were gently scraped off from the culture plate, quickly put into liquid nitrogen for quick freezing, and then moved to −80°C for storage. The proteins extracted from cells were quantified by iTRAQ labeling, and the proteins with p value < 0.05 and ratio multiple change >1.2 or <0.83 were defined as differentially expressed proteins. Then, these differentially expressed proteins were analyzed by GO functional enrichment, and the related differential proteins were found.

Statistical Analysis

The GraphPad Prism 8 was used for statistical analysis. Two independent samples were analyzed by t-test, and the measurement data was described by mean ± Standard deviation (SD). The comparison between groups was conducted by one-way analysis of variance (ANOVA). The p value less than 0.05 indicated that the difference was statistically significant.

RESULTS

LQ can Enhance Cell Viability

To detect the effect of LQ on cell viability, CCK-8 kit was used. First, the safe dose of the drug was detected. As shown in **Figure 1A**, LQ had no effect on cell viability at 0.1–10 μmol/L. Subsequently, in order to find the effective dose of LQ, H/R-HBMECs were established. As shown in **Figure 1B**, LQ could promote the cell viability of H/R-HBMECs at 0.1–1 μmol/L. Ultimately, our study demonstrated that LQ could enhance cell viability in a certain concentration range.

LQ Promotes Migration and Tube Formation of H/R-HBMECs

To assess the migration capacity of LQ on H/R-HBMECs, wound healing assay was examined for healing rate. As shown in **Figures 2A,C**, after the treatment of H/R, the migration capacity of HBMECs reduced, while LQ could reverse this phenomenon dose-dependently. Moreover, to test the effects of LQ on tube formation of HBMECs under the treatment of H/R, Matrigel assay was used to simulate the angiogenesis experiment. Robust and complete tubular-like structures of HBMECs were observed in normal group, while tube formation was disrupted by H/R. However, vessel branch length and number could be increased in a dose-dependent manner under LQ treatment (**Figures 2B,D,E**). Our results indicate that LQ can promote cell migration and angiogenesis in a dose-dependent manner.

LQ can Reduce Apoptosis

It is well known that mitochondrial membrane potential decreases when cells are suffered from early apoptosis. To detect early apoptosis, JC-1 probe was used to detect changes in mitochondrial membrane potential. As shown in **Figures 3A,C**, the green fluorescence intensity was higher in the H/R group, which indicated that the membrane potential decreased and the cells underwent early apoptosis. However, in the presence of LQ, red fluorescence is relatively more, showing that early apoptosis is reduced. In order to further assess apoptosis, flow cytometry can be more intuitive detection. As shown in the **Figures 3B,D**, the apoptotic rate was significantly increased in the H/R group compared with the normal group. LQ can reduce cell apoptosis in a concentration-dependent manner. Our results showed that LQ could reduce apoptosis in a certain concentration range.

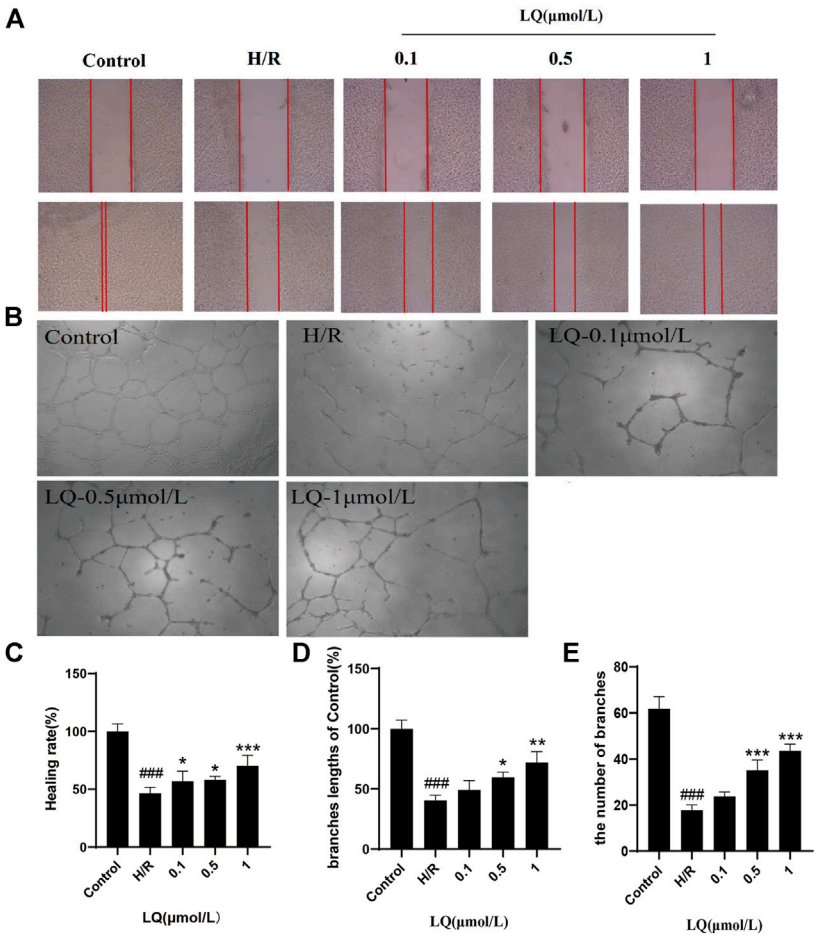

FIGURE 2 | LQ promote migration and tube formation of H/R-HBMECs. **(A)** The distance between scratches could be reduced in the presence of LQ (0.1, 0.5, 1 μmol/L). **(B)** The branches length of the tube could be increased by different concentrations of LQ (0.5, 1 μmol/L). **(C)** The healing rate data analyze. **(D)** The branches length of the tube dada analyze. **(E)** The number of branches of tube data analyze. $^{###}p < 0.001$, compared to control. $^{*}p < 0.05$, $^{**}p < 0.01$, $^{***}p < 0.001$, compared to H/R.

LQ Reduces the Elevation of ICAM-1 and VCAM-1

In order to detect the effect of LQ on the surface adhesion of HBMECs, the levels of ICAM-1 and VCAM-1 were detected by ELISA kit, which are important adhesion molecule mediating the adhesion reaction. As shown in **Figure 4**, LQ can alleviate the elevation of ICAM-1 and VCAM-1 caused by H/R, thereby reducing cell-to-cell or cell-to-matrix adhesion, reducing endothelial cell permeability, and further ensuring the integrity of the BBB.

LQ Regulates ROS, SOD and MDA Levels

Since oxidative stress can occur in ischemic events, we explored whether LQ can reduce oxidative stress caused by H/R. High content cell analysis system was used to detect the fluorescence intensity of ROS. In our study, green fluorescence was enhanced in the model group compared with the control group, indicating that oxidative stress events occurred. As shown in **Figure 5A**, LQ at a concentration of 0.1–1 μmol/L can reduce the production of ROS, then reduce oxidative stress, and protect cells from damage. Meanwhile, the detection of cell supernatant by ELISA indicated, SOD and MDA level increased in H/R group, as shown in **Figures 5B,C**. However, LQ could significantly attenuate the above function of HBMECs.

LQ Regulates Oxidative Stress and Endoplasmic Reticulum (ER) Stress Pathway Proteins to Maintain BBB Integrity

To further understand the protective mechanism of LQ on H/R-HBMECs, we first studied its oxidative stress pathway. Since Nrf2/Keap1 pathway plays a key role in oxidative stress, we investigated whether LQ could regulate the expression of these proteins. As shown in **Figures 6A,B**, LQ dramatically increased the levels of Nrf2 and decreased the expression of Keap1, indicating that Nrf2/Keap1 pathway involved LQ protects HBMECs from oxidative stress. Meanwhile, since ER stress is activated by

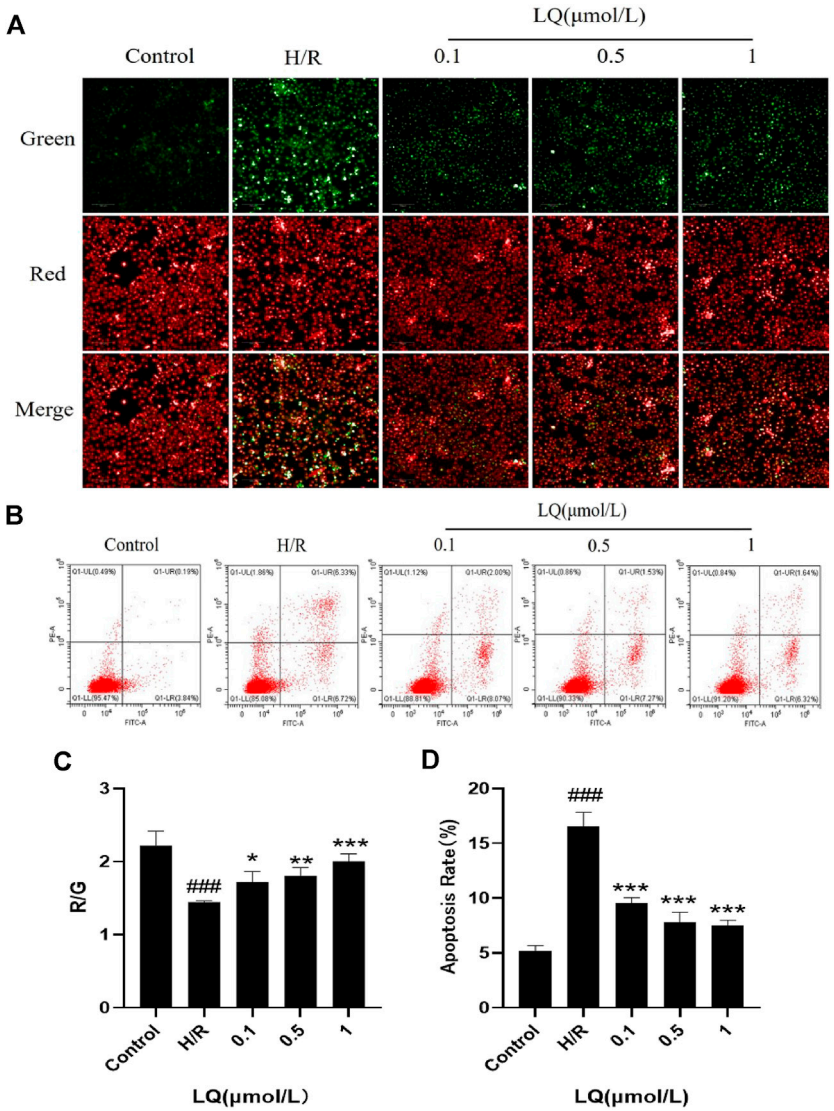

FIGURE 3 | LQ can reduce apoptosis. **(A, C)** The mitochondrial membrane was increased by LQ. Green represents the decrease of membrane potential and red was increased. The results are expressed as the intensity of red fluorescence relative to green fluorescence. **(B, D)** The upper left corner represents necrotic cells due to mechanical injury, the upper right corner represents late apoptotic cells, the lower left corner represents normal cells, and the lower right corner represents early apoptosis. Flow cytometry detection of LQ can reduce cell apoptosis. $^{###}p < 0.001$, compared to control. $^{*}p < 0.05$, $^{**}p < 0.01$, $^{***}p < 0.001$, compared to H/R.

ischemia-reperfusion, we investigated whether LQ could inhibit endoplasmic reticulum (ER) stress after H/R treatment. In our study, LQ reduced the levels of ATF6 and GRP78 in H/R-HBMECs, showing that the inhibitory effect of LQ on ER stress is involved in its protective mechanism, as shown in **Figures 6C,D**.

Furthermore, in order to clarify whether LQ protects HBMECs from H/R injury and can maintain the integrity of the BBB, we studied the expression of ZO-1 and Claudin-5 by LQ, and once the BBB is disrupted, the expression of both will be reduced. As shown in **Figures 6E,F**, ZO-1 and Claudin-5 expression decreased when subjected to H/R injury, indicating that BBB integrity was disrupted, and LQ could increase the expression of ZO-1 and Claudin-5 to maintain BBB integrity. Our results showed that LQ could inhibit oxidative stress and ER stress, protect HBMECs, and further maintain the integrity of BBB.

iTRAQ Proteomics Analysis

Differentially Expression Proteins

To examine the difference in H/R-HBMECs in the presence of LQ or not, we conducted the proteomics analysis by iTRAQ. Proteins exhibiting a p-value < 0.05 and a ratio fold change >1.2 or <0.83 were defined as differentially expressed proteins. In iTRAQ labeling, 172 proteins were identified as differentially expressed proteins between the control and model groups, among which 94 were upregulated and 78 were downregulated in the model group. There were 434 proteins identified as differentially expressed proteins between the model group and the LQ group, of which

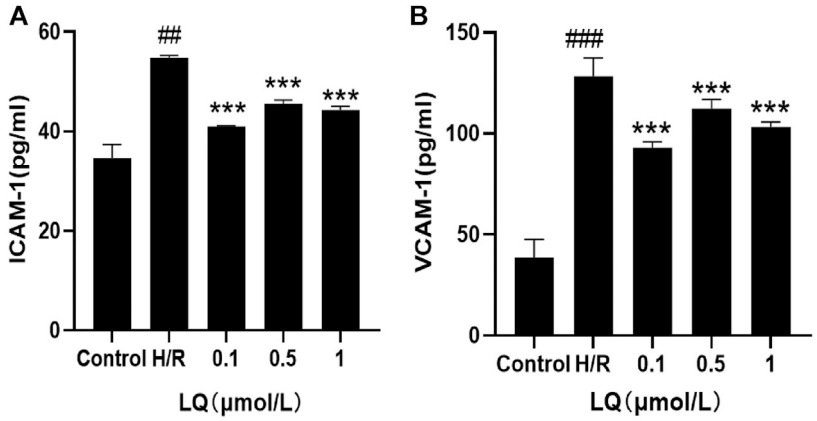

FIGURE 4 | LQ decrease the increase of ICAM-1 and VCAM-1. **(A)** Compared with control, the expression of ICAM-1 was increased in H/R group, and LQ could reduce the elevated ICAM-1. **(B)** Compared with control, the expression of VCAM-1 was increased in H/R group, and LQ could reduce the elevated VCAM-1. $^{\#\#}p < 0.01$, $^{\#\#\#}p < 0.001$, compared to control. $^{***}p < 0.001$, compared to H/R.

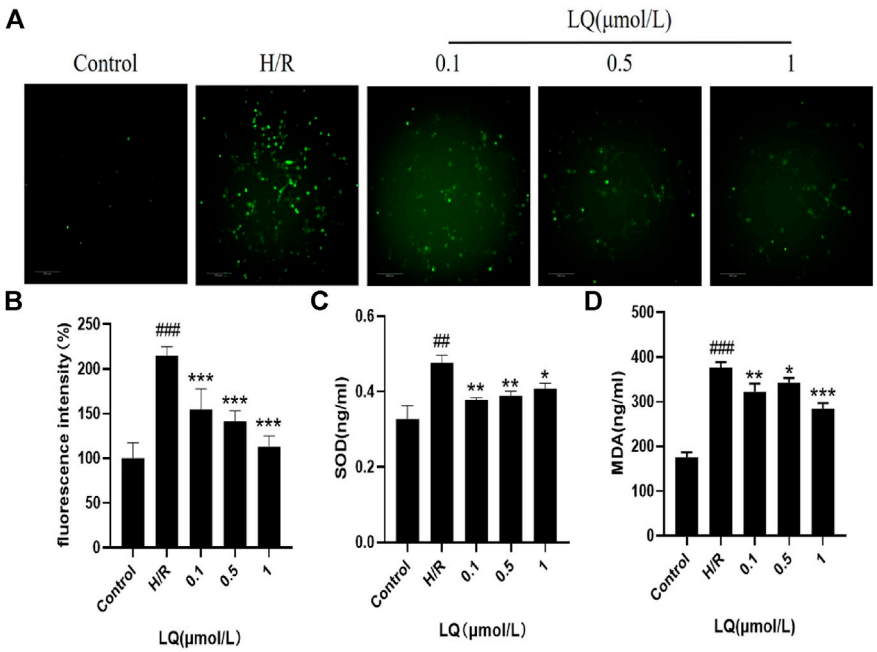

FIGURE 5 | LQ regulates ROS, SOD and MDA levels. **(A, B)** Green fluorescence represents ROS, compared with control, green fluorescence intensity in H/R group is enhanced, representing the increase of ROS level, and LQ can reduce ROS level. **(C)** SOD level was increased by H/R, and LQ reduced SOD level. **(D)** MDA level was increased by H/R, and LQ decreased MDA level. $^{\#\#}p < 0.01$, $^{\#\#\#}p < 0.001$, compared to control. $^{*}p < 0.05$, $^{**}p < 0.01$, $^{***}p < 0.001$, compared to H/R.

270 were up-regulated and 164 were down regulated in the LQ group, as shown in **Figure 7A**. 29 of the same differentially expressed proteins were shared between the two groups, as shown in **Figure 7B**, **Table1**. The expression of these differentially expressed proteins was analyzed by hierarchical clustering as shown in **Figure 7C**.

GO Analysis

To elucidate the biological significance of the 29 differentially expressed proteins, GO analysis was first performed on the differentially expressed proteins and then they were classified according to molecular function, biological process, and cellular component. The data of each category are shown in **Figure 8**. In the biological function category, the negative regulation of apoptosis process appeared significant enrichment. Under the cellular component, there was significant enrichment in the nucleus, cellular exosomes, mitochondria and membrane. In addition, ATP binding and metal ion binding are the most abundant in the category of molecular function.

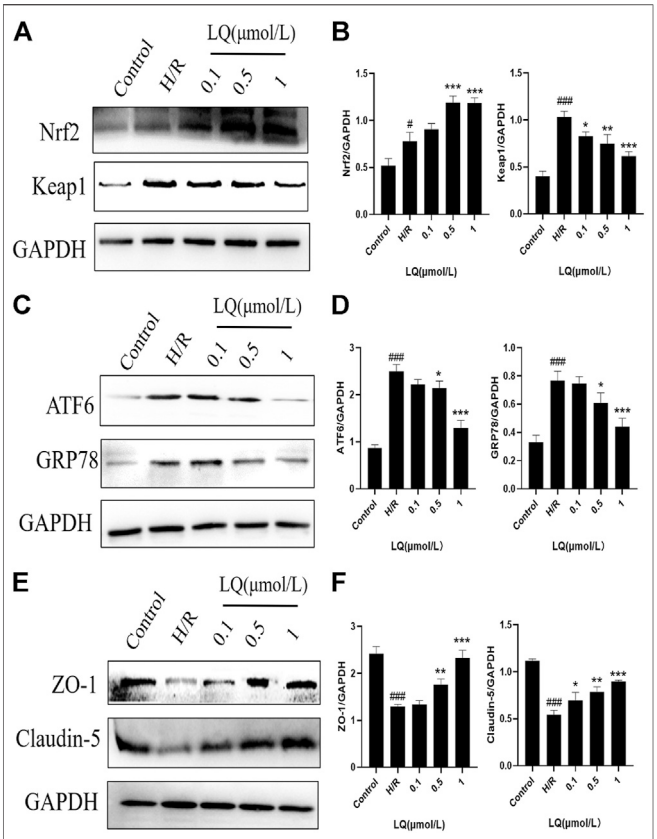

FIGURE 6 | LQ regulations oxidative stress and ER stress pathway proteins and maintains BBB integrity. **(A, B)** The oxidative stress pathway proteins Keap1 and Nrf2 were detected by Western blot. **(C, D)** The ER stress pathway proteins ATF6 and GRP78 were detected by Western blot. **(E, F)** The BBB relative proteins ZO-1 and Claudin-5 were analyzed by Western blot. $^{\#}p < 0.05$, $^{\#\#\#}p < 0.001$, compared to control. $^{*}p < 0.05$, $^{**}p < 0.01$, $^{***}p < 0.001$, compared to H/R.

Among the 29 differentially expressed proteins, five proteins were related to cerebrovascular diseases, including ANXA2, ApoA1, PGK1, CEBPB and MAP3K3. Among them, ANXA2 can be used to rescue cross endothelial cell density and BBB function after brain injury and CNS disease (Li et al., 2019). ApoA1 is reported to regulate the expression of apolipoprotein in brain and reduce atherosclerosis (Button et al., 2019; Contu et al., 2019). The increase of PGK1 can also reduce the formation of atherosclerosis (Zhang et al., 2020). CEBPB is involved in the regulation of brain injury and inflammation (Cortes-Canteli et al., 2008). MAP3K3 plays an important role in maintaining neurovascular integrity (Fisher et al., 2015). This may be the key protein for LQ to protect H/R-HBMECs. Future studies will verify the role of these proteins in LQ to protect H/R-HBMECs.

DISCUSSION

After ischemic stroke, I/R injury-mediated BBB rupture is associated with vascular leakage, circulating cells, and solute infiltration, leading to worsening edema and parenchymal damage (Granger 320 and Kvietys, 2015; Fu et al., 2015). Maintaining the integrity of the BBB may be a promising therapeutic strategy. Studies have shown that the protection of I/R-injured BMECs can reduce the increase of BBB permeability and cerebral infarction area after permanent occlusion of middle cerebral artery in rats caused by ischemic injury (Fang et al., 2016). Moreover, blocking the monolayer hyperosmolarity of HBMECs induced by inflammatory factors, loss of tight junction with surrounding cells and expression of adhesion molecules can effectively alleviate neurological deficits and ischemic injury in rats (Zhang et al., 2017). In this study, we used H/R to simulate ischemia-reperfusion *in vitro*, which is helpful to study the protective effect of LQ on HBMECs.

In this study, the safe and effective dose of LQ was screened out through the detection of cell viability. Subsequent studies were carried out under the premise of ensuring drug safety and non-toxicity. Promoting angiogenesis after restoring blood supply can protect cells against environmental stress including hypoxia (Li et al., 2017). This study was to systematically investigate the potential effects of LQ on angiogenesis using tubule formation assay and endothelial cell migration. Our results showed that LQ could effectively promote angiogenesis under H/R stimulation, such as tube formation and migration. Increasing evidence suggested that endothelial cell apoptosis may mediate brain dysfunction, suggesting that I/R-induced cerebrovascular lesions may involve microvascular endothelial cell apoptosis. Our study showed that LQ could reverse the decrease of mitochondrial membrane potential due to early apoptosis, thereby reducing apoptosis.

When the BBB is threatened, the expression of ICAM and VCAM increases, leading to the release of neurotoxic substances by neutrophils and monocytes, which in turn damage brain cells (Willam et al., 1999; Volcik et al., 2010). In this study, we found that LQ could reverse the elevation of ICAM-1 and VCAM-1, reduce their adhesion to surrounding toxic substances, and ultimately played a role in brain protection. In addition, after cerebral ischemia, cells will produce a large number of free radicals, such as ROS, excessive free radicals are the main mechanism of cell lipid peroxidation, which is one of the important causes of cell damage. At the same time, the activity of oxidases such as MDA will increase, which will destroy the balance of oxidation-antioxidation in the body, leading to severe damage of the blood-brain barrier and further worsen brain injury (Schreibelt et al., 2007). Our study found that LQ could decrease MDA expression, maintain oxidative balance and reduce brain injury. Besides, antioxidant enzymes such as SOD will also be reduced after ischemic events (Schreibelt et al., 2007). However, in our study, SOD level increased in H/R group, and the expression of it decreased after the treatment of LQ. We guessed that stress protection measures occur after cells were injured, forcing SOD level to rise, while LQ alleviated oxidative stress damage, thereby reducing SOD levels.

Nrf2 is an important transcription factor regulator and plays an important role in oxidative stress. Therefore, Nrf2 signaling is considered a therapeutic target for several human diseases (Taguchi et al., 2011). Keap1 is a negative regulator of Nrf2. When the body is subjected to oxidative stress,

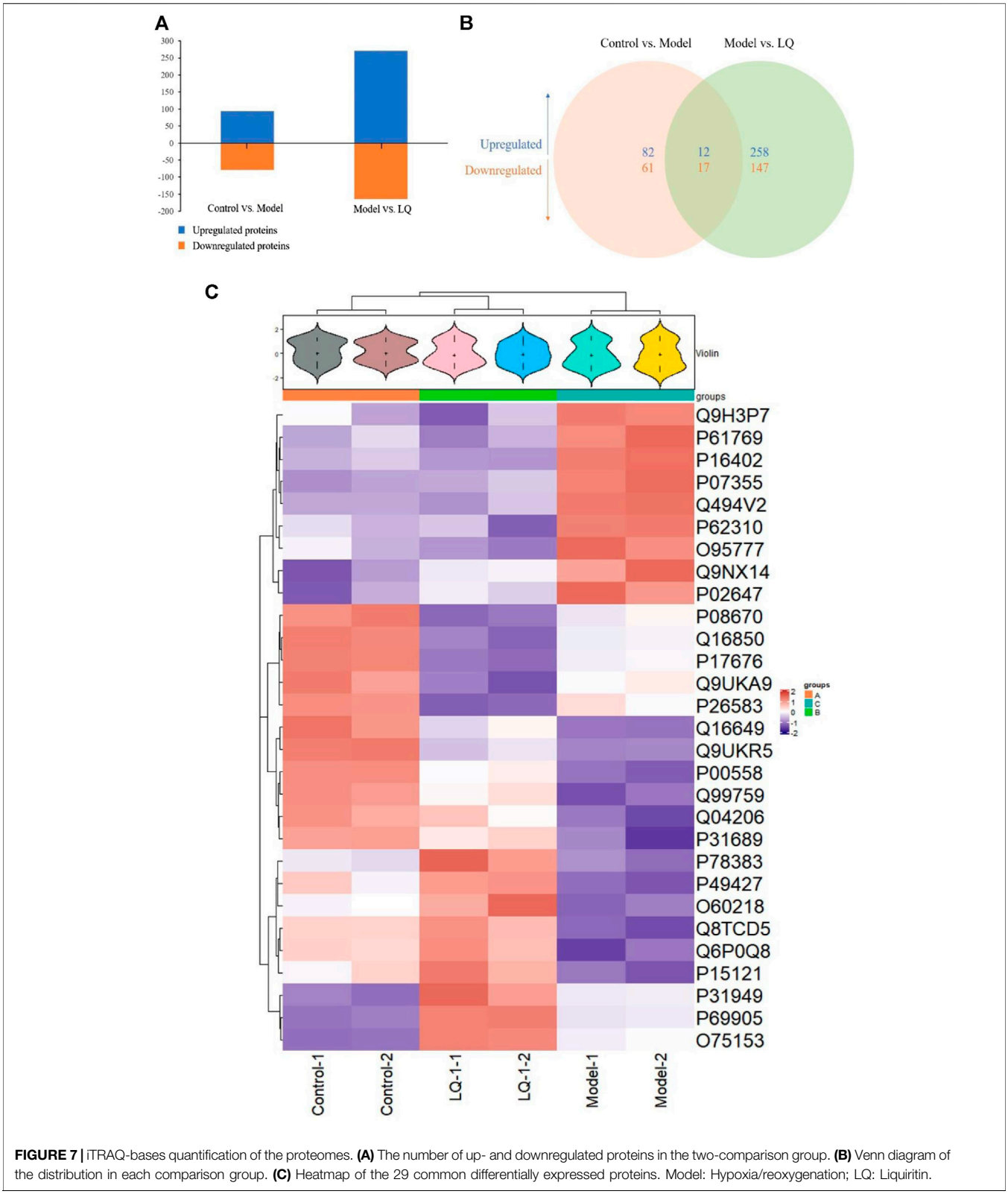

FIGURE 7 | iTRAQ-bases quantification of the proteomes. **(A)** The number of up- and downregulated proteins in the two-comparison group. **(B)** Venn diagram of the distribution in each comparison group. **(C)** Heatmap of the 29 common differentially expressed proteins. Model: Hypoxia/reoxygenation; LQ: Liquiritin.

Keap1 decouples from Nrf2, and Nrf2 transfers into the nucleus. It combines with ARE, an antioxidant response element, and promotes the expression of antioxidants to enhance the antioxidant capacity of cells (Komatsu et al., 2010). When stimulated by oxidative stress, the Keap1/Nrf2 signaling pathway is activated, the body undergoes

TABLE 1 | The common differentially expressed proteins.

Accession	Gene Name	Description
P07355	ANXA2	Annexin A2
P16402	H1-3	Histone H1.3
P31949	S100A11	Protein S100-A11
O75153	CLUH	Clustered mitochondria protein homolog
P69905	HBA1	Hemoglobin subunit alpha
O95777	LSM8	U6 snRNA-associated Sm-like protein LSm8
P61769	B2M	Beta-2-microglobulin
P02647	APOA1	Apolipoprotein A-I
P62310	LSM3	U6 snRNA-associated Sm-like protein LSm3
Q9NX14	NDUFB11	NADH dehydrogenase [ubiquinone] 1 beta subcomplex subunit 11, mitochondrial
Q9H3P7	ACBD3	Golgi resident protein GCP60
Q494V2	CFAP100	Cilia- and flagella-associated protein 100
P08670	VIM	Vimentin
P00558	PGK1	Phosphoglycerate kinase 1
P31689	DNAJA1	DnaJ homolog subfamily a member 1
P26583	HMGB2	High mobility group protein B2
Q9UKA9	PTBP2	Polypyrimidine tract-binding protein 2
P15121	AKR1B1	Aldo-keto reductase family 1 member B1
O60218	AKR1B10	Aldo-keto reductase family 1 member B10
Q16850	CYP51A1	Lanosterol 14-alpha demethylase
Q9UKR5	ERG28	Ergosterol biosynthetic protein 28
Q6P0Q8	MAST2	Microtubule-associated serine/threonine-protein kinase 2
P17676	CEBPB	CCAAT/enhancer-binding protein beta
P78383	SLC35B1	Solute carrier family 35 member B1
Q8TCD5	NT5C	5′ (3′)-deoxyribonucleotidase, cytosolic type
Q99759	MAP3K3	Mitogen-activated protein kinase kinase 3
Q04206	RELA	Transcription factor p65
Q16649	NFIL3	Nuclear factor interleukin-3-regulated protein
P49427	CDC34	Ubiquitin-conjugating enzyme E2 R1

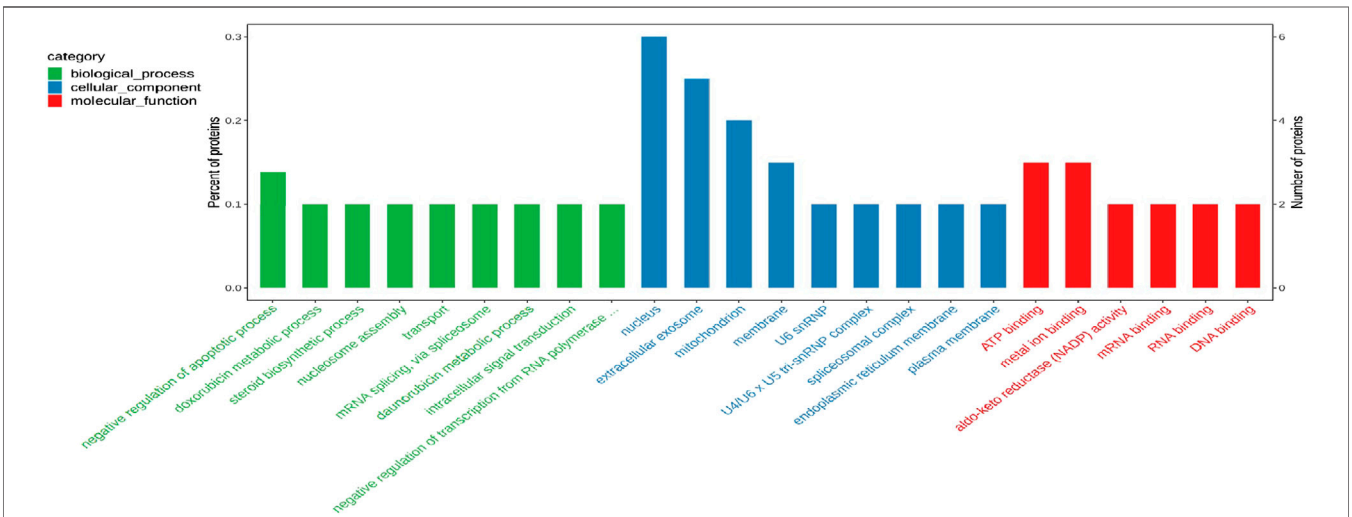

FIGURE 8 | Gene ontology (GO) enrichment analysis of 29 common differentially expressed proteins.

self-antioxidant response, and Nrf2 expression will elevated, but this is not sufficient to guarantee its anti-oxidative stress damage. Our study found that LQ could down-regulate the expression of Keap1, activate the downstream Nrf2/ARE antioxidant pathway, and protect cells from damage caused by H/R.

Meanwhile, ischemia and oxidative stress can lead to disorders in the folding of ER proteins, which can stimulate ER stress (Hetz, 2012). ER stress can be activated through three pathways: PKR-like ER kinase (PERK), inositol requiring enzyme 1 (IRE1), and the activating transcription factor-6 (ATF-6), which signal transduction proteins protect cells from ER stress under

physiological conditions (Hetz et al., 2020). However, when the organism is threatened by the external environment, ER stress can induce apoptosis through these three pathways. And studies have shown that inhibiting ER stress can reduce brain injury after I/R injury (Nakka et al., 2010). Our study showed that H/R led to the activation of ER stress system, elevated expression of ATF6 and GRP78, and caused apoptosis. However, LQ could reduce the expression of both, inhibit ER stress, and then reduce apoptosis.

In addition, in order to find the possible targets of LQ, proteomic analysis was carried out. 29 common differential proteins were detected among the control group, H/R group and LQ group. Among them, ANXA2, ApoA1, PGK1, CEBPB and MAP3K3 were related to atherosclerosis and cerebral inflammation. Therefore, future studies will verify the role of these proteins in the protection of H/R-HBMECs by LQ.

However, there are still many limitations in this experiment. In our study, for BBB integrity experiment, we only detected the expression of ZO-1 and Claudin-5, which are tight junction proteins and play an important role in BBB skeleton maintenance. However, in order to describe the integrity of BBB in many aspects, trans epithelial electric resistance also needs to measure the permeability. Secondly, for proteomic analysis, only five common differential proteins were described in this study, which may be the target proteins of LQ protecting H/R-HBMECs, but still need further experiments to be verified.

In conclusion, we investigated the protective effects of LQ on H/R-HBMECs. Our study showed that LQ could significantly improve the damage of HBMECs caused by H/R, which manifested as: enhancing cell viability, cell migration and reducing cell apoptosis. We further explored the mechanism of action of LQ and found that LQ could reduce ROS and MDA levels, as well as SOD expression, which may be related to its activation of Keap1/Nrf2 antioxidant pathway. Not only that, our study also demonstrated for the first time that LQ can reduce apoptosis by inhibiting ER stress, which provides the experimental basis for the compound ratio in the future. In the future, we should further study its targets in order to provide new treatment ideas for stroke.

DATA AVAILABILITY STATEMENT

The data presented in the study are deposited in the iProX repository, accession number is LMT902.

AUTHOR CONTRIBUTIONS

YH, ML, and HZ contributed to the conception and design of the experiment. ML, JK, and YD performed experiments. CC and YH performed the statistical analysis. YB and SG wrote the first draft of the manuscript. YW processed images. ML and JK wrote sections of the manuscript.

FUNDING

This work was supported by the National Key Research and Development Program of China (no. 2019YFC1711603) and the National Natural Science Foundation of China (no. 81771288 and 81771303).

REFERENCES

Abbott, N. J., Patabendige, A. A. K., Dolman, D. E. M., Yusof, S. R., and Begley, D. J. (2010). Structure and Function of the Blood-Brain Barrier. *Neurobiol. Dis.* 37, 13–25. doi:10.1016/j.nbd.2009.07.030

Button, E. B., Boyce, G. K., Wilkinson, A., Stukas, S., Hayat, A., Fan, J., et al. (2019). ApoA-I Deficiency Increases Cortical Amyloid Deposition, Cerebral Amyloid Angiopathy, Cortical and Hippocampal Astrogliosis, and Amyloid-Associated Astrocyte Reactivity in APP/PS1 Mice. *Alz Res. Ther.* 11, 44. doi:10.1186/s13195-019-0497-9

Chen, K. J., and Lu, A. P. (2006). Situation of Integrative Medicine in China: Results from a National Survey in 2004. *Chin. J. Integr. Med.* 12, 161–165. doi:10.1007/bf02836514

Contu, L., Carare, R. O., and Hawkes, C. A. (2019). Knockout of Apolipoprotein A-I Decreases Parenchymal and Vascular β-amyloid Pathology in the Tg2576 Mouse Model of Alzheimer's Disease. *Neuropathol. Appl. Neurobiol.* 45, 698–714. doi:10.1111/nan.12556

Cortes-Canteli, M., Luna-Medina, R., Sanz-Sancristobal, M., Alvarez-Barrientos, A., Santos, A., and Perez-Castillo, A. (2008). CCAAT/enhancer Binding Protein Deficiency Provides Cerebral Protection Following Excitotoxic Injury. *J. Cell Sci.* 121, 1224–1234. doi:10.1242/jcs.025031

Fang, Z., He, Q. W., Li, Q., Chen, X. L., Baral, S., Jin, H. J., et al. (2016). MicroRNA-150 Regulates Blood-brain Barrier Permeability via Tie-2 after Permanent Middle Cerebral Artery Occlusion in Rats. *FASEB J.* 30, 2097–2107. doi:10.1096/fj.201500126

Fisher, O. S., Deng, H., Liu, D., Zhang, Y., Wei, R., Deng, Y., et al. (2015). Structure and Vascular Function of MEKK3-Cerebral Cavernous Malformations 2 Complex. *Nat. Commun.* 6, 7937. doi:10.1038/ncomms8937

Fu, Y., Liu, Q., Anrather, J., and Shi, F.D. (2015). Immune Interventions in Stroke. *Nat. Rev. Neurol.* 11, 524–535. doi:10.1038/nrneurol.2015.144

GBD 2016 Lifetime Risk of Stroke Collaborators. (2018). Global, Regional, and Country-specific Lifetime Risks of Stroke, 1990 and 2016. *New Engl. J. Med.* 379, 2429–2437. doi:10.1056/NEJMoa1804492

GBD 2017 Causes of Death Collaborators. (2018). Global, Regional, and National Age-sex-specific Mortality for 282 Causes of Death in 195 Countries and Territories, 1980-2017: a Systematic Analysis for the Global Burden of Disease Study 2017. *Lancet* 392, 1736–1788. doi:10.1016/s0140-6736(18)32203-7

Granger, D. N., and Kvietys, P. R. (2015). Reperfusion Injury and Reactive Oxygen Species: The Evolution of a Concept. *Redox Biol.* 6, 524–551. doi:10.1016/j.redox.2015.08.020

Guo, X. Y., Liu, J., Liu, J., Li, H. J., Qi, Y., Qin, L. P., et al. (2013). Use of Traditional Chinese Medicine in Chinese Patients with Coronary Heart Disease. *Biomed. Environ. Sci.* 26, 303–310. doi:10.3967/0895-3988.2013.04.009

Hao, P.P., Jiang, F., Chen, Y.G., Yang, J., Zhang, K., Zhang, M.X., et al. (2015). Traditional Chinese Medication for Cardiovascular Disease. *Nat. Rev. Cardiol.* 12, 115–122. doi:10.1038/nrcardio.2014.177

Hetz, C. (2012). The Unfolded Protein Response: Controlling Cell Fate Decisions under ER Stress and beyond. *Nat. Rev. Mol. Cell Biol.* 13, 89–102. doi:10.1038/nrm3270

Hetz, C., Zhang, K., and Kaufman, R. J. (2020). Mechanisms, Regulation and Functions of the Unfolded Protein Response. *Nat. Rev. Mol. Cell Biol.* 21, 421–438. doi:10.1038/s41580-020-0250-z

Keaney, J., and Campbell, M. (2015). The Dynamic Blood-Brain Barrier. *Febs J.* 282, 4067–4079. doi:10.1111/febs.13412

Keep, R. F., Zhou, N., Xiang, J., Andjelkovic, A. V., Hua, Y., and Xi, G. (2014). Vascular Disruption and Blood-Brain Barrier Dysfunction in Intracerebral Hemorrhage. *Fluids Barriers CNS* 11, 18. doi:10.1186/2045-8118-11-18

Komatsu, M., Kurokawa, H., Waguri, S., Taguchi, K., Kobayashi, A., Ichimura, Y., et al. (2010). The Selective Autophagy Substrate P62 Activates the Stress Responsive Transcription Factor Nrf2 through Inactivation of Keap1. *Nat. Cell Biol.* 12, 213–223. doi:10.1038/ncb2021

Li, H., Ye, M., Zhang, Y., Huang, M., Xu, W., Chu, K., et al. (2015). Blood-brain Barrier Permeability of Gualou Guizhi Granules and Neuroprotective Effects in Ischemia/reperfusion Injury. *Mol. Med. Rep.* 12, 1272–1278. doi:10.3892/mmr.2015.3520

Li, L., Wang, M., Mei, Z., Cao, W., Yang, Y., Wang, Y., et al. (2017). lncRNAs HIF1A-AS2 Facilitates the Up-Regulation of HIF-1α by Sponging to miR-153-3p, Whereby Promoting Angiogenesis in HUVECs in Hypoxia. *Biomed. Pharmacother.* 96, 165–172. doi:10.1016/j.biopha.2017.09.113

Li, W., Chen, Z., Yuan, J., Yu, Z., Cheng, C., Zhao, Q., et al. (2019). Annexin A2 Is a Robo4 Ligand that Modulates ARF6 Activation-Associated Cerebral Trans-endothelial Permeability. *J. Cereb. Blood Flow Metab.* 39, 2048–2060. doi:10.1177/0271678x18777916

Liberale, L., Gaul, D. S., Akhmedov, A., Bonetti, N. R., Nageswaran, V., Costantino, S., et al. (2020). Endothelial SIRT6 Blunts Stroke Size and Neurological Deficit by Preserving Blood-Brain Barrier Integrity: a Translational Study. *Eur. Heart J.* 41, 1575–1587. doi:10.1093/eurheartj/ehz712

Molina, C. A. (2011). Reperfusion Therapies for Acute Ischemic Stroke: Current Pharmacological and Mechanical Approaches. *Stroke* 42, S16–S19. doi:10.1161/strokeaha.110.598763

Nakka, V. P., Gusain, A., and Raghubir, R. (2010). Endoplasmic Reticulum Stress Plays Critical Role in Brain Damage after Cerebral Ischemia/reperfusion in Rats. *Neurotox Res.* 17, 189–202. doi:10.1007/s12640-009-9110-5

Powers, W. J., Rabinstein, A. A., Ackerson, T., Adeoye, O. M., Bambakidis, N. C., Becker, K., et al. (2019). Guidelines for the Early Management of Patients with Acute Ischemic Stroke: 2019 Update to the 2018 Guidelines for the Early Management of Acute Ischemic Stroke: A Guideline for Healthcare Professionals from the American Heart Association/American Stroke Association. *Stroke* 50, e344–e418. doi:10.1161/str.0000000000000211

Schreibelt, G., van Horssen, J., van Rossum, S., Dijkstra, C. D., Drukarch, B., and de Vries, H. E. (2007). Therapeutic Potential and Biological Role of Endogenous Antioxidant Enzymes in Multiple Sclerosis Pathology. *Brain Res. Rev.* 56, 322–330. doi:10.1016/j.brainresrev.2007.07.005

Taguchi, K., Motohashi, H., and Yamamoto, M. (2011). Molecular Mechanisms of the Keap1-Nrf2 Pathway in Stress Response and Cancer Evolution. *Genes Cells* 16, 123–140. doi:10.1111/j.1365-2443.2010.01473.x

Volcik, K. A., Ballantyne, C. M., Hoogeveen, R., Folsom, A. R., and Boerwinkle, E. (2010). Intercellular Adhesion Molecule-1 G241R Polymorphism Predicts Risk of Incident Ischemic Stroke. *Stroke* 41, 1038–1040. doi:10.1161/strokeaha.109.575563

Widimsky, P., Coram, R., and Abou-Chebl, A. (2014). Reperfusion Therapy of Acute Ischaemic Stroke and Acute Myocardial Infarction: Similarities and Differences. *Eur. Heart J.* 35, 147–155. doi:10.1093/eurheartj/eht409

Willam, C., Schindler, R., Frei, U., and Eckardt, K.U. (1999). Increases in Oxygen Tension Stimulate Expression of ICAM-1 and VCAM-1 on Human Endothelial Cells. *Am. J. Physiol. Heart Circul. Physiol.* 276, H2044–H2052. doi:10.1152/ajpheart.1999.276.6.H2044

Wu, K.W., Lv, L. L., Lei, Y., Qian, C., and Sun, F. Y. (2019). Endothelial Cells Promote Excitatory Synaptogenesis and Improve Ischemia-Induced Motor Deficits in Neonatal Mice. *Neurobiol. Dis.* 121, 230–239. doi:10.1016/j.nbd.2018.10.006

Zhang, H., Park, J. H., Maharjan, S., Park, J. A., Choi, K. S., Park, H., et al. (2017). Sac-1004, a Vascular Leakage Blocker, Reduces Cerebral Ischemia-Reperfusion Injury by Suppressing Blood-Brain Barrier Disruption and Inflammation. *J. Neuroinflammation* 14, 122. doi:10.1186/s12974-017-0897-3

Zhang, X., Guan, M. X., Jiang, Q. H., Li, S., Zhang, H. Y., Wu, Z. G., et al. (2020). NEAT1 Knockdown Suppresses Endothelial Cell Proliferation and Induces Apoptosis by Regulating miR-638/AKT/mTOR Signaling in Atherosclerosis. *Oncol. Rep.* 44, 115–125. doi:10.3892/or.2020.7605

Conflict of Interest: The authors declare that the research was conducted in the absence of any commercial or financial relationships that could be construed as a potential conflict of interest.

frontiers in Pharmacology

ORIGINAL RESEARCH
published: 06 August 2021
doi: 10.3389/fphar.2021.732655

Hu-Zhang-Qing-Mai-Yin Inhibits Proliferation of Human Retinal Capillary Endothelial Cells Exposed to High Glucose

Yuan-Yuan Yu[1†], Qiu-Ping Liu[1†], Meng-Ting Li[2], Pei An[1], Yu-Ying Chen[1], Xin Luan[1], Chao Lv[1]* and Hong Zhang[1]**

[1]*Institute of Interdisciplinary Integrative Medicine Research, Shanghai University of Traditional Chinese Medicine, Shanghai, China,* [2]*Department of Neurology, Yueyang Integrated Traditional Chinese and Western Medicine Hospital, Shanghai University of Traditional Chinese Medicine, Shanghai, China*

OPEN ACCESS

Edited by:
Zhang Yuefan,
Shanghai University, China

Reviewed by:
Shi Fei Li,
Shanxi University, China
Fu Peng,
Sichuan University, China

***Correspondence:**
Xin Luan
luanxin@shutcm.edu.cn
Chao Lv
lvchaoanhui@163.com
Hong Zhang
zhanghong@shutcm.edu.cn

†*These authors have contributed equally to this work.*

Specialty section:
This article was submitted to Ethnopharmacology, a section of the journal Frontiers in Pharmacology

Received: *29 June 2021*
Accepted: *29 July 2021*
Published: *06 August 2021*

Citation:
Yu Y-Y, Liu Q-P, Li M-T, An P, Chen Y-Y, Luan X, Lv C and Zhang H (2021) Hu-Zhang-Qing-Mai-Yin Inhibits Proliferation of Human Retinal Capillary Endothelial Cells Exposed to High Glucose. Front. Pharmacol. 12:732655. doi: 10.3389/fphar.2021.732655

Background: Diabetic retinopathy (DR) is one of the serious complications of diabetes and an important cause of blindness. Despite much research on the pathogenesis of DR, there is still a lack of safe and effective treatment methods. Hu-zhang-qing-mai-yin (HZQMY), a Chinese medicine formula, has been clinically used in the safe and effective treatment of DR for many years. However, the systematic pharmacological research is lacking. The aim of this study was to evaluate the anti-DR effects of HZQMY and explore the possible mechanism involved. Methods: The constituents of HZQMY were analyzed by LC-MS/MS. DR model was established by high glucose simulation on human retinal capillary endothelial cells (HRCECs) *in vitro*. The cell viability, cell proliferation, cell apoptosis, and tube formation were assessed. Subsequently the related mechanisms were analyzed by assays for JC-1 mitochondrial membrane potential (MMP), intracellular ROS, ATP, western blot and proteomics. Results: 27 main chemical components contained in HZQMY were identified. HZQMY significantly inhibited the viability and proliferation of HRCECs exposed to high glucose, and promoted the apoptosis. In addition, HZQMY also boosted the release of ROS and suppressed tube formation of HRCECs under high glucose exposure. Meanwhile, HRCECs treated with high glucose released more ROS than normal cells, which could be markedly inhibited by HZQMY in a dose-dependent manner. Additionally, western blot assay indicated that HZQMY increased the expression of proteins related to the P38 signaling pathway and inhibited nuclear factor kappa-B (NF-κB) pathway. Proteomic analysis predicted that HSPA4, MAPK3, ENO1, EEF2 and ERPS may be the candidate targets of HZQMY in HRCECs. Conclusions: HZQMY inhibited the proliferation and promoted the Mitochondria related apoptosis of HRCECs exposed to high glucose possibly through regulating P38 and NF-κB signaling pathway.

Keywords: diabetic retinopathy, Chinese medicine formula, human retinal capillary endothelial cells, proliferation, apoptosis

INTRODUCTION

Diabetes is one of the most common chronic metabolic diseases, with an estimated 592 million diabetics worldwide by 2035 (Duh et al., 2017). Diabetic retinopathy (DR) is a highly specific neurovascular complication of type 1 and type 2 diabetes, which is one of the most common complications of diabetes and affects about one third of diabetic patients (Wong and Sabanayagam, 2020). The prevalence of diabetes among adults (20–79 years old) has risen to 8.8% and diabetic patients are more prone to suffer from cataract, glaucoma and other eye diseases (Bommer et al., 2017). Diabetes has a profound impact on multiple organ systems, but visual impairment and even blindness caused by DR may be one of the diseases that have the greatest impact on patient's quality of life (Antonetti et al., 2021). At present, the main treatment methods for DR include laser therapy, intravitreal injection of steroid hormones or taking anti-VEGF drugs, oral administration of calcium hydroxybenzene sulfonate, etc., but there are problems of ineffective or accompanied by a large number of side effects (Ihnat et al., 2007). Therefore, it is an urgent need for finding the therapy with good safety and effectivity.

In recent years, clinical studies have shown that the application of Chinese medicine in the prevention and treatment of DR has significant advantages due to the definite clinical efficacy (Xiao and Luo, 2018; Zhang et al., 2018). Based on modern pharmacology and clinical trials, Chinese medicines have the advantages of multi-target and multi-channel in the treatment of DR (Behl and Kotwani, 2017; He et al., 2016; Pang et al., 2015; Zhang et al., 2018). Clinical trials have shown that Chinese medicines can promote blood microcirculation, improve vascular endothelial function, protect the blood-retinal barrier, and inhibit oxidation and inflammation (He et al., 2016; Behl and Kotwani, 2017; Zhang et al., 2018).

Hu-zhang-qing-mai-yin (HZQMY) is an empirical Chinese medicine prescription produced by combining the theory of traditional Chinese theory with clinical experience, which is composed of root of *Polygonum cuspidatum* Sieb. et Zucc., fruit of *Forsythia suspensa,* whole herb of *Sedum sarmentosum* Bunge, whole herb of *Siegesbeckia orientalis* L., rattan stem of *Spatholobus suberectus* Dunn, root of *Glycyrrhiza uralensis* Fisch, root of *Stragalus membranaceus* (Fisch.) Bunge and root of *Ligusticum chuanxiong* hort. The formula plays the function of clearing heat and detoxification, promoting blood circulation and removing blood stasis. However, its active components and mechanism of action are still unclear, and systematic pharmacological studies on the treatment of DR are lacking.

In our study, the main ingredients of HZQMY were identified by HPLC-Q-TOF-MS, its anti-DR effects were evaluated and the mechanism of action was explored *in vitro*, so as to provide reference for the prevention and treatment of DR.

MATERIALS AND METHODS

Cells and Regents

Human retinal capillary endothelial cells (HRCECs) were acquired from the Cell Bank of Shanghai Academy of Chinese Sciences (Shanghai, China). Dulbecco's modified eagle medium (DMEM) was purchased from HyClone (Logan, United States), fetal bovine serum (FBS) was bought from GIBCO (Grand Island, United States). Cell Counting Kit-8 (CCK-8) and PBS were obtained from meilun biotechnology co., Ltd. (Dalian, China). ATP Assay Kit, Mitochondrial membrane potential kit and ROS assay kit were purchased from Beyotime Biotechnology (Shanghai, China). Apoptosis Detection Kit and cycle detection kit were provided by KeyGen Biotechnology co., Ltd. (Nanjing, China). Matrigel was provided by Corning (New York, United States). Primary antibody of p-NF-κB, NF-κB, p-P38, P38, BCL-XL, BCL-2 and GAPDH were bought from Cell Signaling Technology (Danvers, United States).

TABLE 1 | Components of HZQMY.

Plant name	Medicinal part	Dosage (g)
Polygonum cuspidatum Sieb. et Zucc	Root	18
Forsythia suspensa	Fruit	18
Sedum sarmentosum Bunge	Whole plant	30
Siegesbeckia orientalis L	Whole plant	18
Spatholobus suberectus Dunn	Rattan stem	15
Glycyrrhiza uralensis Fisch	Root	9
Stragalus membranaceus (Fisch.) Bunge	Root	15
Ligusticum chuanxiong hort	Root	18

Preparation of Hu-Zhang-Qing-Mai-Yin Extract

Root of *Polygonum cuspidatum* Sieb. et Zucc., fruit of *Forsythia suspensa*, whole plant of *Sedum sarmentosum* Bunge, whole plant of *Siegesbeckia orientalis* L., rattan stem of *Spatholobus suberectus* Dunn, root of *Glycyrrhiza uralensis* Fisch, root of *Stragalus membranaceus* (Fisch.) Bunge and root of *Ligusticum chuanxiong* hort. were provided by the ophthalmology Department of Longhua Hospital Affiliated to Shanghai University of Traditional Chinese Medicine (**Table 1**). These Chinese herbal medicines were put into the decocting pot, and extracted with 10 times volume pure water for 1 hour, two times in total. The decocting liquid were concentrated with a rotating evaporator after filtering with a 4-layer gauze. After that, the liquid was further pre-freezed at −50°C for 5 h for a vacuum dry in the material tray of the freeze-dryer. The dryer was heated up and finally fixed to −40°C for lyophilized 72 h to make a lyophilized powder which was stored in a refrigerator at −20°C for later use. The stock solution of the HZQMY extract was prepared with first grade pure water to the concentration of 0.1 g/ml, and then it was filtered and sterilized by 0.22 μm microporous membrane. For temporary use, the medium containing 10% FBS was diluted to the working concentrations.

LC-MS/MS Analysis

1.0 g of HZQMY extract was put into a 25 ml volumetric flask, and then 50% methanol was added to scale, ultrasonic treatment for 30 min, cooling, 50% methanol to make up the amount of loss reduction, fully mixed, filtrated with a 0.45 μm microporous membrane to obtain the test solution, and 10 μL was taken for mass spectrometry detection.

Agilent 6530 four-stage rod-time-of-flight mass spectrometry (Q-TOF-MS) system was performed, chromatographic separations were carried out on an ACQUITY UPLC HSS T3 (2.1 × 150 mm, 1.7 μm) column at 25°C and the drying gas (N_2) was 13 L/min. Gradient elution with mobile phase A (0.1 formic acid water), mobile phase B (acetonitrile): 99% A in 0–2 min; from 99 to 34% A in 2–20 min; from 34 to 5% A in 20–28 min. The mass spectrometry was performed in positive and negative ion scanning patter with a scanning range of 100–1700 m/z and a capillary voltage of 4000 V. The intercepting cone voltage is 60 V.

Cell Culture

HRCECs were cultured in DMEM containing 10% FBS and 1% penicillin-streptomycin at 37°C and 5% CO_2. DR model was established by induction of HRCECs with high glucose *in vitro* (Liu et al., 2020). The cells were divided into normal group (cells were cultured in normal-glucose (5.5 mM) media, NG), high glucose model group (cells were cultured in high-glucose (35 mM) media, HG), and HZQMY different dose groups. Except normal group, all the other groups of cells were given 35 mM glucose to imitate high-glucose environment. Different concentrations of HZQMY extract were used to treat the cells. Cells were collected for subsequent experiments following treatment with HZQMY extract for 24 h or 48 h.

CCK-8 Assay

HRCECs were seeded into 96-well plates (5×10^3 cells/well) for 24 h in a 5% CO_2 incubator at 37°C, then different concentrations of HZQMY extract (10, 25, 50, 100, 150 μg/ml) were added in 96-well plates for 24 and 48 h. Discarding the old medium, 100 μL of 10% CCK-8 kit was added into each well for incubation at 37°C for 30 min. OD value was detected at 450 nm with a microplate analyzer. Cell survival rate (%) = (OD value of experimental group–OD value of blank group)/(OD value of control group–OD value of blank group) ×100%.

Cell Colony Formation Assay

HRCECs were seeded into 6-well plates (600 cells/well) for 24 h in a 5% CO_2 incubator at 37°C, then added with different concentrations of the extract and cultured for 8 days. The cells were fixed with 4% paraformaldehyde for 30 min and stained with crystal violet for 15 min. Clone formation rate (%) = (amount of clones/number of inoculated cells) ×100%.

Cell Cycle Analysis

HRCECs were seeded into 6-well plates (5×10^5 cells/well) for 24 h in a 5% CO_2 incubator at 37°C, then each group was added with different concentrations of the extract for 24 h culture. Cells were harvested, 1 ml of precooled 70% ethanol was added to mix well, and fixed at 4°C for 2 h. The cells were collected, mixed with 0.5 ml PI into the sample tube, and incubated in the dark for 30 min. The red fluorescence was detected by flow cytometry at 488 nm, and the light scattering was recorded at the same time. The Beckman flow cytometer was used for detection.

Tube Formation Assay

60 μL of the dissolved matrigel (9–12 mg/ml) was added in a well in 96-well plate and then placed in the incubator at 37°C for 1 h. HRCECs were cultured under different concentrations of HZQMY with or without HG. Subsequently, 50 μL of cell suspension was collected and added into the pre-solidified matrigel for 8 h in the 37°C incubator. The tube formation was observed under an optical microscope, and photographed. ImageJ was used to calculate the number of lumens and the length of tubules.

Cell Nuclear Staining

HRCECs were seeded into 24-well plates (5×10^4 cells/well) for 24 h in a 5% CO_2 incubator at 37°C, then each group was added with different concentrations of the extract for 24 h culture. Subsequently, the cells were washed by PBS three times, 150 μL of 4% paraformaldehyde was added to each well and fixed at room temperature for 30 min, and remove the fixing solution, add 150 μL of 0.1% Triton X-100 for 10 min. Finally, 150 μL DAPI solution was added in each well for incubation at room temperature for 10 min in dark. The samples were photographed by Operetta CLS high-content analysis system.

Apoptosis Assay

HRCECs were seeded into 6-well plates (5×10^5 cells/well) for 24 h in a 5% CO_2 incubator at 37°C, then each group was added with different concentrations of drugs for 24 h culture. After that, the cells were digested with trypsin without Ethylene Diamine Tetraacetic Acid (EDTA) and centrifuged with a 15 ml centrifuge tube at 2000 rpm for 10 min at 4°C, and the supernatant was discarded. 100 μL 1 × FITC binding solution was added to mix well, then 5 μL FITC dye was added for 10 min incubation at room temperature in dark. Last, 5 μL PI dye was added for 5 min incubation in dark. The Beckman flow cytometer was used for detection.

Intracellular ROS Detection

HRCECs were seeded into a 96-well plate (1×10^5 cells/well) for 24 h in a 5% CO_2 incubator at 37°C, then each group was added with different concentrations of the extract for 6 h. DCFH-DA was added for 1 h incubation in a 37°C cell incubator. The Beckman flow cytometer was used for detection.

ATP Detection

ATP concentration was detected by the ATP Assay Kit. HRCECs were seeded into 6-well plates (5×10^5 cells/well) for 12 h in a 5% CO_2 incubator at 37°C, then added with different concentrations of HZQMY extract to culture for 24 h. Cells were lysed to isolate total protein, then centrifuged at 12,000 g and 4°C for 10 min. Next, 20 μL sample or standard solution were added to 100 μL ATP detection solution, mixed, and luminescence was measured with a multifunctional enzyme plate analyzer.

JC-1 Mitochondrial Membrane Potential Assay

HRCECs were seeded into 24-well plates (5×10^4 cells/well) for 24 h in a 5% CO_2 incubator at 37°C, then added with different

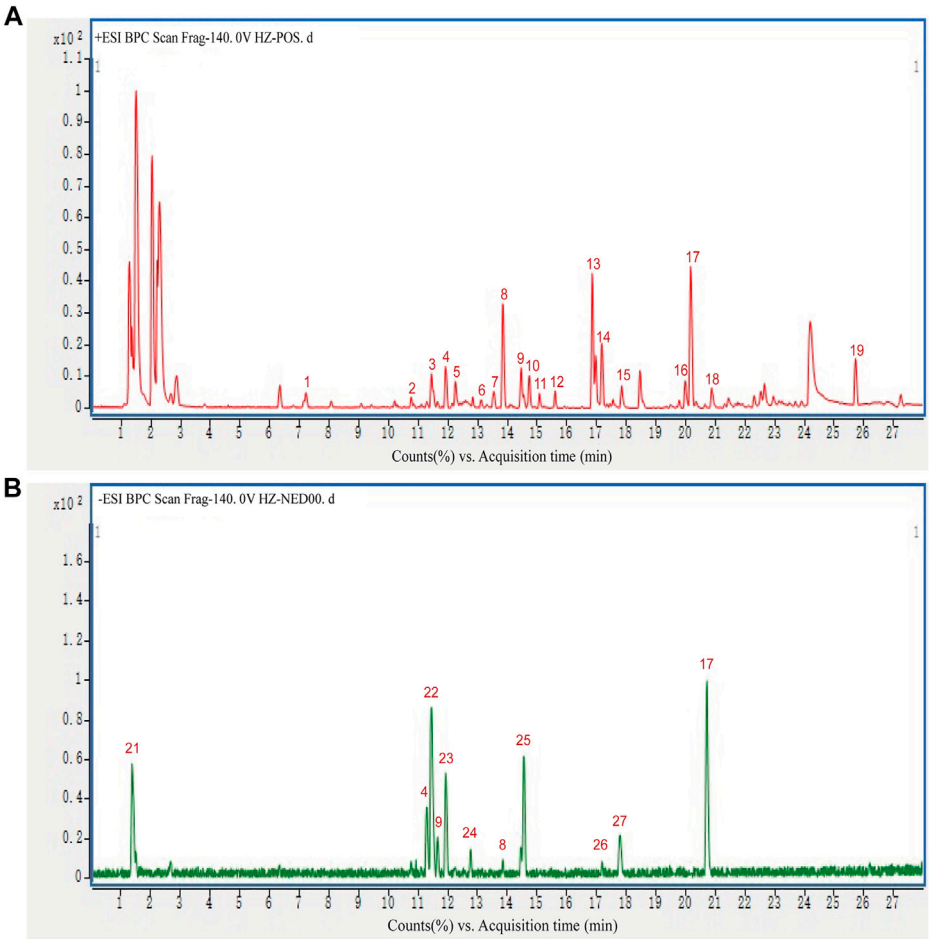

FIGURE 1 | HPLC-Q-TOF-MS chromatogram of 27 constituents in positive and negative mode.

concentrations of the extract for 24 h culture. Apoptotic cells should show green fluorescence after JC-1 staining, while normal cells show red fluorescence. The relative ratio of red-green fluorescence is often used to measure the proportion of mitochondrial depolarization, which was used as one of the early detection indicators of cell apoptosis. The fluorescence quantification was carried out using ImageJ software.

Western Blot Assay

HRCECs were seeded into 6-well plates (5×10^5 cells/well) for 24 h in a 5% CO_2 incubator at 37°C, then each group was added with different concentrations of the extract for 24 h culture. Cells were collected and total proteins were extracted from HRCECs using RIPA lysate and PMSF (RIPA: PMSF = 100: 1). Protein concentration was measured by using the BCA Protein Concentration Assay Kit. The proteins were separated by 10% SDS-polyacrylamide electrophoresis and transferred to PVDF membrane, which was then sealed with QuickBlock™ Blocking Buffer at room temperature for 1 h. After that, the membrane was incubated with the primary antibody overnight at 4°C, followed by washing 3 times with TBST, and the rabbit/mouse antibody was incubated at room temperature for 1 h. Then the membrane was washed 3 times with TBST. Finally, the gray values of the protein bands were detected and photographed by Chemi Scope Mini, and GAPDH was used as internal reference.

TMT Quantitative Proteomic Analysis

HRCECs (cultured with 35 mM glucose) were seeded into 100 mm culture dishes and 100 μg/ml HZQMY extract was added until 60% confluent. After 24 h, cells were harvested and flash-frozen in liquid nitrogen. Identification and analysis were processed by Ouyi Biotechnology Co., Ltd. (Shanghai, China). The proteins were quantified by iTRAQ labeling, and based on UniProt, KEGG, go, KOG/cog databases, the annotated information of the identified proteins was extracted to mine the protein functions. Proteins with quantification changes >1.5 and p value <0.05 were considered as differentially expressed proteins. After the differentially expressed proteins were obtained, GO/KEGG enrichment analysis were performed to describe the functions of these proteins, and the involved

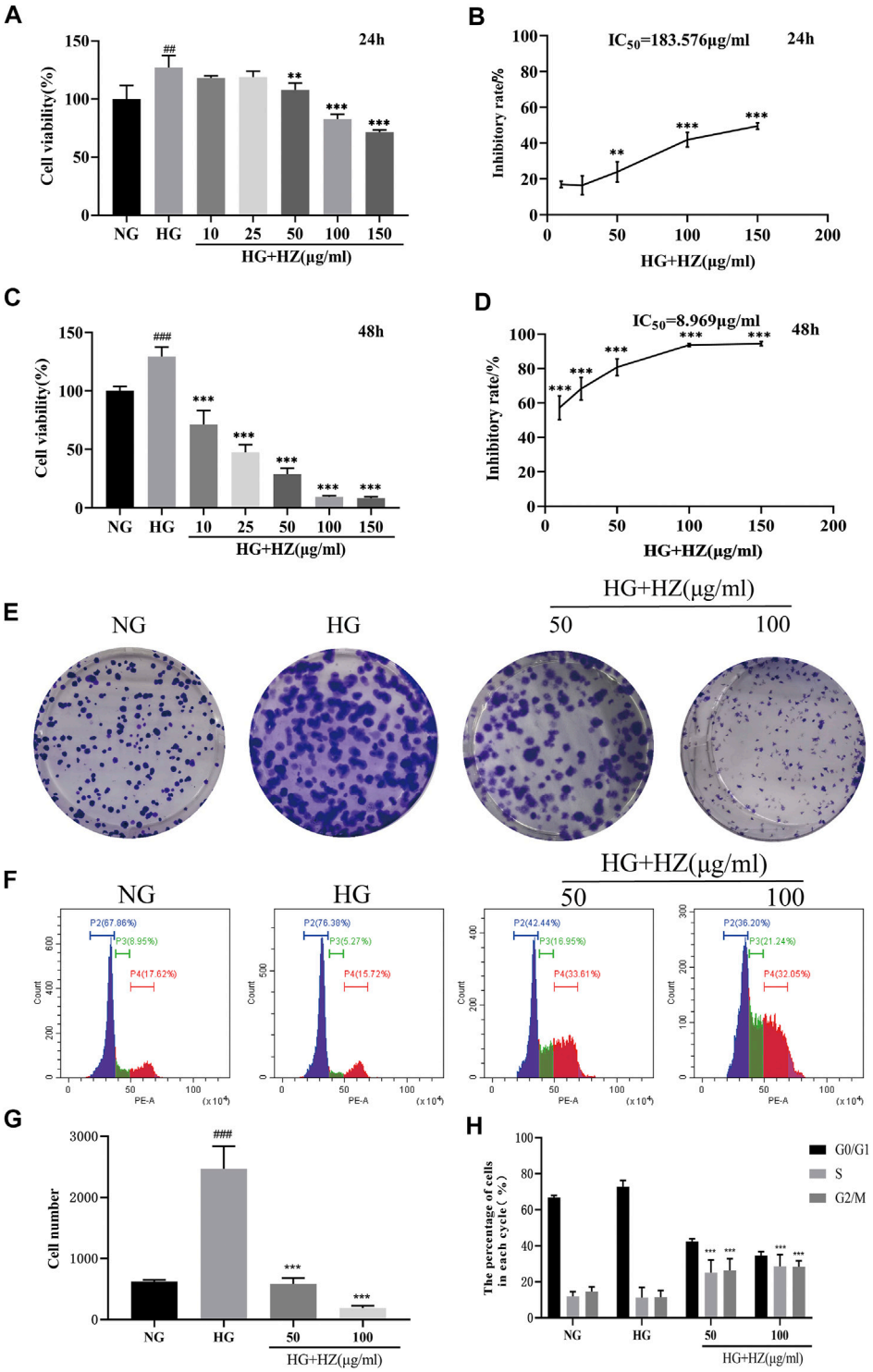

FIGURE 2 | Effects of HZQMY on the viability and proliferation of HRCEC cells exposed to high glucose. Cell viability **(A, C)** and inhibitory rate of cell proliferation **(B, D)** induced by various concentrations of HZQMY for 24 and 48 h, respectively. **(E)** HRCECs were cultured with NG, HG and HG-HZ, respectively, for 8 days **(F)** Cell cycle distribution was detected by flow cytometry. **(G)** The number of cell colonies was analyzed. **(H)** The percentage of cells in each phase was analyzed. $^{\#\#}$ and $^{\#\#\#}$ indicate $p < 0.01$ and $p < 0.001$, respectively, compared with NG group. ** and ***indicate $p < 0.01$ and $p < 0.001$, respectively, compared with HG group. HZ: HZQMY.

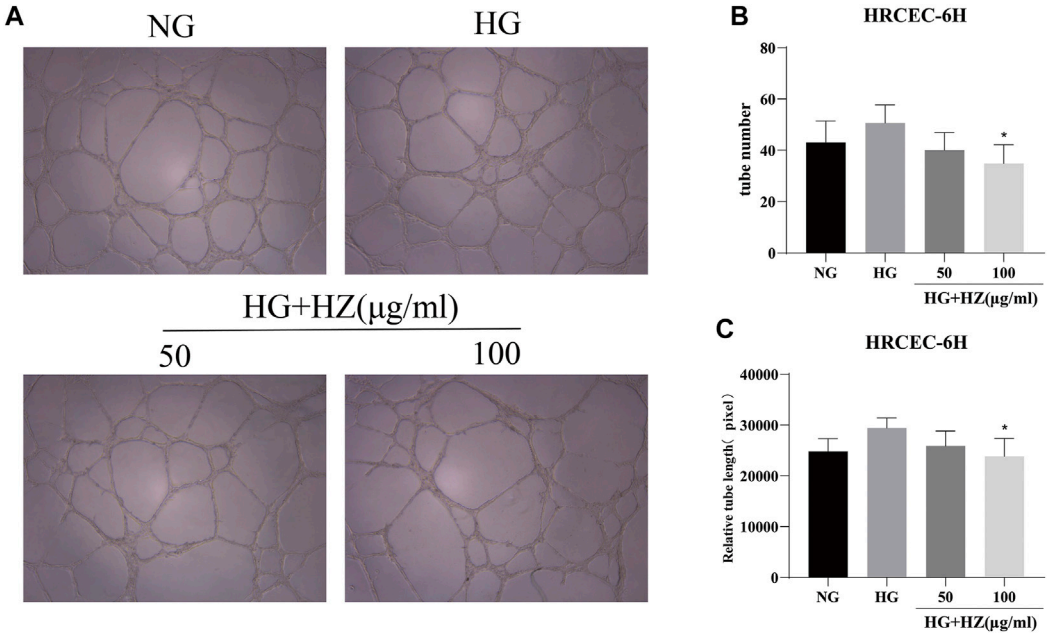

FIGURE 3 | Tube formation assay of HZQMY. **(A)** Tubulogenesis simulates angiogenesis *in vivo*. Magnification, ×40. **(B)** The number and length **(C)** of tube formation were analyzed. * indicates $p < 0.05$ vs HG group. HZ: HZQMY.

interaction network analysis was also executed by using STRING database.

Statistical Analysis

All data were analyzed by SPSS 22.0 statistical software, and the results were expressed as mean ± standard deviation. The comparison of the mean between two groups was performed by *t*-test, and the comparison of the mean between multiple groups was carried out by one-way analysis of variance. $p < 0.05$ was considered statistically significant.

RESULTS

Identification of the Components of Hu-Zhang-Qing-Mai-Yin

HPLC-Q-TOF-MS was used to analyze the constituents of HZQMY, and a total of 27 compounds were identified by comparing databases and literatures, which are Forsythoside E (1), Heteroclitin D (2), Quercetin (3), Forsythoside (4), Pinoresinol 4-O-β-D-glucopyranoside (5), Quercitrin (6), Forsyithin (7), Arctiin (8), Polydatin (9), Liquiritin (10), Apigenin (11), Isorhamnetin (12), Calycosin-7-O-glucoside (13), Kaempferol (14), Afromosin (RG) (15), (-)-Catechin hydrate (16), Genistein (17), Eleutheroside A (18), *trans*-Anethole (19), Oleanic acid (20), Quercetin dihydrate (21), Physcion 8-β-D-glucoside (22), Hyperoside (23), 3-Hydroxy-4-methoxybenzoic acid (24), Luteolin (25), Formononetin (26) and Prunetin (27). The chromatogram of the compounds obtained is shown in **Figure 1**.

Hu-Zhang-Qing-Mai-Yin Inhibited Cell Viability and Proliferation

As shown in **Figure 2**, when compared with NG group (5.5 mmol/L), the cell viability significantly increased in HG group (35 mmol/L). However, 50–150 μg/ml HZQMY significantly reduced the cell viability increased by high glucose after 24 h incubation (**Figures 2A,B**), and the inhibitory effect was more pronounced at 48 h (**Figures 2C,D**). These results suggested that high glucose can improve cell viability, while HZQMY can reverse the promotion effect in a time and dose-dependent manner.

To test the proliferation effect of HZQMY on HRCECs, cell colony formation and cycle assay were performed. **Figures 2E,G** show that high concentration of glucose can promote cell proliferation, while HZQMY could reverse this effect in a dose-dependent manner. Decreased cell proliferation is always associated with changes in the phase of the cell cycle, and the flow cytometry analysis displayed that the G_2/M phase accounted for a higher proportion in the HZQMY group than in the HG group (**Figures 2F,H**). The results suggested that HZQMY inhibits cell proliferation by arresting the cell cycle in the G_2/M phase.

Hu-Zhang-Qing-Mai-Yin Decreased the Tube Formation

Angiogenesis is a characteristic of endothelial cells. Tube formation *in vitro* was used to simulate angiogenesis *in vivo*, and the length of angiogenic branches was finally compared with ImageJ. The results (**Figures 3A–C**) displayed that the number of

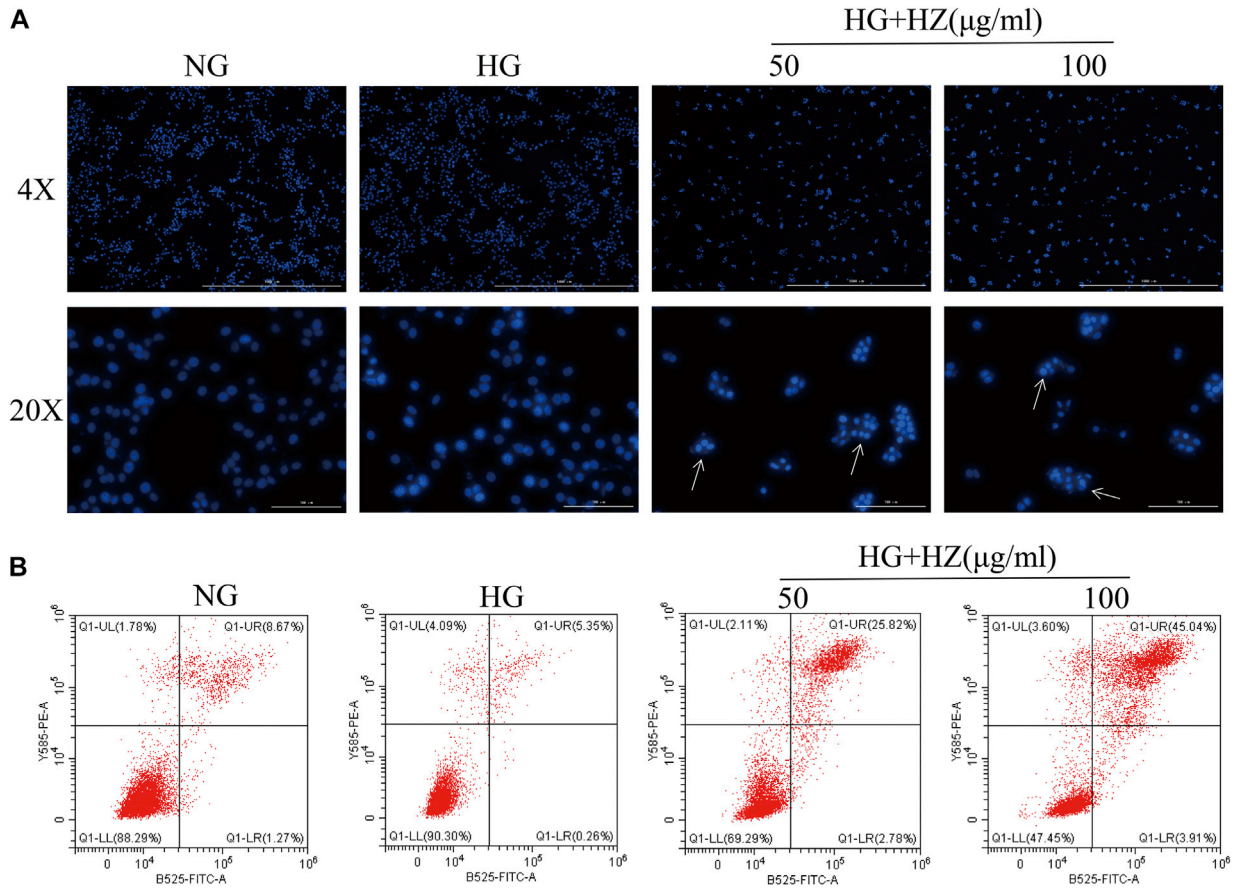

FIGURE 4 | Effect of HZQMY on cell apoptosis. **(A)** Effects of HZQMY on nuclear morphology in HRCECs exposed to high glucose. **(B)** Cell apoptosis was detected by flow cytometry. Magnification, ×40 and ×200. HZ: HZQMY.

tubes and the length of tube branches were decreased after HZQMY treatment, which indicated that HZQMY can slightly inhibit the angiogenesis of HRCECs induced by high glucose.

Hu-Zhang-Qing-Mai-Yin Facilitated Cell Apoptosis

In order to determine whether the inhibitory effect of HZQMY on cell proliferation was related to the induction of cell apoptosis, the nucleus was stained with DAPI to analyze the nuclear morphology. As shown in **Figure 4A**, after HZQMY treatment, the number of cells decreased significantly, nuclear pyknosis and apoptotic bodies were formed in a dose-dependent manner.

Flow cytometry was used to quantitatively analyze the proportion of cells in different stages of apoptosis in each group after Annexin V and PI double staining. Annexin V is used as an indicator of early apoptosis, and PI acts as an indicator of late apoptosis. As shown in **Figure 4B**, with the increase of HZQMY concentration, the sum of early and late apoptosis significantly increased, with the NG group was 9.94%, the HG group was 5.61%, the HG + HZ-50 group was 28.60%, the HG + HZ-100 group was 48.95%, which suggested that HZQMY could induce cell apoptosis in a dose-dependent manner.

Hu-Zhang-Qing-Mai-Yin Regulated ROS and ATP Levels and Induced MMP Collapse

Mitochondria are important organelles responsible for energy generation, which are closely related to ATP synthesis (Tang et al., 2018). What's more, the production of ROS has also closely relation with mitochondria (Indo et al., 2007). Therefore, MMP and the levels of ROS and ATP are often used to evaluate the functional status of mitochondria. To verify whether HZQMY affected the production of ATP and ROS, the cellular ROS levels were detected by DCFH-DA and ATP content was assessed by ATP assay kit. As shown in **Figures 5A,C**, after treatment with 100 μg/ml HZQMY for 24 h, the production of ROS in cells increased sharply. Compared with the NG group (**Figure 5D**), high glucose increased ATP levels in HRCECs, while HZQMY significantly reduced its production.

JC-1 is a fluorescent probe, which can act as an indicator of early cell apoptosis, and is often used in the detection of MMP. In the NG group, the cytoplasm of the cells showed red fluorescence, indicating high MMP. While the cells are injured, MMP will

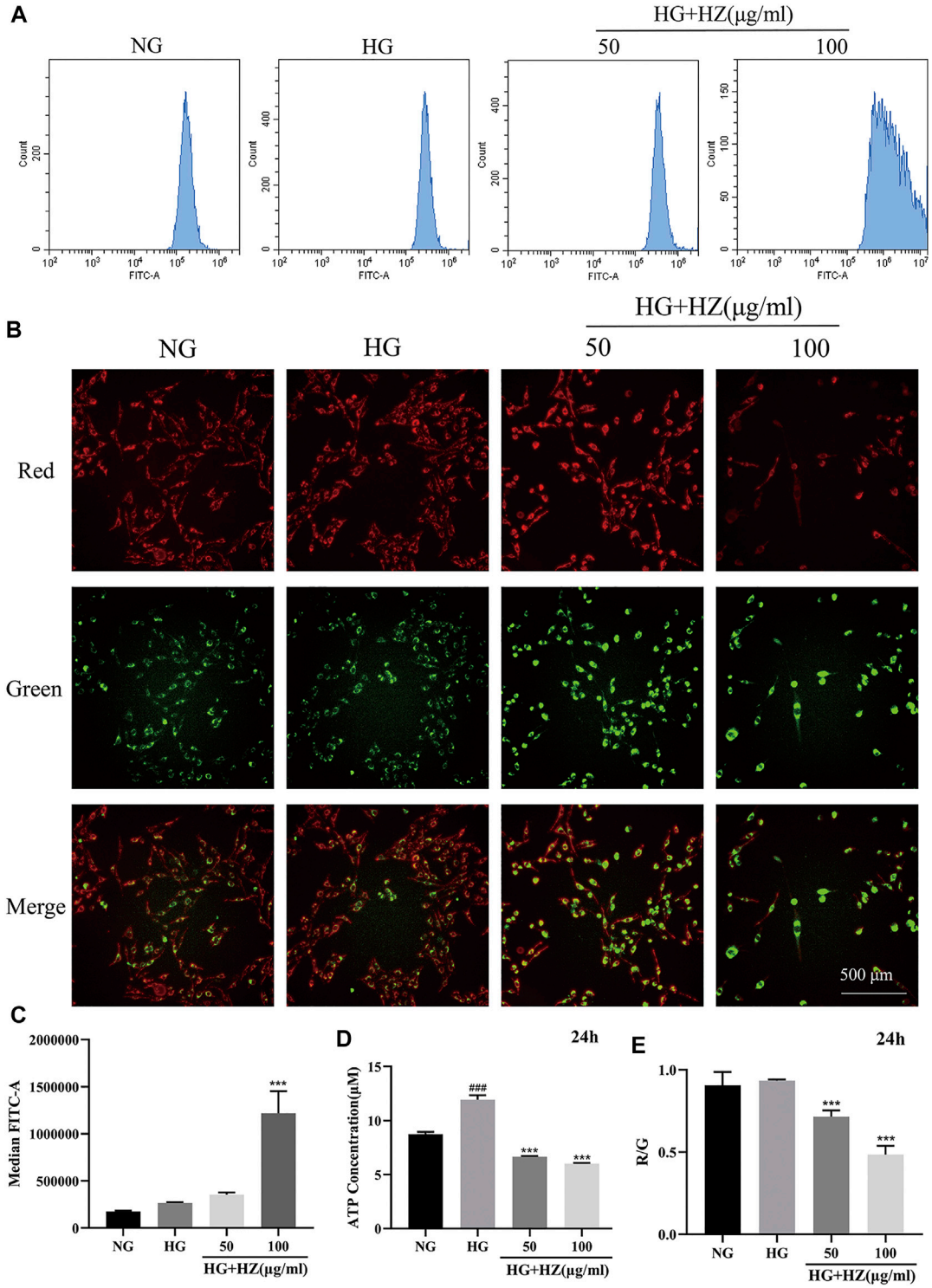

FIGURE 5 | HZQMY regulated ROS and ATP levels, and promoted MMP collapse. **(A)** Cellular ROS level was detected by flow cytometry. **(B)** The red and green fluorescence of the cells was measured by high content cell imager. **(C)** The ROS level was analyzed. **(D)** Cellular ATP level was detected by ATP assay kit. **(E)** R/G represents the change of MMP. $^{###}$ indicates $p < 0.001$ compared with NG group. *** indicates $p < 0.001$ compared with HG group. HZ: HZQMY.

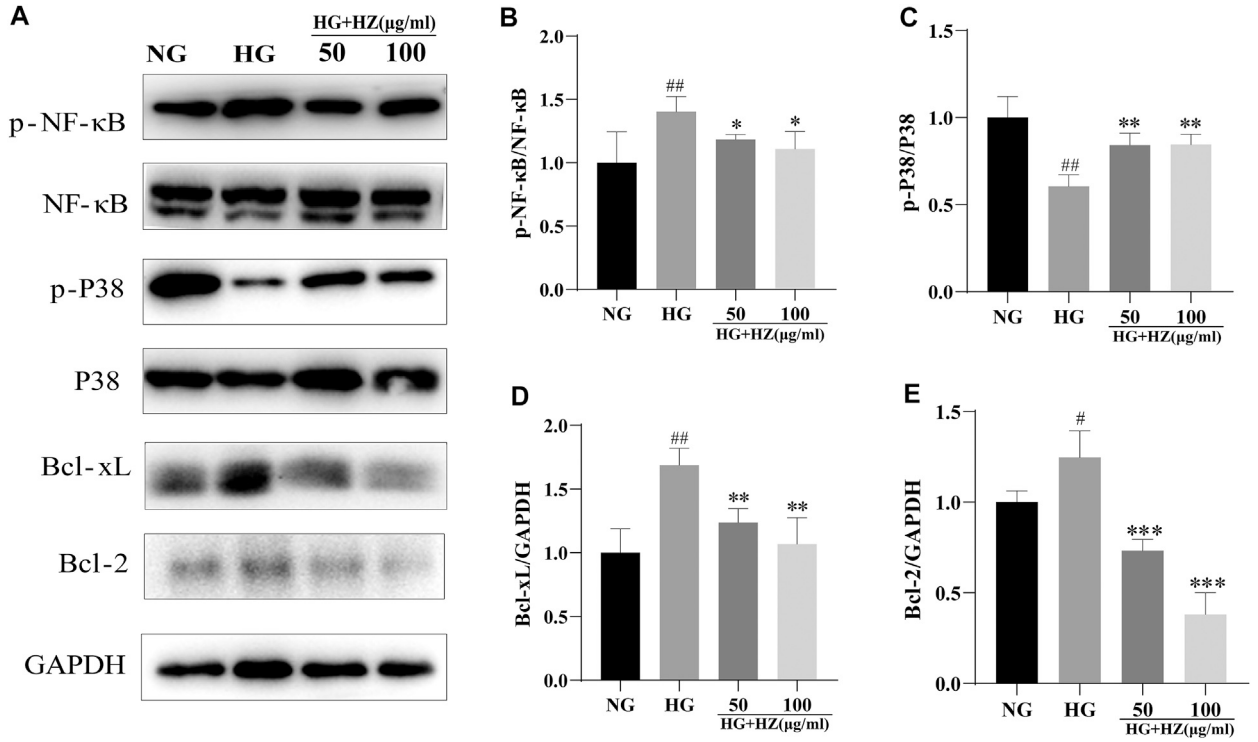

FIGURE 6 | Effect of HZQMY on protein expression of P38 and NF-κB signal pathways in HRCECs. **(A)** p-NF-κB, NF-κB, p-P38, P38, BCL-XL, BCL-2 and GAPDH were measured by western blot. **(B)** The expression of p-NF-κB was analyzed. **(C)** The expression of p-P38 was analyzed. **(D)** The expression of BCL-XL was analyzed. **(E)** The expression of BCL-2 was analyzed. ## and ### indicate $p < 0.01$ and $p < 0.001$ compared with NG group. ** and *** indicate $p < 0.01$ and $p < 0.001$ compared with HG group. HZ: HZQMY.

decrease, the cytoplasmic red fluorescence of the cells will reduce, and the green fluorescence will increase. The ratio of red fluorescence to green fluorescence (R/G) can be used for quantitative comparison. As shown in **Figure 5B**, the red fluorescence significantly decreased and the green fluorescence markedly increased. The higher the concentration of HZQMY is, the lower the ratio of R/G is (**Figure 5E**), indicating promotive effects of HZQMY on MMP collapse.

HZQMY regulated the proteins of P38 and NF-κB signaling pathway to inhibit proliferation of HRCECs.

To explore the mechanism of inhibitory effect of HZQMY on the proliferation of HRCECs in high glucose environment, we studied its mitochondrial apoptosis pathway. The decreased MMP, ROS and ATP levels proved that mitochondrial function was impaired.

As we all know, P38 is a classic pathway of apoptosis. In our study, P-P38 could be upregulated by HZQMY, and BCL-2 and BCL-XL could be downregulated by it, as shown in **Figures 6A,C–E**. Since NF-κB signal pathway plays a significant role in cell proliferation (Mu et al., 2020). Then western blot assay was used to detect the protein expression of NF-κB signaling pathway. As shown in **Figures 6A,B**, HZQMY downregulated the expression of p-NF-κB in HRCECs cultured with high glucose. All these results indicated that HZQMY suppressed cell proliferation possibly through regulating P38 and NF-κB signal transduction pathway.

TMT Quantitative Proteomic Analysis

Enrichment and PPI Analysis of Differentially Expression Proteins

The screening conditions of differentially expression proteins were set as p value <0.05 and quantification fold changes >1.5. After analyze, the two groups between the HG-HRCECs group and the HZQMY-100 group have 852 differentially expression proteins, of which 122 were upregulated and 730 were downregulated. To find the potential target proteins of HZQMY on HRCECs, differentially expression proteins were compared using GO and KEGG analysis.

GO analysis of differentially expression proteins mainly includes three aspects: biological processes, molecular functions and cellular component. As shown in **Figure 7A**, neutrophil degranulation, protein folding process were significantly enriched in the biological processes. Extracellular exosome and membrane were markedly enriched in the cellular component. ATP binding and identical protein binding were obviously enriched in the molecular function analysis.

The result of KEGG enrichment analysis showed that differentially expression proteins were significantly enriched in apoptosis, HIF-1 signaling pathway and AMPK signaling pathway (**Figure 7B**). The distribution of differentially expression proteins at KEGG Level 2 is shown in **Figure 7C**, which further reveals that the underlying mechanism of HZQMY

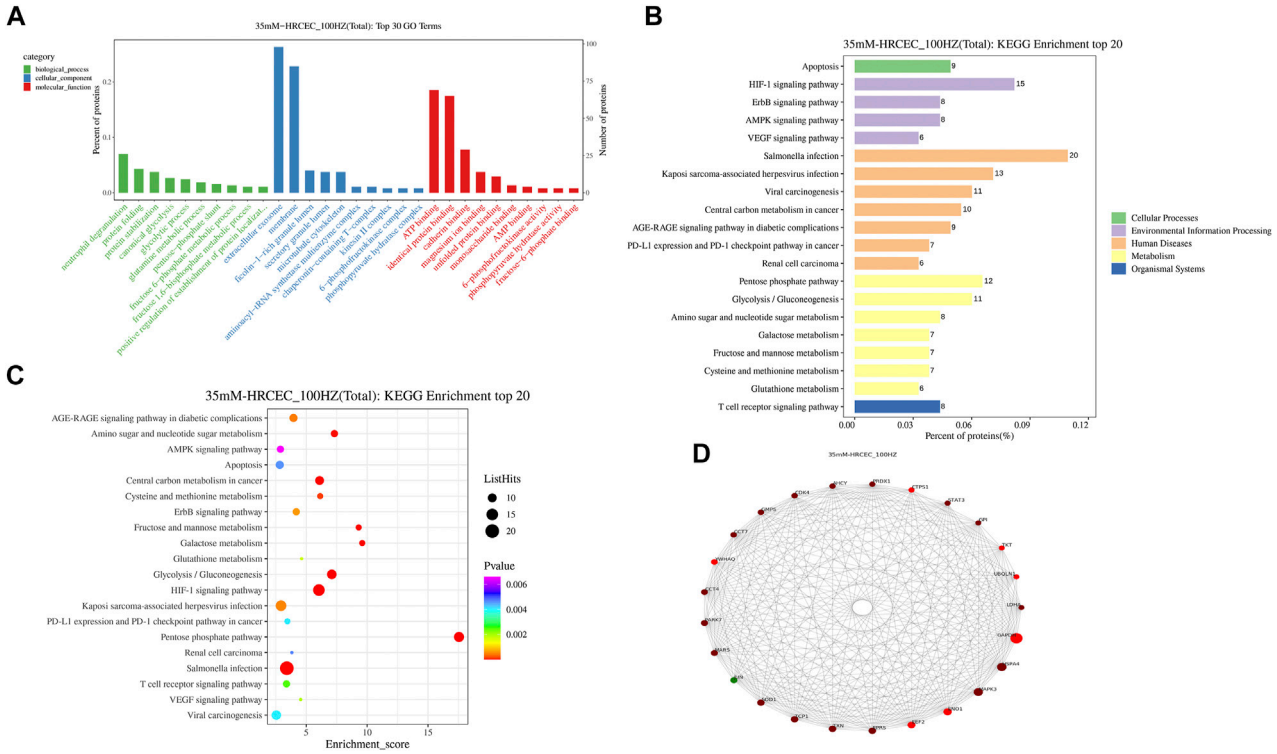

FIGURE 7 | GO/KEGG/PPI analyses of differentially expression proteins. **(A)** GO enrichment of differentially expression proteins. **(B)** Differentially expression proteins distribution at KEGG Level 2. **(C)** Bubble diagram of TOP 20 KEGG enrichment. **(D)** PPI network diagram of differentially expression proteins. HZ: HZQMY.

against DR may be through apoptosis and HIF-1 signaling pathway and AMPK signaling pathway.

The String database is a database of predicted functional correlations between proteins. The species was selected in the String database for analysis of the differentially expression proteins to obtain the interaction relationship between them. Top 25 proteins with connectivity degree were selected and the interaction network diagram was drawn (**Figure 7D**). Top five proteins for connectivity degree are HSPA4, MAPK3, ENO1, EEF2 and ERPS.

DISCUSSION

Proliferative diabetic retinopathy (PDR) is the late manifestation of DR, which is one of the common serious complications of diabetic eyes, and is an important cause of vision loss and even blindness in patients (de Carlo et al., 2016). In the early stage of PDR hyperplasia, intraocular neovascularization can be controlled by total retinal laser photocoagulation, but in the late stage, PDR is often complicated with vitreous hemorrhage or neovascularization, which results in required vitrectomy. Furthermore, bleeding during this operation may affect the surgical field, prolong the operative time, increase complications and influence postoperative recovery (Abouammoh et al., 2016). In recent years, more and more studies believe that vascular endothelial growth factor (VEGF) participates in PDR neovascularization by promoting endothelial cell proliferation and migration, improving vascular permeability and other ways, leading to the progression of PDR. Therefore, it is recommended to use anti-VEGF drugs to control the progression of neovascularization ophthalmopathy (Savastano et al., 2018). However, it has been reported that conventional anti-VEGF drugs such as bevacizumab and leizumab may have certain toxic reactions while inhibiting retinal and choroidal neovascularization, affecting retinal photoreceptor function (Gross and Glassman, 2016).

Traditional Chinese medicine (TCM) in the treatment of diabetic retinopathy has its unique advantages of safety, good efficacy and less side effects. Although TCM is used as a supplement and alternative medicine in many developed countries, more than 70 percent of people take it to prevent and treat diseases in China (Chen and Lu, 2006). HZQMY has been used in clinic due to definite curative effect in DR. However, systematic pharmacological studies on the treatment of DR are lacking. In the present study, HPLC-Q-TOF-MS was used to analyze the constituents of HZQMY, 27 of which were identified. Among them, Quercetin has been reported to be effective in the treatment of type 2 diabetes (Chen et al., 2016), possibly by alleviating ferroptosis of pancreatic β cells (Li et al., 2020). Arctiin inhibits the proliferation of human retinal capillary endothelial cells induced by high glucose by regulating the ROCK 1/PTEN/PI3K/Akt/VEGF pathway (Zhou et al., 2020). Polydatin

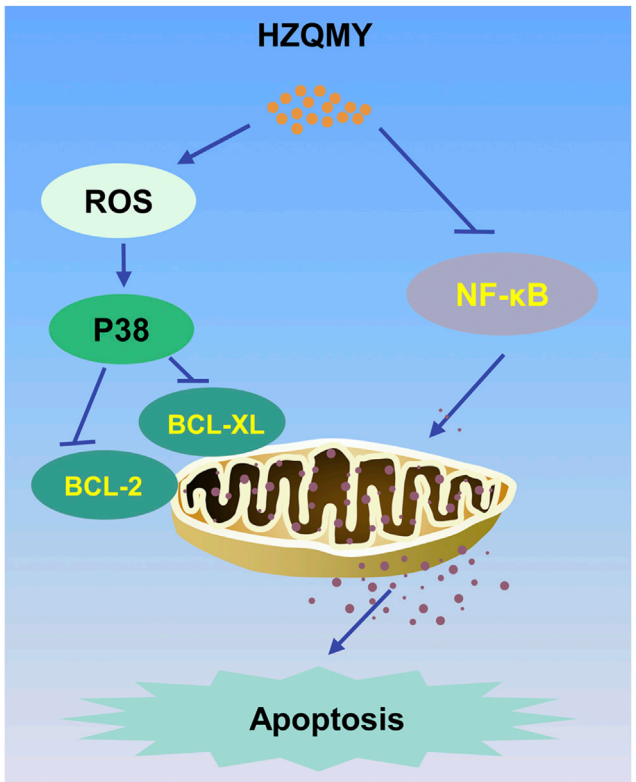

FIGURE 8 | The mechanism of the inhibitory effect of HZQMY in HRCECs. HZQMY regulated ROS/P38 signaling pathway, and then inhibited the expression of BCL-2 and BCL-XL. What's more, HZQMY also inhibited NF-κB signaling pathway to induce mitochondrial apoptosis.

increases glucose and lipid metabolism in insulin resistant HepG 2 cells via the AMPK pathway (Hao et al., 2018). Apigenin improves diabetic nephropathy by MAPK-NF-κB-TNF-α and TGF-β1-MAPK-fibronectin pathways (Malik et al., 2017). Isorhamnetin, genistein, oleanic acid, hyperoside, luteolin and formononetin have the effect of treating diabetes as well (Alkhalidy et al., 2018; Oza and Kulkarni, 2018; Wang et al., 2018; Xu et al., 2018; Wu et al., 2020; Matboli et al., 2021).

In the present study, we demonstrated that high glucose increased cell viability and proliferation, while HZQMY could reverse these phenomena. What's more, since angiogenesis is a property of endothelial cells, the *in vitro* tubulogenesis experiment was carried out to observe the effect of HZQMY on HRCECs exposed to high glucose. As a result, tube formation of the HRCECs could be inhibited by HZQMY. In addition, we also found that HZQMY could increase the apoptosis of HRCECs, which is displayed as accelerating the nuclear pyknosis and cell late apoptosis.

We further explored the mechanism of action on the inhibition of cell proliferation and induction of cell apoptosis by HZQMY. The mitochondrial pathway is the most common apoptotic one (Ou et al., 2017). HZQMY was found to promote MMP collapse. Studies have indicated that promotion of P38 and ROS could promote mitochondrial apoptosis (Rao et al., 2012; Syed et al., 2020). Moreover, studies have also shown that ROS can regulate P38 induced mitochondrial apoptosis (Cui et al., 2019). Upon damage to endothelial cells, p38 is involved in the regulation of ROS mediated damage to endothelial cells (Usatyuk et al., 2003). In our study, HZQMY could increase p-P38 and ROS concentration and decrease ATP level. What's more, HZQMY also downregulated the expression of BCL-XL and BCL-2 in HRCECs, indicating that HZQMY promoted cell apoptosis through the mitochondrial pathway. In addition, NF-κB regulates programmed cell death, cell adhesion, proliferation, innate and adaptive immune responses, and tissue remodeling (Ghosh and Hayden, 2008). Previous study showed that pantoprazole could promotes mitochondrial apoptosis by decreasing NF-κB signaling pathway (Geeviman et al., 2018). Our experiment also showed that high glucose increased the expression of p-NF-κB in HRCECs, while HZQMY could reverse their expression. Meanwhile, it was observed that the G_2/M phase accounted for a higher proportion in the HZQMY group than in the HG group, indicating that HZQMY could regulate P38 and NF-κB pathway and interfere with the cell cycle, thereby inhibiting cell proliferation and promoting apoptosis (**Figure 8**).

With the rapid development of proteomics and the establishment of bioinformatics theory, problems such as low detection sensitivity and few reliable evaluation indexes for clarifying the mechanism of action of numerous active compounds from Chinese medicines have been gradually solved, and a new strategy has been provided for the research on the target of these compounds in the treatment of diseases. KEGG analysis showed that the differentially expression proteins were mainly enriched in apoptosis, and the signaling pathways involved are most likely to be HIF-1. What's more, we also screened out 5 most likely target proteins through PPI analysis, which were HSPA4, MAPK3, ENO1, EEF2 and ERPS. High glucose combined with palmitate can regulate the expression of HSPA4 (Diaz-Ganete et al., 2021). MAPK3 (also known as ERK1) is necessary for pancreatic β cell function (Leduc et al., 2017). In diabetic patients, elevation of glycolytic enzymes including ENO1 is used as a biomarker for endogenous renoprotective factors (Gordin et al., 2019). Aerobic exercise combined with resistance exercise is able to enhance the activation of EEF2, contributing to improved glycemic control and maintenance of muscle health in type 1 diabetes (Minnock et al., 2020). ERPS can also be the potential biomarker to distinguish the type 2 diabetes and healthy person (Chu et al., 2013). What's more, inhibiting ERK1/2-NF-κB pathway could attenuate inflammation of DR (Zhang et al., 2019). These results suggest that these are probably the key proteins of HZQMY acting on HRCECs exposed to high glucose, which need to be further studied.

In conclusion, HZQMY inhibited the proliferation and promoted the mitochondria related apoptosis of HRCECs under high glucose exposure possibly by regulating P38 and NF-κB pathway. The target proteins need to be verified further.

DATA AVAILABILITY STATEMENT

The original contributions presented in the study are included in the article/supplementary material, further inquiries can be directed to the corresponding authors.

AUTHOR CONTRIBUTIONS

HZ, CL and XL contributed to the conception and design of the experiment. YY and QL performed experiments. PA and YC performed the statistical analysis. YY and ML wrote the first draft of the manuscript. CL processed images. YY and ML wrote sections of the manuscript.

FUNDING

This work was supported by funds from the National Natural Science Foundation of China (No. 81773941, 81903654 and 81903510); National Key Subject of Drug Innovation, China (2019ZX09201005-007); National Major Project of China (2019ZX09201004-003-010); National key R & D program for key research project of modernization of traditional Chinese medicine (2019YFC1711602); Program for Professor of Special Appointment (Young Eastern Scholar) at Shanghai Institutions of Higher Learning, China; Shanghai "Chenguang Program" of Education Commission of Shanghai Municipality, China (No. 18CG46); and "Yangfan Program" (No. 19YF1449400) of Science and Technology Commission of Shanghai Municipality, China.

REFERENCES

Abouammoh, M. A., Alsulaiman, S. M., Gupta, V. S., Mousa, A., Hirakata, A., Berrocal, M. H., et al. (2016). Pars Plana Vitrectomy with Juxtapapillary Laser Photocoagulation versus Vitrectomy without Juxtapapillary Laser Photocoagulation for the Treatment of Optic Disc Pit Maculopathy: the Results of the KKESH International Collaborative Retina Study Group. *Br. J. Ophthalmol.* 100, 478–483. doi:10.1136/bjophthalmol-2015-307128

Alkhalidy, H., Moore, W., Wang, Y., Luo, J., McMillan, R., Zhen, W., et al. (2018). The Flavonoid Kaempferol Ameliorates Streptozotocin-Induced Diabetes by Suppressing Hepatic Glucose Production. *Molecules* 23, 2338. doi:10.3390/molecules23092338

Antonetti, D. A., Silva, P. S., and Stitt, A. W. (2021). Current Understanding of the Molecular and Cellular Pathology of Diabetic Retinopathy. *Nat. Rev. Endocrinol.* 17, 195–206. doi:10.1038/s41574-020-00451-4

Behl, T., and Kotwani, A. (2017). Chinese Herbal Drugs for the Treatment of Diabetic Retinopathy. *J. Pharm. Pharmacol.* 69, 223–235. doi:10.1111/jphp.12683

Bommer, C., Heesemann, E., Sagalova, V., Manne-Goehler, J., Atun, R., Bärnighausen, T., et al. (2017). The Global Economic burden of Diabetes in Adults Aged 20-79 Years: a Cost-Of-Illness Study. *Lancet Diabetes Endocrinol.* 5, 423–430. doi:10.1016/S2213-8587(17)30097-9

Chen, K. J., and Lu, A. P. (2006). Situation of Integrative Medicine in China: Results from a National Survey in 2004. *Chin. J. Integr. Med.* 12, 161–165. doi:10.1007/BF02836514

Chen, S., Jiang, H., Wu, X., and Fang, J. (2016). Therapeutic Effects of Quercetin on Inflammation, Obesity, and Type 2 Diabetes. *Mediators Inflamm.* 2016, 1–5. doi:10.1155/2016/9340637

Chu, L., Fu, G., Meng, Q., Zhou, H., and Zhang, M. (2013). Identification of Urinary Biomarkers for Type 2 Diabetes Using Bead-Based Proteomic Approach. *Diabetes Res. Clin. Pract.* 101, 187–193. doi:10.1016/j.diabres.2013.05.004

Cui, S., Nian, Q., Chen, G., Wang, X., Zhang, J., Qiu, J., et al. (2019). Ghrelin Ameliorates A549 Cell Apoptosis Caused by Paraquat via P38-MAPK Regulated Mitochondrial Apoptotic Pathway. *Toxicology* 426, 152267. doi:10.1016/j.tox.2019.152267

de Carlo, T. E., Bonini Filho, M. A., Baumal, C. R., Reichel, E., Rogers, A., Witkin, A. J., et al. (2016). Evaluation of Preretinal Neovascularization in Proliferative Diabetic Retinopathy Using Optical Coherence Tomography Angiography. *Ophthalmic. Surg. Lasers Imaging Retina* 47, 115–119. doi:10.3928/23258160-20160126-03

Diaz-Ganete, A., Quiroga-de-Castro, A., Mateos, R. M., Medina, F., Segundo, C., and Lechuga-Sancho, A. M. (2021). Toxicity Induced by Cytokines, Glucose, and Lipids Increase Apoptosis and Hamper Insulin Secretion in the 1.1E7 Beta Cell-Line. *Int. J. Mol. Sci.* 22, 2559. doi:10.3390/ijms22052559

Duh, E. J., Sun, J. K., and Stitt, A. W. (2017). Diabetic Retinopathy: Current Understanding, Mechanisms, and Treatment Strategies. *JCI Insight* 2, e93751. doi:10.1172/jci.insight.93751

Geeviman, K., Babu, D., and Prakash Babu, P. (2018). Pantoprazole Induces Mitochondrial Apoptosis and Attenuates NF-κB Signaling in Glioma Cells. *Cell Mol. Neurobiol.* 38, 1491–1504. doi:10.1007/s10571-018-0623-4

Ghosh, S., and Hayden, M. S. (2008). New Regulators of NF-κB in Inflammation. *Nat. Rev. Immunol.* 8, 837–848. doi:10.1038/nri2423

Gordin, D., Shah, H., Shinjo, T., St-Louis, R., Qi, W., Park, K., et al. (2019). Characterization of Glycolytic Enzymes and Pyruvate Kinase M2 in Type 1 and 2 Diabetic Nephropathy. *Dia Care* 42, 1263–1273. doi:10.2337/dc18-2585

Gross, J. G., and Glassman, A. R. (2016). A Novel Treatment for Proliferative Diabetic Retinopathy. *JAMA Ophthalmol.* 134, 13–14. doi:10.1001/jamaophthalmol.2015.5079

Hao, J., Huang, K., Chen, C., Liang, Y., Wang, Y., Zhang, X., et al. (2018). Polydatin Improves Glucose and Lipid Metabolisms in Insulin-Resistant HepG2 Cells through the AMPK Pathway. *Biol. Pharm. Bull.* 41, 891–898. doi:10.1248/bpb.b17-01027

He, L., Wang, H., Gu, C., He, X., Zhao, L., and Tong, X. (2016). Administration of Traditional Chinese Blood Circulation Activating Drugs for Microvascular Complications in Patients with Type 2 Diabetes Mellitus. *J. Diabetes Res.* 2016, 1–9. doi:10.1155/2016/1081657

Ihnat, M. A., Thorpe, J. E., and Ceriello, A. (2007). Hypothesis: the ?metabolic Memory?, the New challenge of Diabetes. *Diabetic Med.* 24, 582–586. doi:10.1111/j.1464-5491.2007.02138.x

Indo, H. P., Davidson, M., Yen, H.-C., Suenaga, S., Tomita, K., Nishii, T., et al. (2007). Evidence of ROS Generation by Mitochondria in Cells with Impaired Electron Transport Chain and Mitochondrial DNA Damage. *Mitochondrion* 7, 106–118. doi:10.1016/j.mito.2006.11.026

Leduc, M., Richard, J., Costes, S., Muller, D., Varrault, A., Compan, V., et al. (2017). ERK1 Is Dispensable for Mouse Pancreatic Beta Cell Function but Is Necessary for Glucose-Induced Full Activation of MSK1 and CREB. *Diabetologia* 60, 1999–2010. doi:10.1007/s00125-017-4356-6

Li, D., Jiang, C., Mei, G., Zhao, Y., Chen, L., Liu, J., et al. (2020). Quercetin Alleviates Ferroptosis of Pancreatic β Cells in Type 2 Diabetes. *Nutrients* 12, 2954. doi:10.3390/nu12102954

Liu, L., Xu, H., Zhao, H., and Jiang, C. (2020). STEAP4 Inhibits HIF-1α/PKM2 Signaling and Reduces High Glucose-Induced Apoptosis of Retinal Vascular Endothelial Cells. *Diabetes Metab. Syndr. Obes.* 13, 2573–2582. doi:10.2147/DMSO.S251663

Malik, S., Suchal, K., Khan, S. I., Bhatia, J., Kishore, K., Dinda, A. K., et al. (2017). Apigenin Ameliorates Streptozotocin-Induced Diabetic Nephropathy in Rats via MAPK-NF-κB-TNF-α and TGF-β1-MAPK-Fibronectin Pathways. *Am. J. Physiol. Ren. Physiol.* 313, F414–F422. doi:10.1152/ajprenal.00393.2016

Matboli, M., Saad, M., Hasanin, A. H., A. Saleh, L., Baher, W., Bekhet, M. M., et al. (2021). New Insight into the Role of Isorhamnetin as a Regulator of Insulin Signaling Pathway in Type 2 Diabetes Mellitus Rat Model: Molecular and Computational Approach. *Biomed. Pharmacother.* 135, 111176. doi:10.1016/j.biopha.2020.111176

Minnock, D., Annibalini, G., Le Roux, C. W., Contarelli, S., Krause, M., Saltarelli, R., et al. (2020). Effects of Acute Aerobic, Resistance and Combined Exercises

on 24-h Glucose Variability and Skeletal Muscle Signalling Responses in Type 1 Diabetics. *Eur. J. Appl. Physiol.* 120, 2677–2691. doi:10.1007/s00421-020-04491-6

Mu, Y.-T., Feng, H.-H., Yu, J.-Q., Liu, Z.-K., Wang, Y., Shao, J., et al. (2020). Curcumin Suppressed Proliferation and Migration of Human Retinoblastoma Cells through Modulating NF-κB Pathway. *Int. Ophthalmol.* 40, 2435–2440. doi:10.1007/s10792-020-01406-4

Ou, L., Lin, S., Song, B., Liu, J., Lai, R., and Shao, L. (2017). The Mechanisms of Graphene-Based Materials-Induced Programmed Cell Death: a Review of Apoptosis, Autophagy, and Programmed Necrosis. *Int. J. Nanomedicine* 12, 6633–6646. doi:10.2147/IJN.S140526

Oza, M. J., and Kulkarni, Y. A. (2018). Formononetin Treatment in Type 2 Diabetic Rats Reduces Insulin Resistance and Hyperglycemia. *Front. Pharmacol.* 9, 739. doi:10.3389/fphar.2018.00739

Pang, B., Zhou, Q., Zhao, T.-Y., He, L.-S., Guo, J., Chen, H.-D., et al. (2015). Innovative Thoughts on Treating Diabetes from the Perspective of Traditional Chinese Medicine. *Evid. Based Complement. Altern. Med.* 2015, 1–12. doi:10.1155/2015/905432

Rao, P. S., Satelli, A., Moridani, M., Jenkins, M., and Rao, U. S. (2012). Luteolin Induces Apoptosis in Multidrug Resistant Cancer Cells without Affecting the Drug Transporter Function: Involvement of Cell Line-specific Apoptotic Mechanisms. *Int. J. Cancer* 130, 2703–2714. doi:10.1002/ijc.26308

Savastano, M. C., Federici, M., Falsini, B., Caporossi, A., and Minnella, A. M. (2018). Detecting Papillary Neovascularization in Proliferative Diabetic Retinopathy Using Optical Coherence Tomography Angiography. *Acta Ophthalmol.* 96, 321–323. doi:10.1111/aos.13166

Syed, A. A., Reza, M. I., Shafiq, M., Kumariya, S., Singh, P., Husain, A., et al. (2020). Naringin Ameliorates Type 2 Diabetes Mellitus-Induced Steatohepatitis by Inhibiting RAGE/NF-κB Mediated Mitochondrial Apoptosis. *Life Sci.* 257, 118118. doi:10.1016/j.lfs.2020.118118

Tang, G., Zhang, C., Ju, Z., Zheng, S., Wen, Z., Xu, S., et al. (2018). The Mitochondrial Membrane Protein FgLetm1 Regulates Mitochondrial Integrity, Production of Endogenous Reactive Oxygen Species and Mycotoxin Biosynthesis inFusarium Graminearum. *Mol. Plant Pathol.* 19, 1595–1611. doi:10.1111/mpp.12633

Usatyuk, P. V., Vepa, S., Watkins, T., He, D., Parinandi, N. L., and Natarajan, V. (2003). Redox Regulation of Reactive Oxygen Species-Induced P38 MAP Kinase Activation and Barrier Dysfunction in Lung Microvascular Endothelial Cells. *Antioxid. Redox Signal.* 5, 723–730. doi:10.1089/152308603770380025

Wang, S., Du, L.-B., Jin, L., Wang, Z., Peng, J., Liao, N., et al. (2018). Nano-oleanolic Acid Alleviates Metabolic Dysfunctions in Rats with High Fat and Fructose Diet. *Biomed. Pharmacother.* 108, 1181–1187. doi:10.1016/j.biopha.2018.09.150

Wong, T. Y., and Sabanayagam, C. (2020). Strategies to Tackle the Global Burden of Diabetic Retinopathy: From Epidemiology to Artificial Intelligence. *Ophthalmologica* 243, 9–20. doi:10.1159/000502387

Wu, W., Xie, Z., Zhang, Q., Ma, Y., Bi, X., Yang, X., et al. (2020). Hyperoside Ameliorates Diabetic Retinopathy via Anti-Oxidation, Inhibiting Cell Damage and Apoptosis Induced by High Glucose. *Front. Pharmacol.* 11, 797. doi:10.3389/fphar.2020.00797

Xiao, E., and Luo, L. (2018). Alternative Therapies for Diabetes: A Comparison of Western and Traditional Chinese Medicine (TCM) Approaches. *Curr. Diabetes Rev.* 14, 487–496. doi:10.2174/1573399813666170519103230

Xu, J., Xu, H., Yu, Y., He, Y., Liu, Q., and Yang, B. (2018). Combination of Luteolin and Solifenacin Improves Urinary Dysfunction Induced by Diabetic Cystopathy in Rats. *Med. Sci. Monit.* 24, 1441–1448. doi:10.12659/msm.904534

Zhang, H. W., Zhang, H., Grant, S. J., Wan, X., and Li, G. (2018). Single Herbal Medicine for Diabetic Retinopathy. *Cochrane Database Syst. Rev.* 2018, CD007939. doi:10.1002/14651858.CD007939.pub2

Zhang, T., Ouyang, H., Mei, X., Lu, B., Yu, Z., Chen, K., et al. (2019). Erianin Alleviates Diabetic Retinopathy by Reducing Retinal Inflammation Initiated by Microglial Cells via Inhibiting Hyperglycemia-mediated ERK1/2-NF-κB Signaling Pathway. *FASEB J.* 33, 11776–11790. doi:10.1096/fj.201802614RRR

Zhou, M., Li, G., Zhu, L., Zhou, H., and Lu, L. (2020). Arctiin Attenuates High Glucose-induced Human Retinal Capillary Endothelial Cell Proliferation by Regulating ROCK1/PTEN/PI3K/Akt/VEGF Pathway *In Vitro*. *J. Cel Mol. Med.* 24, 5695–5706. doi:10.1111/jcmm.15232

Conflict of Interest: The authors declare that the research was conducted in the absence of any commercial or financial relationships that could be construed as a potential conflict of interest.

Publisher's Note: All claims expressed in this article are solely those of the authors and do not necessarily represent those of their affiliated organizations, or those of the publisher, the editors and the reviewers. Any product that may be evaluated in this article, or claim that may be made by its manufacturer, is not guaranteed or endorsed by the publisher.

frontiers in Pharmacology

ORIGINAL RESEARCH
published: 20 October 2021
doi: 10.3389/fphar.2021.732874

The Protective Effect of Quercetin on Endothelial Cells Injured by Hypoxia and Reoxygenation

Meng-Ting Li[1†], Jia Ke[1†], Shu-Fen Guo[1], Yang Wu[1], Yue-Feng Bian[1], Li-Li Shan[1], Qian-Yun Liu[1], Ya-Jing Huo[1], Cen Guo[1], Ming-Yuan Liu[1], Ya-Jie Liu[2] and Yan Han[1]**

[1]Department of Neurology, Yueyang Hospital of Integrated Traditional Chinese and Western Medicine, Shanghai University of Traditional Chinese Medicine, Shanghai, China, [2]Department of Neurology, Shenzhen Hospital, Southern Medical University, Shenzhen, China

OPEN ACCESS

Edited by:
Tie-Jun Li,
Second Military Medical University, China

Reviewed by:
Carina Rodrigues Boeck,
UFN - Universidade Franciscana, Brazil
Zhong Ping,
Shanghai Shidong Hospital of Yangpu District, China

***Correspondence:**
Yan Han
hanyan.2006@aliyun.com
Ya-Jie Liu
docliu18@qq.com

[†]*These authors have contributed equally to this work*

Specialty section:
This article was submitted to Neuropharmacology, a section of the journal Frontiers in Pharmacology

Received: *29 June 2021*
Accepted: *04 October 2021*
Published: *20 October 2021*

Citation:
Li M-T, Ke J, Guo S-F, Wu Y, Bian Y-F, Shan L-L, Liu Q-Y, Huo Y-J, Guo C, Liu M-Y, Liu Y-J and Han Y (2021) The Protective Effect of Quercetin on Endothelial Cells Injured by Hypoxia and Reoxygenation. Front. Pharmacol. 12:732874. doi: 10.3389/fphar.2021.732874

Background: Cerebral small vessel disease (CSVD) is a group of clinical syndromes covering all pathological processes of small vessels in the brain, which can cause stroke and serious dementia. However, as the pathogenesis of CSVD is not clear, so the treatment is limited. Endothelial cell dysfunction is earlier than clinical symptoms, such as hypertension and leukosis. Therefore, the treatment of endothelial cells is expected to be a new breakthrough. Quercetin, a flavonoid present in a variety of plants, has the function of anti-inflammation and anti-oxidation. This study aimed to investigate the protective effect of quercetin on endothelial cell injury and provide a basic theory for subsequent application in the clinic.

Methods: Human brain microvascular endothelial cells (HBMECs) were cultured *in vitro*, and the injury model of endothelial cells was established by hypoxia and reoxygenation (H/R). The protective effects of quercetin on HBMECs were studied from the perspectives of cell viability, cell migration, angiogenesis and apoptosis. In order to further study the mechanism of quercetin, oxidative stress and endoplasmic reticulum stress were analyzed. What's more, blood-brain barrier (BBB) integrity was also studied.

Results: Quercetin can promote the viability, migration and angiogenesis of HBMECs, and inhibit the apoptosis. In addition, quercetin can also activate Keap1/Nrf2 signaling pathway, reduce ATF6/GRP78 protein expression. Further study showed that quercetin could increase the expression of Claudin-5 and Zonula occludens-1.

Conclusions: Our experiments show that quercetin can protect HBMECs from H/R, which contains promoting cell proliferation, cell migration and angiogenesis, reducing mitochondrial membrane potential damage and inhibiting cell apoptosis. This may be related to its antioxidation and inhibition of endoplasmic reticulum stress. At the same time, quercetin can increase the level of BBB connexin, suggesting that quercetin can maintain BBB integrity.

Keywords: cerebral small vessel disease, endothelial cells, quercetin, oxidative stress, endoplasmic reticulum stress, blood brain barrier

INTRODUCTION

Cerebral small vessel disease (CSVD) is an umbrella term that encompasses all pathological processes involving the small vessels in the brain and refers to a group of clinical, imaging, and pathological syndromes with various etiologies containing the intracranial arterioles to venules (diameter <400 μm) (Wardlaw et al., 2013; Wardlaw et al., 2019).The most common symptoms include mainly new onset subcortical small infarcts, lacunar foci of vascular origin, cerebral white matter hyperintensities, microbleeds, cerebral atrophy, and enlarged perivascular spaces (Wardlaw et al., 2013). With the progression of the disease, subclinical and early-stage patients can have emotional abnormalities, gait, memory, disorientation, and even stroke and dementia and other serious consequences. Up to 25% of stroke and 45% of dementia are caused by CSVD (Cannistraro et al., 2019), which brings a heavy socioeconomic burden and is a major problem that needs to be addressed by slow disease and health strategies.

Scholar has used dynamic contrast enhanced-MRI technique to find that blood-brain barrier (BBB) leakage is more prevalent in CSVD patients (Zhang et al., 2017). Extravasation of blood components may lead to local vascular changes and diffuse brain tissue damage. The BBB is a junction of endothelial cells, pericytes and astrocyte tight junctions (Keaney and Campbell, 2015). In addition, more and more scholars also believe that endothelial dysfunction plays a key role in the early development of CSVD (Hainsworth et al., 2015). Therefore, protecting endothelial cells may be a potential therapeutic strategy for CSVD.

Quercetin, a flavonoid present in several plants, such as *Polygonum cuspidatum* Sieb. et Zucc, has strong antioxidant and anti-inflammatory activities and can exert protective effects in various pathological conditions including cardiovascular disease, metabolic disorders, neurodegenerative diseases, diabetes, cancer and obesity (Dok-Go et al., 2003; Comalada et al., 2005; Cho et al., 2006). Pretreatment with quercetin significantly increased the expression levels of endogenous antioxidant enzymes in hippocampal CA1 pyramidal neurons of ischemia injured animals, showing strong antioxidant and neuroprotective effects (Chen et al., 2017). Recent studies have also found that quercetin has neuroprotective effects against ischemic injury while maintaining BBB integrity (Jin et al., 2019). However, its effect on brain microvascular endothelial cells (BMECs) under hypoxia and reoxygenation (H/R) injury is poorly studied, and the target protein of quercetin protecting BMECs has not been reported.

In our study, we explored the protective effect of quercetin on human brain microvascular endothelial cells (HBMECs) injured by H/R in culture. At the same time, we further studied the possible mechanism of its protective effect, so as to provide more theoretical basis for the clinical promotion of quercetin, and provide new ideas for the treatment of CSVD.

MATERIALS AND METHODS

Media, Reagents and Antibodies

Quercetin (purity>98%) was acquired from Best Biological Technology Co., Ltd. (Chengdu, China). HBMECs were purchased from Qingqi Biotechnology Development Co., Ltd (Shanghai, China). Fetal bovine serum (FBS) was obtained from Biological Industries (Kibbutz Beit Haemek, Israel). Penicillin/streptomycin and dulbecco's modified eagle medium (DMEM) were purchased from Hyclone (GA, United States). Mitochondrial membrane potential (JC-1) test kit, BCA protein test kit, 2,7-dichlorodi-hydrofluorescein diacetate (DCFH-DA) and NP40 lysate were purchased from Beyotime Biotechnology (Shanghai, China). Phosphatase preparation and Complete protease inhibitor were purchased from Roche (Shanghai, China). Apoptosis Kit was purchased from BD Biosciences (Sparks, MD, United States). Malondialdehyde (MDA), Superoxide dismutase (SOD), Intercellular cell adhesion molecule-1 (ICAM-1), Vascular cell adhesion molecule-1 (VCAM-1) enzyme linked immunosorbent assay (ELISA) was purchased from Abcam company (Cambridge, United Kingdom). Antibodies against Nuclear factor E2-related factor 2 (Nrf2), Kelch Like ECH Associated Protein 1 (Keap1), Activating transcription factor 6 (ATF6), Glucose-regulated protein 78 (GRP78), Zonula occludens 1 (ZO-1), Claudin-5, GAPDH was purchased from Cell Signaling Technology (Danvers, United States). Horseradish peroxidase (HRP)-conjugated anti-rabbit IgG was obtained from Jackson company (Pennsylvania, United States). SDS-PAGE rapid dispensing kit and ECL chromogenic solution were purchased from EpiZyme Biotechnology (Shanghai, China).

Cell Culture and Injury Model

HBMECs were cultured in DMEM containing 10% FBS and 1% penicillin-streptomycin, at 37°C incubator with 5% CO_2. To cause endothelial cell damage, HBMECs were treated with 12 h hypoxia followed by 8 h reoxygenation, and the specific procedures were as follows (Warpsinski et al., 2020): HBMECs were first incubated with serum-free medium in a hypoxia incubator (1% O_2, 5% CO_2, 94% N_2) for 12 h, and then the medium was changed to normal medium containing 10% FBS, while they were incubated in a normoxia incubator (95% O_2, 5% CO_2) for 8 h.

Quercetin Treatment

2 mg Quercetin was dissolved in 331 μL DMSO to form a stock solution with a concentration of 1 mmol/L and stored at −20°C. The working solution was diluted to 0.1, 0.5, 1, 2, 5, 10 μmol/L with DMEM, in which the percentage of DMSO was below 0.1%. Once cells had been adherent, quercetin with serum-free medium was added, and the plates were subsequently placed into the hypoxia incubator. After 12 h, cells were removed, changed to quercetin with serum medium, and placed in a normoxia incubator for 8 h.

Cell Viability Assay

The effects of quercetin on the viability of HBMECs were examined by Cell Counting Kit-8 according to the operator's manual. The safe doses of quercetin to the cells in the absence of damage to the endothelial cells were first assessed, and then the protective effects of it in the condition of cell damage were tested. All experimental results were repeated at least three times.

Scratch Healing and Tube Formation Assay

Migration experiments were performed using a cell scratch method. Before quercetin treatment, a straight perpendicular line was drawn at the bottom of the culture plate and photographed for recording for 0 h, and the cells were subsequently subjected to quercetin and modeling treatment before taking photographs for recording. The anterior and posterior areas were contrasted twice.

Tube formation mimicking cell angiogenic ability, the Matrigel (9–12 mg/ml) was placed on the bottom of the culture plate, then quercetin and modeling treated cells were plated on top, after 8 h, pictures were taken. The branching generation of blood vessels was analyzed and compared using ImageJ.

Mitochondrial Membrane Potentials and Apoptosis Assay

The mitochondrial membrane potential change and apoptosis kit were used to detect cell apoptosis. The alteration of mitochondrial membrane potential was detected by staining HBMECs with JC-1 fluorescent probe. JC-1 (1 ×) staining working solution was added and incubated in a 37°C incubator for 20 min before being washed twice with JC-1 (1 ×) staining buffer and finally added to each well for PBS. Then, the high content cell imager was used to analysis.

HBMECs were collected from the 6-well plates, centrifuged to remove the supernatant, subsequently add 1 × Annexin V binding solution to blow and mix the cells, then add FITC Annexin V dye to incubate in the dark at room temperature for 10 min, add propidium iodide (PI) staining solution 5 min before the machine, and Beckman flow cytometer was employed to detect.

ELISA

After the cells were treated with H/R or quercetin, the supernatant was collected. ICAM-1, VCAM-1, SOD and MDA were detected using ELISA kits according to the operator's manual.

Reactive Oxygen Species (ROS) Assay

The ability of ROS generation was detected by the DCFH-DA probe, which was evaluated by the high content cell imager, and analyzed by fluorescence using ImageJ.

Western Blotting

HBMECs were collected from culture plates, NP40 lysate adding phosphatase preparation and complete protease inhibitor was used to extract proteins from cells. Protein content was determined and 30 μg protein was taken for immunoblotting experiments. SDS-PAGE gel was used for electrophoresis, blocked with 5% nonfat dry milk after electrotransfer to PVDF membrane for 1 h at room temperature. Then anti-Nrf2 (rabbit, 1:1,000), anti-Keap1 (rabbit, 1:1,000), anti-ATF6 (rabbit,1: 1,000), anti-GRP78 (rabbit, 1:1,000), anti-ZO-1 (rabbit, 1:1,000), anti-Claudin-5 (rabbit, 1:1,000) antibodies were incubated overnight at 4°C. After washing the next day, diluted Goat anti rabbit secondary antibodies (IgG HRP, 1:10,000) were added and incubated for 1 h. Finally, detection was developed after washing three times in TBST.

Proteomic Analysis

HBMECs were treated with H/R in the present of quercetin (1 μmol/L). Subsequently, the cells were gently scraped from the culture plate with a cell scraper, collected in cryovials, quickly placed in liquid nitrogen, and then stored at −80°C for 5 min iTRAQ technology was used to do the proteomic analysis, the proteins with p value <0.05 and ratio multiple change >1.2 or <0.83 were defined as differentially expressed proteins.

Statistical Analysis

Data were fit with normal distribution, and mean ± standard deviation was used to express the data. The GraphPad Prism 8 was used for statistical analysis. Two independent samples were analyzed by t-test, and the measurement data were described by mean ± Standard deviation (SD). The comparison between groups was conducted by one-way analysis of variance (ANOVA). p value <0.05 indicated that the difference was statistically significant.

RESULTS

Results

Effect of Quercetin on Cell Viability

To test the effect of quercetin on cell viability, we first examined a safe dose of quercetin on the cells, as shown in **Figure 1A**, which had no impact for cell viability at 0.1–10 μmol/L. Next, for searching for an effective dose on the basis of endothelial cell damage, we showed that quercetin at 0.1–1 μmol/L could promote cell viability in H/R-HBMECs, as shown in **Figure 1B**. Subsequent experiments were carried out around this concentration range. It is worth noting that when the drug concentration reached 10 μmol/L, cytotoxicity appeared. We thought that when HBMECs were damaged by H/R, its tolerance decreases. Therefore, when the drug concentration was slightly higher, the damage to cells increased. Therefore, cytotoxicity occurred when the drug concentration is 10 μmol/L.

Effect of Quercetin on Cell Migration and Angiogenesis

To examine the effects of quercetin on the migratory and angiogenic capacities of endothelial cells, HBMECs were subjected to H/R treatment while quercetin was administered. We performed a scratch assay to test the cell migration ability, which showed that H/R treatment weakened the migration ability of H/R-HBMECs compared with the control, and quercetin could significantly promote cell migration at a concentration of 0.1–1 μmol/L. Tubulogenesis was used to mimic *in vitro* angiogenesis, and its branch length represents angiogenic capacity. The results showed that H/R treatment resulted in reduced angiogenic capacity, but quercetin 0.1–1 μmol/L could reverse this injury, as shown in **Figure 2**.

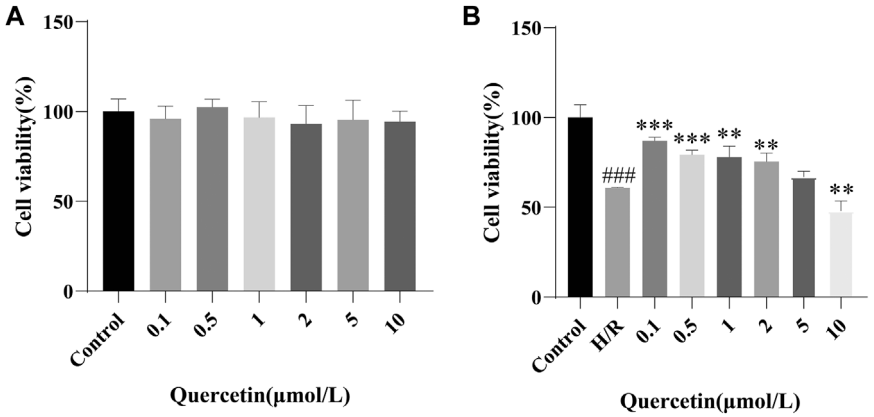

FIGURE 1 | (A) HBMECs were treated with quercetin (0, 0.1, 0.5, 1, 2, 5, 10 μmol/L) for 24 h, viability was measured using CCK-8 method (B) HBMECs were treated with quercetin (0, 0.1, 0.5, 1, 2, 5, 10 μmol/L) and H/R treatment, viability was measured using CCK-8 method. $^{###}p < 0.001$ compared to control group; $^{**}p < 0.01$, $^{***}p < 0.001$ compared to H/R group. H/R: hypoxia and reoxygenation, n = 3.

Effect of Quercetin on Cell Apoptosis

To test the potential of quercetin to inhibit endothelial cell apoptosis, we employed mitochondrial membrane potential and apoptosis for evaluation. When cells were injured to undergo apoptotic events, the mitochondrial membrane potential was reduced, cytoplasmic red fluorescence was significantly reduced, green fluorescence was increased, and Red/Green (R/G) was finally adopted to represent the alteration of mitochondrial membrane potential, which will decrease when the mitochondrial membrane potential is compromised. Our results showed that after H/R treatment, the mitochondrial membrane potential of the cells decreased, as indicated by increased green fluorescence. With increasing doses of quercetin, red fluorescence was constantly enhanced, indicating that quercetin can dose dependently elevate mitochondrial membrane potential (**Figure 3A, C**). Further, Flow cytometry was employed to directly examine cell apoptosis. The results showed that HBMECs exhibited an elevated rate of apoptosis after H/R treatment, whereas quercetin at 0.1–1 μmol/L exhibited a clear ability to inhibit apoptosis (**Figure 3B, D**).

Effect of Quercetin on Cell Adhesion

Once endothelial cells are damaged, some adhesion molecules, such as ICAM-1 and VCAM-1 are produced, adsorbing toxic substances into the BBB, and damaging the brain parenchyma (Hauptmann et al., 2020). To examine the effect of quercetin on the ability of H/R-HBMECs to produce adhesion molecules, ICAM-1 and VCAM-1 were measured using ELISA. In our study, H/R resulted in increased levels of ICAM-1 and VCAM-1, but the addition of quercetin under the concentration of 0.1–1 μmol/L decreased this effect (**Figure 4**).

Quercetin Could Inhibit Oxidative Stress

Quercetin is a flavonoid with strong antioxidant capacity, so we employed DCFH-DA probe to detect ROS. We observed increased ROS generation in HBMECs exposed to H/R, which was markedly reduced by quercetin treatment at the concentrations of 0.1–1 μmol/L. Meanwhile, we detected the level changes of oxidative stress products SOD and MDA with ELISA, and the results showed that quercetin at the concentration of 0.1–1 μmol/L was able to decrease SOD and MDA, which were elevated by H/R, thus indicating that quercetin could reduce the damage of HBMECs from oxidative stress (**Figure 5**).

Quercetin Could Regulate Keap1/Nrf2 and ATF6/GRP78 Proteins

To further explore the protective mechanism of quercetin on HBMECs, we analyzed the expression levels of oxidative stress and endoplasmic reticulum stress-related proteins. Keap1/Nrf2 is known to regulate antioxidant responses *in vivo*. Oxidative stress injury forces endothelial cells to undergo a stress response, resulting in increased Keap1/Nrf2 levels (Warpsinski et al., 2020). In the present study, H/R resulted in the activation of cellular antioxidant response mechanisms and increased levels of Keap1 and Nrf2, which could be further strengthened by quercetin at 0.5–1 μmol/L to enhance the antioxidant capacity of HBMECs. ATF6/GRP78 is one of the pathways that regulate endoplasmic reticulum (ER) homeostasis. ER stress can aggravate endothelial cell injury (Nie et al., 2020). In our study, ER stress was activated by H/R, and the levels of ATF6 and GRP78 were increased. Quercetin at 1 μmol/L was able to significantly reduce the protein levels of both, inhibit ER stress, and protect HBMECs from H/R injury (**Figure 6**).

Quercetin Could Maintain BBB Integrity

BMECs are the backbone of BBB structure, and their death or apoptosis after H/R injury affects BBB integrity and functionality (Ding et al., 2019). In this paper, the function of endothelial cells was reflected by the detection of changes in the expression of BBB associated proteins ZO-1 and Claudin-5. Compared with the control group, the expression of ZO-1 and Claudin-5 was

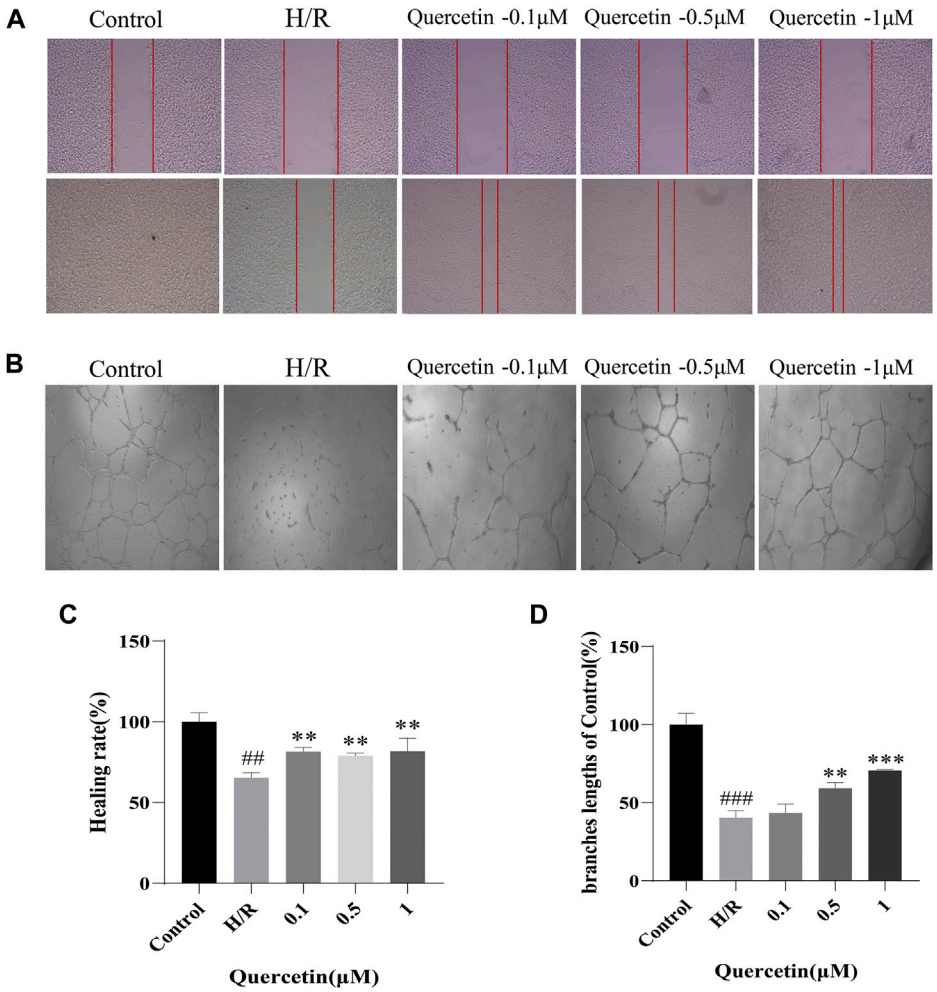

FIGURE 2 | (A) The distance between scratches in the presence of quercetin (0.1, 0.5, 1 μmol/L) was measured using scratch method **(B)** The branches length of the tube under the different concentrations of quercetin (0.1, 0.5, 1 μmol/L) was detected with tube formation method **(C)** Healing rate was calculated **(D)** Branches length data was displayed. $^{\#\#}p < 0.01$, $^{\#\#\#}p < 0.001$ compared to control group; $^{**}p < 0.01$, $^{***}p < 0.001$ compared to H/R group. μM: μmol/L; H/R: hypoxia and reoxygenation, n = 3.

decreased in H/R injury, indicating that the BBB was damaged and this damage could be reversed by quercetin at the concentrations of 0.5–1 μmol/L, indicating that quercetin can maintain the function of endothelial cells (**Figure 7**).

Proteomic Analysis

To find the differentially expression proteins (DEPs) of H/R injured HBMECs in the presence of quercetin or not, iTRAQ was used to conduct the proteomics analysis. Proteins exhibiting a $p < 0.05$ and a ratio fold change >1.2 or <0.83 were defined as DEPs. In our study, the differences in protein among the control, H/R, and quercetin groups were compared. The results showed that 172 proteins were identified as DEPs between the control and H/R groups, among which 94 were upregulated and 78 were downregulated in the H/R group. There were 1,016 proteins identified as DEPs between H/R group and the quercetin group, of which 553 were up-regulated and 463 were down-regulated in the quercetin group, as shown in **Figure 8A**. Between control vs H/R and H/R vs quercetin group, 56 of the same DEPs were shared between the two groups. The expressions of these DEPs were analyzed by hierarchical clustering as shown in **Figure 8B**. Among these DEPs, top 20 were shown in **Table1**. Among these 20 commons, insulin receptor-related protein (INSRR), dual specificity protein phosphatase 3 (DUSP3), annexin A2 (ANXA2), hemoglobin subunit alpha (HBA1), phosphoglycerate kinase 1 (PGK1), vitronectin (VTN), glucose-6-phosphate isomerase (GPI) are related to endothelial cells.

DISCUSSION

CSVD, as an increasing medical and socioeconomic burden, has rapidly attracted attention. But surprisingly, the pathogenesis of CSVD remains obscure at present, rendering no clear scheme for its treatment either. Given that the later stages of CSVD can

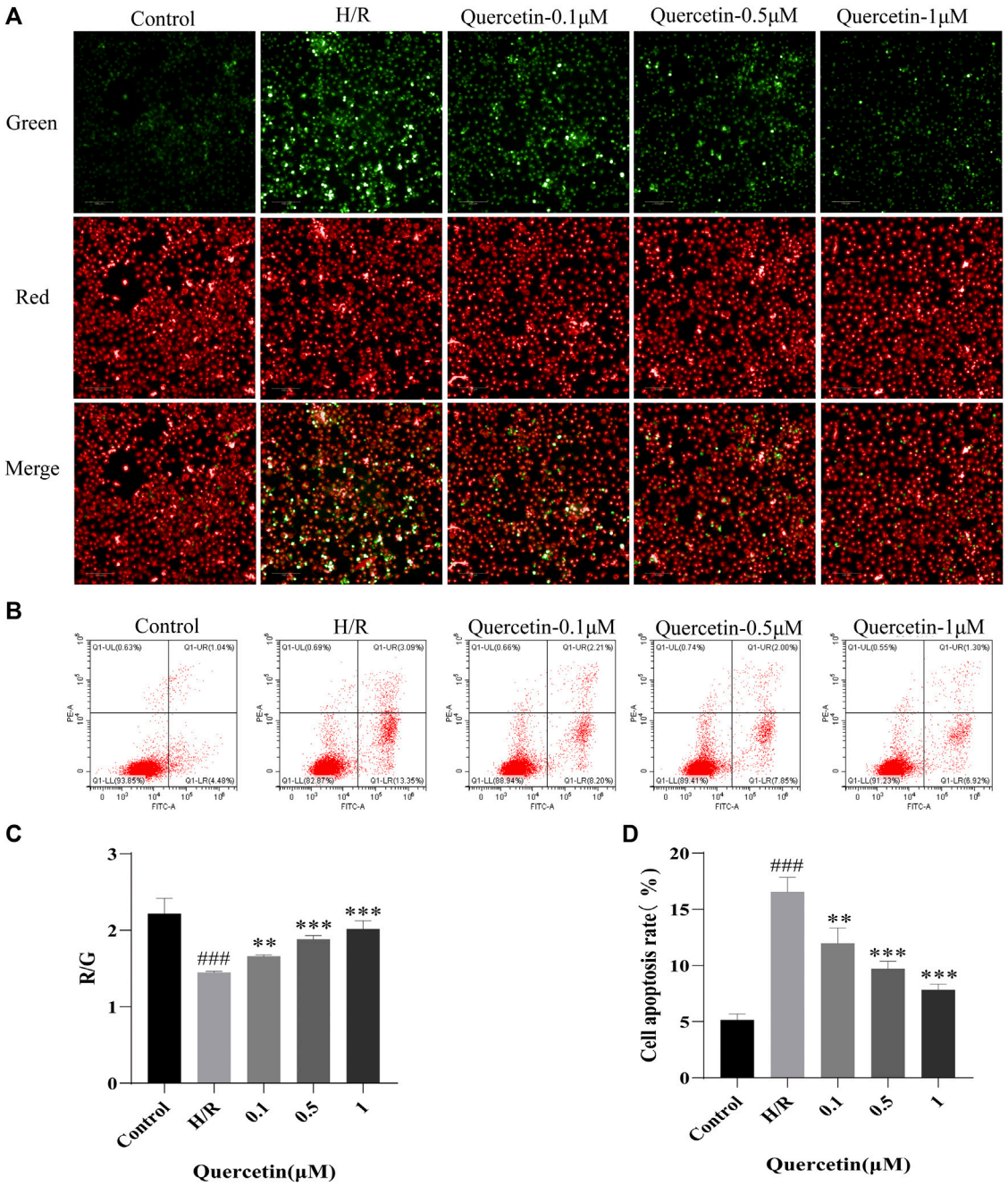

FIGURE 3 | (A) The mitochondrial membrane was examined using JC-1 probe **(B)** Apoptosis was evaluated using flow cytometry **(C)** R/G represents altered mitochondrial membrane potential **(D)** Apoptosis data was analyzed. $^{###}p < 0.001$ compared to control group; $^{**}p < 0.01$, $^{***}p < 0.001$ compared to H/R group. μM: μmol/L; R/G: Red/Green; H/R: hypoxia and reoxygenation, n = 3.

progress to severe outcomes such as stroke and dementia, targeting the early lesions for treatment can effectively delay the progression of CSVD (Cannistraro et al., 2019). It has been shown that the early pathological changes of CSVD lie in endothelial cell dysfunction and drugs that stabilize its dysfunction may improve the vulnerability of cerebral white matter in CSVD lesions (Rajani et al., 2018). Given the role played by endothelial cells in CSVD, we set out to investigate the protective effects of traditional Chinese medicine on endothelial cells using HBMECs.

Quercetin is a flavonoid present in a variety of plants (Nawrot-Hadzik et al., 2019). It has strong antioxidant and anti-inflammatory activities and can exert protective effects in various pathological conditions. In this study, we demonstrated that quercetin can ameliorate H/R injury, and several experimental data confirm our conclusion that

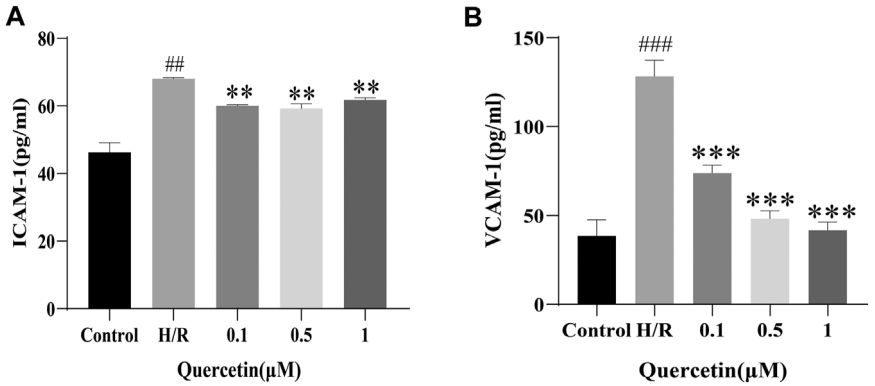

FIGURE 4 | (A) ICAM-1 was detected with ELISA **(B)** VCAM-1 was evaluated using ELISA. $^{\#\#}p < 0.01$, $^{\#\#\#}p < 0.001$ compared to control group; $^{**}p < 0.01$, $^{***}p < 0.001$ compared to H/R group. μM: μmol/L; ICAM-1: Intercellular cell adhesion molecule-1; VCAM-1: Vascular cell adhesion molecule-1; H/R: Hypoxia and reoxygenation, n = 3.

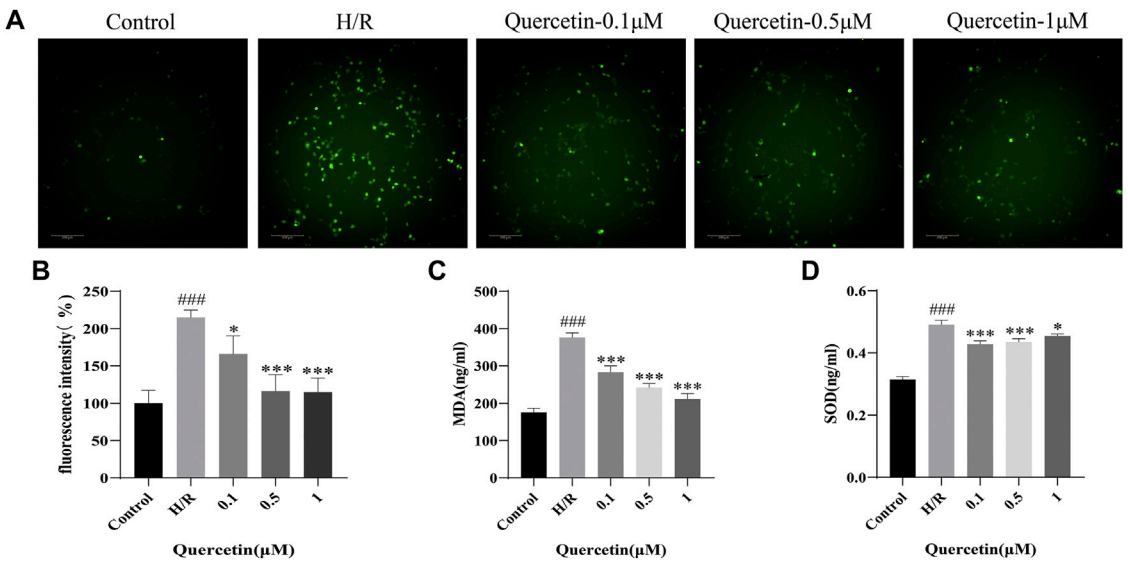

FIGURE 5 | (A) HBMECs was treated with quercetin (0.1, 0.5, 1 μmol/L) and H/R, ROS level was measured using DCFH-DA probe **(B)** Fluorescence intensity represents ROS expression **(C)** MDA was detected with ELISA **(D)** SOD was evaluated using ELISA. $^{\#\#\#}p < 0.001$ compared to control group; $^{*}p < 0.05$, $^{***}p < 0.001$ compared to H/R group. μM: μmol/L; ROS: Reactive oxygen species; MDA: Malondialdehyde; SOD: Superoxide dismutase; H/R: Hypoxia and reoxygenation, n = 3.

quercetin can promote cell viability, cell migration, angiogenesis, increase mitochondrial membrane potential and inhibit apoptosis.

Considering that quercetin has strong antioxidant activity, we investigated the mechanism by which quercetin protects HBMECs in terms of antioxidation. ROS levels can be significantly increased by oxidative stress (Wu et al., 2018), and the accumulation of ROS can cause many diseases, including cardiovascular diseases, endothelial dysfunction and aging related diseases, and neurodegenerative diseases (Chen et al., 2015; Jakaria et al., 2018; Santos et al., 2018). Moreover, oxidative stress occurs lipid peroxidation, producing MDA, which will destroy the body's oxidative antioxidant balance and increase endothelial cell damage (Yang et al., 2021). Keap1/Nrf2 is considered to be the most important self-anti-oxidative stress pathway at present, and activation of this pathway can significantly improve endothelial cell dysfunction. In particular, ROS help promote the activation of the Nrf2 signaling pathway (Selimoglu-Buet et al., 2017). We have demonstrated that quercetin can decrease ROS and MDA generation, while increasing Keap1 and Nrf2 protein expression, suggesting that quercetin may attenuate endothelial cell injury by decreasing oxidative stress responses via activating the Keap1/Nrf2 signaling pathway.

Not only that, sustained ER stress activates the unfolded protein response and alters the expression of antioxidant genes, leading to endothelial cell apoptosis (Tang et al., 2019). Moreover, oxidative stress can also cause the disturbance of

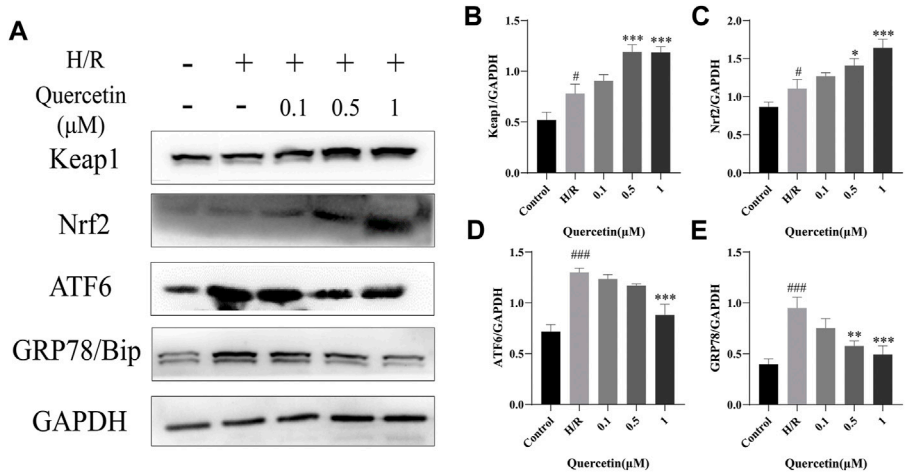

FIGURE 6 | (A) Protein expressions were evaluated with Western blotting **(B)** Keap1 quantification of Western blotting result was calculated **(C)** Nrf2 expression quantification of Western blotting result was inhibited **(D)** ATF6 expression data was analyzed **(E)** GRP78 expression data was analyzed. $^{\#}p < 0.05$, $^{\#\#\#}p < 0.001$ compared to control group; $^{*}p < 0.05$, $^{**}p < 0.01$, $^{***}p < 0.001$ compared to H/R group. μM: μmol/L; Keap1: Kelch Like ECH Associated Protein 1; Nrf2: Nuclear factor E2-related factor 2; ATF6: Activating transcription factor 6; GRP78: Glucose-regulated protein 78; H/R: Hypoxia and reoxygenation, n = 3.

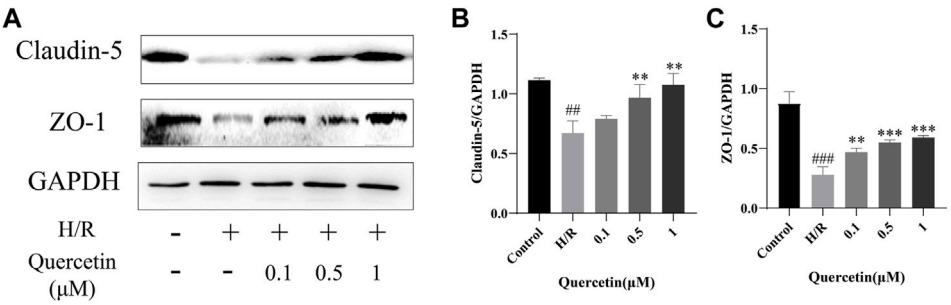

FIGURE 7 | (A) Protein expressions were evaluated with Western blotting **(B)** Claudin-5 quantification of Western blotting result was calculated **(C)** ZO-1 expression quantification of Western blotting result was inhibited. $^{\#\#}p < 0.01$, $^{\#\#\#}p < 0.001$ compared to control group; $^{**}p < 0.01$, $^{***}p < 0.001$ compared to H/R group. μM: μmol/L; ZO-1: Zonula occludens 1; H/R: Hypoxia and reoxygenation, n = 3.

protein folding in the ER, provoke ER stress, and aggravate endothelial cell injury (Hetz, 2012). ER stress can be activated by these three pathways: PKR-like ER kinase (PERK), inositol requiring enzyme 1 (IRE1), and the activating ATF-6, which protect cells from ER stress under homeostatic conditions (Hetz et al., 2020). But when affected by external adverse stimuli, these three pathways would activate the ER stress response and induce cell apoptosis. Moreover, studies have shown that inhibition of the ER stress response can reverse H/R-induced endothelial cell dysfunction (Chen et al., 2020).In our study, quercetin could reduce the elevated ATF6/GRP78 content caused by H/R, inhibit the endoplasmic reticulum stress response, and protect endothelial cells.

As a major component of the BBB, the functions of endothelial cells include maintaining its integrity. BBB dysfunction causes leakage of fluids, proteins, and other plasma components into perivascular tissues, further impairing cerebral vasodilation and nutrient transport (Wardlaw et al., 2019). When endothelial cells are damaged and the integrity of BBB will be destroyed, so protecting endothelial cells can further maintain the integrity of BBB.Claudin-5 is highly expressed in BMECs and is involved in constituting the backbone of tight junction chains to regulate BBB permeability (Yang et al., 2020). Endothelial cells are anchored to the actin cytoskeleton by scaffolding proteins such as ZO-1, rendering tight junctions between endothelial cells that maintain the tightness of the BBB (Zhang et al., 2020). In our study, the expression of claudin-5 and ZO-1 was used to represent BBB integrity. Our results showed that the protein levels of claudin-5 and ZO-1 were decreased in HBMECs subjected to H/R injury, indicating that BBB integrity was disrupted, and quercetin could reduce this injury by elevating claudin-5 and ZO-1 protein levels.

Furthermore, to find the potential targets of quercetin on HBMECs, i-TRAQ was labeled into cells. After proteomic analysis, top 20 of the common differentially expressed proteins were investigated. Among them, INSRR, DUSP3,

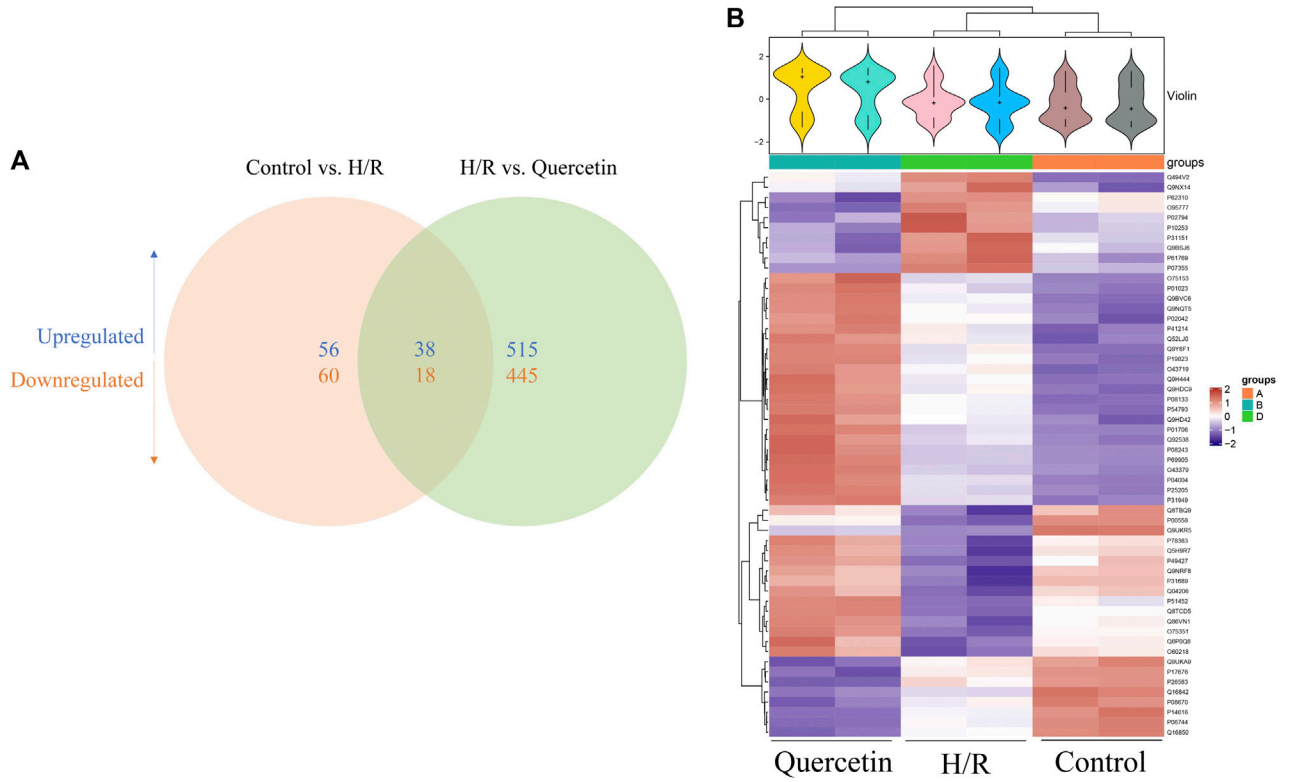

FIGURE 8 | (A) Venn diagram of the distribution in each comparison group **(B)** Heatmap of the 56 common differentially expressed proteins. H/R: Hypoxia and reoxygenation.

TABLE 1 | Top 20 of the common differentially expressed proteins.

Accession	Gene name	Description
P14616	INSRR	Insulin receptor-related protein
P31949	S100A11	Protein S100-A11
P51452	DUSP3	Dual specificity protein phosphatase 3
Q8TCD5	NT5C	5′ (3′)-deoxyribonucleotidase, cytosolic type
P07355	ANXA2	Annexin A2
O95777	LSM8	U6 snRNA-associated Sm-like protein LSm8
P25205	MCM3	DNA replication licensing factor MCM3
O43379	WDR62	WD repeat-containing protein 62
P49427	CDC34	Ubiquitin-conjugating enzyme E2 R1
Q9UKR5	ERG28	Ergosterol biosynthetic protein 28
P69905	HBA1	Hemoglobin subunit alpha
P00558	PGK1	Phosphoglycerate kinase 1
O75351	VPS4B	Vacuolar protein sorting-associated protein 4B
P54793	ARSF	Arylsulfatase F
Q16850	CYP51A1	Lanosterol 14-alpha demethylase
Q9BVC6	TMEM109	Transmembrane protein 109
P04004	VTN	Vitronectin
P06744	GPI	Glucose-6-phosphate isomerase
P01706	IGLV2-11	Immunoglobulin lambda variable 2–11
P19823	ITIH2	Inter-alpha-trypsin inhibitor heavy chain H2

ANXA2, HBA1, PGK1, VTN, GPI are related to endothelial cells. INSRR is considered as a tumor endothelial marker and its overexpression can promote angiogenesis (Nowak-Sliwinska et al., 2019). Recombinant ANXA2 can reduce endothelial permeability under hypoxic and flammatory factor injury states, indicating that ANXA2 may be involved in the maintenance of endothelial cell tightness (Li et al., 2019). In staining human cervical sections, strong expression of DUSP3 was found in endothelial cells, and experiments also demonstrated that DUSP3 is necessary for basic fibroblast growth factor induced microvascular growth (Amand et al., 2014). HBA1 expression in endothelial cells has been shown to control vascular tone and function (Sangwung et al., 2017). PGK1 is also thought to reduce atherogenesis (Zhang et al., 2020). What's more, VTN is considered critical for thrombus formation in the setting of vascular injury (Bowley et al., 2017). GPI is enriched in the microvascular endothelial cells of synovial tissue from rheumatoid arthritis patients under hypoxic environment, and regulates the secretion of vascular endothelial growth factor from rheumatoid arthritis synovial fibroblasts to induce angiogenesis (Lu et al., 2017). In addition, the study of differentially expressed proteins related to varicocele mediated infertility showed that Nrf2 was an upstream regulator of ANXA2 (Panner Selvam et al., 2021). Inhibition of PGK1 can activate Keap1/Nrf2 pathway and stimulate cell protective antioxidant response (Bollong et al., 2018). The two proteins may be the potential targets of quercetin through Keap1/Nrf2 pathway. Further study can verify the role of these proteins on the effect of quercetin on H/R-HBMECs.

Admittedly, quercetin can exert protective effects on endothelial cells. But the specific targets of action still require further investigation, and whether there are additional pathways of action remains unknown.

In conclusion, this study showed that quercetin maintained the integrity of the blood-brain barrier by protecting endothelial cells. At the molecular level, quercetin may play a role in protecting endothelial cells by protecting against oxidative stress through the Keap1/Nrf2 pathway and inhibiting endoplasmic reticulum stress through the ATF6/GRP78 pathway. This study lays the foundation for TCM to treat CSVD by protecting endothelial cells.

DATA AVAILABILITY STATEMENT

The datasets presented in this study can be found in online repositories. The names of the repository/repositories and accession number(s) can be found in the article/supplementary material.

AUTHOR CONTRIBUTIONS

YH contributed to the conception and design of the experiment. ML, JK and LS performed experiments. QL, YH and CG performed the statistical analysis. YB and SG wrote the first draft of the manuscript. YW and ML processed images. YL and JK wrote sections of the manuscript.

FUNDING

This work was supported by the National Key Research and Development Program of China (No. 2019YFC1711603); Clinical Research Plan of SHDC (No. SHDC2020CR 2046B) and the National Natural Science Foundation of China (No. 81771288).

REFERENCES

Amand, M., Erpicum, C., Bajou, K., Cerignoli, F., Blacher, S., Martin, M., et al. (2014). DUSP3/VHR Is a Pro-angiogenic Atypical Dual-Specificity Phosphatase. *Mol. Cancer* 13, 108. doi:10.1186/1476-4598-13-108

Bollong, M. J., Lee, G., Coukos, J. S., Yun, H., Zambaldo, C., Chang, J. W., et al. (2018). A Metabolite-Derived Protein Modification Integrates Glycolysis with KEAP1-NRF2 Signalling. *Nature* 562, 600–604. doi:10.1038/s41586-018-0622-0

Bowley, S. R., Fang, C., Merrill-Skoloff, G., Furie, B. C., and Furie, B. (2017). Protein Disulfide Isomerase Secretion Following Vascular Injury Initiates a Regulatory Pathway for Thrombus Formation. *Nat. Commun.* 8, 14151. doi:10.1038/ncomms14151

Cannistraro, R. J., Badi, M., Eidelman, B. H., Dickson, D. W., Middlebrooks, E. H., and Meschia, J. F. (2019). CNS Small Vessel Disease: A Clinical Review. *Neurology* 92, 1146–1156. doi:10.1212/WNL.0000000000007654

Chen, B., Lu, Y., Chen, Y., and Cheng, J. (2015). The Role of Nrf2 in Oxidative Stress-Induced Endothelial Injuries. *J. Endocrinol.* 225, R83–R99. doi:10.1530/JOE-14-0662

Chen, B. H., Park, J. H., Ahn, J. H., Cho, J. H., Kim, I. H., Lee, J. C., et al. (2017). Pretreated Quercetin Protects Gerbil Hippocampal CA1 Pyramidal Neurons from Transient Cerebral Ischemic Injury by Increasing the Expression of Antioxidant Enzymes. *Neural Regen. Res.* 12, 220–227. doi:10.4103/1673-5374.200805

Chen, L., Luo, W., Zhang, W., Chu, H., Wang, J., Dai, X., et al. (2020). circDLPAG4/HECTD1 Mediates Ischaemia/reperfusion Injury in Endothelial Cells via ER Stress. *RNA Biol.* 17, 240–253. doi:10.1080/15476286.2019.1676114

Cho, J. Y., Kim, I. S., Jang, Y. H., Kim, A. R., and Lee, S. R. (2006). Protective Effect of Quercetin, a Natural Flavonoid against Neuronal Damage after Transient Global Cerebral Ischemia. *Neurosci. Lett.* 404, 330–335. doi:10.1016/j.neulet.2006.06.010

Comalada, M., Camuesco, D., Sierra, S., Ballester, I., Xaus, J., Gálvez, J., et al. (2005). *In Vivo* quercitrin Anti-inflammatory Effect Involves Release of Quercetin, Which Inhibits Inflammation through Down-Regulation of the NF-kappaB Pathway. *Eur. J. Immunol.* 35, 584–592. doi:10.1002/eji.200425778

Ding, Y., Wang, R., Zhang, J., Zhao, A., Lu, H., Li, W., et al. (2019). Potential Regulation Mechanisms of P-Gp in the Blood-Brain Barrier in Hypoxia. *Curr. Pharm. Des.* 25, 1041–1051. doi:10.2174/1381612825666190610140153

Dok-Go, H., Lee, K. H., Kim, H. J., Lee, E. H., Lee, J., Song, Y. S., et al. (2003). Neuroprotective Effects of Antioxidative Flavonoids, Quercetin, (+)-dihydroquercetin and Quercetin 3-methyl Ether, Isolated from Opuntia Ficus-Indica Var. Saboten. *Brain Res.* 965, 130–136. doi:10.1016/s0006-8993(02)04150-1

Hainsworth, A. H., Oommen, A. T., and Bridges, L. R. (2015). Endothelial Cells and Human Cerebral Small Vessel Disease. *Brain Pathol.* 25, 44–50. doi:10.1111/bpa.12224

Hauptmann, J., Johann, L., Marini, F., Kitic, M., Colombo, E., Mufazalov, I. A., et al. (2020). Interleukin-1 Promotes Autoimmune Neuroinflammation by Suppressing Endothelial Heme Oxygenase-1 at the Blood-Brain Barrier. *Acta Neuropathol.* 140, 549–567. doi:10.1007/s00401-020-02187-x

Hetz, C. (2012). The Unfolded Protein Response: Controlling Cell Fate Decisions under ER Stress and beyond. *Nat. Rev. Mol. Cel Biol* 13, 89–102. doi:10.1038/nrm3270

Hetz, C., Zhang, K., and Kaufman, R. J. (2020). Mechanisms, Regulation and Functions of the Unfolded Protein Response. *Nat. Rev. Mol. Cel Biol* 21, 421–438. doi:10.1038/s41580-020-0250-z

Jakaria, M., Cho, D. Y., Ezazul Haque, M., Karthivashan, G., Kim, I. S., Ganesan, P., et al. (2018). Neuropharmacological Potential and Delivery Prospects of Thymoquinone for Neurological Disorders. *Oxid Med. Cel Longev* 2018, 1209801. doi:10.1155/2018/1209801

Jin, Z., Ke, J., Guo, P., Wang, Y., and Wu, H. (2019). Quercetin Improves Blood-Brain Barrier Dysfunction in Rats with Cerebral Ischemia Reperfusion via Wnt Signaling Pathway. *Am. J. Transl Res.* 11, 4683–4695.

Keaney, J., and Campbell, M. (2015). The Dynamic Blood-Brain Barrier. *Febs j* 282, 4067–4079. doi:10.1111/febs.13412

Li, W., Chen, Z., Yuan, J., Yu, Z., Cheng, C., Zhao, Q., et al. (2019). Annexin A2 Is a Robo4 Ligand that Modulates ARF6 Activation-Associated Cerebral Trans-endothelial Permeability. *J. Cereb. Blood Flow Metab.* 39, 2048–2060. doi:10.1177/0271678X18777916

Lu, Y., Yu, S. S., Zong, M., Fan, S. S., Lu, T. B., Gong, R. H., et al. (2017). Glucose-6-Phosphate Isomerase (G6PI) Mediates Hypoxia-Induced Angiogenesis in Rheumatoid Arthritis. *Sci. Rep.* 7, 40274. doi:10.1038/srep40274

Nawrot-Hadzik, I., Ślusarczyk, S., Granica, S., Hadzik, J., and Matkowski, A. (2019). Phytochemical Diversity in Rhizomes of Three Reynoutria Species and Their Antioxidant Activity Correlations Elucidated by LC-ESI-MS/MS Analysis. *Molecules* 24, 1136. doi:10.3390/molecules24061136

Nie, X., Tang, W., Zhang, Z., Yang, C., Qian, L., Xie, X., et al. (2020). Procyanidin B2 Mitigates Endothelial Endoplasmic Reticulum Stress through a PPARδ-dependent Mechanism. *Redox Biol.* 37, 101728. doi:10.1016/j.redox.2020.101728

Nowak-Sliwinska, P., van Beijnum, J. R., Huijbers, E. J. M., Gasull, P. C., Mans, L., Bex, A., et al. (2019). Oncofoetal Insulin Receptor Isoform A marks the Tumour Endothelium; an Underestimated Pathway during Tumour Angiogenesis and Angiostatic Treatment. *Br. J. Cancer* 120, 218–228. doi:10.1038/s41416-018-0347-8

Panner Selvam, M. K., Agarwal, A., Sharma, R., Samanta, L., Gupta, S., Dias, T. R., et al. (2021). Protein Fingerprinting of Seminal Plasma Reveals Dysregulation of Exosome-Associated Proteins in Infertile Men with Unilateral Varicocele. *World J. Mens Health* 39, 324–337. doi:10.5534/wjmh.180108

Rajani, R. M., Quick, S., Ruigrok, S. R., Graham, D., Harris, S. E., Verhaaren, B. F. J., et al. (2018). Reversal of Endothelial Dysfunction Reduces white Matter Vulnerability in Cerebral Small Vessel Disease in Rats. *Sci. Transl Med.* 10, eaam9507. doi:10.1126/scitranslmed.aam9507

Sangwung, P., Zhou, G., Lu, Y., Liao, X., Wang, B., Mutchler, S. M., et al. (2017). Regulation of Endothelial Hemoglobin Alpha Expression by Kruppel-like Factors. *Vasc. Med.* 22, 363–369. doi:10.1177/1358863X17722211

Santos, A. L., Sinha, S., and Lindner, A. B. (2018). The Good, the Bad, and the Ugly of ROS: New Insights on Aging and Aging-Related Diseases from Eukaryotic and Prokaryotic Model Organisms. *Oxid Med. Cel Longev* 2018, 1941285. doi:10.1155/2018/1941285

Selimoglu-Buet, D., Badaoui, B., Benayoun, E., Toma, A., Fenaux, P., Quesnel, B., et al. (2017). Accumulation of Classical Monocytes Defines a Subgroup of MDS that Frequently Evolves into CMML. *Blood* 130, 832–835. doi:10.1182/blood-2017-04-779579

Tang, V., Fu, S., Rayner, B. S., and Hawkins, C. L. (2019). 8-Chloroadenosine Induces Apoptosis in Human Coronary Artery Endothelial Cells through the Activation of the Unfolded Protein Response. *Redox Biol.* 26, 101274. doi:10.1016/j.redox.2019.101274

Wardlaw, J. M., Smith, C., and Dichgans, M. (2013). Mechanisms of Sporadic Cerebral Small Vessel Disease: Insights from Neuroimaging. *Lancet Neurol.* 12, 483–497. doi:10.1016/S1474-4422(13)70060-7

Wardlaw, J. M., Smith, C., and Dichgans, M. (2019). Small Vessel Disease: Mechanisms and Clinical Implications. *Lancet Neurol.* 18, 684–696. doi:10.1016/S1474-4422(19)30079-1

Wardlaw, J. M., Smith, E. E., Biessels, G. J., Cordonnier, C., Fazekas, F., Frayne, R., et al. (2013). Neuroimaging Standards for Research into Small Vessel Disease and its Contribution to Ageing and Neurodegeneration. *Lancet Neurol.* 12, 822–838. doi:10.1016/S1474-4422(13)70124-8

Warpsinski, G., Smith, M. J., Srivastava, S., Keeley, T. P., Siow, R. C. M., Fraser, P. A., et al. (2020). Nrf2-regulated Redox Signaling in Brain Endothelial Cells Adapted to Physiological Oxygen Levels: Consequences for Sulforaphane Mediated protection against Hypoxia-Reoxygenation. *Redox Biol.* 37, 101708. doi:10.1016/j.redox.2020.101708

Wu, C. R., Chang, H. C., Cheng, Y. D., Lan, W. C., Yang, S. E., and Ching, H. (2018). Aqueous Extract of Davallia Mariesii Attenuates 6-Hydroxydopamine-Induced Oxidative Damage and Apoptosis in B35 Cells through Inhibition of Caspase Cascade and Activation of PI3K/AKT/GSK-3β Pathway. *Nutrients* 10, 1449. doi:10.3390/nu10101449

Yang, J., Liu, J., Wang, P., Sun, J., Lv, X., and Diao, Y. (2021). Toxic Effect of Titanium Dioxide Nanoparticles on Corneas *In Vitro* and *In Vivo*. *Aging* 13, 5020–5033. doi:10.18632/aging.202412

Yang, Z., Lin, P., Chen, B., Zhang, X., Xiao, W., Wu, S., et al. (2020). Autophagy Alleviates Hypoxia-Induced Blood-Brain Barrier Injury via Regulation of CLDN5 (Claudin 5). *Autophagy*, 1–20. doi:10.1080/15548627.2020.1851897

Zhang, C. E., Wong, S. M., van de Haar, H. J., Staals, J., Jansen, J. F., Jeukens, C. R., et al. (2017). Blood-brain Barrier Leakage Is More Widespread in Patients with Cerebral Small Vessel Disease. *Neurology* 88, 426–432. doi:10.1212/WNL.0000000000003556

Zhang, X., Guan, M. X., Jiang, Q. H., Li, S., Zhang, H. Y., Wu, Z. G., et al. (2020). NEAT1 Knockdown Suppresses Endothelial Cell Proliferation and Induces Apoptosis by Regulating miR-638/AKT/mTOR S-ignaling in A-therosclerosis. *Oncol. Rep.* 44, 115–125. doi:10.3892/or.2020.7605

Zhang, X., Tang, X., Ma, F., Fan, Y., Sun, P., Zhu, T., et al. (2020). Endothelium-targeted Overexpression of Krüppel-like Factor 11 Protects the Blood-Brain Barrier Function after Ischemic Brain Injury. *Brain Pathol.* 30, 746–765. doi:10.1111/bpa.12831

Conflict of Interest: The authors declare that the research was conducted in the absence of any commercial or financial relationships that could be construed as a potential conflict of interest.

Publisher's Note: All claims expressed in this article are solely those of the authors and do not necessarily represent those of their affiliated organizations, or those of the publisher, the editors and the reviewers. Any product that may be evaluated in this article, or claim that may be made by its manufacturer, is not guaranteed or endorsed by the publisher.

frontiers in Neuroscience

REVIEW
published: 16 November 2021
doi: 10.3389/fnins.2021.755902

Research Progress on the Ability of Astragaloside IV to Protect the Brain Against Ischemia-Reperfusion Injury

Xianhui Kang[1,2†], Shuyue Su[3†], Wandong Hong[4], Wujun Geng[1,5] and Hongli Tang[1*]*

[1] Department of Anesthesiology, The First Affiliated Hospital of Wenzhou Medical University, Wenzhou, China, [2] Department of Anesthesiology, The First Affiliated Hospital, Zhejiang University School of Medicine, Hangzhou, China, [3] Wenzhou Medical University, Wenzhou, China, [4] Department of Gastroenterology and Hepatology, The First Affiliated Hospital of Wenzhou Medical University, Wenzhou, China, [5] Wenzhou Key Laboratory of Perioperative Medicine, Wenzhou, China

Stroke, a disease with a sudden onset and high morbidity and mortality rates, is difficult to treat in the clinic. Traditional Chinese medicine has become increasingly widely used in clinical practice. Modern pharmacological studies have found that Radix Astragali has a variety of medicinal properties, i.e., immunoregulatory, antioxidative, anti-cancer, anti-diabetes, myocardial protective, hepatoprotective, and antiviral functions. This article reviews the protective effect and mechanism of astragaloside IV, which is extracted from Radix Astragali, on stroke, discusses the cerebroprotective effect of astragaloside IV against ischemia-reperfusion-related complications, offers insight into research prospects, and expands the idea of integrating traditional Chinese and Western medicine treatment strategies and drugs to provide a theoretical reference for the clinical treatment of cerebral ischemia-reperfusion injury and the improvement of stroke prognosis.

Keywords: Radix Astragali, astragaloside-IV, stroke, cerebral protection, ischemia reperfusion

OPEN ACCESS

Edited by:
Zhang Yuefan,
Shanghai University, China

Reviewed by:
Ivana Grković,
University of Belgrade, Serbia
Sergei V. Fedorovich,
Belarusian State University, Belarus

****Correspondence:***
Hongli Tang
tanghongliok@126.com
Wujun Geng
gengwujun@126.com

† These authors have contributed equally to this work

Specialty section:
This article was submitted to Neuropharmacology, a section of the journal Frontiers in Neuroscience

Received: *09 August 2021*
Accepted: *13 October 2021*
Published: *16 November 2021*

Citation:
Kang X, Su S, Hong W, Geng W and Tang H (2021) Research Progress on the Ability of Astragaloside IV to Protect the Brain Against Ischemia-Reperfusion Injury. Front. Neurosci. 15:755902. doi: 10.3389/fnins.2021.755902

INTRODUCTION

Stroke has a high incidence and is the main cause of death worldwide. Restoration of cerebral blood supply as soon as possible, i.e., reperfusion, is currently the best method for protecting the brain against ischemic injury. Recombinant tissue plasminogen activator (rtPA), which is the only FDA-approved treatment for ischemic stroke, has a significant time-dependent therapeutic effect. rtPA is most effective when administered within 90 min before symptoms appear (Lansberg et al., 2009), and the prognosis of elderly patients and patients with severe stroke treated with rtPA is still poor (Saposnik et al., 2013). Due to the injury caused by reperfusion and the narrow 4.5 h therapeutic window of rtPA, few patients are suitable for rtPA treatment. In clinical practice, only approximately 3% of patients can be treated with rtPA (Armstead et al., 2010). If rtPA is administered after beyond the therapeutic window thrombolysis, the risk of hemorrhagic transformation and fatal edema due to cerebral ischemia-reperfusion injury is elevated (Shafi and Levine, 2010).

Astragaloside IV, a monomer extracted from Radix Astragali (**Figure 1**; Li et al., 2019), protects brain tissue by inhibiting the expression of peripheral benzodiazepine receptors in the ischemic penumbra and reducing apoptosis. It can also regulate M1/M2 microglia/macrophage polarization and improve the inflammatory response in the ischemic penumbra area, thus protecting brain tissue. Astragaloside IV can ameliorate memory impairment and neuroinflammation in mice with bilateral common carotid artery occlusion by decreasing the expression of Toll-like receptor

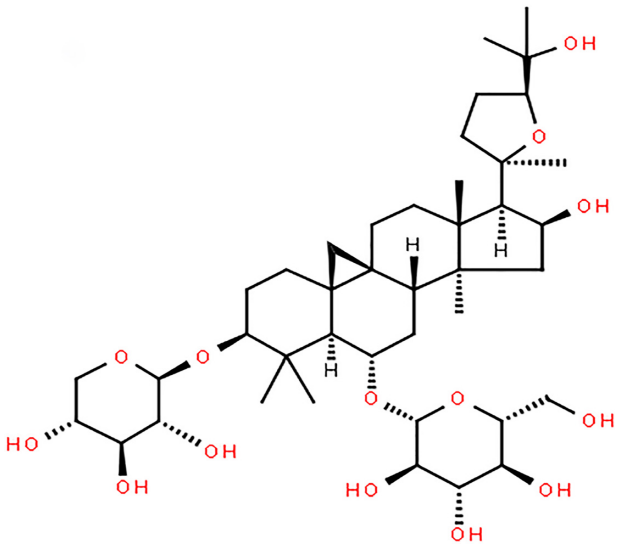

FIGURE 1 | Chemical structure of Astragaloside IV.

(TLR)4 and its downstream receptor proteins, including MyD88, TRIF, and TRAF6, and inhibiting the phosphorylation of NF-κB. In addition, astragaloside IV exerts a protective effect on neural stem cells by inhibiting the JNK/C-Jun pathway through miR-138. Other researchers have shown that astragaloside IV can protect the brain against ischemia-reperfusion injury by reducing the permeability of the blood-brain barrier (BBB) under pathological conditions by upregulating Bal-2 expression and downregulating Bax, caspase-3, BIP, CHOP, P-PERK, and P-eif2α expression, thereby reducing endothelial cell apoptosis and inhibiting endoplasmic reticulum stress. Recently, some scholars have confirmed the ability of astragaloside IV to cross the BBB through computational studies, and model analysis has verified the ability of astragaloside IV to cross the BBB (Stępnik and Kukula-Koch, 2020). This lays the foundation for the clinical application of astragaloside IV in the future.

MECHANISM UNDERLYING THE AMELIORATION OF ISCHEMIA-REPERFUSION INJURY BY ASTRAGALOSIDE IV

There are many mechanisms of ischemia-reperfusion injury: ischemia-induced neuronal apoptosis, oxidative stress (Chan, 1996), BBB damage (del Zoppo and Mabuchi, 2003), leukocyte adhesion to vessel walls (del Zoppo et al., 1991), parenchymal infiltration (Zhang et al., 1994a,b), hemorrhagic transformation, and inflammatory responses triggered by ischemia and exacerbated by reperfusion (Jean et al., 1998; Lindsberg and Grau, 2003; Liu et al., 2011). Several studies have shown that astragaloside IV can alleviate brain injury caused by ischemia-reperfusion through multiple pathways (**Table 1**).

Ischemia-Induced Neuronal Apoptosis

Glutamate-releasing enzyme-mediated excitotoxicity is the main cause of ischemic brain injury (Tymianski, 2011). Elevation of glutamate concentrations in the ischemic area of the brain activates neuronal N-methyl-D-aspartate receptor (NMDAR), mediates extracellular calcium influx, and increases intracellular calcium concentrations, and intracellular calcium triggers the apoptosis cascade, leading to cell dysfunction (Lai et al., 2014). Glutamate stimulation induces dissociation of mitochondrial hexokinase II (HK-II) from mitochondria, resulting in impaired mitochondrial function, as evidenced by opening of the mitochondrial permeability transition pore (mPTP) (Nederlof et al., 2014), collapse of the mitochondrial membrane potential, and decreased neuronal mitochondrial oxygen consumption, accompanied by apoptosis, oxidative DNA damage, PAR formation (Alano et al., 2004), and nuclear translocation of apoptosis-inducing factor (AIF), which is indicative of dependent cell death (Yu et al., 2006). Moreover, calcium overload is an important link between apoptosis and neuronal necrosis. Extracellular calcium can be absorbed and transported to mitochondria during ischemia-reperfusion injury, increasing mitochondrial permeability and promoting oxidative reactions and apoptosis (Yin et al., 2020). CaSR, a G-protein-coupled receptor, plays an important role in maintaining calcium homeostasis and regulating calcium influx (Lu et al., 2010; **Figure 2**).

Astragaloside IV can preserve mitochondrial HK-II, reduce the release of proapoptotic proteins and AIF, and subsequently protect neurons from apoptosis and cell death by promoting the binding of Akt to HK-II, thus activating Akt to protect mitochondrial HK-II, improving the activity of glycolysis, and protecting hexokinase (Li et al., 2019). It has been found that during cerebral ischemia-reperfusion, the protein expression of CaSR and calcium influx increase. Astragaloside IV can inhibit the protein expression of CaSR after ischemia-reperfusion injury to reduce calcium reflux (Du et al., 2021). Radix Astragali exerts a protective effect not only on neurons but also against ischemic apoptosis of neural stem cells. Previous studies have found that ischemia and hypoxia promote neural stem cell proliferation through a feedback mechanism. Stem cell viability increases after 2 h of ischemia and hypoxia. However, with the prolongation of ischemia and hypoxia, stem cell viability decreases in a time-dependent manner (Li et al., 2007). It has been found that the expression of miR-138 is increased in neural stem cells exposed to hypoxia. miR-138, which plays a critical role in promoting the growth and survival of self-renewing tumor-initiating cells, was previously identified as a molecular marker of glioma stem cells (GSCs) (Chan et al., 2012). It has also been reported that the JNK/C-Jun pathway mediates the effect of miR-138 on hypoxia-induced myocardial apoptosis (He et al., 2013). In a recent study, a 50% decline in stem cell viability was observed after an 8-h ischemic preconditioning regimen. Studies have shown that pretreatment of rat neural stem cells with 2.5 or 5 mg/ml Astragalus polysaccharides for 2 h before

TABLE 1 | Protective effect and mechanism of astragaloside IV against cerebral ischemia-reperfusion injury.

No.	Study object/model	Test indicator	Mechanism	Effect	References
1	OGD	(+) Number of surviving cells HK-II expression p-Akt expression (-) Glutamate concentration TUNEL staining DAPI staining PAR expression	(+) Akt phosphorylation (+) Akt binding to HK-II	(+) Hexokinase activity Mitochondrial HK-II (-) Release of proapoptotic proteins and apoptosis-inducing factor (AIF)	Li et al., 2019
2	MCAO SD rats OGD PC12 cells	(+) Cell viability (-) Apoptosis rate of PC12 cells Caspase-3 expression Calcium concentration CaSR expression	(-) CaSR expression	(-)reduce calcium reflux	Du et al., 2021
3	Hypoxia-treated neural stem cells in SD rats	(+) Cell viability Bcl-2 expression miR-138 expression (-) Apoptosis rate Caspase-3 expression Caspase-9 expression Bax expression p-JNK expression p-c-Jun expression p-p38MAPK expression	(+) miR-138 expression (-) JNK/p38 MAPK pathway	(+) Cell survival Anti-apoptotic factor expression (-) Apoptosis rate Pro-apoptotic factor expression	Zheng and Zhao, 2018
4	C57BL/6 mice	(+) Cell survival rate Nrf2 mRNA and protein expression HO-1 mRNA and protein expression	(+) Nrf2/HO-1 pathway	(+) Expression of Nrf2 in nuclei Nrf2 nuclear translocation rate HO-1 expression (-) Expression of Nrf2 in cytoplasm	Huang et al., 2014
5	OGD	(+) Cell viability ATP levels JC-1 expression p-PKA expression p-CREB expression (-) LDH levels ROS levels Caspase-3 expression	(+) PKA/CREB pathway	(+) Nerve cell viability (-) Release of LDH Fragmentation of neuronal fibers and cell bodies Expression of caspase-3	Xue et al., 2019
6	MCAO Bend.3 cells C57BL/6 mice	(+) ZO-1 expression Nrf2 expression HO-1 expression NQO1 expression TEER Occludin expression CLDN5 expression (-) BBB permeability ROS levels VCAM-1 expression IL-1β expression TNF-α expression	(+) Nrf2/HO-1 pathway	(+) Expression of tight junction protein (-) VCAM-1 expression Adhesion of monocytes to vascular endothelial cells	Qu et al., 2009; Li et al., 2018
7	MCAO	(+) Neurological score (-) Infarct size MPO levels TNF-α expression IL-1β expression Number of CD11b/CD18-positive neutrophils ICAM-1 expression NF-κB expression	/	(-) TNF-α and IL-1b production Levels of NF-κB Proportion of CD11b/CD18-positive neutrophils Expression of intercellular adhesion molecule-1 (ICAM-1)	Li et al., 2012

(Continued)

TABLE 1 | (Continued)

No.	Study object/model	Test indicator	Mechanism	Effect	References
8	BV-2 microglial cells	(+) Cell viability IL-10 expression Arg-1 expression (-) NO expression IL-1β expression IL-6 expression TNF-α expression IL-4 expression TLR4 expression MyD88 expression NF-êB expression iNOS expression	(-) TLR4/MyD88/NF-B pathway	(+) Expression of anti-inflammatory factor (IL-10) (-) LPS-induced M2 to M1 transition in microglia NO production Expression of proinflammatory factors (IL-6, TNF-α)	Yu et al., 2019
9	MCAO SD rats	(+) PPARγ mRNA expression PPARγ protein expression Number of CD206+/Iba1+(M2) cells Number of BrdU+/NeuN+ cells Number of BrdU+/GFAP+ cells Number of BrdU+/vWF+ cells (-) Number of CD16/32+/Iba1+ (M1) cells	(+) PPARγ pathway	(+)M1 microglia/macrophages convert to M2 microglia/macrophages	Li et al., 2021

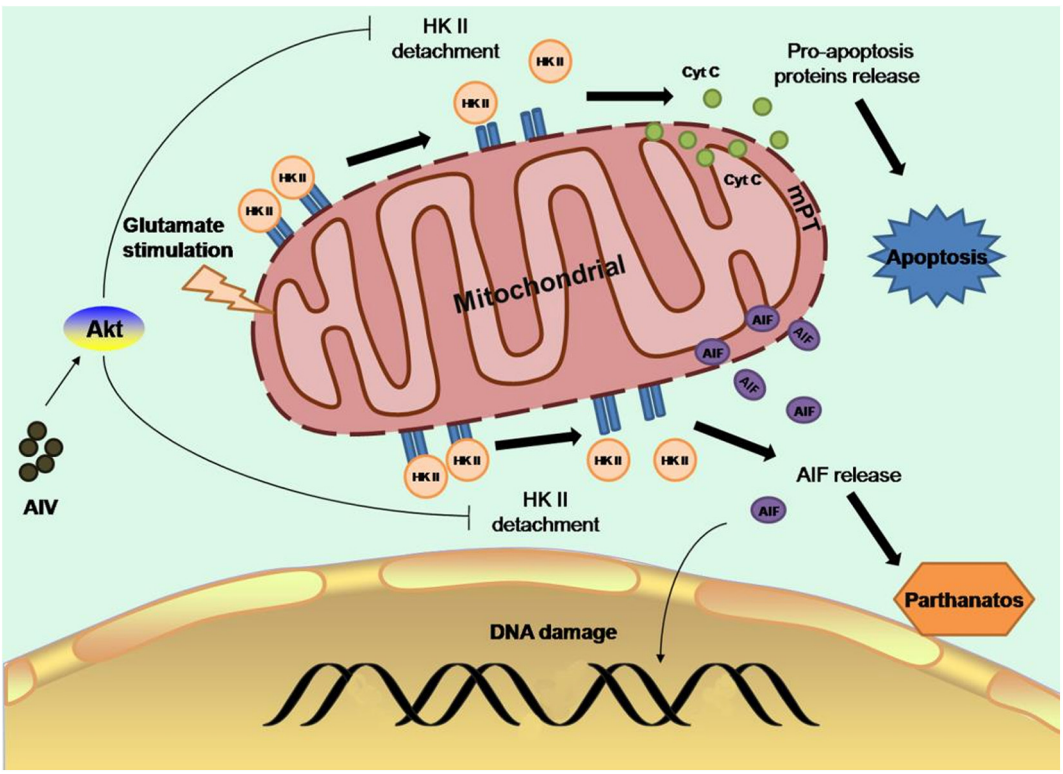

FIGURE 2 | Astragaloside IV can preserve mitochondrial HK-II and subsequently protect neurons from apoptosis and cell death by promoting the binding of Akt to HK-II, which activates Akt and protects mitochondrial HK-II, improving glycolysis, and protecting hexokinase (Springer).

treatment can increase cell survival, decrease the apoptosis rate, decrease the expression of proapoptotic factors, and increase the expression of antiapoptotic factors. In this study, the mechanism under the effect of Astragalus polysaccharides was also discussed. miR-138 expression was significantly elevated in the Astragalus polysaccharide-treated group compared with the control group, and the expression of phosphorylated JNK and c-Jun was decreased. In contrast, the protective effect of Astragalus polysaccharides on ischemic neural stem cells was abolished after miR-138 inhibitor treatment, suggesting that the protective effect of Astragalus polysaccharides on ischemic neural stem cells is achieved through upregulation of miR-138 expression in NSCs exposed to hypoxia and inhibition of the JNK/C-Jun pathway (Zheng and Zhao, 2018). This finding provides an experimental basis for the treatment of perinatal hypoxic-ischemic encephalopathy (HIE) with Astragalus polysaccharides.

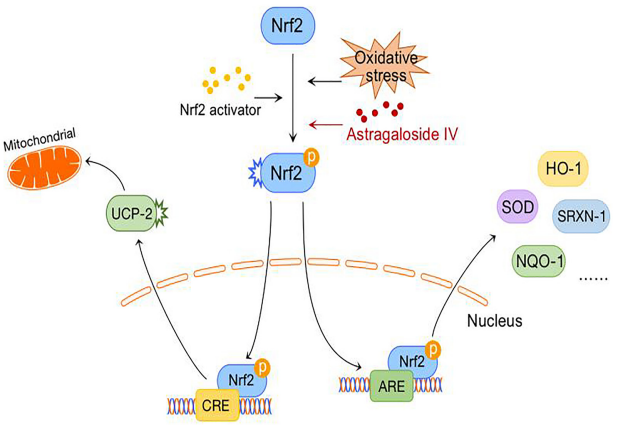

FIGURE 3 | Antioxidative stress mechanism of astragaloside IV.

Oxidative Stress

After cerebral ischemia-reperfusion, the large number of free radicals produced by the brain have a severely damaging effect on nerve cells, and inhibition of the oxidative stress response is an important means for preventing ischemic injury. AREs are *cis*-regulatory elements in the promoter regions of many important antioxidant genes. Nrf2, as a transcription factor, regulates the basic and induced expression of a large number of antioxidant genes by binding to AREs and is one of the key regulators of endogenous antioxidant defense (Kensler et al., 2007). Studies have shown that activation of the Nrf2/ARE pathway increases the nuclear localization of Nrf2; induces the expression of Nrf2/ARE-dependent genes such as HO-1, NQO-1, and SRXN-1; and attenuates cerebral ischemic injury (Zhang et al., 2017).

A comparison of the reactive oxygen species (ROS) levels in an OGD model before and after the administration of astragaloside IV inhibitors explicitly showed that astragaloside IV can inhibit the accumulation of ROS and that this effect is particularly evident at an astragaloside IV concentration of 50 μM. Real-time PCR showed that when the concentration of astragaloside IV is increased, the expression of the Nrf2/ARE-dependent genes HO-1, NQO-1, and SRXN-1 increases in a dose-dependent manner in an OGD model. After lentiviral shRNA-mediated inhibition of Nrf2 in cortical neurons, the scavenging effect of astragaloside IV on ROS is significantly inhibited, showing that the Nrf2/ARE pathway is required for the antioxidative and neuroprotective effects of astragaloside IV against OGD (Gu et al., 2015). Furthermore, astragaloside IV combined with ginsenoside Rg1 or ginsenoside Rb1 and notoginseng R1, which are ineffective when used alone, can activate the Nrf2/HO-1 signaling pathway to a greater extent after cerebral ischemia-reperfusion to downregulate Nrf2 expression in the cytoplasm, upregulate Nrf2 expression in the nucleus, increase the nuclear translocation rate, and increase HO-1 mRNA and protein expression; thus, the antagonistic effect of astragaloside IV against ischemia-reperfusion and oxidative stress injury is enhanced when the drug is combined with these agents (Huang et al., 2014). This provides meaningful guidance for combining drugs in the clinic to reduce their adverse effects and increase their safety. Can astragaloside alleviate neuronal oxidative stress after ischemia-reperfusion through other mechanisms? A previous study revealed that astragaloside IV acts as a key regulator of NO and angiogenesis through the JAK2/STAT3 and ERK1/2 pathways (Wang et al., 2013). In a recent study, astragaloside IV was shown to activate the JAK2/STAT3 signaling pathways, while the JAK2 inhibitor AG490 was found to reverse JAK2/STAT3 activation and the neuroprotective effects of astragaloside IV during OGD/R (Xu et al., 2020).

Abnormal energy metabolism after cerebral ischemia causes mitochondrial damage, resulting in decreased respiration, excessive ROS production, adenosine triphosphate (ATP) depletion (Fiskum et al., 1999; Perez-Pinzon, 2004), and inhibition of the PKA-CREB signaling pathway. The PKA-CREB signal transduction pathway can promote the survival, regeneration and differentiation of neural cells, and its downstream protein UCP-2 can reduce the mitochondrial membrane potential, resulting in mild mitochondrial decoupling and thus reducing ROS production. However, the exact mechanism by which UCP-2 regulates ROS production remains unclear (Ježek et al., 2018). Recently, the "decoupled survival" hypothesis, which is associated with UCP-2, was further confirmed in models of traumatic brain injury and ischemic stroke (Normoyle et al., 2015).

A previous study found that astragaloside IV might activate the PKA/CREB pathway, increase the mitochondrial membrane potential, and reduce the release of ROS in an OGD model. In contrast, it increases the release of ATP and improves mitochondrial function. Furthermore, astragaloside IV significantly reverses the release of LDH during OGD and the fragmentation of neuronal fibers and cell bodies, reduces the expression of caspase-3, and improves neuronal viability (Xue et al., 2019; **Figure 3**).

Astragaloside IV increases SOD activity and SOD mRNA expression in astrocytes. Supplementation with astragaloside IV after OGD/R exposure promotes the expression of oxidation and apoptosis markers, and further research has demonstrated that astragaloside IV inhibits the CXCR4 receptor and decreases

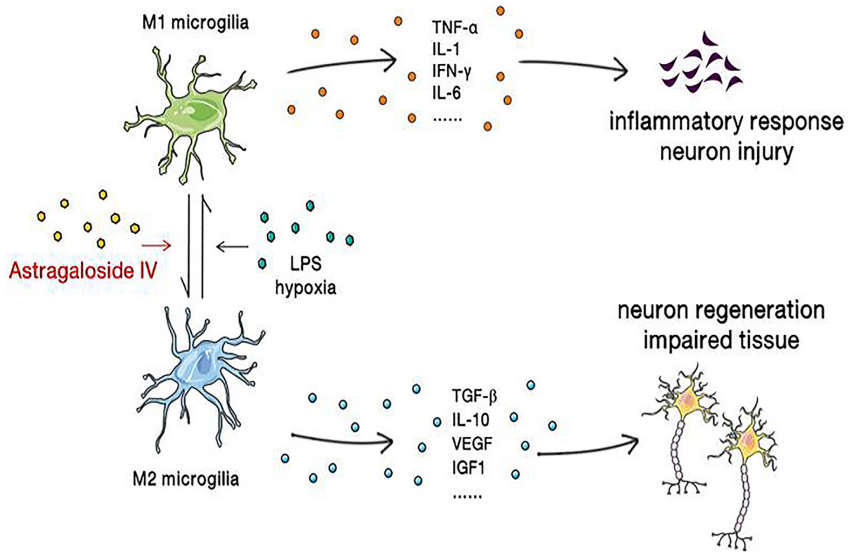

FIGURE 4 | Astragaloside IV reverses microglial polarization, reduces the inflammatory response, ameliorates neuronal injury, and promotes the regeneration of neurons and the repair of brain tissue.

the activation of the p-JNK/JNK pathway, thus suppressing the expression of Bax/Bcl-2 and ultimately promoting Nrf2/Keap1 signaling (Yang et al., 2021).

Damage to the Blood-Brain Barrier

The BBB consists of a continuous layer of brain capillary endothelial cells, pericytes, basement membranes, and astrocytes. Tight junctions between endothelial cells form metabolic and physical barriers, which limit the movement of macromolecules between the blood and the brain to maintain homeostasis in the brain (Kago et al., 2006). Following ischemic stroke, tight junction complexes in vascular endothelial cells are altered, causing increased paracellular solute leakage. Regulation of transporters and changes in intracellular transport mechanisms lead to disturbances in the transcellular transport of certain substances (Abdullahi et al., 2018). Therefore, protecting the BBB facilitates neuronal recovery after ischemia-reperfusion injury. Hemorrhagic stroke, such as aneurysmal hemorrhage, can lead to increased intracranial pressure, reduced cerebral blood flow, total cerebral ischemia, cerebral edema, blood component spillage, and decomposition product accumulation; in addition, it can damage the BBB, expose neural tissues to neurotoxic blood and immune cells and result in the development of delayed vasospasm, which leads to poor prognosis of stroke patients. This pathophysiological process may be mediated by TLR4, netrin-1, lipocalin-2, tropomyosin-associated kinase receptor B and the tyrosine kinase ErbB4 (Li et al., 2020).

Lanthanum staining was performed in an ischemia model and a sham operation model to compare the localization of lanthanum. Lanthanum was found in the sham operation group, while it was found in the perivascular tissues in the ischemia group. These results confirm that ischemia leads to dysfunction of the BBB. In the astragaloside IV-treated group, lanthanum was mainly confined to the cerebral capillaries, suggesting that astragaloside IV may maintain the integrity of the BBB in rats subjected to ischemia-reperfusion. A decrease in Evans blue leakage and an increase in the expression of the tight junction protein ZO-1 have also been reported, strongly supporting this idea (Qu et al., 2009). Other studies have found that astragaloside IV has an effect on BBB endothelial cells and inhibits the deterioration of inflammation to reduce the adhesion of JAWS II cells to bEnd.3 cells, decrease the expression of cellular VCAM-1, and increase the expression of cellular tight junction proteins (e.g., zo-1, occludin, and CLDN5). However, Nrf2 siRNA abolishes these effects of astragaloside IV and its protective effect on tight junctions, indicating that the protective effect of astragaloside IV against LPS-induced BBB endothelial cell injury is dependent on the Nrf2 signaling pathway (Li et al., 2018).

Moreover, experiments have demonstrated that astragaloside IV reduces the expression of TLR4 in rats with experimental arachnoid hemorrhage, thus reducing the activation of Nrf2 and decreasing the occurrence of delayed cerebral spasm (Ma et al., 2018). This finding suggests that astragaloside-IV also has a protective effect against delayed cerebral spasm after hemorrhagic stroke.

Leukocyte Adhesion to the Vascular Wall and Cerebral Parenchymal Infiltration

Inflammatory injury plays an important role in cerebral ischemia-reperfusion injury, and cerebral blood flow is interrupted after arterial occlusion. The acute inflammatory response is caused by neutrophil adhesion to ischemic endothelial cells (Chou et al., 2004; Yilmaz and Granger, 2010). Integrins and the immunoglobulin superfamily play a major role in this process (Huang et al., 2006). CD11b/CD18 is one of the major integrins in neutrophils and can recognize and

TABLE 2 | Protective effect and mechanism of astragaloside IV against cerebral ischemia-reperfusion complications.

No.	Study object/model	Test indicator	Mechanism	Effect
1	MCAO	(+) Neurological score (-) Brain water content BBB permeability MMP-9 expression AQP4 expression	(-) MMP-9 and AQP4 expression	(+) BBB function (-) Water enters astrocytes from microvessels Cerebral edema
2	BCCAO	(+) SOD levels (-) IL-1β expression TNF-α expression MDA levels ROS levels TLR4 expression TRIF expression TRAF6 expression p-P6 expression NLRP3 expression Caspase-1 expression Iba1 expression	(-) TLR4/MyD88, TRIF, and TRAF6/NF-κB pathways	(+) Memory function (-) Excessive activation of astrocytes and microglia Inflammatory reaction

bind to immunoglobulin superfamily members on the surface of endothelial cells (Springer, 1990; de Fougerolles et al., 1991; Shen et al., 1998).

Astragaloside IV has been found to play a protective role by significantly reducing the production of TNF-a and IL-1b, decreasing the level of NF-κB, significantly reducing the proportion of CD11b/CD18-positive neutrophils, and downregulating the expression of intercellular adhesion molecule-1 (ICAM-1). However, interestingly, this protective effect is not significantly correlated with the dose of astragaloside IV (Li et al., 2012).

Inflammatory Reaction in the Ischemic Penumbra

M1 microglia/macrophages can be activated by factors such as LPS, IFN-γ, TNF-α, hypoxia, and amyloid β, which increase the synthesis of proinflammatory factors, chemokines, and oxidative metabolites and worsen the inflammatory response, thereby aggravating neuronal injury and death. In contrast, M2 microglia/macrophages inhibit the inflammatory response by secreting cytokines and neurotrophic factors and promote neuronal repair and regeneration (Kanazawa et al., 2017). Activated microglia/macrophages can be detected in the border zone of ischemic lesions 30 min after permanent middle cerebral artery occlusion (MCAO) (Qin et al., 2019), and it has been demonstrated that the expression of the TLR family members TLR2, TLR4, and TLR9 increases after ischemic brain injury. Elevated TLR4 expression leads to activation of the NF-κB pathway and activates microglia/macrophages, allowing them to undergo the transition from the M2 phenotype to the M1 phenotype (Zhao et al., 2017). In addition, peroxisome proliferator–activated receptor γ (PPARγ), which is widely expressed in macrophages and microglia, is a member of the nuclear receptor superfamily and a ligand-activated transcription factor (Straus and Glass, 2007). PPARγ agonists have been reported to increase M2 microglial/macrophage polarization and promote neurogenesis and angiogenesis after cerebral ischemia-reperfusion (Kinouchi et al., 2018). Therefore, the PPARγ receptor is considered an effective therapeutic target for a variety of central nervous system diseases, including ischemic stroke (Cai et al., 2018).

It was found that 5 μmol/l astragaloside IV can inhibit the LPS-induced transition from the M2 phenotype to the M1 phenotype, NO production, and the expression of proinflammatory factors (IL-6, TNF-α) in microglia/macrophages but increase the expression of anti-inflammatory factors (IL-10). Immunofluorescence staining revealed that the expression of TLR4, MyD88, and NF-κB is elevated under stimulation with LPS and that this change can be inhibited by astragaloside IV, suggesting that astragaloside IV exerts its effect through the TLR4/MyD88/NF-κB signaling pathway (Yu et al., 2019). It was recently reported that astragaloside IV is a natural PPARγ agonist (Wang et al., 2017). It was found that astragaloside IV increases the M2 polarization of microglia/macrophages and the expression of PPARγ mRNA and protein. Immunofluorescence staining showed that after administration of the PPARγ antagonist T0070907, the number of CD16/32+/Iba1+ (M1) cells increases, the number of CD206+/Iba1+ (M2) cells decreases, the numbers of BrdU+/NeuN+, BrdU+/GFAP+, and BrdU+/vWF+ cells dramatically decreases and astragaloside IV-mediated neurogenesis and angiogenesis is blocked. The results indicate that astragaloside IV promotes M2 microglial/macrophage polarization through the PPARγ pathway (Li et al., 2021) (**Figure 4**).

PROTECTIVE EFFECT AND MECHANISM OF ASTRAGALOSIDE IV AGAINST CEREBRAL ISCHEMIA-REPERFUSION COMPLICATIONS

Astragaloside IV also exerts protective effects against cerebral ischemia-reperfusion complications (**Table 2**).

Cerebral Edema

Cerebral edema after intravenous thrombolysis is a rare but potentially fatal complication (Cruz-Flores et al., 2001) that occurs mainly due to cytotoxic edema resulting from ischemia and vasogenic edema aggravated by reperfusion. The aforementioned disturbance of the BBB caused by ischemia-reperfusion can lead to vasogenic brain edema and play an important role in the course of brain edema. Matrix metalloproteinases (MMPs) are proteolytic enzymes, and MMP-9 expression after cerebral ischemia leads to degradation of several important structural proteins, thus impairing the microvascular wall, increasing microvascular permeability, and disrupting the BBB (Dong et al., 2009; Liu et al., 2009). AQP4 is a member of the transmembrane aquaporin family and the water/glycerol transporter family (Agre, 2006), and AQP4 gene deficiency ameliorates brain edema caused by cerebral ischemia (Manley et al., 2000).

Studies have found that astragaloside IV can reduce the expression of MMP-9 and AQP4, ameliorate BBB dysfunction, and reduce cerebral edema complications. An experiment also revealed that there is no significant correlation between the protective effect and dose of astragaloside IV (Li et al., 2013).

Memory Impairment

There is a direct relationship between hypoperfusion in the hippocampal CA1 region and memory impairment after cerebral ischemia (Zhang et al., 2010). BBB breakdown (Winkler et al., 2014) and neurovascular dysfunction (Winkler et al., 2015) are also significant pathological features of Alzheimer's disease. In addition, neuroinflammation also plays an important role in impairing cognitive performance during the progression of neurodegenerative diseases (Harrison et al., 2014).

Astragaloside IV significantly decreases TLR4 expression and the synthesis of downstream adaptor proteins, including MyD88, TRIF, and TRAF6, and then suppresses NF-κB phosphorylation while inhibiting the excessive activation of astrocytes and microglia, alleviating the inflammatory response, and significantly improving memory impairment in mice with bilateral common carotid artery occlusion (BCCAO) (Li et al., 2017). Moreover, as a natural PPARγ agonist, astragaloside IV reduces the formation of neuritic plaques and Aβ plaques by inhibiting the expression of BACE1 to improve cognitive performance in Alzheimer's disease patients (Wang et al., 2017).

LIMITATIONS AND PROSPECTS

The mechanism underlying the cerebroprotective effect of astragaloside IV against ischemia-reperfusion is clear. Astragaloside significantly ameliorates injury caused by ischemia-reperfusion at multiple levels. Astragaloside IV acts on multiple signaling pathways to relieve neuronal apoptosis, oxidative stress, BBB injury, leukocyte adhesion to the vascular wall and parenchymal infiltration caused by ischemia-reperfusion and the inflammatory response triggered by ischemia and aggravated reperfusion to improve brain injury and complications after ischemia-reperfusion and improve prognosis.

However, most of the data have been obtained in cells, rats and mice, as there have been few clinical trials on the effect of astragaloside IV in stroke patients. We searched for articles on clinical trials of astragaloside IV and found that astragaloside IV has ameliorative effects on skeletal muscle injury (Jiang et al., 2020), precancerous lesions of gastric carcinoma (Zhang et al., 2018), liver fibrosis (Wang et al., 2021), induction of natriuresis (Ai et al., 2008), and heart failure (Luo et al., 1995). However, there are very few clinical publication on the protective effect of astragaloside IV on the brain. In addition, astragaloside IV was shown to have a dose-independent effect on some aspects of injury, such as leukocyte adhesion to the vascular wall and parenchymal infiltration.

Astragaloside IV has a certain toxic effect at specific doses, as 10 μmol/l astragaloside IV significantly decreases cell viability (Yu et al., 2019), but the appropriate dose of astragaloside IV can achieve a certain synergistic effect when administered in combination with other drugs such as ligustrazine (Cai et al., 2014) and notoginseng (Huang et al., 2017), providing guidance for clinical practice. Clinically, the use of rtPA for the treatment of acute ischemic stroke is limited not only by the small therapeutic window but also by the occurrence hemorrhagic transformation during ischemia-reperfusion injury. The incidence of spontaneous hemorrhagic transformation after acute ischemic stroke ranges from 13 to 43%, although autopsy results have suggested that the incidence is as high as 38–71%, and the use of rtPA increases this risk by 10-fold (Zhu et al., 2015). However, there is little evidence showing whether astragaloside IV exerts a cerebroprotective effect against intracerebral hemorrhage injury. We need to more comprehensively explore the cerebroprotective effect of astragaloside IV against ischemia-reperfusion through a more in-depth study of astragaloside IV.

AUTHOR CONTRIBUTIONS

WG and HT were involved in the study design. WG, HT, and WH provided and prepared the samples. XK and SS wrote the manuscript. All authors contributed to the article and approved the submitted version.

FUNDING

This work was supported by the National Natural Science Foundation of China (81973620 and 81774109), Wenzhou Science and Technology Project (ZY2019015), National Natural Science Foundation of Zhejiang Provincial (LGD20H290002), and Wenzhou Key Laboratory of Perioperative Medicine (2021HZSY0069).

REFERENCES

Abdullahi, W., Tripathi, D., and Ronaldson, P. T. (2018). Blood-brain barrier dysfunction in ischemic stroke: targeting tight junctions and transporters for vascular protection. *Am. J. Physiol.* 315, C343–C356. doi: 10.1152/ajpcell.00095.2018

Agre, P. (2006). The aquaporin water channels. *Proc. Am. Thorac. Soc.* 3, 5–13. doi: 10.1513/pats.200510-109JH

Ai, P., Yong, G., Dingkun, G., Qiuyu, Z., Kaiyuan, Z., and Shanyan, L. (2008). Aqueous extract of Astragali Radix induces human natriuresis through enhancement of renal response to atrial natriuretic peptide. *J. Ethnopharmacol.* 116, 413–421. doi: 10.1016/j.jep.2007.12.005

Alano, C. C., Ying, W., and Swanson, R. A. (2004). Poly(ADP-ribose) polymerase-1-mediated cell death in astrocytes requires NAD+ depletion and mitochondrial permeability transition. *J. Biol. Chem.* 279, 18895–18902. doi: 10.1074/jbc.M313329200

Armstead, W. M., Ganguly, K., Kiessling, J. W., Riley, J., Chen, X. H., Smith, D. H., et al. (2010). Signaling, delivery and age as emerging issues in the benefit/risk ratio outcome of tPA For treatment of CNS ischemic disorders. *J. Neurochem.* 113, 303–312. doi: 10.1111/j.1471-4159.2010.06613.x

Cai, J., Pan, R., Jia, X., Li, Y., Hou, Z., Huang, R. Y., et al. (2014). The combination of astragalus membranaceus and ligustrazine ameliorates microhaemorrhage by maintaining blood-brain barrier integrity in cerebrally ischaemic rats. *J. Ethnopharmacol.* 158, 301–309. doi: 10.1016/j.jep.2014.10.019

Cai, W., Yang, T., Liu, H., Han, L., Zhang, K., Hu, X., et al. (2018). Peroxisome proliferator-activated receptor γ (PPARγ): a master gatekeeper in CNS injury and repair. *Prog. Neurobiol.* 163-164, 27–58. doi: 10.1016/j.pneurobio.2017.10.002

Chan, P. H. (1996). Role of oxidants in ischemic brain damage. *Stroke* 27, 1124–1129. doi: 10.1161/01.str.27.6.1124

Chan, X. H., Nama, S., Gopal, F., Rizk, P., Ramasamy, S., Sundaram, G., et al. (2012). Targeting glioma stem cells by functional inhibition of a prosurvival oncomiR-138 in malignant gliomas. *Cell Rep.* 2, 591–602. doi: 10.1016/j.celrep.2012.07.012

Chou, W. H., Choi, D. S., Zhang, H., Mu, D., McMahon, T., Kharazia, V. N., et al. (2004). Neutrophil protein kinase Cdelta as a mediator of stroke-reperfusion injury. *J. Clin. Invest.* 114, 49–56. doi: 10.1172/jci21655

Cruz-Flores, S., Thompson, D. W., and Boiser, J. R. (2001). Massive cerebral edema after recanalization post-thrombolysis. *J. Neuroimaging* 11, 447–451. doi: 10.1111/j.1552-6569.2001.tb00079.x

de Fougerolles, A. R., Stacker, S. A., Schwarting, R., and Springer, T. A. (1991). Characterization of ICAM-2 and evidence for a third counter-receptor for LFA-1. *J. Exp. Med.* 174, 253–267. doi: 10.1084/jem.174.1.253

del Zoppo, G. J., and Mabuchi, T. (2003). Cerebral microvessel responses to focal ischemia. *J. Cereb. Blood Flow Metab.* 23, 879–894. doi: 10.1097/01.Wcb.0000078322.96027.78

del Zoppo, G. J., Schmid-Schonbein, G. W., Mori, E., Copeland, B. R., and Chang, C. M. (1991). Polymorphonuclear leukocytes occlude capillaries following middle cerebral artery occlusion and reperfusion in baboons. *Stroke* 22, 1276–1283. doi: 10.1161/01.str.22.10.1276

Dong, H., Fan, Y. H., Zhang, W., Wang, Q., Yang, Q. Z., and Xiong, L. Z. (2009). Repeated electroacupuncture preconditioning attenuates matrix metalloproteinase-9 expression and activity after focal cerebral ischemia in rats. *Neurol. Res.* 31, 853–858. doi: 10.1179/174313209x393960

Du, S. J., Zhang, Y., Zhao, Y. M., Dong, Y. J., Tang, J. L., Zhou, X. H., et al. (2021). Astragaloside IV attenuates cerebral ischemia-reperfusion injury in rats through the inhibition of calcium-sensing receptor-mediated apoptosis. *Int. J. Mol. Med.* 47, 302–314. doi: 10.3892/ijmm.2020.4777

Fiskum, G., Murphy, A. N., and Beal, M. F. (1999). Mitochondria in neurodegeneration: acute ischemia and chronic neurodegenerative diseases. *J. Cereb. Blood Flow Metab.* 19, 351–369. doi: 10.1097/00004647-199904000-00001

Gu, D. M., Lu, P. H., Zhang, K., Wang, X., Sun, M., Chen, G. Q., et al. (2015). EGFR mediates astragaloside IV-induced Nrf2 activation to protect cortical neurons against *in vitro* ischemia/reperfusion damages. *Biochem. Biophys. Res. Commun.* 457, 391–397. doi: 10.1016/j.bbrc.2015.01.002

Harrison, N. A., Doeller, C. F., Voon, V., Burgess, N., and Critchley, H. D. (2014). Peripheral inflammation acutely impairs human spatial memory via actions on medial temporal lobe glucose metabolism. *Biol. Psychiatry* 76, 585–593. doi: 10.1016/j.biopsych.2014.01.005

He, S., Liu, P., Jian, Z., Li, J., Zhu, Y., Feng, Z., et al. (2013). miR-138 protects cardiomyocytes from hypoxia-induced apoptosis via MLK3/JNK/c-jun pathway. *Biochem. Biophys. Res. Commun.* 441, 763–769. doi: 10.1016/j.bbrc.2013.10.151

Huang, J., Upadhyay, U. M., and Tamargo, R. J. (2006). Inflammation in stroke and focal cerebral ischemia. *Surg. Neurol.* 66, 232–245. doi: 10.1016/j.surneu.2005.12.028

Huang, X. P., Qiu, Y. Y., Wang, B., Ding, H., Tang, Y. H., Zeng, R., et al. (2014). Effects of Astragaloside IV combined with the active components of Panax notoginseng on oxidative stress injury and nuclear factor-erythroid 2-related factor 2/heme oxygenase-1 signaling pathway after cerebral ischemia-reperfusion in mice. *Pharmacogn. Mag.* 10, 402–409. doi: 10.4103/0973-1296.141765

Huang, X. P., Tan, H., Chen, B. Y., and Deng, C. Q. (2017). Combination of total Astragalus extract and total Panax notoginseng saponins strengthened the protective effects on brain damage through improving energy metabolism and inhibiting apoptosis after cerebral ischemia-reperfusion in mice. *Chin. J. Integr. Med.* 23, 445–452. doi: 10.1007/s11655-015-1965-0

Jean, W. C., Spellman, S. R., Nussbaum, E. S., and Low, W. C. (1998). Reperfusion injury after focal cerebral ischemia: the role of inflammation and the therapeutic horizon. *Neurosurgery* 43, 1382–1396. doi: 10.1097/00006123-199812000-00076

Ježek, P., Holendová, B., Garlid, K. D., and Jabůrek, M. (2018). Mitochondrial Uncoupling Proteins: subtle Regulators of Cellular Redox Signaling. *Antioxid. Redox Signal.* 29, 667–714. doi: 10.1089/ars.2017.7225

Jiang, B., Yang, Y. J., Dang, W. Z., Li, H., Feng, G. Z., Yu, X. C., et al. (2020). Astragaloside IV reverses simvastatin-induced skeletal muscle injury by activating the AMPK-PGC-1α signalling pathway. *Phytother. Res.* 34, 1175–1184. doi: 10.1002/ptr.6593

Kago, T., Takagi, N., Date, I., Takenaga, Y., Takagi, K., and Takeo, S. (2006). Cerebral ischemia enhances tyrosine phosphorylation of occludin in brain capillaries. *Biochem. Biophys. Res. Commun.* 339, 1197–1203. doi: 10.1016/j.bbrc.2005.11.133

Kanazawa, M., Ninomiya, I., Hatakeyama, M., Takahashi, T., and Shimohata, T. (2017). Microglia and Monocytes/Macrophages Polarization Reveal Novel Therapeutic Mechanism against Stroke. *Int. J. Mol. Sci.* 18:2135. doi: 10.3390/ijms18102135

Kensler, T. W., Wakabayashi, N., and Biswal, S. (2007). Cell survival responses to environmental stresses via the Keap1-Nrf2-ARE pathway. *Annu. Rev. Pharmacol. Toxicol.* 47, 89–116. doi: 10.1146/annurev.pharmtox.46.120604.141046

Kinouchi, T., Kitazato, K. T., Shimada, K., Yagi, K., Tada, Y., Matsushita, N., et al. (2018). Treatment with the PPARγ Agonist Pioglitazone in the Early Post-ischemia Phase Inhibits Pro-inflammatory Responses and Promotes Neurogenesis Via the Activation of Innate- and Bone Marrow-Derived Stem Cells in Rats. *Transl. Stroke Res.* 9, 306–316. doi: 10.1007/s12975-017-0577-8

Lai, T. W., Zhang, S., and Wang, Y. T. (2014). Excitotoxicity and stroke: identifying novel targets for neuroprotection. *Prog.Neurobiol.* 115, 157–188. doi: 10.1016/j.pneurobio.2013.11.006

Lansberg, M. G., Schrooten, M., Bluhmki, E., Thijs, V. N., and Saver, J. L. (2009). Treatment time-specific number needed to treat estimates for tissue plasminogen activator therapy in acute stroke based on shifts over the entire range of the modified Rankin Scale. *Stroke* 40, 2079–2084. doi: 10.1161/strokeaha.108.540708

Li, H., Wang, P., Huang, F., Jin, J., Wu, H., Zhang, B., et al. (2018). Astragaloside IV protects blood-brain barrier integrity from LPS-induced disruption via activating Nrf2 antioxidant signaling pathway in mice. *Toxicol. Appl. Pharmacol.* 340, 58–66. doi: 10.1016/j.taap.2017.12.019

Li, L., Gan, H., Jin, H., Fang, Y., Yang, Y., Zhang, J., et al. (2021). Astragaloside IV promotes microglia/macrophages M2 polarization and enhances neurogenesis and angiogenesis through PPARγ pathway after cerebral ischemia/reperfusion

injury in rats. *Int. Immunopharmacol.* 92:107335. doi: 10.1016/j.intimp.2020.107335

Li, M., Li, H., Fang, F., Deng, X., and Ma, S. (2017). Astragaloside IV attenuates cognitive impairments induced by transient cerebral ischemia and reperfusion in mice via anti-inflammatory mechanisms. *Neurosci. Lett.* 639, 114–119. doi: 10.1016/j.neulet.2016.12.046

Li, M., Ma, R. N., Li, L. H., Qu, Y. Z., and Gao, G. D. (2013). Astragaloside IV reduces cerebral edema post-ischemia/reperfusion correlating the suppression of MMP-9 and AQP4. *Eur. J. Pharmacol.* 715, 189–195.

Li, M., Qu, Y. Z., Zhao, Z. W., Wu, S. X., Liu, Y. Y., Wei, X. Y., et al. (2012). Astragaloside IV protects against focal cerebral ischemia/reperfusion injury correlating to suppression of neutrophils adhesion-related molecules. *Neurochem. Int.* 60, 458–465. doi: 10.1016/j.neuint.2012.01.026

Li, X., Zhu, L., Chen, X., and Fan, M. (2007). Effects of hypoxia on proliferation and differentiation of myoblasts. *Med. Hypotheses* 69, 629–636. doi: 10.1016/j.mehy.2006.12.050

Li, Y., Wu, P., Bihl, J. C., and Shi, H. (2020). Underlying Mechanisms and Potential Therapeutic Molecular Targets in Blood-Brain Barrier Disruption After Subarachnoid Hemorrhage. *Curr. Neuropharmacol.* 18, 1168–1179. doi: 10.2174/1570159x18666200106154203

Li, Y., Yang, Y., Zhao, Y., Zhang, J., Liu, B., Jiao, S., et al. (2019). Astragaloside IV reduces neuronal apoptosis and parthanatos in ischemic injury by preserving mitochondrial hexokinase-II. *Free Radic. Biol. Med.* 131, 251–263. doi: 10.1016/j.freeradbiomed.2018.11.033

Lindsberg, P. J., and Grau, A. J. (2003). Inflammation and infections as risk factors for ischemic stroke. *Stroke* 34, 2518–2532. doi: 10.1161/01.Str.0000089015.51603.Cc

Liu, W., Hendren, J., Qin, X. J., Shen, J., and Liu, K. J. (2009). Normobaric hyperoxia attenuates early blood-brain barrier disruption by inhibiting MMP-9-mediated occludin degradation in focal cerebral ischemia. *J. Neurochem.* 108, 811–820. doi: 10.1111/j.1471-4159.2008.05821.x

Liu, Z., Li, P., Zhao, D., Tang, H., and Guo, J. (2011). Anti-inflammation effects of Cordyceps sinensis mycelium in focal cerebral ischemic injury rats. *Inflammation* 34, 639–644. doi: 10.1007/s10753-010-9273-5

Lu, F. H., Tian, Z., Zhang, W. H., Zhao, Y. J., Li, H. L., Ren, H., et al. (2010). Calcium-sensing receptors regulate cardiomyocyte Ca2+ signaling via the sarcoplasmic reticulum-mitochondrion interface during hypoxia/reoxygenation. *J. Biomed. Sci.* 17:50. doi: 10.1186/1423-0127-17-50

Luo, H. M., Dai, R. H., and Li, Y. (1995). Nuclear cardiology study on effective ingredients of Astragalus membranaceus in treating heart failure. *Zhongguo Zhong Xi Yi Jie He Za Zhi* 15, 707–709.

Ma, Y., Qiao, G., Yin, Y., Zhang, Y., Yu, Y., and Yu, X. (2018). Protective Effects of Astragaloside IV on Delayed Cerebral Vasospasm in an Experimental Rat Model of Subarachnoid Hemorrhage. *World Neurosurg.* 118, e443–e448. doi: 10.1016/j.wneu.2018.06.212

Manley, G. T., Fujimura, M., Ma, T., Noshita, N., Filiz, F., Bollen, A. W., et al. (2000). Aquaporin-4 deletion in mice reduces brain edema after acute water intoxication and ischemic stroke. *Nat. Med.* 6, 159–163. doi: 10.1038/72256

Nederlof, R., Eerbeek, O., Hollmann, M. W., Southworth, R., and Zuurbier, C. J. (2014). Targeting hexokinase II to mitochondria to modulate energy metabolism and reduce ischaemia-reperfusion injury in heart. *Br. J.Pharmacol.* 171, 2067–2079. doi: 10.1111/bph.12363

Normoyle, K. P., Kim, M., Farahvar, A., Llano, D., Jackson, K., and Wang, H. (2015). The emerging neuroprotective role of mitochondrial uncoupling protein-2 in traumatic brain injury. *Transl. Neurosci.* 6, 179–186. doi: 10.1515/tnsci-2015-0019

Perez-Pinzon, M. A. (2004). Neuroprotective effects of ischemic preconditioning in brain mitochondria following cerebral ischemia. *J. Bioenerg. Biomembr.* 36, 323–327. doi: 10.1023/B:JOBB.0000041762.47544.ff

Qin, C., Zhou, L. Q., Ma, X. T., Hu, Z. W., Yang, S., Chen, M., et al. (2019). Dual Functions of Microglia in Ischemic Stroke. *Neurosci. Bull.* 35, 921–933. doi: 10.1007/s12264-019-00388-3

Qu, Y. Z., Li, M., Zhao, Y. L., Zhao, Z. W., Wei, X. Y., Liu, J. P., et al. (2009). Astragaloside IV attenuates cerebral ischemia-reperfusion-induced increase in permeability of the blood-brain barrier in rats. *Eur. J. Pharmacol.* 606, 137–141. doi: 10.1016/j.ejphar.2009.01.022

Saposnik, G., Guzik, A. K., Reeves, M., Ovbiagele, B., and Johnston, S. C. (2013). Stroke Prognostication using Age and NIH Stroke Scale: SPAN-100. *Neurology* 80, 21–28. doi: 10.1212/WNL.0b013e31827b1ace

Shafi, N., and Levine, J. M. (2010). Emergency management of acute ischemic stroke. *Curr. Atheroscler. Rep.* 12, 230–235. doi: 10.1007/s11883-010-0116-5

Shen, Y. C., Sung, Y. J., and Chen, C. F. (1998). Magnolol inhibits Mac-1 (CD11b/CD18)-dependent neutrophil adhesion: relationship with its antioxidant effect. *Eur. J. Pharmacol.* 343, 79–86. doi: 10.1016/s0014-2999(97)01519-7

Springer, T. A. (1990). Adhesion receptors of the immune system. *Nature* 346, 425–434. doi: 10.1038/346425a0

Stępnik, K., and Kukula-Koch, W. (2020). In Silico Studies on Triterpenoid Saponins Permeation through the Blood-Brain Barrier Combined with Postmortem Research on the Brain Tissues of Mice Affected by Astragaloside IV Administration. *Int. J. Mol. Sci.* 21:2534. doi: 10.3390/ijms21072534

Straus, D. S., and Glass, C. K. (2007). Anti-inflammatory actions of PPAR ligands: new insights on cellular and molecular mechanisms. *Trends Immunol.* 28, 551–558. doi: 10.1016/j.it.2007.09.003

Tymianski, M. (2011). Emerging mechanisms of disrupted cellular signaling in brain ischemia. *Nat.Neurosci.* 14, 1369–1373. doi: 10.1038/nn.2951

Wang, S. G., Xu, Y., Chen, J. D., Yang, C. H., and Chen, X. H. (2013). Astragaloside IV stimulates angiogenesis and increases nitric oxide accumulation via JAK2/STAT3 and ERK1/2 pathway. *Molecules* 18, 12809–12819. doi: 10.3390/molecules181012809

Wang, X., Wang, Y., Hu, J. P., Yu, S., Li, B. K., Cui, Y., et al. (2017). Astragaloside IV, a Natural PPARγ Agonist. Reduces Aβ Production in Alzheimer's Disease Through Inhibition of BACE1. *Mol. Neurobiol.* 54, 2939–2949. doi: 10.1007/s12035-016-9874-6

Wang, Y., Li, Y., Zhang, H., Zhu, L., Zhong, J., Zeng, J., et al. (2021). Pharmacokinetics-based comprehensive strategy to identify multiple effective components in Huangqi decoction against liver fibrosis. *Phytomedicine* 84:153513. doi: 10.1016/j.phymed.2021.153513

Winkler, E. A., Nishida, Y., Sagare, A. P., Rege, S. V., Bell, R. D., Perlmutter, D., et al. (2015). GLUT1 reductions exacerbate Alzheimer's disease vasculo-neuronal dysfunction and degeneration. *Nat. Neurosci.* 18, 521–530. doi: 10.1038/nn.3966

Winkler, E. A., Sagare, A. P., and Zlokovic, B. V. (2014). The pericyte: a forgotten cell type with important implications for Alzheimer's disease? *Brain Pathol.* 24, 371–386. doi: 10.1111/bpa.12152

Xu, Z., Liu, W., and Huang, H. (2020). Astragaloside IV Alleviates Cerebral Ischemia-Reperfusion Injury by Activating the Janus Kinase 2 and Signal Transducer and Activator of Transcription 3 Signaling Pathway. *Pharmacology* 105, 181–189. doi: 10.1159/000503361

Xue, B., Huang, J., Ma, B., Yang, B., Chang, D., and Liu, J. (2019). Astragaloside IV Protects Primary Cerebral Cortical Neurons from Oxygen and Glucose Deprivation/Reoxygenation by Activating the PKA/CREB Pathway. *Neuroscience* 404, 326–337. doi: 10.1016/j.neuroscience.2019.01.040

Yang, J., Shao, C., Li, W., Wan, H., He, Y., and Yang, J. (2021). Protective effects of Astragaloside IV against oxidative injury and apoptosis in cultured astrocytes by regulating Nrf2/JNK signaling. *Exp. Brain Res.* 239, 1827–1840. doi: 10.1007/s00221-021-06096-7

Yilmaz, G., and Granger, D. N. (2010). Leukocyte recruitment and ischemic brain injury. *Neuromol. Med.* 12, 193–204. doi: 10.1007/s12017-009-8074-1

Yin, F., Zhou, H., Fang, Y., Li, C., He, Y., Yu, L., et al. (2020). Astragaloside IV alleviates ischemia reperfusion-induced apoptosis by inhibiting the activation of key factors in death receptor pathway and mitochondrial pathway. *J. Ethnopharmacol.* 248:112319. doi: 10.1016/j.jep.2019.112319

Yu, S. W., Andrabi, S. A., Wang, H., Kim, N. S., Poirier, G. G., Dawson, T. M., et al. (2006). Apoptosis-inducing factor mediates poly(ADP-ribose) (PAR) polymer-induced cell death. *Proc. Natl. Acad. Sci. U.S.A.* 103, 18314–18319. doi: 10.1073/pnas.0606528103

Yu, J., Guo, M., Li, Y., Zhang, H., Chai, Z., Wang, Q., et al. (2019). Astragaloside IV protects neurons from microglia-mediated cell damage through promoting

microglia polarization. *Folia Neuropathol.* 57, 170–181. doi: 10.5114/fn.2019.86299

Zhang, C., Cai, T., Zeng, X., Cai, D., Chen, Y., Huang, X., et al. (2018). Astragaloside IV reverses MNNG-induced precancerous lesions of gastric carcinoma in rats: regulation on glycolysis through miRNA-34a/LDHA pathway. *Phytother. Res.* 32, 1364–1372. doi: 10.1002/ptr.6070

Zhang, L., Fu, F., Zhang, X., Zhu, M., Wang, T., and Fan, H. (2010). Escin attenuates cognitive deficits and hippocampal injury after transient global cerebral ischemia in mice via regulating certain inflammatory genes. *Neurochem. Int.* 57, 119–127. doi: 10.1016/j.neuint.2010.05.001

Zhang, R., Xu, M., Wang, Y., Xie, F., Zhang, G., and Qin, X. (2017). Nrf2-a Promising Therapeutic Target for Defensing Against Oxidative Stress in Stroke. *Mol. Neurobiol.* 54, 6006–6017. doi: 10.1007/s12035-016-0111-0

Zhang, R. L., Chopp, M., Chen, H., and Garcia, J. H. (1994a). Temporal profile of ischemic tissue damage, neutrophil response, and vascular plugging following permanent and transient (2H) middle cerebral artery occlusion in the rat. *J. Neurol. Sci.* 125, 3–10. doi: 10.1016/0022-510x(94)90234-8

Zhang, R. L., Chopp, M., Li, Y., Zaloga, C., Jiang, N., Jones, M. L., et al. (1994b). Anti-ICAM-1 antibody reduces ischemic cell damage after transient middle cerebral artery occlusion in the rat. *Neurology* 44, 1747–1751. doi: 10.1212/wnl.44.9.1747

Zhao, S. C., Ma, L. S., Chu, Z. H., Xu, H., Wu, W. Q., and Liu, F. (2017). Regulation of microglial activation in stroke. *Acta Pharmacol. Sin.* 38, 445–458. doi: 10.1038/aps.2016.162

Zheng, Z., and Zhao, B. (2018). Astragalus polysaccharide protects hypoxia-induced injury by up-regulation of miR-138 in rat neural stem cells. *Biomed. Pharmacother.* 102, 295–301. doi: 10.1016/j.biopha.2018.03.040

Zhu, Z., Fu, Y., Tian, D., Sun, N., Han, W., Chang, G., et al. (2015). Combination of the Immune Modulator Fingolimod With Alteplase in Acute Ischemic Stroke: a Pilot Trial. *Circulation* 132, 1104–1112. doi: 10.1161/circulationaha.115.016371

Conflict of Interest: The authors declare that the research was conducted in the absence of any commercial or financial relationships that could be construed as a potential conflict of interest.

Publisher's Note: All claims expressed in this article are solely those of the authors and do not necessarily represent those of their affiliated organizations, or those of the publisher, the editors and the reviewers. Any product that may be evaluated in this article, or claim that may be made by its manufacturer, is not guaranteed or endorsed by the publisher.

Advantages of publishing in Frontiers

OPEN ACCESS
Articles are free to read for greatest visibility and readership

FAST PUBLICATION
Around 90 days from submission to decision

HIGH QUALITY PEER-REVIEW
Rigorous, collaborative, and constructive peer-review

TRANSPARENT PEER-REVIEW
Editors and reviewers acknowledged by name on published articles

Frontiers
Avenue du Tribunal-Fédéral 34
1005 Lausanne | Switzerland

Visit us: www.frontiersin.org
Contact us: frontiersin.org/about/contact

REPRODUCIBILITY OF RESEARCH
Support open data and methods to enhance research reproducibility

DIGITAL PUBLISHING
Articles designed for optimal readership across devices

FOLLOW US
@frontiersin

IMPACT METRICS
Advanced article metrics track visibility across digital media

EXTENSIVE PROMOTION
Marketing and promotion of impactful research

LOOP RESEARCH NETWORK
Our network increases your article's readership